Bifunctional Ligand Systems for the Radiolabeling of Nanoparticles and Biomolecules with the *fac*-[^{99m}Tc(CO)$_3$]$^+$-Core

Dissertation

zur

Erlangung der naturwissenschaftlichen Doktorwürde

(Dr. sc. nat.)

vorgelegt der

Mathematisch-naturwissenschaftlichen Fakultät

der

Universität Zürich

von

Michael Felber

aus Römerswil LU

Promotionskomitee

Prof. Dr. Roger Alberto (Vorsitz)

Prof. Dr. Roland K. O. Sigel

Zürich, 2015

To my Family

Pra minha Família

Table of Contents

Summary

The application of nanoparticles (NPs) in the medical field is increasingly growing in importance. NPs such as mesoporous silica NPs, polymeric NPs, magnetic NPs, gold NPs (AuNPs), and quantum dots (QDs) are promising candidates for the design of novel imaging, drug delivery or theranostic agents. A major challenge after administration of NPs to living organisms is the exact localization. Among the various techniques to assess the biodistribution of functional nanostructures, radiolabeling and subsequent detection of the emitted γ-photons allows for noninvasive imaging by single photon emission computed tomography (SPECT) or positron emission tomography (PET). Moreover, radiolabeling provides an accurate quantification of nanostructure localization in different organs or tissues by performing an *ex vivo* biodistribution.

For the ^{99m}Tc labeling of AuNPs and QDs a novel coating ligand was synthesized, containing a thiol group as an anchor for the NP surface, a spacer (e.g. polyethylene glycol PEG) and the 2,3-diaminopropionic acid (DAP) chelator for the $[^{99m}Tc(CO)_3]^+$ fragment. This ligand is multi-functional; it combines the metal chelate with conjugating functions to biological vectors in one single molecule. The concept allows coupling of any targeting function to the chelator. An example with a small molecule target for the prostate specific membrane antigen (PSMA) is given. Derivatized AuNPs and QDs can directly be labeled in one step with $[^{99m}Tc(OH_2)_3(CO)_3]^+$. The AuNPs in particular are highly stable in buffer and serum, a prerequisite for *in vivo* studies excluding misinterpretation of the biodistribution data. AuNPs with differing sizes (7 nm and 14 nm core diameter) were administered intravenously into nude NMRI mice bearing LNCaP xenografts. MicroSPECT images show for both probes rapid clearance from the blood pool *via* the hepatobiliary pathway. The 7 nm AuNPs revealed a significantly higher bone uptake than the 14 nm AuNPs. The high affinity towards bone mineral is further confirmed *in vitro* with hydroxyapatite.

In case NPs have an intrinsic property for contrast, radiolabeling automatically leads to multi-modal imaging agents. Particularly the development of NP-based dual-modality probes for magnetic resonance imaging (MRI)/PET or MRI/SPECT is intensively investigated. One of the most commonly used radionuclide for clinical SPECT imaging is ^{99m}Tc and the labeling of Fe_3O_4 NPs with ^{99m}Tc was shown to be a successful strategy to obtain dual-modality imaging agents. The focus in this thesis is on the ^{99m}Tc labeling of gold containing magnetic

nanomaterials (Fe_3O_4-Au core-shell and heterostructured Fe_3O_4-Au Dumbbell-like NPs). The key elements for the labeling are novel coating ligands, consisting of mono- or dithiol anchors for the gold surface, a PEG linker and various chelators for the $[^{99m}Tc(CO)_3]^+$ fragment. In a variety of labeling experiments, favorable coatings were examined and their stability tested. The findings presented herein can form the basis for the development of potential, NP-based SPECT/MRI dual-modality imaging agents.

The versatility of the established ligand system was further shown with an intermediate along the synthethic pathway. The terminal hydroxyl group of the triethylene glycol linker conjugated to DAP was combined with L-tyrosine *via* a Mitsunobu reaction to the *para*-hydroxy of L-tyrosine. The ^{99m}Tc-L-tyrosine derivative was evaluated in healthy and nude NMRI mice bearing a C6 tumor xenograft. Radiolabeled amino acid derivatives in general are highly interesting for tumor imaging due to enhanced amino acid metabolism and protein synthesis in tumors compared to normal peripheral tissue. However, uptake in the tumor and pancreas at 1 h post injection (p.i.) was low, indicating that the tracer was not recognized as an amino acid analogue. Although the ^{99m}Tc-L-tyrosine derivative was not suitable for tumor imaging, it may be useful to image and to assess the functionality of the gallbladder. At 1 h p.i., the uptake in the gallbladder was unexpectedly high and the microSPECT images showed a high uptake after already 15 min p.i.

In addition, the bifunctional ligand system HS-PEG-DAP is not only well suitable for NP coating, but also for the labeling of biomolecules with a free thiol group. The basis for this novel labeling approach is the well known thiol-disufide exchange reaction. Therefore, the complex HS-PEG-DAP-$^{99m}Tc(CO)_3$ was activated with 2,2'-dithiodipyridine to form the pyridyl disulfide derivative. This compound allows the radiolabeling of biomolecues bearing a thiol functionality, exemplified with thioglucose, cysteine and glutathione. The scope of this labeling strategy can be extended to small peptides or even proteins containing a free thiol group.

Zusammenfassung

Die Anwendung von Nanopartikeln (NP) in der Medizin gewinnt immer mehr an Bedeutung. NP wie mesoporöse Silica NP, polymerische NP, magnetische NP, Gold NP (AuNP), und Quantenpunkte (QP) sind vielversprechende Kandidaten für die Entwicklung von neuartigen Kontrastmitteln für bildgebende Verfahren, die gezielte Pharmakotherapie oder theragnostischen Substanzen. Die genaue Lokalisierung nach der Verabreichung an lebende Organismen stellt jedoch eine besonders grosse Herausforderung dar. Unter den verschiedenen Techniken zur Bestimmung der Biodistribution von funktionalen Nanostrukturen erlaubt die Markierung mit Radionukliden und die entsprechende Detektion der emittierten γ-Strahlung mittels Einzelphotonen-Emissions-Computer-Tomographie (SPECT) oder Positronen-Emissions-Tomographie (PET) noninvasive Bildgebung. Zudem kann mithilfe von Radionuklid-Markierung eine *ex vivo* Biodistributionsanalyse durchgeführt und somit die exakte Menge in den verschiedenen Organen ermittelt werden.

Für die Markierung von AuNP und QP mit ^{99m}Tc wurde in dieser Arbeit ein neuartiger Oberflächen-Ligand synthetisiert, bestehend aus einer Thiolgruppe für die Verankerung an der NP Oberfläche, einem Linker (z.B. Polyethylenglykol PEG) und dem 2,3-Diaminpropionsäure-Chelator (DAP) für das $[^{99m}Tc(CO)_3]^+$ Fragment. Dieser Ligand ist multifunktional durch die Kombination vom Chelat und konjugierenden Funktionen für biologische Vektoren in einem einzigen Molekül. Dieses Konzept ermöglicht die Kopplung von jeglicher biologischer Zielfunktion mit dem Chelator. Als Beispiel wird eine niedermolekulare Zielfunktion für das Prostata-spezifische Membranantigen (PSMA) gezeigt. Derivatisierte AuNP und QP können direkt in einem Schritt mit $[^{99m}Tc(CO)_3(OH_2)_3]^+$ markiert werden. Die AuNP sind extrem stabil in Pufferlösung und im Serum, eine Voraussetzung für *in vivo* Studien um eine Fehlinterpretation der Biodistributionsdaten zu vermeiden. AuNP mit unterschiedlichen Grössen (7 und 14 nm Kerndurchmesser) wurden intravenös an NMRI Mäuse mit einem LNCaP Tumor verabreicht. Kleintier-SPECT Analysen zeigten für beide Substanzen eine schnelle Ausscheidung vom Blut in die Leber. Die 7 nm AuNP hatten eine signifikant grössere Aufnahme in den Knochen als die 14 nm AuNP. Die grosse Affinität für Knochenmineral wurde zusätzlich *in vitro* mit Hydroxylapatit bestätigt.

Falls NP eine intrinsische Eigenschaft als Kontrastmittel besitzen führt die Radionuklid-Markierung automatisch zu multimodalen Substanzen. Vor allem die Entwicklung von NP

basierten bimodalen Substanzen für Magnetresonanztomographie (MRI)/PET oder MRI/SPECT wird intensiv erforscht. Das am häufigsten verwendete Radionuklid für die klinische SPECT-Bildgebung ist ^{99m}Tc und die Markierung von Fe_3O_4 NP mit ^{99m}Tc hat sich als eine erfolgreiche Strategie für die Synthese von bimodalen Kontrastmitteln erwiesen. Der Fokus dieser Arbeit ist auf die ^{99m}Tc-Markierung von Fe_3O_4-Au Kern-Schalen NP und Fe_3O_4-Au Dumbbell-ähnlichen NP gerichtet. Das wichtigste Element für die Markierung sind neuartige Liganden, zusammengesetzt aus Mono- oder Dithiolgruppen für die Befestigung an der NP Oberfläche, einem PEG Linker und verschiedenen Chelatoren für das $[^{99m}Tc(CO)_3]^+$ Fragment. In diversen Experimenten wurde die optimale Kombination von Liganden eruiert und deren Stabilität getestet. Die gewonnen Erkenntnisse bilden die Basis von potentiellen NP basierten bimodalen MRI/SPECT Kontrastmittel.

Die vielfältige Anwendung der synthetisierten Ligandsysteme wurde an einem weiteren Beispiel gezeigt, wobei die terminale Hydroxygruppe des an den DAP gekoppelten PEG Linker durch eine Mitsunobu Reaktion mit der *para*-Hydroxygruppe von L-Tyrosin verbunden wurde. Das entsprechende ^{99m}Tc-L-Tyrosin Derivat wurde in gesunden und NMRI Mäusen mit einem C6 Tumor evaluiert. Markierte Aminosäuren sind generell interessant für die Bildgebung von Tumoren aufgrund des verstärkten Aminosäuren Metabolismus und Proteinsynthese im Vergleich zu normalem peripherem Gewebe. Der synthetisierte Tracer zeigte jedoch eine sehr geringe Tumoraufnahme und wird somit nicht als Aminosäure-Analog erkannt. Das Derivat zeigte aber sehr interessante Charakteristika für die Bildgebung der Gallenblasenfunktion. Eine Stunde nach intravenöser Verabreichung war die Aufnahme in der Gallenblase unerwartet hoch und auf den Kleintier-SPECT Bildern ist bereits nach 15 min eine hohe Aufnahme zu erkennen.

Das bifunktionale Ligandsystem HS-PEG-DAP ist nicht nur für die Oberflächenbeschichtung von NP geeignet, sondern auch für die Markierung von Biomolekülen mit einer freien Thiolgruppe. Die Grundlage für diese neuartige Markierungsmethode bildet die bekannte Thiol-Disulfid Austauschreaktion. Dabei wurde der Komplex HS-PEG-DAP-^{99m}Tc(CO)$_3$ mit 2,2‘-Dithiodipyridin aktiviert, wodurch das Pyridyl-Disulfid Derivat entstand. Diese Verbindung ermöglicht die Markierung von Biomolekülen mit einer Thiolgruppe, beispielsweise Thioglucose, Cystein oder Glutathion. Die Möglichkeiten dieser Markierungsstrategie können auf kleine Peptide oder sogar Proteine mit einer freien Thiolgruppe erweitert werden.

1. Introduction

1.1 Nanomedicine – An Emerging Field

Nanomedicine is defined as the application of nanotechnology to medicine for specific diagnostic or therapeutic purposes.[1] This includes materials in the scale range of 1-100 nm, which offer unique tools for the development of highly engineered, effective and safe medicines.[2,3] The field of nanomedicine combines the expertise of chemists, material scientists, physicists, biologists and biomedical engineers, and has evolved as one of the most exciting research field during the last decade.[4] Due to the importance and potential of nanomedicine, the US National Institutes of Health (NIH) recognizes it as a priority area in the roadmap for medical research. Therefore, NIH launched in 2005 an initiative to support basic and applied biomedical research of nanotechnology with about USD 300 million until 2015.[5] The fascination of nanomaterials arises from their exclusive properties that bulk materials do not have, especially quantum-size and surface effects.[2] As a consequence of the small size, nanomaterials have an increased surface area to volume ratio and this enables the development of materials with various functions, such as targeting, imaging or therapy.[6] The landscape of nanomaterials used for biomedical applications can be categorized into three groups.[7,8] The first group consists inorganic nanostructures, namely magnetic nanoparticles (MNPs), gold nanoparticles (AuNPs), mesoporous silica nanoparticles (mSiNPs), quantum dots (QDs) and upconverting nanoparticles (UCNPs). The second group comprises polymeric NPs made of dendrimers or amphiphilic polymers. Lipid NPs, including liposomes and solid lipid containing NPs, represent the third group. In addition, the biomedical application of carbon nanotubes (CNTs) has also been widely explored, but CNTs do not fit in any of the three groups.[9] Each type of material listed above has its own advantages and very specific properties, but the translation into the clinic requires biocompatibility or biodegradability. This is a major limitation for most of the inorganic nanomaterials and the main focus lies on their modification in order to guarantee a safe behavior after administration to living organisms. This was achieved with iron oxide nanoparticles (IONPs), widely used magnetic resonance imaging (MRI) contrast agents, such as Feridex, Combidex or Feraheme.[10] Excellent biocompatibility, biodegradability and structural versatility are the characteristics of polymeric and lipid NPs.[11] Therefore, these materials constitute a large number of the nanomedicines in routine clinical use, mainly for

drug delivery purposes.[12] The ultimate goal of drug delivery is the development of so-called "magic bullets", highly efficient therapeutics that can distinguish between malignant and benign cells, and selectively target cancerous tissues.[1] Besides the targeting capability, nanocarriers also improve the pharmaceutical formulation of conventional therapeutic agents, because most of them are poorly water soluble.[12] In addition, drug delivery systems control the release rate of the drug for an optimal therapeutic effect.[13] Examples of NP-based therapeutics in clinical use are Abraxane and Genexol-PM for the delivery of the chemotherapeutic drug Paclitaxel; or Caelyx, Doxil and Myocet for the delivery of the anticancer drug Doxorubicin. A detailed list of all drug delivery systems in clinical use and under clinical investigation can be found in the review by Xia and co-workers.[1]

1.2 Functionalization of Nanomaterials for Biomedical Applications

Chemistry is absolutely crucial for the fabrication of nanomaterials, not only to control the size and chemical composition, but also to provide functional groups, stabilizers and targeting functions on the surface. The combination of the surface chemistry and the physical properties, like the size and shape, are the determining element for the biophysicochemical behavior of the nanomaterial, which in turn dictates its biological fate (see section 1.4).[14] Many synthetic methods provide inorganic NPs with a hydrophobic coating and there are essentially two strategies to access water soluble NPs, a prerequisite for biomedical applications.[15]

The first strategy is based on a replacement of the native hydrophobic coating with small bifunctional molecules or polymers. This requires strong anchoring groups with a high affinity to the surface of the NPs, as well as hydrophilic groups to ensure water solubility and biocompatibility.[16] Mono- or dithiolated ligands are predominantly used as anchors for AuNPs and CdSe/ZnS core-shell QDs due to the strong binding of thiol-groups to these materials.[17,18] However, in biological milieu L-cysteine is present in various forms (as free amino acid, in glutathione or as protein residue) and could adsorb on the thiophilic NP surface, leading to undesired changes of the coating layer. The question if monodentate or bidentate anchors are better in preventing nonspecific binding of thiols has been addressed by Heyes and co-workers.[19] In their study, CdSe/ZnS QDs were coated with either monodentate mercaptopropanoic acid or bidentate dihydrolipoic acid (DHLA) (Figure 1). At

low thiol concentration, they found that a coating with monodentate ligands inhibits nonspecific binding better than a coating with bidentate ligands. At high thiol concentration they observed the inverse situation. This result highlights that nonspecific adsorption depends on a balance between the free thiol concentration and the dentate nature. Another possibility to prevent surface exposure is the usage of polyethylene glycol (PEG) ligands conjugated to the thiolate-anchors. This type of ligand system provides highly water soluble NPs, biocompatibility and protection of the inorganic core from degradation.[20] Moreover, PEG-based ligand systems prevent aggregation and endow the particles with great stability, which is described as colloidal stability.[21] In a typical experimental setup the colloidal stability is investigated with dynamic light scattering (DLS) techniques over time and expressed as changes in the hydrodynamic diameter (HDD).[22] An alternative to PEG on the outer sphere of the coating are zwitterionic groups like phosphobetaine, sulfobetaine or carboxybetaine (Figure 1).[23] Zwitterionic groups have very similar attributes as PEG, including hydrophilicity and overall charge neutrality, but ligands with these groups are generally shorter in length and, as a consequence, leading to smaller HDDs.[24] The same coating ligand rationale can be applied to IONPs, however, the iron oxide surface requires anchoring groups different than thiolates due to the low affinity of thiol-groups to Fe^{III}. The anchor with highest affinity to INOPs was evaluated by Gao and co-workers.[25] In their study, they compared the binding affinities of three different coating ligands: diphosphate-PEG-OCH_3, hydroxamate-PEG-OCH_3 and dopamine-PEG-OCH_3 (PEG with $M_W \approx 2000$ Da, Figure 1). They found that the binding affinity follows the order of diphosphate, dopamine and hydroxamate. In addition to the binding affinity of the anchoring groups, their effect on the magnetic properties of IONPs is equally important. In the same study they showed that the ratio of the transverse relaxivity (r_2) to longitudinal relaxivity (r_1) is highest with dopamine, followed by hydroxamate and disphosphate. Taking into account the largely enhanced T_2 effect, high binding affinity and commercial availability, dopamine is the ligand of choice for many research groups for developing novel IONP-based MRI contrast agents.[26,27] IONPs used nowadays in clinics are usually coated with dextran or starch, but these biopolymers do not exhibit the same strong interaction as dopamine with its vicinal diol-groups.[28]

The second strategy to make NPs water soluble relies on the utilization of amphiphilic block copolymers or phospholipid micelles.[16] With this route the native hydrophobic coating of NPs is not replaced, but encapsulated in an entropy-driven process. The hydrophobic

segments of the amphiphilic coating interact with the native hydrophobic coating of the NPs and the hydrophilic parts are on the outer sphere of the coating. Although this phase transfer approach is straight forward and guarantees high long-term colloidal stability, it results in large HDDs.

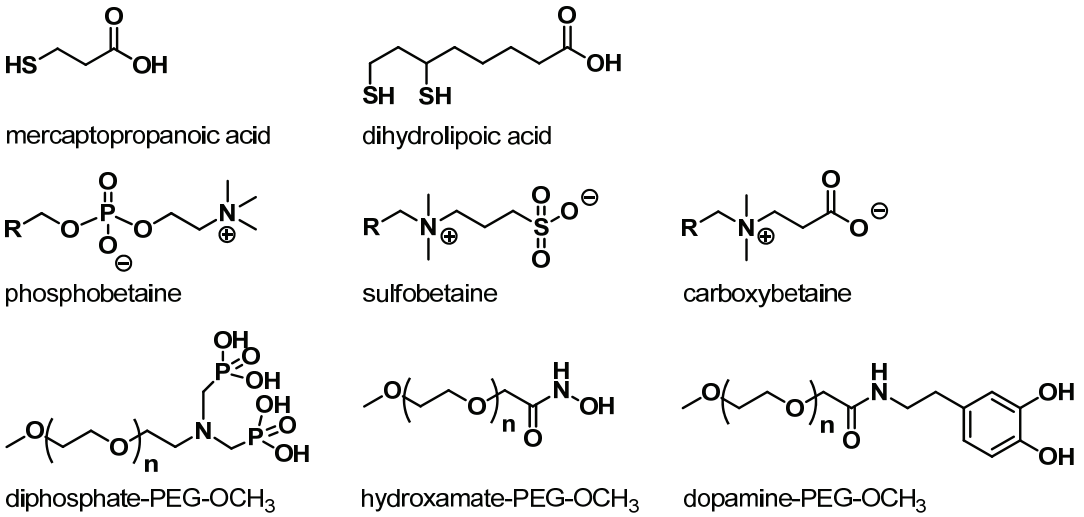

Figure 1. A typical monodentate and bidentate thiolate-ligand for AuNPs or CdSe/ZnS QDs (top row); various zwitterionic functionalities (middle row); and different anchoring-groups for IONPs.

1.3 Radiolabeling of Nanomaterials

In order to use nanomaterials as highly efficient platforms to design imaging and therapeutic agents for cancer or other human disorders, targeting functions such as monoclonal antibodies, aptamers, peptides or receptor-specific small molecules are an integral part of the construct.[29] However, the attachment of a targeting function does not automatically mean accumulation at the target site, particularly because a biological system is extremely complex and reliable predictions are difficult. Therefore, it is absolutely critical to monitor the pharmacokinetics and biodistribution of a nanomaterial after administration, preferably in a noninvasive and quantitative manner.[30] The imaging modalities that allow noninvasive investigations are broadly classified into techniques producing an image of anatomy (computed tomography CT and MRI) and techniques producing an image with details on function, namely: contrast-enhanced CT and MRI, optical imaging, single photon emission computed tomography (SPECT) and positron emission tomography (PET).[31] The second group is especially relevant in context with nanomaterials. AuNPs, for instance, can be used as CT contrast agents, but the low sensitivity does not allow accurate quantification.[32] IONPs

as part of MNPs are already used as MRI contrast agents, but the poor sensitivity and rather long acquisition time clearly limits this modality for tracking purposes.[30] Many classes of nanomaterials are used for optical imaging (QDs, UCNPs, AuNPs and CNTs), but the poor tissue penetration is the major limitation of this modality for noninvasive imaging.[31] SPECT and PET, on the other hand, are based on the detection of photons emitted by radionuclides. These highly sensitive modalities are not limited in tissue penetration and provide an accurate quantification of radionuclide uptake in live subjects.[33] However, SPECT and PET have different detector setups, originating from different decay modes. Radionuclides used for SPECT applications emit γ photons that are usually detected with two opposite and collimated γ cameras rotating around the patient.[34] PET radionuclides emit positrons, which travel a short distance (between 0.1-2 mm depending on the radionuclide) in tissue before they interact with electrons, resulting in annihilation.[34] Consequently, two γ photons (each 511 keV) per decay are emitted in an angle of 180° and detected in a ring array of detectors.[35] Based on the different detector setups, the sensitivity of SPECT is between one and two orders of magnitude less than PET, but the SPECT radionuclides are more readily available and have favorable decay times.[36] The most commenly used radioisotope in nuclear medicine is ^{99m}Tc, due to its ideal physical properties ($t_{1/2}$ = 6 h, E_γ = 140 keV), low cost and widespread availability from generators.[37] There are roughly twenty ^{99m}Tc radiopharmaceuticals in clinical use and each day approximately 50'000 procedures with ^{99m}Tc are performed in the US.[38] It is estimated that the demand for ^{99m}Tc increases at an annual rate of 3%-5% and the future challenge will be to ensure the production and supply of ^{99}Mo/^{99m}Tc-generators.[39] Besides ^{99m}Tc, PET isotopes (^{18}F, ^{64}Cu or ^{68}Ga) are increasingly available in Western countries and, therefore, radionuclides in general offer an excellent platform for the labeling of nanomaterials.[40] In pharmacokinetic and biodistributional analyses with SPECT and PET, important parameters such as circulation time in the blood pool, accumulation at the target site and clearance pathway can be perfectly assessed in a noninvasive fashion.[41] Due to this fact the radiolabeling of nanomedicines has drawn a lot of attention by several research groups in the last couple of years. In the next sections it is discussed how nanomaterials are radiolabeled and which strategies have been established so far, shown by means of examples. It is noteworthy that ^{99m}Tc labeled NPs have a longstanding history and the so-called ^{99m}Tc radiocolloids were first employed over 50 years ago for sentinel lymph node imaging.[42] These particles are composed of sulfur colloid or

human serum albumin and the most widely used nanomedicine for imaging applications.[43] However, the advances in nanotechnology for biomedical applications over the last years have revived this research field and open up new and enriching opportunities.

1.3.1 Extrinsic Radiolabeling – Conjugation of a Chelator to the Coating Ligands

The idea behind this approach is the covalent attachment of a chelator to the surface of the NP coating or on functional groups of polymeric NPs. The latter was shown by Line and co-workers in 2006, using *N*-(2-hydroxypropyl)methacrylamide (HPMA) as a co-polymer.[44] They derivatized the polymer backbone with the dipicolylamine (DPA) chelator for the $[^{99m}Tc(CO)_3]^+$ fragment and diethylenetriaminepentaacidic acid (DTPA) for ^{90}Y labeling. The co-polymer was further equipped with a peptide-based targeting function (RGD4C) for the $\alpha_v\beta_3$ integrin (overexpressed in the tumor neovasculature and various tumor types, such as osteosarcoma, neuroblastoma, glioblastoma, melanoma, lung carcinoma and breast cancer). This conjugate served as a diagnostic tool for tumor imaging (with ^{99m}Tc) and arrested tumor growth with its radiotherapeutic unit (^{90}Y). In 2007, Gambhir and co-workers radiolabeled CdSe/ZnS core-shell QDs with a terminal carboxyl-group or coated with PEG-NH_2 ($M_W \approx 2000$ Da).[45] In this pioneering work, they conjugated 1,4,7,10-tetraazacyclododecane-1,4,7,10-tetraacetic acid (DOTA) to QD-PEG-NH_2 or DOTA-lysine to QD-COOH *via* standard 1-ethyl-3-(3-dimethylaminopropyl)carbodiimide (EDC) / *N*-hydroxysuccinimide (NHS) coupling chemistry and labeled the QDs with $^{64}Cu^{II}$. *In vivo* studies revealed a rapid uptake by the liver and spleen, whereas PEGylated QDs exhibited slightly slower uptake into these organs. This example is also interesting due the combination of two imaging modalities (optical imaging and PET) and the concomitant synergistic effects.[46] The radiolabeling allows whole-body imaging to visualize the location of the tumor and the luminescence of the QDs can potentially be used to illuminate the exact tumor boarders during surgical excision of the tumor.[47] In a similar way as QDs, gold nanocages (AuNCs) coated with HS-PEG-NH_2 ($M_W \approx$ 5000 Da) were conjugated with DOTA-NHS-ester and labeled with $^{64}Cu^{II}$.[48] The study of Xia and co-workers focused on the evaluation of two different sized AuNCs (HDD of 96 nm and 64 nm). The small AuNCs demonstrated superior *in vivo* pharmacokinetics, higher tumor uptake and high retention in the blood pool, which is favorable for drug delivery applications with AuNCs. In 2013, Cai and co-workers published for the first time a radiolabeling procedure of mSiNPs (80 nm diameter), modified with thiol-groups on the surface.[33] They functionalized the surface with Mal-PEG-NH_2 (Mal = maleimide, $M_W \approx$ 5000 Da) and in a

second step *(S)*-2-(4-isothiocyanatobenzyl)-1,4,7-triazacyclononane-1,4,7-triacetic acid (*p*-SCN-Bn-NOTA) and SCM-PEG-Mal (SCM = succinimidyl carboxy methyl ester, $M_W \approx 5000$ Da) were coupled to mSiNP-S-Mal-PEG-NH_2 *via* amide bond formation. Finally, the modified antibody HS-TRC105 was conjugated to the Mal group on the outer coating surface and the mSiNPs were radiolabeled with $^{64}Cu^{II}$. Their study indicated the antibody to be the controlling factor for enhanced tumor uptake for this potential nanocarrier system, although quite high liver uptake was found. Penades and co-workers used the NOTA chelator for the radiolabeling of non-targeted and targeted glucose-coated AuNPs (2-3 nm core diameter) with $^{68}Ga^{III}$.[49] NOTA was attached on the NP surface through a linker and a thiolate anchor. The *in vivo* evaluation of the targeted AuNPs showed an increased capability to reach and bind to the natural targets as compared to the non-targeted AuNPs. In a recent study by Grimm and co-workers, the approach of chelator conjugation to the NP coating was extended to radiolabeling with $^{89}Zr^{II}$.[43] In their work, terminal amine-groups were introduced in Ferumoxytol (IONPs with a carboxymethyl dextran shell) *via* EDC-coupling of ethylenediamine. Subsequent conjugation of the $^{89}Zr^{II}$ chelator desferrioxamine (DFO) in its activated form (DFO-*p*-SCN) allowed labeling with the ^{89}Zr-oxalate precursor. Successful preclinical *in vivo* studies make $^{89}Zr^{II}$-labeled Ferumoxytol a promising dual-modality imaging agent for lymphatic drainage.

1.3.2 Extrinsic Radiolabeling – Anchoring of Preformed Complexes on the NP Surface

Another approach for the radiolabeling of NPs is based on bifunctional ligands, bearing a chelating moiety for the radionuclide and an anchoring group for the NP surface. In this two step procedure, the bifunctional ligand is initially labeled and then attached on the NP surface by either ligand exchange or diffusion through the existing coating to reach exposed gaps of the surface.[50] This strategy was first published in 2011 by Blower and co-workers for the development of PET-MRI dual-modality agents.[51] They synthesized a dithiocarbamatebisphosphonate ligand with a dithiolate moiety for $^{64}Cu^{II}$ chelation and a bisphosphonate anchor for the IONP surface. Two dithiolate units are coordinating to $^{64}Cu^{II}$ and the preformed complex was attached on the surface of Endorem, clinically applied IONPs (Figure 2A). NP labeling was achieved by heating a mixture of IONPs and $^{64}Cu^{II}$ complex at 100 °C for 15 min, assuming a loosening of the dextran coating at this temperature, which allows permeation of the complex to the surface. The same principle was adopted for a bifunctional ligand to label Endorem with the $[^{99m}Tc(CO)_3]^+$-core.[52]

Therefore, the dithiolate moiety was replaced with DPA and the preformed $^{99m}Tc^{I}$-DPA-alendronate was bound to the IONP surface under the same conditions as the $^{64}Cu^{II}$ analogue (Figure 2B). A drawback associated with Endorem is rapid clearance from the blood pool into the liver and spleen. To address this, Torres and co-workers coated IONPs (5.5 nm core diameter) with bisphosphonate-PEG-OCH_3 (M_W ≈ 5000 Da) to obtain a final HDD of 24 nm.[50] The radiolabeling with preformed $^{99m}Tc^{I}$-DPA-alendronate allowed them precise investigation of the pharmacokinetics. They observed a long blood half-life of 3 h and no sign of accumulation in the liver. This system has great potential to serve as a platform for the development of SPECT-MRI imaging agents. In general, the next generation after the SPECT-CT and PET-CT hybrid devices is the combination of PET or SPECT with MRI. Several benefits come along with this technology advancement: no additional radiation dose to the patients from the anatomic modality, higher soft tissue contrast and the possibility of simultaneous acquisition of the two modalities.[52] The only issue which has to be kept in mind is that SPECT and PET agents are used in extremely low concentrations, whereas MRI agents have to be administered in higher concentrations and, thereby, additional non-radioactive agent is needed for dual-modality imaging.

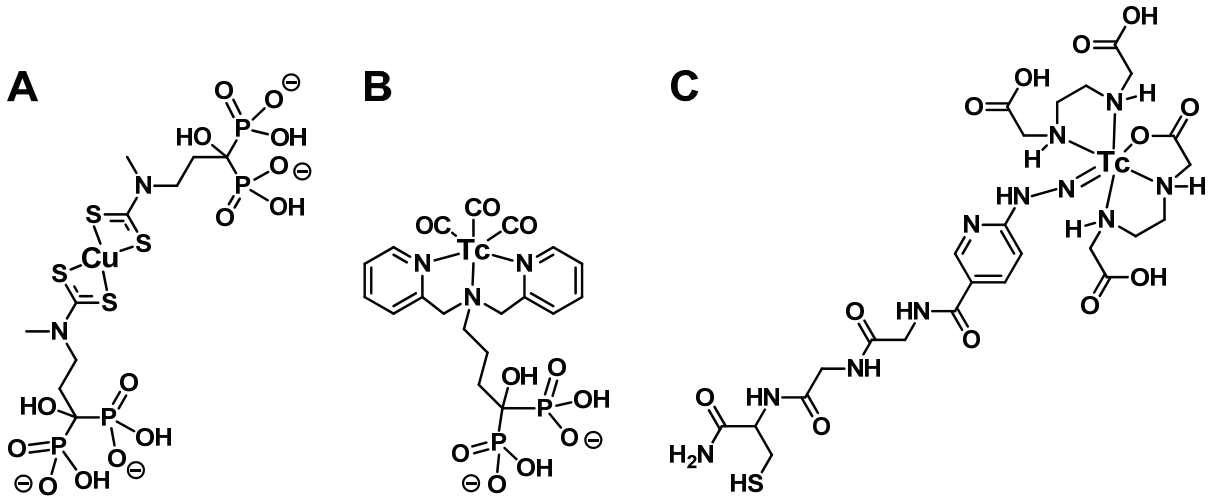

Figure 2. Bifunctional ligand systems labeled with (A) $^{64}Cu^{II}$ for the attachment on the surface of IONPs, (B) $^{99m}Tc^{I}$ for IONPs and (C) $^{99m}Tc^{V}$ for AuNPs.

Gómez-Oliván and co-workers synthesized the hydrazinonicotinamide (HYNIC) derivative HYNIC-Gly-Gly-Cys-NH_2 and they obtained the $^{99m}Tc^{V}$-complex upon addition of $[^{99m}TcO_4]^-$, $SnCl_2$, EDDA (N,N-ethylene diamine diacetic acid) and tricine (N-tris[hydroxymethyl]methylglycine) (Figure 2C).[53] The terminal L-cysteine served as an anchor for the surface of AuNPs (20 nm core diameter) and in addition to the radiolabel they

modified the gold surface with cyclo[Arg-Gly-Asp-D-Phe-Lys-(Cys)] as a targeting function for the $\alpha_v\beta_3$ integrin. The AuNP conjugate is a good example of a multimeric system and it showed up to 8% tumor uptake at 3 h after intraperitoneal administration.

1.3.3 Extrinsic Radiolabeling – Conjugation of Preformed Complexes to the NP Coating

Instead of binding the preformed complexes on the NP surface *via* an anchoring group, it is also possible to covalently conjugate preformed complexes to functional groups on the NP coating. This approach was decisively shaped by the work of Frangioni and co-workers.[54] They used preformed ^{99m}Tc-MAS$_3$-NHS (NHS activated *S*-acetylmercaptoacetyltriserine) and conjugated it to the L-cysteine coating of CdSe/ZnS QDs via amide bond formation (Figure 3A). Various QD sizes, ranging from 2.9 to 4.3 nm core diameter (resulting HDDs between 4.6 and 7.2 nm), were radiolabeled in this way and the excretion pathway was investigated. In this pathbreaking study an HDD threshold of 5.5 nm was determined for rapid and efficient urinary excretion. Nanostructures with HDDs larger than 5.5 nm are typically cleared from the body into the liver and spleen. With the same concept Frangioni and co-workers examined the effect of the PEG length on the clearance, using InAs/ZnS core-shell QDs (3.2 nm core diameter) coated with DHLA-PEG$_n$ (n = 2, 3, 4, 8, 14, 22).[55] They found that QDs coated with DHLA-PEG$_4$ were cleared most efficiently *via* the urinary pathway. Chen and co-workers labeled NHS-DOTA with ^{64}Cu^{II} and conjugated the radiolabel to the human serum albumin (HSA) coating of IONPs (Figure 3B).[56] Radiolabeled HSA-IONPs manifested a prolonged circulation time and high accumulation in lesions.

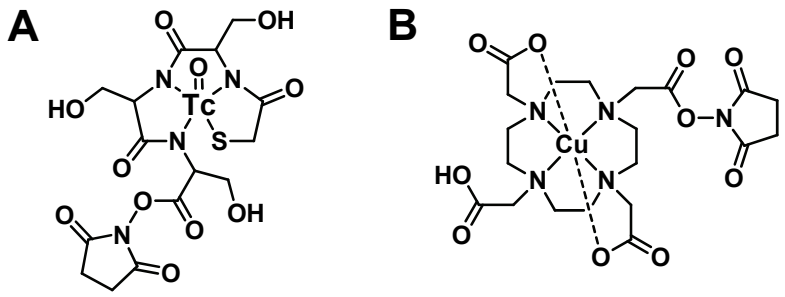

Figure 3. NHS-activated ligand systems labeled with (A) ^{99m}Tc^{V} for the conjugation to L-cysteine on the surface of QDs and (B) ^{64}Cu^{II} for the conjugation to HSA on the surface of IONPs.

1.3.4 Intrinsic Radiolabeling – General Idea

Although extrinsic NP radiolabeling and the concomitant use of chelators was shown by various research groups, the disadvantage of this approach is the chance of transmetallation

induced by proteins.[57] Consequently, radionuclide detachment from its ligand leads to uptake in non-targeted organs and, therefore, misinterpretation of reconstructed images and inaccurate pharmacokinetic information.[58] That is why high stability is an important criterion and in the focus of so-called intrinsic radiolabeling strategies, which do not require a chelator for the radionuclide. A detailed overview of this relatively young but rapidly growing research field is depicted in a recent review by Cai and co-workers.[59] The four different approaches for extrinsic radiolabeling are briefly described in the following sections by means of examples.

1.3.5 Intrinsic Radiolabeling – Hot-Plus-Cold Precursors

Some of the elements used for NP synthesis have radioactive isotopes which feature suitable decay characteristics for medical imaging and the isotopes can be produced with, for example, cyclotrons available in the clinical environment. A prominent material for NPs is gold and radioactive ^{198}Au ($t_{1/2}$ = 2.7 days; E_γ = 411 keV) fulfills the requirements for SPECT applications. Zheng and co-workers synthesized in one step NIR-emitting glutathione coated [^{198}Au]AuNPs *via* thermal reduction of non-radioactive ^{197}Au and radioactive ^{198}Au ions in the presence of glutathione as reducing agent.[60] The obtained radioactive NPs were renally cleared due to their small size (3 nm core diameter) and exhibited preferable *in vivo* kinetics. By using a mixture of ^{197}Au and ^{198}Au, Xia and co-workers synthesized radioluminescent Au nanocages.[61] They reported for the first time Cerenkov luminescence of the ^{198}Au isotope, which is light emitted during the decay of the radionuclide. The ^{198}Au nanocages showed high accumulation in tumor and serve as a potential platform for dual-modality imaging with SPECT and optical imaging. In another study Liu and co-workers alloyed ^{64}Cu directly into the lattice of the nanostructure to obtain ^{64}CuAuNPs, starting from $HAuCl_4$, non-radioactive [$Cu(acac)_2$] and $^{64}CuCl_2$.[58] The radioactive NPs were further modified with HS-PEG-OCH_3 to improve the *in vivo* blood circulation, which was mirrored in a long blood retention time after administration and passive tumor targeting.

1.3.6 Intrinsic Radiolabeling – Specific Trapping

Alternatively, radionuclides can specifically be trapped on the surface of certain NPs, presumably IONPs. This strategy strikes by its simplicity and avoids challenging, multi-step and nuclide-specific chelation. Mareque-Rivas and co-workers, for example, demonstrated that the *fac*-$[M(CO)_3]^+$-core (M = ^{99m}Tc, Re) interacts with the hydroxyl-groups at the IONP

surface.[62] This ligand-like behavior of the NP surface was taken advantage of for the radiolabeling of iron oxide filled micelles for potential dual-modality imaging applications. These radiolabeled micelles were further modified with a fluorescence label (rhodamine), loaded with dsRNA and used as a theranostic platform to target lymph nodes and strongly activated cells of the immune system.[63] High affinity to the *fac*-$[^{99m}Tc(CO)_3]^+$-core was also observed on the ZnS surface as part of CdSe/ZnS core-shell QDs.[47] Analogously to the work with IONPs, Mareque-Rivas and co-workers formed radiolabeled QD-filled PEG-micelles, loaded with a Pt^{IV} prodrug that was activated upon light emission of the QDs. In another example IONPs coated with poly(acrylic acid) were radiolabeled with a mixture of $[H_2{*}AsO_4]^{1-}$ and $[H{*}AsO_4]^{2-}$ (*As includes the four positron emitting 70/71/72/74 As and the three electron emitting 74/76/77 As radioisotopes).[64] The As^VO_4 fragment occupies vacant FeO_4 tetrahedral sites on the octahedrally terminated surface of IONPs, leading to highly stable NPs for dual-modal PET/MRI applications. Using the same type of poly(acrylic acid) coated IONPs, Cai and co-workers labeled the surface with ^{69}Ge ions ($t_{1/2}$ = 1.6 days; positron emitter) since Ge has a strong binding affinity to metal oxides.[65] Although radiolabeled NPs showed mainly uptake in the liver, this is the first example for successful utilization of a ^{69}Ge-based agent for PET/MRI imaging. In a recent work by Holland and co-workers, various radioisotopes ($^{64}Cu^{II}$, $^{111}In^{III}$ and $^{89}Zr^{IV}$) were bound on the IONP surface in a heat-induced procedure.[66] With their technique clinically applied Feraheme was labeled in high yields and they showed in mice models the ability of the tracers to detect tissues enriched with activated macrophages. Chelator-free labeling was also achieved by integration of ^{64}Cu onto as-prepared gold nanomaterials (spheres, rods and hexapods), stabilized with PEG. In the study by Chen and co-workers, $^{64}Cu^{II}$ was reduced with hydrazine and grown on the nanomaterial surface.[67] Further derivatization with an RGD peptide yielded in high tumor targeting ability and successful photothermal therapy of cancerous tissue.

1.3.7 Intrinsic Radiolabeling – Cation Exchange

Cation exchange between $^{64}Cu^{II}$ and the original cations of CdSe/ZnS QDs was reported in a profound study by Chen and co-workers.[68] With their results they showed that $^{64}Cu^{II}$ could replace Zn^{II} of the QD shell. When tuning the reaction conditions, $^{64}Cu^{II}$ diffuses even inside the core to replace Cd^{II} cations. Due to Cerenkov luminescence of ^{64}Cu, the emitted blue light induces a self-illuminating property of QDs which allows *in vivo* optical imaging. Unlike other luminescence probes for imaging, external light is not required to illuminate QDs and

eliminates the usual strong background autofluorescence of biomolecules.[69] The synergistic effects of radionuclide doping inside QDs make this agent a promising candidate for dual-modal imaging.

1.3.8 Intrinsic Radiolabeling – Proton Beam Activation

The last approach for intrinsic radiolabeling is the harshest and most difficult to achieve. Llop and co-workers presented two strategies for proton beam activation, suitable for metal oxide NPs.[70] They synthesized ^{18}O enriched aluminum oxide NPs and irradiated them with protons to yield ^{18}F labeled NPs *via* the $^{18}O(p,n)^{18}F$ nuclear reaction. However, this method is time consuming and extremely costly because ^{18}O is utilized. For this reason they directly irradiated aluminum oxide NPs with a 16 MeV proton beam to obtain ^{13}N labeled NPs *via* the $^{16}O(p,\alpha)^{13}N$ nuclear reaction. Although this activation can be applied to any metal oxide containing NP, the resulting PET nuclide ^{13}N has a short half-life of only 10 min.

1.4 Nanomaterial Characteristics and the Impact on the *In Vivo* Behavior

For successful translation of nanomedicines into clinical applications, a number of requirements have to be fulfilled, including targeting capability (active or passive), reasonable blood circulation time, minimal off-target, metabolism to clearable components, effective clearance from the human body and minimal toxicity.[31] These different parameters can be mediated by the interplay of the size, shape and surface coating of nanomaterials.[71] The following sections highlight the most important findings over the last years in order to correlate the properties of nanomaterials with their concomitant physiological behavior.

1.4.1 Size and Shape of Nanomaterials

After administering nanomaterials to living subjects, their biological fate is mainly determined by the mononuclear phagocyte system (MPS) and the renal system.[1] The MPS system consists of organs that are rich in phagocytic cells (macrophages, Kupffer cells and monocytes), such as liver, spleen and bone marrow.[72] Its mechanisms are generally coming into play with NPs having an HDD larger than 10 nm.[73] Various studies have shown that particles with an HDD in the range of 10 to 20 nm are rapidly taken up by the liver and large NPs (HDD >200 nm) are filtered in the spleen.[74] NPs smaller than 6 nm are filtered out by the glomular filtration system in the kidneys and, therefore, renally cleared.[54] NPs with an HDD

between 6 and 8 nm are cleared less efficiently by the renal system and NPs larger than 8 nm are not subjected to glomular filtration anymore.[75] However, at this point it is important to mention that the combination of the size and surface coating dictates how rapidly nanomaterials are removed from the blood circulation and cleared *via* the two different systems. As described in section 1.4.2, surface engineering enables to endow NPs with so-called "stealth"-properties that prolong the blood circulation time substantially.

The size of nanomaterials is not only decisive for the clearance pathway, but also for tumor uptake. It is well known that the tumor vasculature has leaky walls as a result of tumor angiogenesis.[30] Throughout angiogenesis, the endothelial cells undergo rapid proliferation, leading to reduced density and discontinuous arrangement of the endothelium.[76] As a consequence, tumor vessels lack of tight junctions and this effect is referred to as the "enhanced permeability and retention (EPR)" effect. This allows NPs with HDD sizes between 30 and 200 nm to accumulate passively in the tumor lesion.[77] Because of this effect, it has been evidenced that macromolecular drugs and NPs are able to target tumors more efficiently than small molecule drugs.[78] Nevertheless, it has to be kept in mind that tumor angiogenesis is a disorganized and inhomogeneous process in a solid tumor and enhanced permeability might not always be given. Therefore, it is still favorable to equip NP with a targeting function to combine synergistically the benefits from active and passive targeting.

Most of the nanomaterials used for biomedical applications have a spherical shape, which is beneficial in context with circulation properties. Ferrari and co-workers demonstrated that spherical NPs show a laminar flow pattern, facilitating the extravasation into tumor tissue.[79] Rod- and bar-shaped NPs, on the other hand, have the tendency to fail a laminar flow pattern in the blood stream, resulting in reduced tumor accumulation. Moreover, the shape of NPs has a crucial impact on the cellular uptake profile. In a study by Lehr and co-workers distinct uptake mechanisms were inhibited to investigate the influence on the shape-specific NP uptake.[80] They concluded that spherical NPs undergo a clathrin-mediated uptake, whereas cylindrical and worm-like NPs follow a macropinocytotic uptake pathway.

1.4.2 Surface Coating

The surface characteristics of the NP coating are, besides the overall NP size, a determining factor for the interactions in biological milieu and, therefore, the biological fate. A very important factor is the overall surface charge of a nanomaterial, expressed as the Zeta

potential (ζ-Pot.). It has been shown that positive surface charges exhibit high systemic toxicity, inducing complications like hemolysis and platelet aggregation.[81] This is primarily due to the fact that the cationic surfaces of NPs strongly interact with the negatively charged phospholipid functionalities on cell membranes which cause disruption of the plasma membrane.[75] In addition, positively charged NPs have a high nonspecific internalization rate and a very short blood circulation half-life.[82] This was also observed by Jallet and co-workers when they compared the pharmacokinetics of IONPs with a positive (ζ-Pot. of +20 mV), negative (-30 mV) and neutral surface charge.[83] Neutral and negatively charged IONPs showed a prolonged circulation half-life and significant higher liver uptake as compared to positively charged IONPs. Although negatively charged NPs have reduced nonspecific adsorption on biomolecules and accordingly a longer blood circulation time than positively charged NPs, neutral NPs have the longest circulation half-life. For both diagnostic and therapeutic applications a reasonable circulation half-life is necessary in order to allow nanomaterials to pass by a lesion several times, increasing the chance of accumulation in clinically relevant concentrations. Neutral surface charge can be achieved by coating NPs with PEG or zwitterionic ligands (see section 1.2). The two ligand systems have the same mechanism of action, binding a large number of water molecules through electrostatic interactions and hydrogen bonding.[84] The additional water shell around the NPs provides the aforementioned "stealth"-property and prevents efficiently the adsorption of serum proteins, known as opsonization.[85] The avoidance of opsonization is absolutely crucial, because otherwise the HDD of NPs increases dramatically and the NPs are recognized by the phagocytic cells of the MPS. PEG is the most widely used polymer for minimizing opsonization and PEG coating (> $M_W \approx 2000$ Da) increases the circulation time by a factor of 2-10.[30,86] However, PEG on the surface of NPs has a large effect on the HDD and it might induce undesirable immune responses.[87] That is why zwitterions became an attractive alternative to the use of PEG due to the strong interaction with water and, associated therewith, the anti-fouling properties.[88] Rotello and co-workers compared the anti-fouling properties of PEG and zwitterionic coatings (carboxybetaines and sulfobetaines).[89] They found that zwitterionic coating exhibits lower adsorption of plasma proteins and lower non-specific cellular uptake in comparison to PEG coating. The question with zwitterionic coating ligands is, whether the negative or the positive charge should be exposed on the outermost layer of the NP conjugates. The answer to this question was provided by Bawendi and co-

workers in experiments with InAs/CdZnS core-shell QDs.[90] They observed non-specific adsorption of proteins in case the positive charges are located on the outermost layer, for both *in vitro* and *in vivo* experiments. QDs exposing negative charges, on the other hand, are far less susceptible to interactions with proteins.

Nevertheless, the two types of coating have their own advantages and this was impressively demonstrated by Zheng and co-workers.[91] They synthesized zwitterionic NIR-emitting AuNPs coated with glutathione (2.5 nm core diameter, 3.3 nm HDD) and neutral NIR-emitting AuNPs coated with PEG (2.3 nm core diameter, 5.5 nm HDD). The results revealed an enhancement of the EPR effect upon PEGylation relative to zwitterionization, as a consequence of an increased retention time and concentration in the blood. Based on the insights, they suggested PEG-AuNPs to be more suitable for cancer therapy due to their high passive targeting efficiency and long tumor retention. In their opinion, glutathione-AuNPs have more potential for use in cancer diagnosis because of their short circulation time and rapid renal clearance from normal tissue.

1.4.3 Toxicity

Nanomaterials can be classified as biodegradable and non-biodegradable.[75] If metabolism into clearable components is not possible, it must be guaranteed that the materials show a safe behavior after administration. The research activities in this context are part of nanotoxicology, a field that has emerged along with the initiation of nanomedicine.[4] There is still little understanding of the long-term effects on living organisms and the exact toxicological properties.[92] It is known that intracellular and *in vivo* toxicity of IONPs is related to the generation of excess reactive oxygen species (ROS), leading to oxidative stress, DNA damage, inflammation and injury to the immune system.[93] The chemical activity of AuNPs inside a living organism is the gold-catalyzed NO formation in blood plasma.[94] However, the overall toxicity is very complex and depends on numerous factors such as the administered dose, chemical composition, size, structure, solubility, surface chemistry, route of administration, biodegradability, pharmacokinetics and biodistribution.[95] These factors have to be understood and exploited extensively to make the nanomaterial's way to clinical applications.

2. Results & Discussion

2.1 The Development of a Novel ^{99m}Tc Labeling Strategy of NPs – Ligand Synthesis and Preliminary Experiments

The main goal of this thesis was to establish a method for facile radiolabeling of NPs with the $[^{99m}Tc(OH_2)_3(CO)_3]^+$ precursor. We have found the inspiration for a potential strategy in a study by Frangioni and co-workers, one of the most cited publications in the field of nanomaterials for biomedical applications.[54] As described in section 1.3.3, they radiolabeled L-cysteine coated CdSe/ZnS QDs with preformed ^{99m}Tc-MAS$_3$-NHS and conjugated the activated complex to the QD surface (Figure 4A). Although their technique worked well in reasonable radiochemical yields (RCYs), there are some limitations associated with this method: ^{99m}Tc-MAS$_3$-NHS has to be synthesized in an aprotic solvent (e.g. DMSO) since the NHS-ester is prone to undergo ester hydrolysis in protic solvents. Thus, ^{99m}Tc-MAS$_3$ was synthesized in aqueous solution, starting from $[^{99m}TcO_4]^-$ in saline (from the ^{99}Mo generator eluate), MAS$_3$ and stannous(II) chloride dihydrate. ^{99m}Tc-MAS$_3$ was isolated with an Oasis HLB cartridge and eluted with dry DMSO for the coupling with NHS, using *N,N,N',N'*-tetramethyl-*O*-(*N*-succinimidyl)uronium tetrafluoroborate (TSTU) and *N,N*-diisopropylethylamine (DIEA).[96] After purification, ^{99m}Tc-MAS$_3$-NHS was finally conjugated to the amine functionalities on the QD surface. Taking into account the different synthetic and purification steps, this technique is rather complicated from a radiochemical point of view. Therefore, we aimed at designing a bifunctional coating ligand for QDs, which allows direct radiolabeling with $[^{99m}Tc(OH_2)_3(CO)_3]^+$ in one and last step.

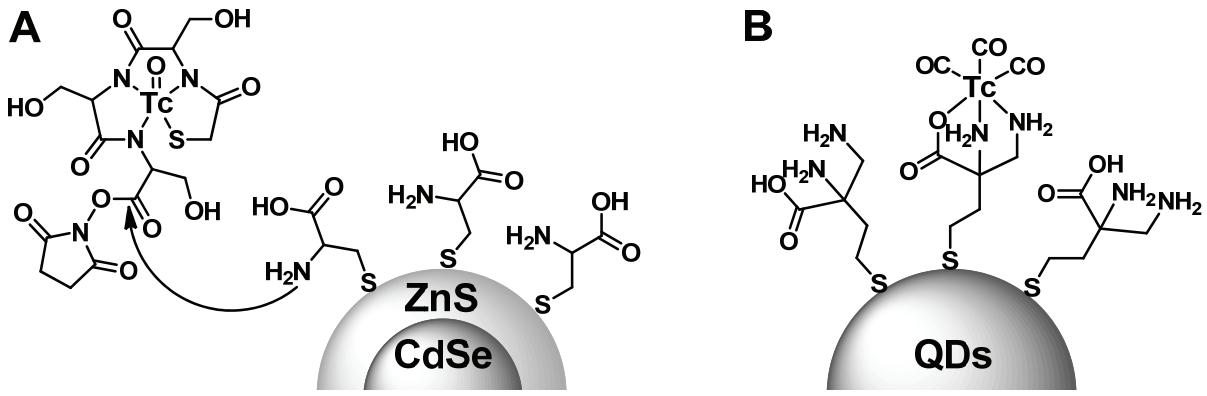

Figure 4. (A) Schematic illustration of the technique developed by Frangioni and co-workers to radiolabel L-cysteine coated QDs with activated ^{99m}Tc-MAS$_3$-NHS; (B) Our approach to radiolabel QDs, functionalized with the bifunctional coating ligand HS-CH$_2$-CH$_2$-DAP, directly in one step with $[^{99m}Tc(OH_2)_3(CO)_3]^+$ (the stereochemistry is omitted for simplicity).

The idea was to synthesize a ligand system that has certain similarity to L-cysteine, comprising a thiol-group as an achor for the NP surface, a short linker and a hydrophilic chelator at the outermost layer of the organic coating (Figure 4B). 2,3-Diaminopropionic acid (DAP) seemed to be predestined, because of its small size, hydrophilicity and high potency to coordinate the $[^{99m}Tc(CO)_3]^+$ fragment.[97] The approach to synthesize the bifunctional coating ligand HS-CH_2-CH_2-DAP is described in the next section.

2.1.1 The Synthesis of HS-CH_2-CH_2-DAP

The precursor for the DAP chelator is racemic ethyl 2-*N*-(*tert*-butoxycarbonyl)-3-nitriloalaninate **3**, which was synthesized according to a literature procedure in three steps starting from ethyl cyanoacetate.[98] The oxime **1** was prepared *via* nitrosation in aqueous acetic acid and the addition of sodium nitrite.[99] After reduction to the amine with sodium dithionite under basic conditions, the tosylate salt **2** was directly formed.[100] Protection with $(Boc)_2O$ was achieved with DIEA in refluxing toluene to give **3** as a racemate (Scheme 1).[101]

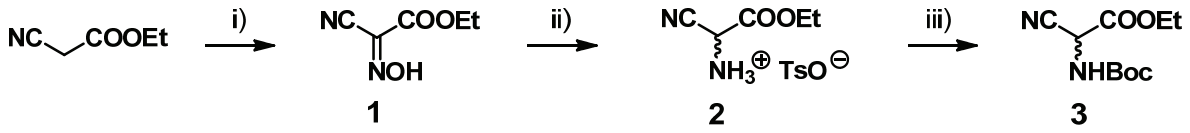

Scheme 1. Synthesis of the DAP precursor ethyl 2-*N*-(*tert*-butoxycarbonyl)-3-nitriloalaninate **3**. i) HOAc (45%), $NaNO_2$, r.t., 5 h, 97%; ii) a) $NaHCO_3$, $Na_2S_2O_4$, H_2O, r.t., 1 h, 67%; b) HOTs, Et_2O, EtOH, r.t., 37%; iii) $(Boc)_2O$, toluene, *i*-Pr_2NEt, reflux, 6 h, 70%.

The DAP precursor **3** can be derivatized at its α-carbon position, for instance by deprotonation with KO^tBu and alkylation with a primary halide.[97] In a first attempt we chose {[(2-iodoethyl)sulfanyl]methyl}benzene **5** as a primary halide, bearing a benzyl protected thiol group and iodine as a leaving group for the S_N2 displacement reaction. Accordingly, compound **5** was synthesized by alkylation of phenylmethanethiol with 1,2-dibromoethane and in a second step the bromine was converted into an iodine *via* a Finkelstein reaction (Scheme 2).[102]

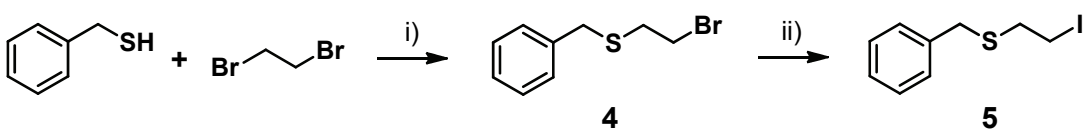

Scheme 2. Synthesis of {[(2-iodoethyl)sulfanyl]methyl}benzene **5**. i) KO^tBu, EtOH, r.t., 13 h, 77%; ii) NaI, acetone, r.t., 14 h, 90%.

The alkylation of deprotonated **3** with the primary halide **5** gave compound **6** in 50% yield. It has previously been shown in our laboratory that the reduction of the nitrile to the amine can be accomplished with $NaBH_4$ in combination with catalytic amounts of $NiCl_2$.[97] In this reaction, the Ni^{II} metal cation coordinates to the nitrile and activates it for an efficient and exclusive reduction to the amine.[103] Combined with *in situ* Boc-protection, the DAP derivative **7** was synthesized in 82% yield. Compound **8** was obtained in 53% yield by basic ester hydrolysis of the ethyl ester and subsequent deprotectoin of the Boc-groups under acidic conditions. There are several methods to cleave the benzyl protecting group of the thioether **7**, but most of them are rather harsh and involve alkali metals in liquid ammonia, hydrofluoric acid or electrolysis.[104] Therefore we applied a method reported by Fujii and co-workers, using trifluoroacetic acid (TFA) solutions of Ph_2SO and $MeSiCl_3$.[105] Although the disulfide **9** is formed in this cleavage reaction, it is quick and the reagents are easier to handle compared to the reagents needed for the other methods.

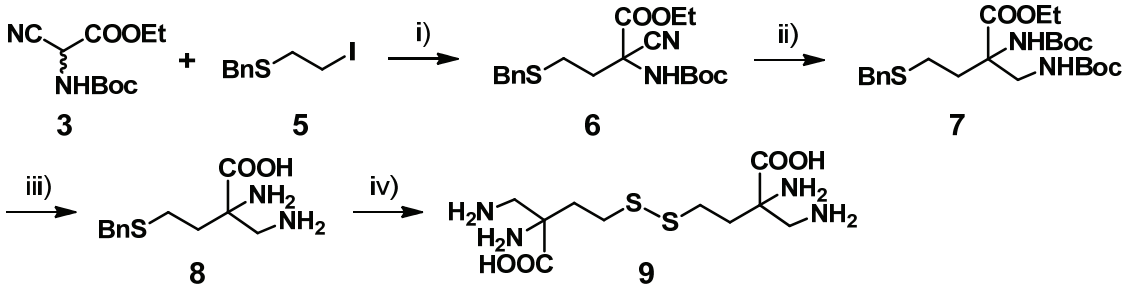

Scheme 3. Synthesis of 4,4'-disulfanediylbis[2-amino-2-(aminomethyl)butanoic acid] **9**. i) KO^tBu, HO^tBu, 80 °C, 14 h, 50%; ii) $NiCl_2 \cdot 6\ H_2O$, $NaBH_4$, $(Boc)_2O$, MeOH, 20 °C, 16 h, 82%; iii) a) 1 M NaOH, MeOH, 80 °C, 12 h; b) 1 M HCl, MeOH, 80 °C, 8 h, 53%; iv) 0.4 M Ph_2SO, 1 M $MeSiCl_3$, TFA, 0 °C, 4 h, 53%.

A commonly used thiol-protecting group is triphenylmethyl and we exploited in a set of synthetic routes its applicability to obtain the target molecule **9** in its reduced form (thiol instead of a disulfide). Triphenylmethanethiol, a well-known building block in organic synthesis for the introduction of a protected thiol, was particularly suited for this approach. Firstly, we synthesized compound **14**, bearing a primary bromide for an S_N2 reaction with deprotonated triphenylmethanethiol and the protected DAP chelator. The starting point of this five step reaction is commercially available 2-(benzyloxy)ethanol and its terminal hydroxyl group was converted into a bromide by performing an Appel reaction.[106] The tertiary carbon of **3** was deprotonated with *in situ* generated NaOEt and alkylated with **10**. In analogy to the above described reaction, the nitrile was reduced to the Boc-protected

amine. After deprotection of the benzyl group in **12** with 10% Pd/C and H_2, the resulting hydroxyl group was converted into a bromide to obtain compound **14** (Scheme 4). However, the desired insertion of deprotonated triphenylmethanethiol into **14** was not successful (Scheme 5). We believe that the nucleophilic attack does not occur because both the nucleophile and the electrophile **14** are sterically too hindered. Once the spatial distance between the leaving group (bromide) and the protected DAP chelator is increased, for instance with additional ethylene glycol units, the reaction takes place in high yields (see section 2.2.1). In another experiment we attempted to couple derivatized triphenylmethanethiol **15** with deprotonated **3** (Scheme 5). Like the previously discussed reaction, the product was not formed due to sterical reasons.

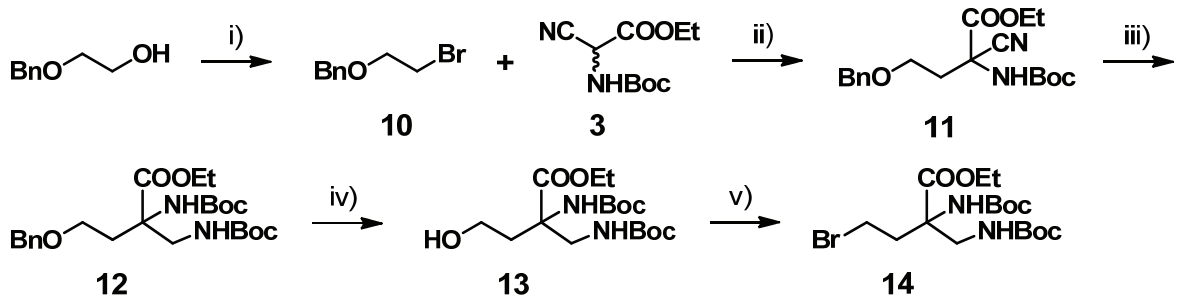

Scheme 4. Synthesis of ethyl 4-bromo-*N*-(*tert*-butoxycarbonyl)-2'-[(*tert*-butoxycarbonyl)amino]-isovalinate **14**. i) CBr_4, PPh_3, CH_2Cl_2, 0-20 °C, 5 h, 75%; ii) Na, EtOH, reflux, overnight, 42%; iii) $NiCl_2 \cdot 6 H_2O$, $NaBH_4$, $(Boc)_2O$, MeOH, 20 °C, 14 h, 78%; iv) H_2 (1 atm), 10% Pd/C, MeOH, 20 °C, overnight, 83%; v) CBr_4, PPh_3, CH_2Cl_2, 0-20 °C, 5 h, 75%.

Finally, we investigated the reaction of two equivalents of deprotonated **3** and the terminal halide containing disulfide **17**. Product formation was only observed in trace amounts, assuming that the nucleophile **3** cleaves the disulfide instead of attacking the electrophile.[107]

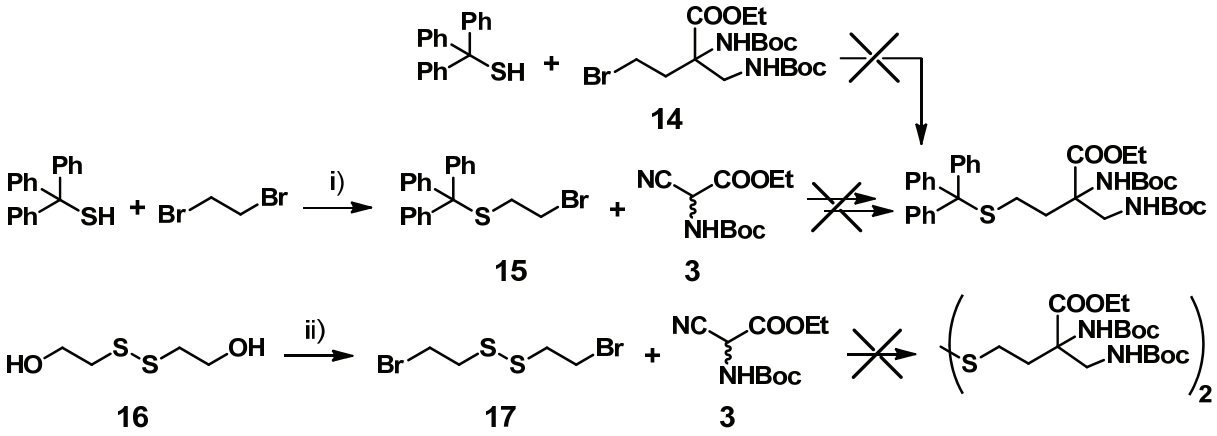

Scheme 5. Attempts to synthesize the DAP derivative with a triphenylmethane-protected thiol group. i) KO^tBu, MeOH, r.t., 13 h, 70%; ii) HBr (48%), conc. H_2SO_4, 0-80 °C, 24 h, 37%.[108]

The investigation of different synthetic pathways to obtain the bifunctional ligand HS-CH_2-CH_2-DAP led to the conclusion that triphenylmethane is not feasible as a thiol protecting group due to its bulky nature. A successful way to synthesize the target molecule **9** involves benzyl protection of the thiol, even though deprotection results in the disulfide.

2.1.2 Functionalization of CdTe/ZnTe QDs with HS-CH_2-CH_2-DAP and ^{99m}Tc Labeling

In 2009 Prasad and co-workers reported a novel procedure for the aqueous-phase synthesis of highly luminescent CdTe/ZnTe core-shell QDs.[109] In their approach, a reduced Te species was generated upon mixing sodium borohydride with tellurium powder in water. The Te solution was injected into a basic solution containing L-cysteine, Cd^{II} and Zn^{II} precursors. The emission maximum of the QDs was easily tuned by varying the reflux time. This elegant synthesis drew our attention and our first idea was to use HS-CH_2-CH_2-DAP in place of L-cysteine to synthesize CdTe/ZnTe QDs. Based on the fact that we obtained HS-CH_2-CH_2-DAP as the disulfide **9**, we first reproduced Prasad's synthesis with L-cystine, the oxidized form of L-cysteine. Therefore, L-cystine was reduced in a separate flask and added to the Cd^{II}/Zn^{II} precursor solution shortly before the addition of the Te solution. The synthesized QDs showed a core diameter of 2.90 ± 0.70 nm, the first excitonic peak at 550 nm and the emission maximum at 572 nm (Figure 5). The relative quantum yield (QY) was calculated to be 46%, using Rhodamine 6G as a reference.

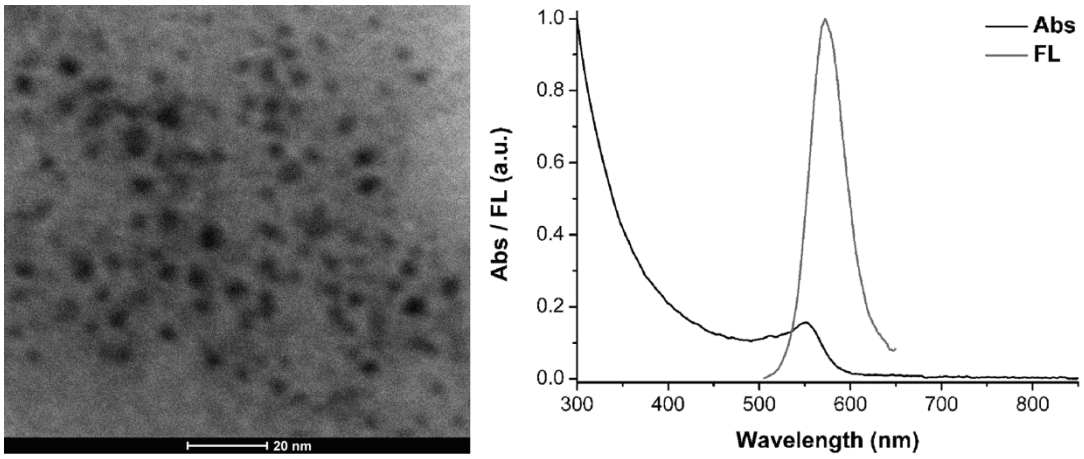

Figure 5. Representative TEM micrograph of CdTe/ZnTe core-shell QDs with a core diameter of 2.90 ± 0.70 nm (left) and normalized fluorescence (grey line) and UV/Vis absorption (black line) spectra in water (right).

In a control experiment L-cystine was added without sodium borohydride reduction and as a consequence the reaction mixture became completely black, lacking the formation of QDs.

Given that it was possible to synthesize QDs with *in situ* reduced L-cystine in an analogoues manner as reported in the literature, we concluded that the applied reaction conditions allow cleavage of the disulfide bond. Therefore, L-cystine was replaced with the disulfide **9** and the synthesis was carried out in the same way as described above. However, we did not evidence the formation of QDs, even after prolonged reaction times and increased reducing agent concentration to cleave the disulfide. Our hypothesis is that DAP chelates the Cd^{II} cations and thus Cd^{II} is no longer available for the QD core synthesis, resulting in the absence of emission upon excitation with UV light. ESI-MS measurements of the reaction mixture provided indications for Cd^{II}-chelation by the DAP ligand, but the spectra were not fully conclusive. Further investigations have not been undertaken since the synthesis of QDs did not work at all. The second approach to functionalize CdTe/ZnTe QDs with HS-CH_2-CH_2-DAP was based on an exchange of the existing L-cysteine coating with *in situ* reduced **9**. For this attempt, QDs were mixed with SH-CH_2-CH_2-DAP and purified to remove excess bifunctional coating ligand. According to the integrals of the NMR signals 50% of the surface is coated with HS-CH_2-CH_2-DAP and the other half is coated with L-cysteine. The analysis of the derivatized QDs did not reveal significant changes in the absorption and emission spectra, but the QY dropped from 46% to 22%. A possible explanation for this drop might be an increased interaction of the QD surface with the polar media, because HS-CH_2-CH_2-DAP is bulkier than L-cysteine and hence the overall coating density lower as compared to the native QDs.[110] Nevertheless, the functionalized QDs were applied in experiments with $[^{99m}Tc(OH_2)_3(CO)_3]^+$ to have a proof of concept for the aspired direct radiolabeling strategy. In a typical experiment an aqueous solution of $[^{99m}Tc(OH_2)_3(CO)_3]^+$ (0.5 ml, pH 7-8) was added to derivatized QDs in water (0.5 ml) to obtain a final QD concentration of 1 mg/ml. The labeling progress was monitored by high performance liquid chromatography (HPLC), equipped with a size-exclusion column and two detectors (UV-Vis and γ-counter). We chose phosphate buffered saline (PBS) pH 6.7, supplemented with 1 mM L-cysteine, as the mobile phase, analogously to Frangioni and co-workers.[54] Best labeling yields for derivatized QDs were achieved at 45 °C after 60 min (69%), although not quantitatively due to highly dilute chelator concentrations (see calculations in section 2.2.3). Besides the product peak at 11.30 min retention time, we also observed $[^{99m}Tc(OH_2)_3(CO)_3]^+$ as a double peak (Figure 6A). The reason for the double peak appearance is most likely the L-cysteine in the mobile phase, yielding L-cysteine complexes with the $[^{99m}Tc(CO)_3]^+$ fragment. The radiolabeled QDs were

isolated upon multiple precipitations with ethanol, centrifugation, removal of the supernatant and redispersion in 0.9% saline solution (Figure 6B). The chemical stability of the purified QDs was checked after 12 h at 37 °C under normal atmosphere and HPLC analysis did not reveal the formation of additional ^{99m}Tc species, underscoring the high stability of the radiolabeled QDs (Figure 6C). In a control experiment we incubated underivatized QDs (coated only with L-cysteine) with $[^{99m}Tc(OH_2)_3(CO)_3]^+$ at 45 °C for 60 min. The HPLC analysis showed a small peak at 11.30 min (7%), presumably due to non-specific binding of the $[^{99m}Tc(CO)_3]^+$-core to the L-cysteine coating. However, this peak disappeared in the HPLC trace of the gamma detector after QD isolation, corroborating the non-specific interaction of the L-cysteine coated QDs as compared to the chelation in case of the derivatized QDs.

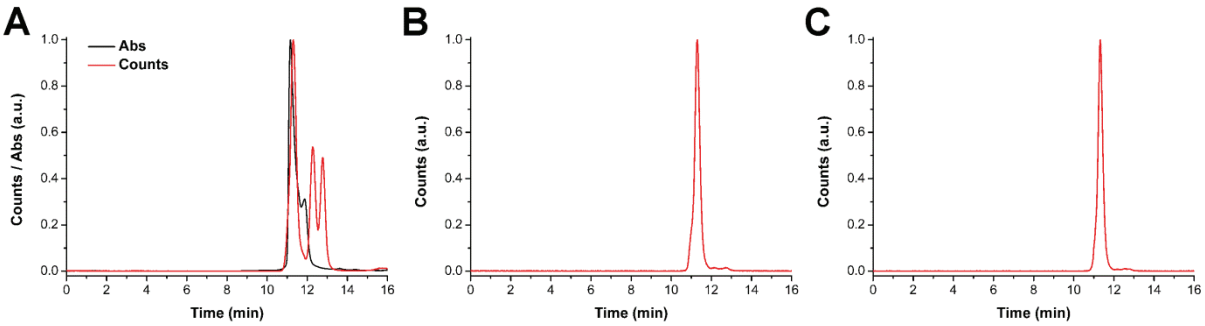

Figure 6. Normalized HPLC traces of (A) radiolabeled CdTe/ZnTe QDs after 60 min at 45 °C, (B) purified and radiolabeled CdTe/ZnTe QDs and (C) purified CdTe/ZnTe QDs after 12 h under normal atmosphere. Please note that the difference of 0.1 min between the absorbance and γ-counts is due to the detector setup in which the γ-detector is located after the UV-detector.

With this set of experiment we showed the feasibility of direct NP radiolabeling with the $[^{99m}Tc(OH_2)_3(CO)_3]^+$ precursor *via* coating NPs with a novel type of a bifunctional ligand system. In the next sections, the focus lies on optimization of this ligand system, the application for various NP types and the introduction of targeting functions to obtain site-specificity.

2.2 ^{99m}Tc Radiolabeling and Biological Evaluation of Targeted Nanoparticles Functionalized with a Versatile Coating Ligand

One of the outstanding characteristic of NPs is the large surface area to volume ratio, which enables the addition of a large payload of functional groups and targeting components on a relatively small volume of material.[111] In order to study noninvasively the effects of the coating and the targeting capability, NPs are radiolabeled for SPECT or PET investigations. As described in detail in section 1.3, radiolabeling of NPs follows essentially two strategies; an "extrinsic" one in which potent, NP surface bound chelators such as DOTA or NOTA, are directly labeled with ^{64}Cu or ^{68}Ga,[33,45,46,48,49,112-114] or direct NP labeling with complexes of preformed bifunctional chelators and their subsequent coating on the NP surface.[50,51,53,54,115] In the "intrinsic" approach, the radiolabel is an integral part of the NP and no chelators are required.[59] All the ^{99m}Tc NP radiolabeling procedures reported so far require preformation of a ^{99m}Tc complex which is, in a second step, combined with NPs *via* covalent bonds or ligand exchange reactions (see section 1.3). For NP drug finding and development, it would be much more convenient to label a biovector bearing NP after its full constitution with a building block which does not need to be adapted to the chelator or the receptor binding ligand. Following this strategy, we synthesized similarly to HS-CH_3-CH_3-DAP a coating ligand for CdSe/ZnS core-shell QDs and AuNPs which allows a direct labeling with the $[^{99m}Tc(OH_2)_3(CO)_3]^+$ precursor in one and last step. This ligand comprises functional groups which can covalently be bound to any biological vector while underivatized ligands maintain their coordinating properties. Specifically, this ligand contains a thiol group as an anchor for the NP surface, a PEG linker and the DAP chelator for the $[^{99m}Tc(CO)_3]^+$ fragment. In addition, a small molecule inhibitor for the prostate specific membrane antigen (PSMA) was conjugated to the coating ligand for introducing a targeting function for prostate cancer. After functionalization and radiolabeling of the NPs, the *in vitro* stability and cellular uptake was examined. Moreover, imaging with small animal microSPECT and *ex vivo* biodistribution studies in nude NMRI mice harboring LNCaP xenografts were carried out.

2.2.1 Synthesis of the Coating Ligands

As already mentioned, DAP is a small, hydrophilic and very strong chelator for the $[^{99m}Tc(CO)_3]^+$ fragment, efficiently preventing trans-metallation in biological milieu which may lead to potential misinterpretation of microSPECT images and biodistribution data.

Derivatization at the α-carbon position allows the introduction of further functionalities such as linkers to NP surfaces. For conjugation to a PEG linker, two precursors are required; ethyl 2-*N*-(*tert*-butoxycarbonyl)-3-nitriloalaninate **3** and 13-bromo-1-phenyl-2,5,8,11-tetraoxatridecane **19**, obtained in a two step reaction from tetraethylene glycol.[106,116] Compound **23** was synthesized analogously to compound **14** (see section 2.1.1). The trityl (Trt)-protected thiol was introduced *via* an S_N2 displacement of the halide with triphenylmethanethiol. The final, multifunctional compound HS-PEG-DAP **26** was obtained as a racemate by basic ester hydrolysis of **24** and subsequent deprotection of the Trt- and Boc-group under acidic conditions (Scheme 6).

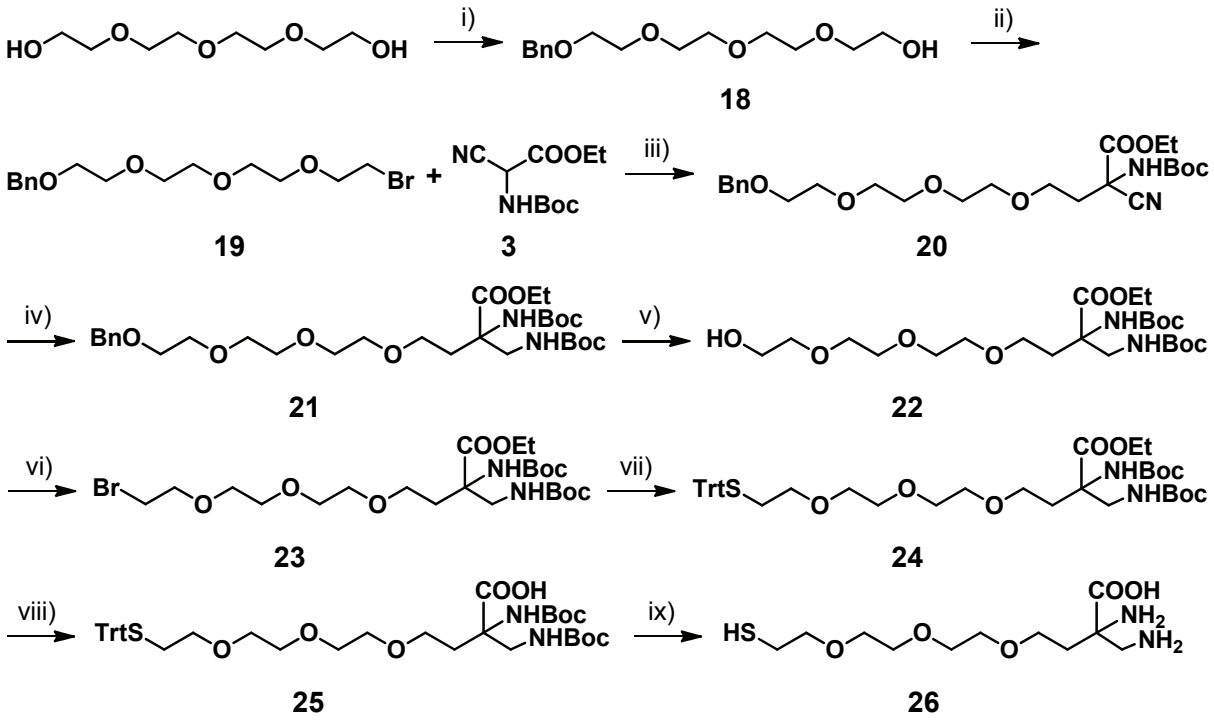

Scheme 6. Synthesis of HS-PEG-DAP **26**. i) BnBr, NaH (60% suspension in oil), THF, 0-20 °C, overnight, 86%; ii) CBr_4, PPh_3, CH_2Cl_2, 0-20 °C, 4 h, 98%; iii) Na, EtOH, reflux, overnight, 64%; iv) $NiCl_2 \cdot 6\ H_2O$, $NaBH_4$, $(Boc)_2O$, MeOH, 20 °C, 14 h, 77%; v) H_2 (1 atm), 10% Pd/C, MeOH, 20 °C, overnight, 98%; vi) CBr_4, PPh_3, CH_2Cl_2, 0-20 °C, 4 h, 71%; vii) HSTrt, NaH (60% suspension in oil), THF, reflux, 3 h, 90%; viii) MeOH / 1 M NaOH (1:1), 80 °C, overnight, 97%; ix) CH_2Cl_2 / TFA / TES (20:8:1.5), 20 °C, 2 h, 98%. The stereochemistry of the DAP chelating moiety is omitted for simplicity.

After basic ester hydrolysis of **24**, the carboxylic acid in **25** can be activated to e.g. **32** for subsequent conjugation with amines of bioactive molecules (Scheme 7). We emphasize the strength of this approach; compound **32** can be conjugated to essentially any amine containing targeting vector due to the multiple functions of DAP-based ligand systems. To exemplify this strategy, we selected as a cancer receptor-specific targeting function a small

molecule inhibitor of PSMA, a type II integral membrane protein that is overexpressed on prostate cancer cells.[117] This inhibitor is part of a ^{99m}Tc labeled prostate cancer imaging agent or targeted polymeric NPs containing the chemotherapeutic Docetaxel, both in clinical trials.[118,119] Its basic structure is lysine-urea-glutamate. The glutamate moiety is essential for binding to the pharmacophore pocket of PSMA.[120] Therefore a linker to the ε-amino group of lysine is required. Pomper and co-workers determined 20 Å as the minimum distance between the lysine moiety and a large fragment such as NPs in order to not affect the PSMA binding affinity.[121] Consequently, the inhibitor with *tert*-butyl ester protected carboxylic acids was coupled to Boc-protected 6-aminohexanoic acid. After removal of the protecting groups, the inhibitor **31** was conjugated to the NHS-activated compound **32** (Scheme 7).

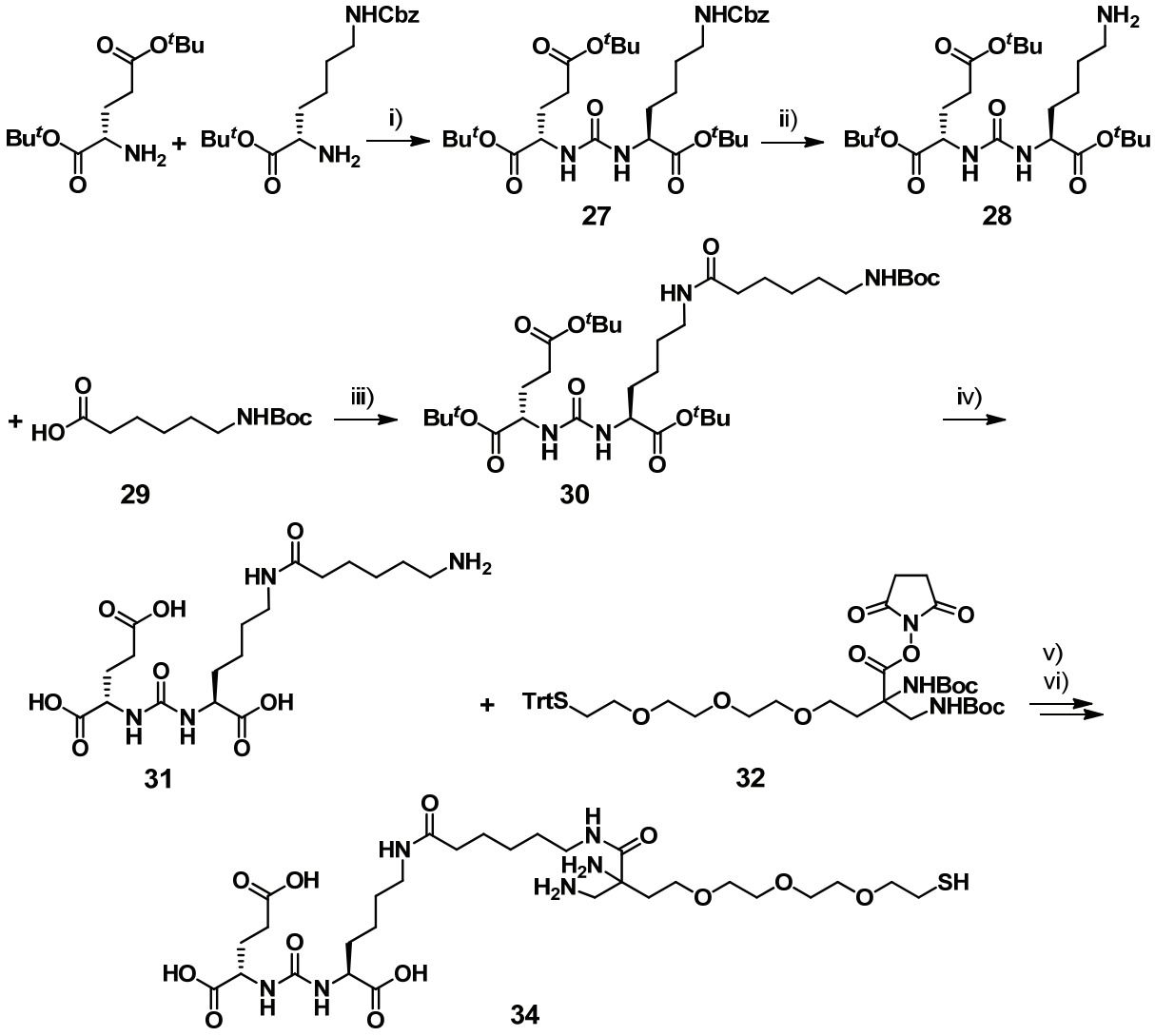

Scheme 7. Synthesis of HS-PEG-DAP-TF **34**. i) Triphosgene, TEA, CH_2Cl_2, 0-25 °C, 6 h, 69%; ii) H_2 (1 atm), 10% Pd/C, MeOH, 20 °C, overnight, 98%; iii) DCC, DMAP, CH_2Cl_2, 0-25 °C, 42 h, 69%; iv) CH_2Cl_2 / TFA / TES (20:8:1.5), 25 °C, 2 h, 99%; v) DMF, H_2O, TEA, 20 °C, 48 h, 82%; vi) CH_2Cl_2 / TFA / TES (20:8:1.5), 20 °C, 2 h, 97%. The stereochemistry of the DAP chelating moiety is omitted for simplicity.

We note that linking of the enantiomerically pure inhibitor to racemic **32** leads to a diastereomeric mixture. The two diastereomers could not be separated with preparative HPLC. We continued the study without further separation, assuming that the distant (racemic) chelating moiety does not impede the interaction of the enantiomerically pure receptor ligand with the target. The final compound HS-PEG-DAP-TF **34** with the targeting function (TF) was obtained after another deprotection step. In **34**, the distance between the ε-nitrogen of lysine and the thiol-group is 21.3 Å and meets therefore the aforementioned requirements (Figure 7).

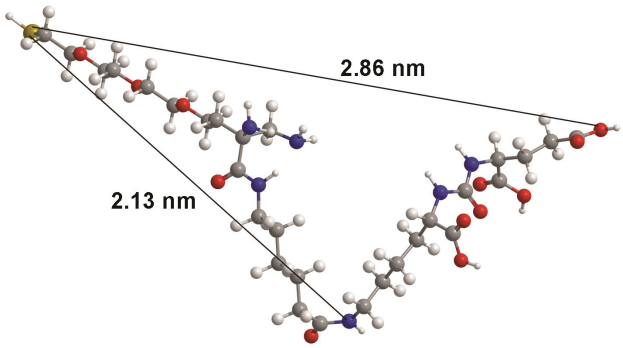

Figure 7. MM2 energy minimized structure of HS-PEG-DAP-TF **34**, calculated with ChemBio3D (CambridgeSoft, Version 12.0.2.1076).

Starting from commercially available compounds, the synthesis of **26** requires twelve and the one of **34** an additional eight steps. Still, the individual steps are fast and of good to very good yields. Flexibility of the design of this multifunctional ligand system is only restricted for synthetic and analytical reasons by the length of the PEG linker. It is well known that PEGs of molecular weights higher than 2 kDa reduce (undesired) fast clearance *via* the reticuloendothelial system (RES) by endowing the NPs with "stealth" properties.[22] However, commercially available PEGs of high molecular weights for a reasonable price consist of a distribution of chain lengths which is not compatible with a well defined design. Our synthetic procedure, especially careful characterization, requires PEGs with clearly defined chain lengths; hence, we used tetraethylene glycol due to its high purity which allows silica gel column chromatography separations of single products.

2.2.2 Synthesis, Functionalization and Characterization of NPs

Hydrophobic QDs and AuNPs, both having high affinity for thiol groups, were synthesized following published procedures.[122,123] In a subsequent step, the hydrophobic surfactants

from the standard syntheses were quantitatively replaced by HS-PEG-DAP **26** and HS-PEG-DAP-TF **34**. Oleylamine stabilized AuNPs were prepared by reduction of tetrachloroauric acid trihydrate with oleylamine in refluxing toluene. This method limits particle sizes from 6 to 14 nm in diameter, depending on the respective reflux time. AuNPs with two different core diameters (6.6 ± 0.3 nm and 13.8 ± 0.4 nm, referred to as $Au^{(7)}$NPs and $Au^{(14)}$NPs respectively in this thesis) were synthesized for assessing the size effect throughout biological evaluations (Figures 8B and 8C). Trioctylphosphine (TOP)/trioctylphosphine oxide (TOPO)-capped CdSe/ZnS core-shell QDs were obtained by reacting the corresponding organometallic precursors at high temperatures in a coordinating solvent mixture. For biological comparison with $Au^{(7)}$NPs, red emissive QDs with a diameter of 6.4 ± 0.1 nm were synthesized (Figure 8A). The QDs showed the first excitonic peak at 642 nm, an emission maximum at 648 nm and a QY of 42% (Figure 8D). The characteristic optical property of AuNPs is the surface plasmon resonance (SPR) peak.[42] This peak was found at 520 nm for $Au^{(7)}$NPs and at 522 nm for $Au^{(14)}$NPs, respectively (Figure 8E and 8F).

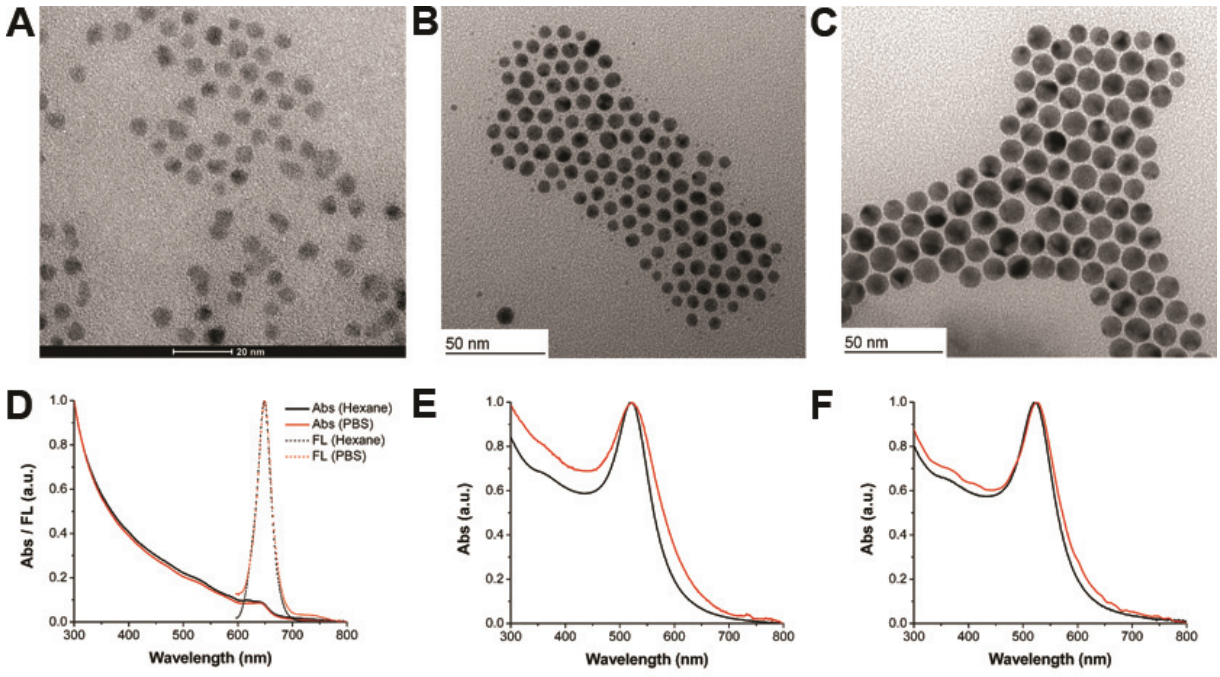

Figure 8. Representative TEM micrographs of (A) TOP/TOPO-coated 6.4 ± 0.1 nm QDs, (B) oleylamine-capped 6.6 ± 0.3 nm AuNPs and (C) 13.8 ± 0.4 nm AuNPs (A was recorded with an Eagle CCD camera; B and C with a Gatan camera). Normalized fluorescence and UV/Vis absorption spectra before (black line, measured in hexane) and after (red line, measured in PBS pH 7.4) functionalization with HS-PEG-DAP **26** and HS-PEG-DAP-TF **34**: (D) QDs, (E) $Au^{(7)}$NPs and (F) $Au^{(14)}$NPs.

For radiolabeling experiments and biological studies, water solubility of the synthesized NPs is a crucial issue which is achieved by substituting the hydrophobic encapsulation with hydrophilic HS-PEG-DAP **26** and HS-PEG-DAP-TF **34**, respectively. Recently, Mattoussi and co-workers reported a UV-promoted, biphasic approach for the phase transfer of ZnS-overcoated CdSe QDs.[110] For this procedure, a nonpolar phase containing the NPs was vigorously mixed under UV-irradiation with a polar phase, containing the water-soluble coating ligands. They applied this method to lipoic acid derivatives and showed a reduction of the disulfide upon UV-excitation, followed by replacement of TOP/TOPO capping ligands. Ligands **26** and **34** described in here are not based on lipoic acid but the same strategy was still successfully applied for achieving a phase transfer. We note that several other, commonly applied methods such as biphasic exchange with $CHCl_3$ and PBS pH 7.4,[54] a two step procedure using histidine as an intermediate coating,[20] or mixing hydrophobic NPs and thiol-ligands in CH_2Cl_2 or tetrahydrofuran all failed. In a typical functionalization process, QDs or AuNPs were dispersed in hexane and mixed with an excess of ligands **26** and **34** in methanol for 50 min under UV-irradiation at 365 nm. This photo-mediated ligand exchange led to precipitation of the NPs, functionalized with **26** and **34**. The NPs were centrifuged and the supernatant, containing excess ligand, was removed. The precipitated NPs were washed with methanol and re-dispersed in PBS. We note that a 1:1 mixture of **26** and **34** resulted in highly water soluble NP conjugates, whereas NPs coated with HS-PEG-DAP **26** alone are poorly soluble in PBS. We assume that the zwitter-ionic nature of the DAP ligand induces electrostatic attractions during the phase transfer and, therefore, aggregation of NPs. The additional introduction of HS-PEG-DAP-TF **34** with its negatively charged carboxylate groups leads to electrostatic repulsion and thus good solubility. Several ratios of **26** and **34** were evaluated for the phase transfer reaction, but the 1:1 ratio displayed the best solubility. Functionalized NPs were finally purified with a PD-10 size-exclusion column (Sephadex G-25 medium and PBS pH 7.4 as mobile phase) to remove any free ligand. Free ligand would compete in the radiolabeling with ligand bound to the NPs and, therefore, lower RCYs.

Phase transfer of QDs did not affect spectroscopic properties such as first excitonic peak or emission maxima (Figure 8D). The QY dropped from 42% to 10% after phase transfer, attributed to an increased interaction of the QDs with the polar media.[110] A good indication of surface modification and particle aggregation of AuNPs is provided by the SPR peak.[18] The functionalized AuNPs exhibited only a weak bathochromic shift ($\Delta\lambda$ = 3 nm for $Au^{(7)}$NPs and

$Au^{(14)}$NPs) compared to the oleylamine-stabilized AuNPs (Figure 8E and 8F). The slight red shifts indicate no significant particle aggregation which is further supported by DLS measurements. The NPs were found to be mono-disperse in PBS with a HDD of 13.1 nm (QDs), 13.5 nm ($Au^{(7)}$NPs) and 20.1 nm ($Au^{(14)}$NPs), respectively. The increase of ~6.5 nm for all NPs as compared to the diameter determined in TEM is in accordance with the length of the organic coating ligand HS-PEG-DAP-TF **34**, which is ~2.8 nm based on the minimum energy structure (Figure 7). All three NPs revealed negative ζ-pot. values between -21.2 and -22.1 mV in PBS. The negative ζ-pot. values confirm the negative coating induced by the carboxylate groups of the ligand **34**. Functionalization was further evidenced by FT-IR spectroscopy. The hydrophobic NPs showed the typical bands at 2916 cm^{-1} and 2850 cm^{-1} of C-H stretching vibrations of the long alkyl chains and the terminal methyl groups (Figure 9). The intensities of these bands decreased substantially after ligand exchange. Only a weak band at 2860 cm^{-1} was still present, likely due to the alkyl moieties in **20**. The appearance of characteristic urea vibrations in the region between 1626 and 1260 cm^{-1} and a PEG-stretching at 1086 cm^{-1} supported the evidence of a ligand exchange. The relevant analytical data after surface modification are summarized in Table 1.

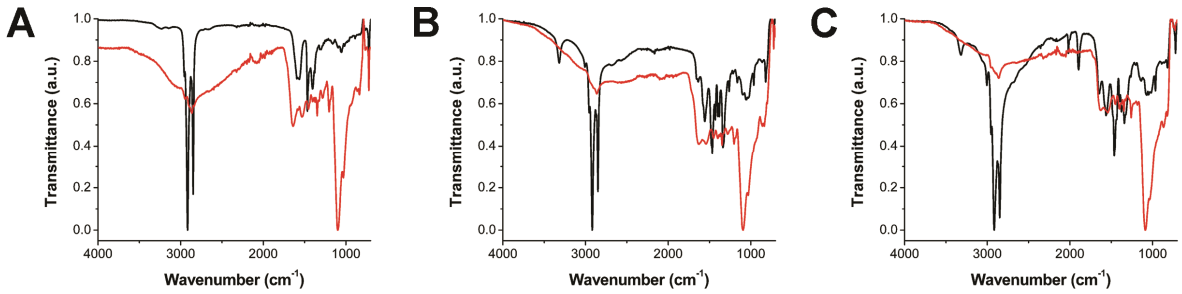

Figure 9. Normalized FT-IR spectra of hydrophobic NPs (black line) and phase transfer (red line): (A) QDs, (B) $Au^{(7)}$NPs and (C) $Au^{(14)}$NPs.

2.2.3 Radiolabeling

$[^{99m}Tc(OH_2)_3(CO)_3]^+$ was prepared with the commercially available IsoLink™ kit from $[^{99m}TcO_4]^-$.[124] The three water ligands of $[^{99m}Tc(OH_2)_3(CO)_3]^+$ are labile and readily exchangeable with tridentate chelators such as DAP. In a typical radiolabeling experiment, a PBS solution of $[^{99m}Tc(OH_2)_3(CO)_3]^+$ was added to NP solutions in PBS (final NP concentration 1.0 mg/ml, Figure 10A). The labeling progress was monitored by HPLC, equipped with a size-exclusion column and three detectors (UV-Vis, fluorescence and γ-counter). The presence of

strong NP bound chelators allows now for their direct labeling, no preformation of complexes with NP affine groups is required. Best labeling yields for AuNPs were achieved with a temperature gradient from 50 °C to 70 °C over one hour and a subsequent incubation for another hour at 70 °C. Labeling temperature for QDs should not exceed 60 °C since formation of a precipitate was observed at higher temperatures.

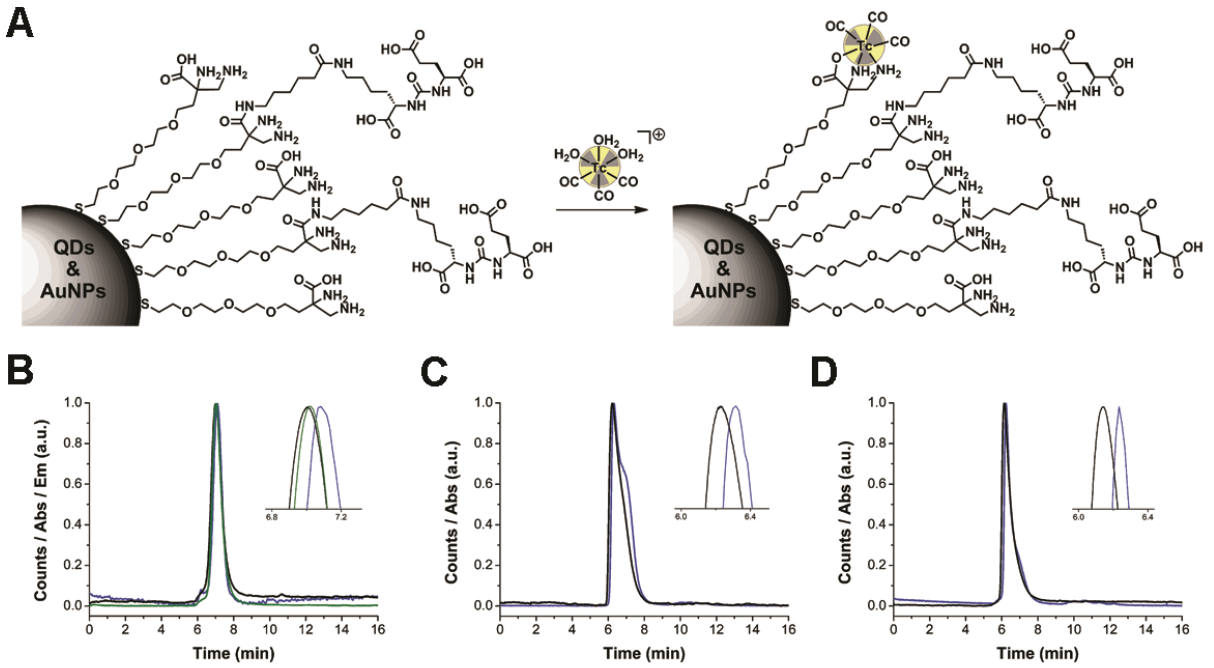

Figure 10. (A) Radiolabeling scheme of NPs. Normalized HPLC traces of (B) QDs, (C) Au$^{(7)}$NPs and (D) Au$^{(14)}$NPs after purification. The analyses include absorbance at 365 nm (black lines), fluorescence at 650 nm (green lines) and γ-counts (blue lines). Please note that the difference of 0.1 min between the absorbance and γ-counts is due to the detector setup in which the γ-detector is located after the UV-detector.

Due to the highly dilute concentrations of chelators and ^{99m}Tc complexes, quantitative labeling can hardly be achieved in these bimolecular reactions for kinetic reasons. Estimating the maximum theoretical number of HS-PEG-DAP **24** units on AuNPs results in a ligand concentration between 10^{-5} to 10^{-6} M for 1 mg/ml NPs according to the following calculations:

- *Calculation of theoretical density HS-PEG-DAP (**24**) ligands on Au$^{(7)}$NPs*

  The volume of a particle is $1.4 \cdot 10^{-25}$ m^3 and the volume of a single gold atom is $1.9 \cdot 10^{-29}$ m^3 (based on the Van-der-Waals-radius of 166 pm). This leads to a theoretical number of 7368 atoms per particle and, therefore, a molecular weight of $1.45 \cdot 10^6$ g/mol per particle. Hence, the amount of AuNPs per mg is $6.9 \cdot 10^{-10}$ mol which is

equal to $4.15 \cdot 10^{14}$ NPs per mg. The surface of one particle is $1.3 \cdot 10^{-16}$ m^2 and assuming the coating ligand as a cylinder with a radius of 5 Å, the surface of its top area is $7.9 \cdot 10^{-19}$ m^2. Using these values, the theoretical maximum number of coating ligands that can bind to a 6.6 nm AuNP is 164. By multiplying this number with $6.9 \cdot 10^{-10}$ mol AuNPs per mg, the amount of coating ligand is $113 \cdot 10^{-9}$ mol. Since this amount is in 1 ml of solvent, the concentration of chelating moieties for the labeling with ^{99m}Tc is $113 \cdot 10^{-6}$ M.

- *Calculation of theoretical density HS-PEG-DAP (**24**) ligands on $Au^{(14)}$NPs*

  The volume of a particle is $1.38 \cdot 10^{-24}$ m^3 and the volume of a single gold atom is $1.9 \cdot 10^{-29}$ m^3 (based on the Van-der-Waals-radius of 166 pm). This leads to a theoretical number of 72'424 atoms per particle and, therefore, a molecular weight of $14.3 \cdot 10^6$ g/mol per particle. Hence, the amount of AuNPs per mg is $7.0 \cdot 10^{-11}$ mol which is equal to $4.21 \cdot 10^{13}$ NPs per mg. The surface of one particle is $6.0 \cdot 10^{-16}$ m^2 and assuming the coating ligand as a cylinder with a radius of 5 Å, the surface of its top area is $7.9 \cdot 10^{-19}$ m^2. Using these values, the theoretical maximum number of coating ligands that can bind to a 13.8 nm AuNP is 759. By multiplying this number with $7.0 \cdot 10^{-11}$ mol AuNPs per mg, the amount of coating ligand is $53 \cdot 10^{-9}$ mol. Since this amount is in 1 ml of solvent, the concentration of chelating moieties for the labeling with ^{99m}Tc is $53 \cdot 10^{-6}$ M.

- *Assumptions:*

  AuNPs are perfect spheres with a fixed diameter (6.5 nm & 13.8 nm). For the sake of simplicity the contribution of oleylamine to the weight of the particles was neglected.

This maximum concentration is certainly lowered by the actual density of bound ligands on the NP surface and by further dilution with the DAP derived targeting molecule **20**. Therefore, a concentration between 10^{-6} and 10^{-7} M is probably a better approximation. With a typical $[^{99m}Tc(OH_2)_3(CO)_3]^+$ concentration between 10^{-8} and 10^{-9} M, such bimolecular reactions become very slow especially when including kinetically inert d^6 centers like the present Tc^I core. Taking these factors into account, the obtained RCY of 10% (QDs), 78% ($Au^{(7)}$NPs) and 49% ($Au^{(14)}$NPs) after PD-10 purification are remarkable and mirror the potency of the DAP chelator (Figures 10B, 10C and 10D, Table 1). If higher temperatures are compatible with NPs, the RCY could become quantitative. At the same mg/ml amounts,

$Au^{(7)}$NPs exhibit a higher RCY since the larger surface area as compared to $Au^{(14)}$NPs leads to a higher chelator concentration (for equal amounts of NP) for labeling.

Table 1. Characteristic analytical data of functionalized NPs.

	QDs	*$Au^{(7)}$NPs*	*$Au^{(14)}$NPs*
λ_{max} (nm)	642 (648)[a]	520	522
Diameter in nm	6.4 ± 0.1	6.6 ± 0.3	13.8 ± 0.4
HDD in nm (PDI)[b]	13.1 (0.4)	13.5 (0.3)	20.1 (0.22)
ζ-pot. in mV (STD)[c]	-22.1 (1.9)	-22.2 (2.0)	-21.2 (1.9)
Retention time (min)[d]	7.01	6.21	6.14
RCY[e] (%)	10	78	49
RCP[f] (%)	≥ 95	≥ 95	≥ 95

[a] λ_{em} (nm); [b] polydispersity index; [c] standard deviation; [d] size-exclusion HPLC analysis; [e] radiochemical yield; [f] radiochemical purity.

2.2.4 Chemical and Serum Stability

For stability assessment, the labeled NPs were kept under air at 40 °C for 12 h in PBS and at 40 °C for 3 h in fetal bovine serum (FBS), whereas 10 µl of radiolabeled NP solution were mixed with 100 µl FBS. HPLC analysis of the AuNP samples revealed for both stability experiments trace amounts of released $[^{99m}Tc(OH_2)_3(CO)_3]^+$ (12.2 min retention time) and $[^{99m}TcO_4]^-$ (12.8 min). The radiochemical purity (RCP) was still >95%, underlying the robustness of the DAP complex bound to the AuNP conjugates (Figures 11B and 11C). No released **26**, coordinated to the *fac*-$[^{99m}Tc(CO)_3]^+$ moiety was though detected. The high stability of radiolabeled AuNP conjugates arises from the formation of the so-called "staple motif", in which the sulfur atom from the ligands **26** and **34** forms a highly stable bridge to two gold atoms.[125] Labeled QDs are more sensitive and precipitates were observed after 12 h at 40 °C. Centrifugation and HPLC analysis of the supernatant revealed a new species at R_t=10.6 min (Figure 11A), identified as ^{99m}Tc-labeled HS-PEG-DAP and released as an entity from the QD surface. Released coating ligand was also observed in the experiments with FBS (Figure 11A). Loss of complex and free ligand from the surface of the QDs reduced their hydrophilic character. Thereby, the hydrophobic ZnS shell was increasingly exposed and the

QDs started to precipitate. AuNPs did not show this behavior (no cleavage of ligand or complex) emphasizing their superior stability over QDs. For evaluating long term chemical stabilities, NPs were kept at 4 °C for one week after labeling. After this time period, radioactivity decreased to zero. The colloidal stabilities of the now "inactive" NP samples could be studied. DLS and HPLC investigations confirmed that the HDD of the AuNPs was not affected by the radiolabeling process. Furthermore, the optical properties of the AuNPs were preserved and no shift or broadening of the SPR peaks was observed. For QDs, wavelength of the first excitonic peak and the emission maximum did not change after one week at 4 °C but the QY decreased from 10% to 7%. The drop in QY confirms coating ligand detachment, known to lead to decreased colloidal stability[15] and in agreement with the appearance of a second peak in DLS analysis as a result of partial aggregation.

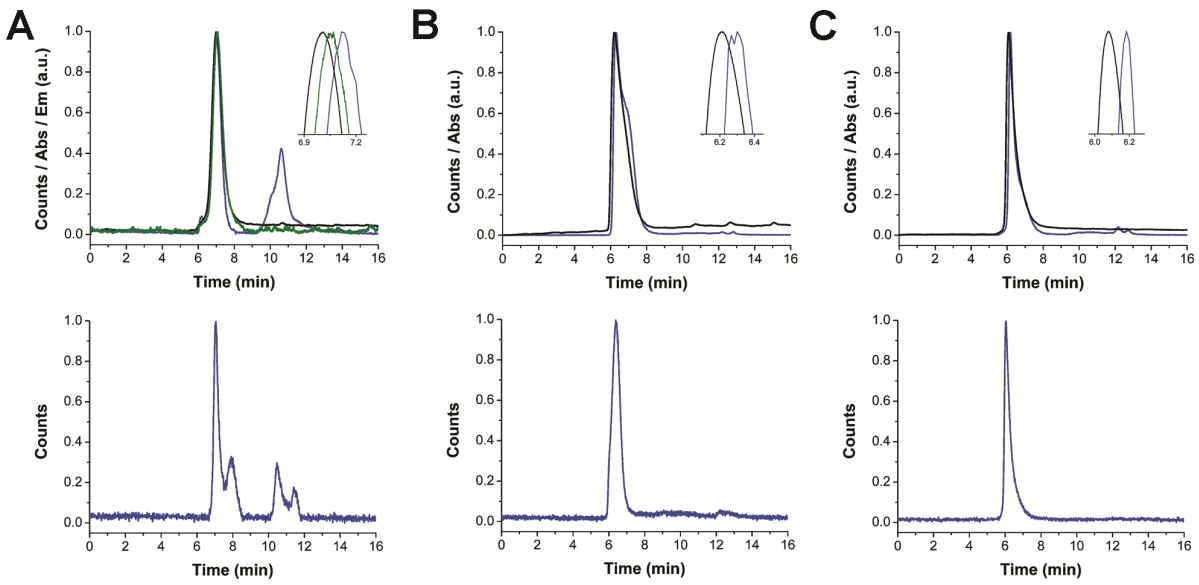

Figure 11. Normalized HPLC traces of (A) QDs, (B) Au$^{(7)}$NPs and (C) Au$^{(14)}$NPs after 12 h at 40 °C in PBS pH 7.4 (top row) and after 3 h at 40 °C in FBS (bottom row). The analyses include absorbance at 365 nm (black lines), fluorescence at 650 nm (green lines) and γ-counts (blue lines). Please note that the difference of 0.1 min between the absorbance and γ-counts is due to the detector setup in which the γ-detector is located after the UV-detector.

High stabilities are very crucial for *in vitro* and *in vivo* applications. Dissociation of the radiolabel would automatically lead to a false assessment of the NP's location. Hence, we focused on Au$^{(7)}$NPs and Au$^{(14)}$NPs and did not include the QDs conjugates in the biological evaluation. The stability problem might be overcome by anchoring the ligands with multiple thiol groups to the surface of QDs.[126,127]

2.2.5 Colloidal Stability and Cellular Uptake Studies

Beside purely chemical stability, the colloidal stability of NPs under physiological conditions is equally important for biomedical investigations. The SPR band is very sensitive to changes in the gold NP environment, thus, respective shifts are good indicators for adsorbed serum proteins.[128,129] $Au^{(7)}$NPs and $Au^{(14)}$NPs in PBS were mixed with FBS in a 1:1 ratio and incubated at 37 °C. UV/Vis spectra were recorded after 0, 3, 6, 12 and 24 h (Figure 12). Insignificant changes in the spectra and SPR band of $Au^{(7)}$NPs indicated little to no interaction with serum proteins, whereas $Au^{(14)}$NPs exhibited a red shift of ~1 nm. Shifts of 1 nm are not fully conclusive and, therefore, an HPLC size-exclusion analysis was performed after 24 h incubation for both probes. We found unchanged retention times for both AuNPs. In agreement with literature, reporting reduced binding of negatively charged serum proteins to neutral or negatively charged NP surfaces, substantial blood serum protein binding can therefore be ruled out.[74,82]

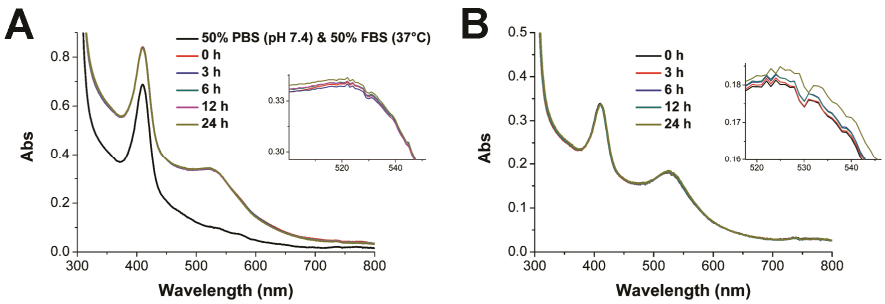

Figure 12. UV-Vis spectra of $Au^{(7)}$NPs (A) and $Au^{(7)}$NPs (B) in a 1:1 mixture of PBS pH 7.4 and FBS at 37 °C and different time points (please note that the peak at 410 nm is from FBS).

The assessed serum stabilities of the AuNPs lead us to the *in vitro* evaluation of the NP bioconjugates. LNCaP is a cancer cell line which overexpresses PSMA and is therefore well suited for following eventual uptake of the AuNPs by TEM. Literature studies confirmed that cellular uptake of NPs depends on the size, shape and the surface coating.[71] Since the cell membrane consists of an anionic, hydrophilic outer surface, the charge of the NP coating is a particularly important factor.[130] Cationic NPs show generally a higher intracellular uptake as anionic or neutral NPs.[131] Uptake preferences are different if the NPs are actively transported into the cell *via* receptor-mediated endocytosis, i.e. the urea-glutamate targeting function may still efficiently dock to the cell surface bound PSMA. LNCaP cells were seeded on glass coverslips, placed in well plates and incubated with $Au^{(7)}$NPs (179 µg/ml) and $Au^{(14)}$NPs (189 µg/ml) for 30 s. After washing and fixing the cells, the samples were

embedded in Epon resin to cut ultrathin sections for TEM analysis. The images clearly show a localization of AuNPs as black spots on the cell surface (Figures 13A, 13B and 14A). EDX confirmed the identity of the black spots and control experiments without AuNPs did not exhibit similar black spots in the TEM images (Figure 15). In additional experiments, the cells were incubated under the same conditions for 90 min in order to localize AuNPs within the cells. $Au^{(7)}$NPs were found entrapped in endomembrane compartments, either as single particles or as aggregates (Figures 13C and 13D). $Au^{(14)}$NPs were mainly present as single particles in the cytosol without being integrated in endosomes (Figure 14B). In order to exclude non-specific uptake of AuNPs, we carried out control experiments under the same conditions with Cos7 cells, not overexpressing PSMA. None of the TEM images evidenced AuNPs inside the cells (Figure 16), corroborating the hypothesis of PSMA receptor-mediated uptake.

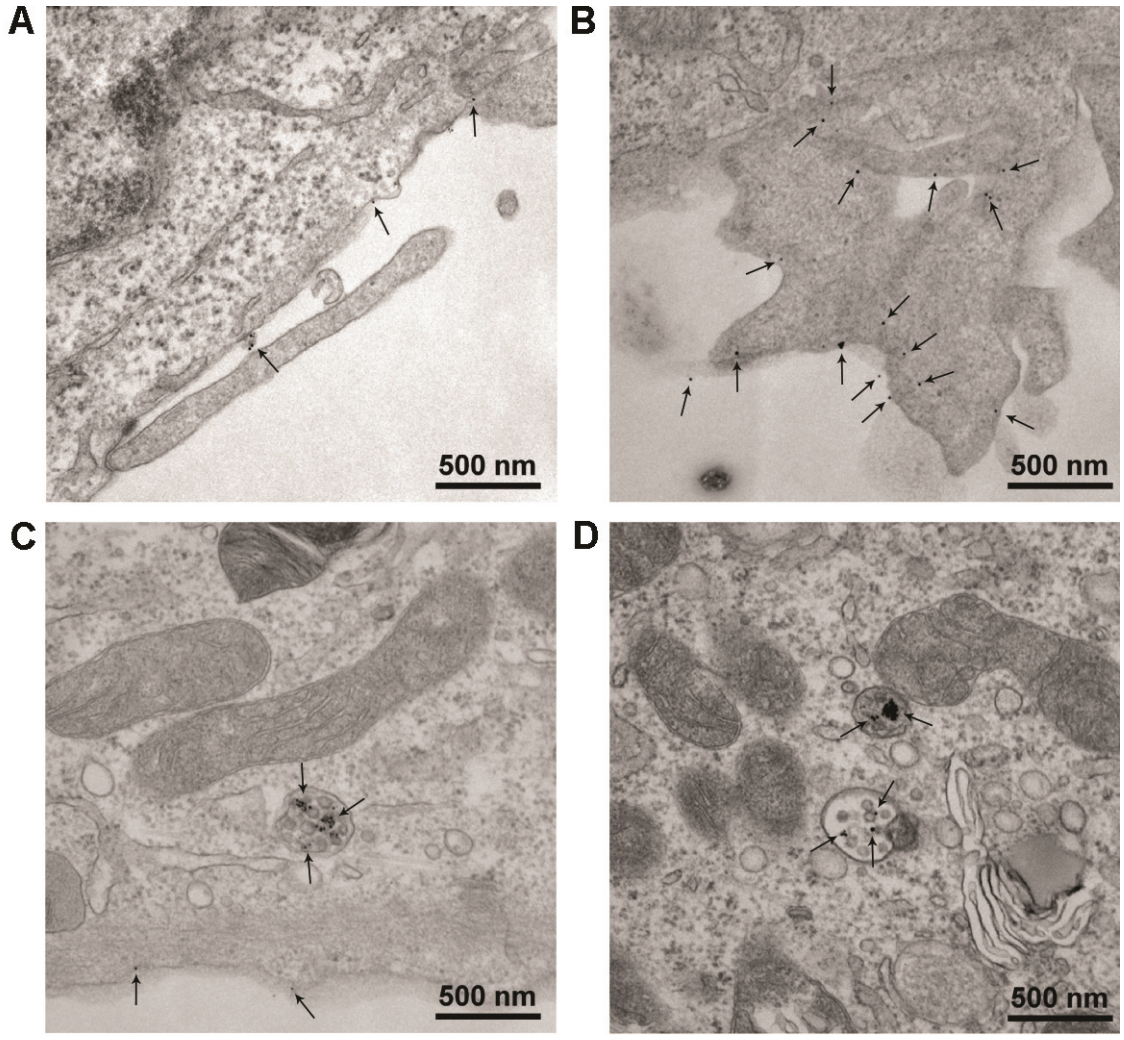

Figure 13. Representative TEM images of LNCaP cells after 30 s (A and B) and 90 min (C and D) incubation of $Au^{(7)}$NPs. Due to the high contrast of AuNPs, the sections were used without further contrasting. The location of the AuNPs is indicated with black arrows.

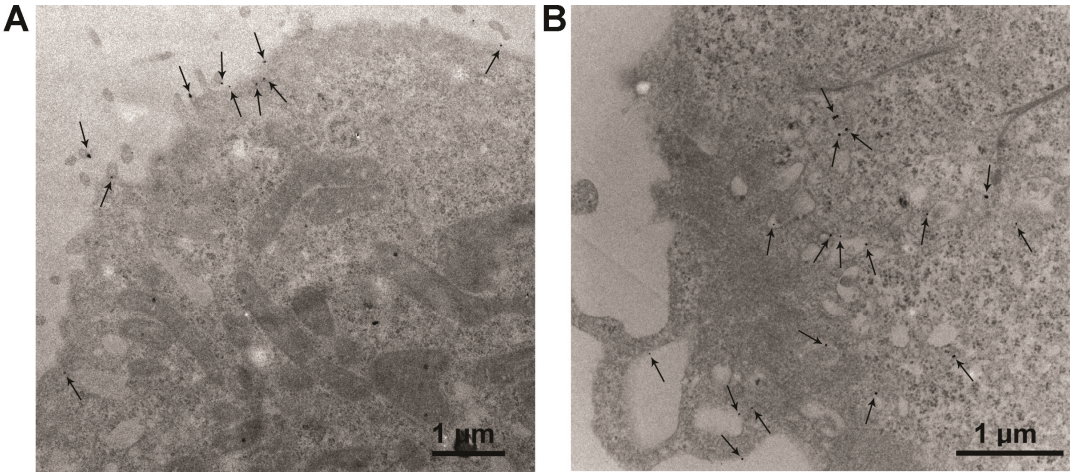

Figure 14. Representative TEM images of LNCaP cells after 30 s (A) and 90 min (B) incubation of $Au^{(14)}$NPs. The location of the AuNPs is indicated with black arrows.

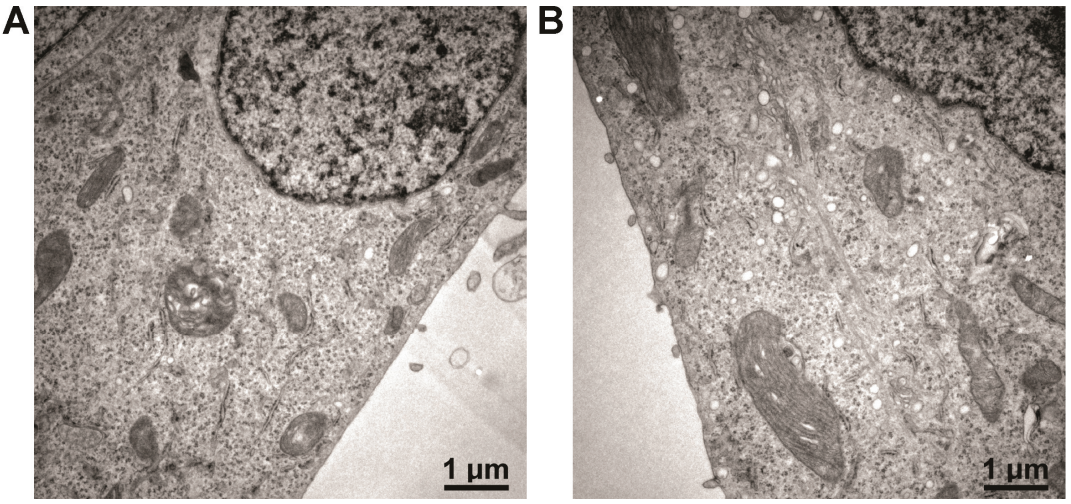

Figure 15. Representative TEM images of LNCaP cells after 30 s (A) and 90 min (B) incubation of medium without AuNPs (control experiment).

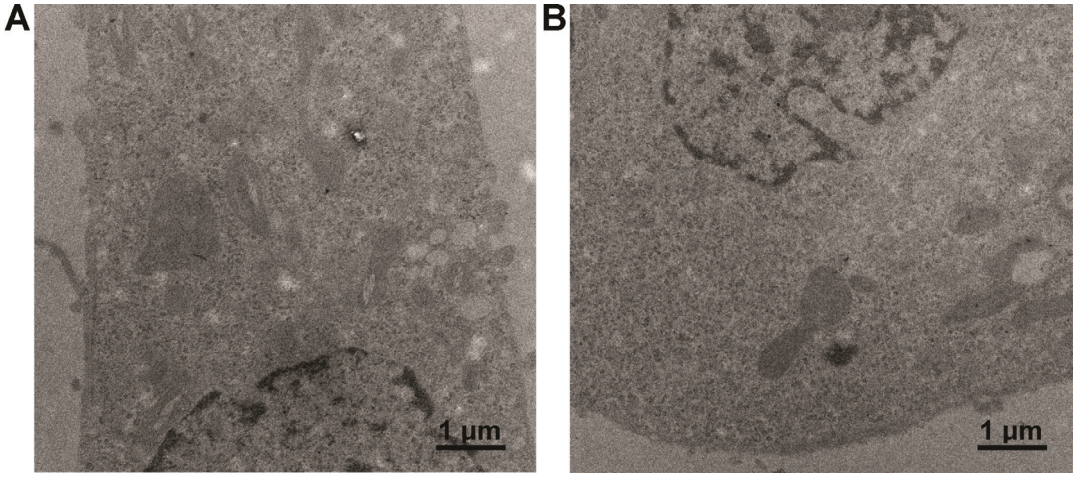

Figure 16. Representative TEM images of Cos7 cells after 90 min incubation of $Au^{(7)}$NPs (A) and $Au^{(14)}$NPs (B) (control experiment).

To conclude the *in vitro* stability experiments and cellular uptake studies, we found that the derivatized AuNPs are stable under physiological conditions and taken up by prostate cancer cells *via* receptor-mediated endocytosis. With this knowledge in hand, we went one step further and evaluated the functionalized and radiolabeled AuNPs *in vivo.*

2.2.6 *In Vivo* microSPECT Imaging and *Ex Vivo* Biodistribution Studies

The *in vivo* behavior of the radiolabeled $Au^{(7)}$NPs and $Au^{(14)}$NPs was studied in nude NMRI mice bearing LNCaP tumor xenografts in the region of the left shoulder. After radiolabeling and purification of 1.0 mg AuNPs as described before, the compounds were administered *via* intravenous injection (i.v.) in concentrations ranging from 50 to 250 µg AuNPs per 0.2 ml injected volume. The mice were imaged with a small animal microSPECT scanner within three different stages over 60 min (0-20 min, 20-40 min and 40-60 min). Figure 17 shows the percent injected dose per gram (%ID/g) uptake data in selected organs for the two probes 60 min post injection (p.i.). The *ex vivo* biodistribution data revealed a high uptake in the liver and the spleen for $Au^{(7)}$NPs and $Au^{(14)}$NPs, respectively (detailed %-numbers in Table 2).

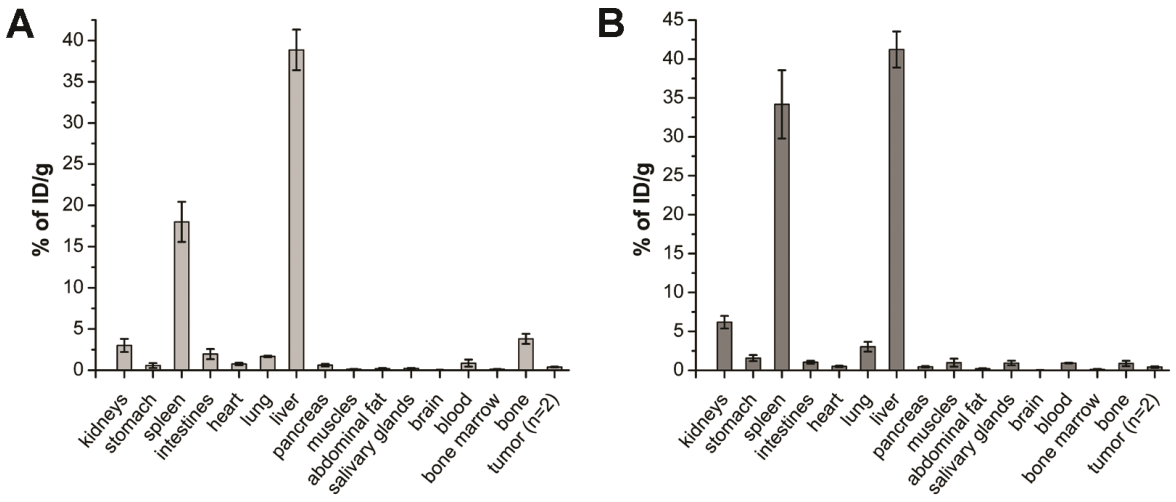

Figure 17. *Ex vivo* biodistribution in LNCaP xenograft mice of $Au^{(7)}$NPs (A) and $Au^{(14)}$NPs (B), expressed as percentage of injected dose (%ID) per gram organ (mean ± standard deviation, n=5).

Clearance *via* the hepatobiliary pathway was expected for both AuNPs based on the HDD and negative surface charge.[57] The radiolabeled NPs showed a low non-specific tissue uptake and tumor uptake was very low for both probes. $Au^{(7)}$NPs and $Au^{(14)}$NPs are rapidly cleared out of the circulation to the liver and spleen and therefore do not accumulate at the tumor site.

Table 2. *Ex vivo* biodistribution data in LNCaP xenograft mice (%ID/g) expressed as mean value ± standard error of the mean (n=5).

organ / tissue	*$Au^{(7)}$NPs*	*$Au^{(14)}$NPs*
kidneys	3.01 ± 0.80	6.18 ± 0.81
stomach	0.57 ± 0.29	1.58 ± 0.39
spleen	18.00 ± 2.44	34.17 ± 4.39
intestines	1.96 ± 0.62	1.04 ± 0.19
heart	0.76 ± 0.14	0.51 ± 0.09
lung	1.67 ± 0.09	3.03 ± 0.64
liver	38.87 ± 2.46	41.22 ± 2.31
pancreas	0.62 ± 0.16	0.46 ± 0.09
muscles	0.13 ± 0.03	0.99 ± 0.51
abdominal fat	0.19 ± 0.08	0.19 ± 0.06
salivary glands	0.23 ± 0.05	0.94 ± 0.30
brain	0.04 ± 0.01	0.04 ± 0.01
blood	0.86 ± 0.43	0.93 ± 0.05
bone marrow	0.13 ± 0.02	0.12 ± 0.07
bone (femur)	3.81 ± 0.61	0.88 ± 0.34
tumor (n=2)	0.39 ± 0.04	0.43 ± 0.10
urine (%ID only)	2.08 ± 0.16	2.78 ± 0.91

This fact is mirrored in the microSPECT images at an early stage (0-20 min), whereas almost the entire injected dose was seen in the liver and spleen (Figure 18). Due to the short blood half-life of the compounds, it is assumed that the NPs are quickly captured by the phagocytic cells of the MPS, which consequently decreases the chance of adequate tumor uptake. This could be improved by preparing NP formulations with a neutral surface charge (ζ-pot. ~ ± 5 mV), although this is very challenging with ligand **34** bearing multiple carboxylate functionalities on the very outer surface.

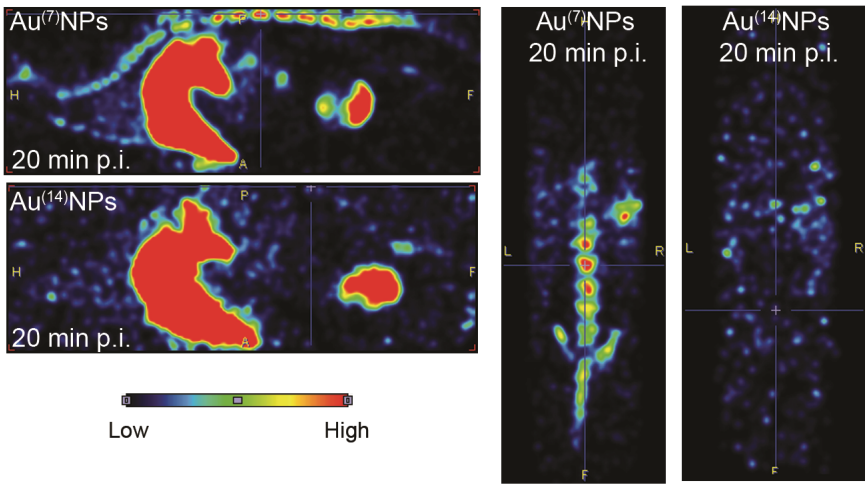

Figure 18. *In vivo* microSPECT images at early scan stage (0-20 min) of $Au^{(7)}$NPs and $Au^{(14)}$NPs (sagittal planes on the left and coronal planes on the right). The injected dose for $Au^{(7)}$NPs probe was 71 MBq and for $Au^{(14)}$NPs probe 66 MBq.

Interestingly, in the early stage microSPECT images of $Au^{(7)}$NPs, the spine, the ribs and the skull are clearly visible, features which are not found for $Au^{(14)}$NPs. The same observation holds true for images at later stages. We first interpreted this observation as the result of uptake by the RES organs, which include the bone marrow. In order to elicit this hypothesis, we isolated the femur of the left leg and bone marrow from the spinal column for *ex vivo* biodistribution analyses. The bone marrow uptake of $Au^{(7)}$NPs (0.13 ± 0.02 %ID/g) and $Au^{(14)}$NPs (0.12 ± 0.07 %ID/g) are small and almost identical for both AuNPs. The bone uptake of the $Au^{(7)}$NPs (3.81 ± 0.61 %ID/g) on the other hand is significantly higher as compared to the $Au^{(14)}$NPs (0.88 ± 0.34 %ID/g). These data are in agreement with the microSPECT images and point to an interaction with the bone mineral itself rather than to an uptake by the bone marrow. More importantly, these are clear indications that overall bone uptake depends on the size of AuNPs, a conclusion which is supported by the biodistribution analyses.

In order to gain further insights into the molecular background of this uncommon, size dependent bone uptake, we performed metabolite analyses of the blood plasma and urine. HPLC analysis of the blood plasma 1 h p.i. showed that 49% of radiolabeled $Au^{(7)}$NPs remained stable, whereas only 7% of the injected $Au^{(14)}$NPs appeared intact (Figure 19). In the urine of the injected $Au^{(7)}$NPs (2.08 ± 0.16 %ID) and $Au^{(14)}$NPs probes (2.78 ± 0.91 %ID) ^{99m}Tc was mostly present as a low molecular weight species, in coincidence with the clearly identifiable bladder in the microSPECT images depicted in Figure 18.

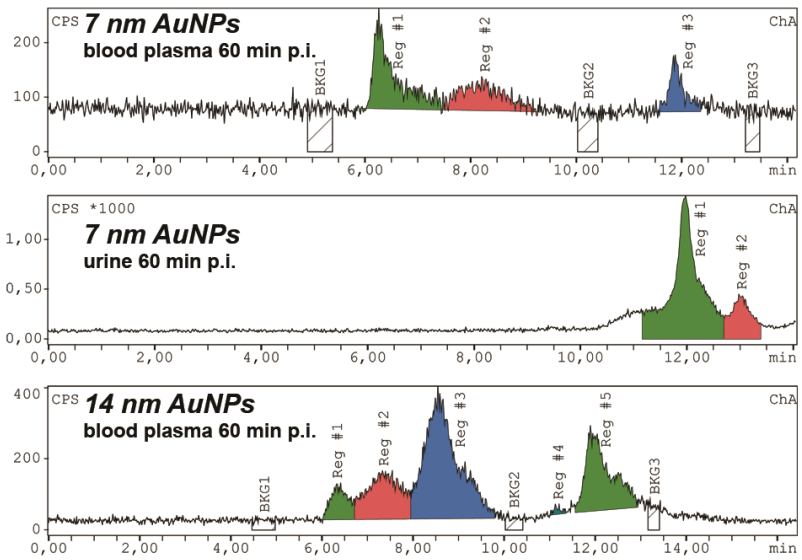

Figure 19. HPLC traces of the blood plasma and urine at 60 min p.i.

Eventual metabolites upon degradation of the NP coating might also be the reason for the uptake in the kidneys since renal clearance of the radiolabeled AuNPs can be ruled out. The high *in vivo* stability of $Au^{(7)}$NPs leads to lower amounts of ^{99m}Tc bearing metabolites, consequently, these AuNPs accumulate better at the bones and show higher resolved images of these organs. Based on the HPLC analysis of the blood plasma, $Au^{(14)}$NPs are metabolized to a higher degree than $Au^{(7)}$NPs. In particular, *in vivo* degradation of the coating ligands and concomitant loss of the carboxylate functions has a crucial impact on the surface charge of the AuNPs. Glutamic acid residues in proteins such as osteonectin have a high binding affinity for hydroxyapatite (synthetic analog for bone mineral).[132] Therefore, the loss of carboxylate groups, especially from the glutamate residues, will lead to decreased affinity towards bone mineral. Furthermore, Roeder and co-workers suggested in a recent study glutamic acid-functionalized AuNPs as X-ray contrast agents for damaged bone tissue.[133] For assessing the affinity of $Au^{(7)}$NPs for bone mineral, we added water-insoluble hydroxyapatite as a nanopowder (2 mg) to a 1.0 ml solution of $Au^{(7)}$NPs (1.0 mg/ml) in PBS (pH 7.4). The suspension was mixed at 37 °C and UV/Vis spectra taken at different time points. A constant decrease of the SPR peak evidenced successive binding of the negatively charged AuNPs to the hydroxyapatite surface. Since the AuNPs were literally extracted by the hydroxyapatite nanopowder, the solution slowly decolorized (Figure 20).

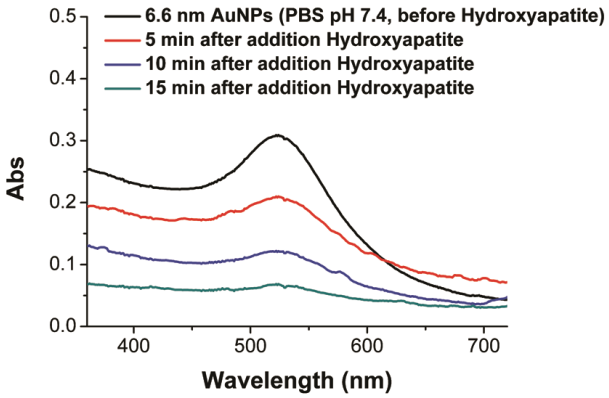

Figure 20. UV-Vis spectra before the addition of hydroxyapatite nanopowder (2 mg) to 1.0 ml AuNP solution in PBS (black line) and at different time points after the addition (red, blue and green line).

The microSPECT images together with the quantitative ^{99m}Tc biodistribution data are a good but not unambiguous indication for intact, radiolabeled $Au^{(7)}$NPs binding to the bones. However, one might still argue that these *in vivo* data are not the result of NP binding but rather caused by a metabolite or leaching of radiolabeled ligand from $Au^{(7)}$NPs. Only

quantitative data on the gold distribution, which should parallel the one of ^{99m}Tc, could rule out this hypothesis. We therefore determined the Au amount on the femur with ICP-MS (of the imaged mice shown in Figure 18). After washing the femur with water and PBS to remove blood remainders, the entire bones were digested in nitrohydrochloric acid for 5 h at room temperature. The femur of the mice injected with Au$^{(7)}$NPs (71 MBq ID) exhibited an amount of 0.63 µg of Au on the bone (57 mg), whereas 0.11 µg of Au was measured on the femur (51 mg) injected with the Au$^{(14)}$NPs sample (66 MBq ID). These values are fully consistent with the data as obtained from the *ex vivo* biodistribution studies with ^{99m}Tc. They strongly support the affinity of the intact radiolabeled AuNPs towards bone mineral.

2.2.7 Conclusion

In summary, we synthesized a novel coating ligand for thiophilic NPs, containing a terminal thiol group, a PEG linker and the DAP chelator (HS-PEG-DAP). The same time, the chelator can be coupled to targeting functions without changing its principal affinity for NP surfaces. Such a conjugation was exemplified with a small molecule inhibitor of PSMA by amide formation between the activated carboxylate of DAP and one primary amine of the targeting function (HS-PEG-DAP-TF). AuNPs (7 and 14 nm) and QDs (6 nm) were derivatized with a 1:1 mixture of HS-PEG-DAP/HS-PEG-DAP-TF and directly labeled with $[^{99m}Tc(OH_2)_3(CO)_3]^+$, demonstrating the high potency of the DAP chelator even at high dilution. Radiolabeled QDs revealed a partial detachment of the coating ligands under normal atmosphere and in serum, whereas the radiolabeled AuNPs were highly stable. *In vitro* cellular uptake studies and *in vivo* biodistribution were performed with 7 nm and 14 nm AuNPs. LNCaP cells showed binding and uptake of AuNPs, indicative for an interaction between the targeting function on the AuNPs and the membrane antigen PSMA. *In vivo* evaluation in nude NMRI mice harboring LNCaP xenografts exhibited fast clearance from the blood pool *via* hepatobiliary excretion and low tumor uptake. Metabolite analysis uncovered a higher stability of 7 nm AuNPs in the blood and a 4-5 times higher bone uptake compared to 14 nm AuNPs. The high affinity towards bone mineral was additionally shown with *in vitro* experiments with hydroxyapatite. For the future, the major challenge will consist in the design of probes with decent blood retention for tumor accumulation. The conjugation of molecules, which allow a tunable surface charge, to the HS-PEG-DAP building block, will fulfill the requirements for a prolonged blood retention time of DAP based coating ligands. Efforts in this direction are currently underway in our laboratories.

2.3 ^{99m}Tc Radiolabeling of Fe_3O_4-Au Core-Shell and Au-Fe_3O_4 Dumbbell-Like Nanoparticles

The work described in section 2.2 is based on coating ligands with a monothiol anchor for the NP surface. We wanted to extend the ligand system to a dithiolate anchoring group. A commonly used precursor for a dithiolate anchor is lipoic acid (LA), which can be readily reduced to dihydrolipoic acid (DHLA). Therefore, we investigated the conversion of the terminal hydroxyl group of compound **22** into an amine function for subsequent amide bond formation with LA (Scheme 8).[134]

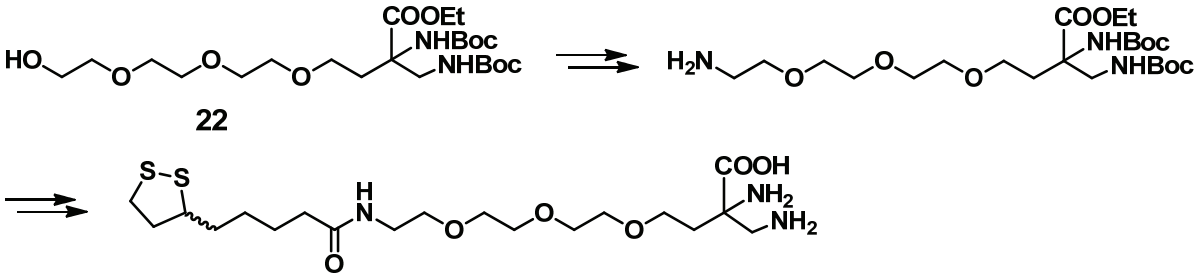

Scheme 8. The key intermediates for the synthesis of the DAP-containing lipoic acid derivative, starting from compound **22**.

In a first attempt of the synthesis, a direct azide formation was aspired *via* activation of the hydroxyl group with mesyl chloride and *in situ* S_N2 displacement with sodium azide. However, the yield was only 17% and it was shown when the mesylate of **22** was isolated, the azide could be obtained in an overall yield of 76%. Reduction of the azide to the amine was achieved either with palladium over carbon in hydrogen atmosphere or by means of the Staudinger reaction in the presence of triphenylphospine and water. Quite unexpectedly, these reactions afforded a side product which proved to be very difficult to separate from the product itself.[134] Due to this complication we decided to apply other tripodal chelators than DAP, such as DPA, picolylacetic acid and iminoacetic acid. As described in section 2.3.1, the synthetic pathway of these chelators and the conjugation to LA is substantially easier as compared to DAP-derivatives. In addition, the basic coating ligand structure, consisting of LA and PEG, was coupled to biotin as a model for a bioactive molecule. With the novel bifunctional coating ligands (bearing LA as an anchor, a PEG linker and the different chelators for the $[^{99m}Tc(CO)_3]^+$ fragment) we aimed at labeling magnetic Fe_3O_4-Au core-shell and Au-Fe_3O_4 Dumbbell-like NPs. We focused our attention on these nanocomposites

because it has recently been reported that the degradation products of IONPs increase free radical production in physiological environments which might lead to cell death.[135] Optimal surface coating is absolutely necessary to avoid degradation and the addition of a gold shell onto IONPs was described to be a promising approach to achieve the desired stability.[136] In general, the development of NP-based dual-modality probes for MRI and PET or SPECT is increasingly growing in importance. The main reason for this combination is the fact that T_2-weighted acquisitions with paramagnetic NPs contrast agents suffer from poor sensitivity and this modality cannot be used for real time imaging.[30] These limitations can be overcome by introducing a radiolabel and subsequent detection of the emitted γ-photons, which is a highly sensitive imaging technique. Moreover, PET-MRI scanners for clinical and SPECT-MRI for preclinical imaging have become commercially available. That is why the combination of paramagnetic NPs with a radiolabel was brought into focus by several research groups and there are three strategies to radiolabel paramagnetic NPs (summary of section 1.3): One strategy is based on bifunctional ligands with a chelate for the radionuclide and an anchor for the IONP surface. Torres and co-workers developed bisphosphonate ligands with a DPA-chelator for the $[^{99m}Tc(CO)_3]^+$ fragment or a dithiocarbamate chelator for $^{64}Cu^{II}$.[50-52] This approach involves initial radiolabeling of the ligands, followed by coating on the IONP surface. Another possibility to radiolabel IONPs is the covalent attachment of a chelator to the existing coating and subsequent labeling with a radionuclide. This concept was, for instance, carried out with DOTA for chelation of $^{64}Cu^{II}$.[112,137] The third strategy are intrinsically radiolabeled IONPs not requiring chelators for the radionuclides.[59] This was achieved by incorporating ^{111}In during the synthesis of IONPs or *via* adsorption of ^{69}Ge, radioactive As oxides or ^{89}Zr on the IONP surface.[57,64-66] Mareque-Rivas and co-workers showed that the $[^{99m}Tc(CO)_3]^+$ fragment can also be adsorbed on the IONP surface, presumably due to the high affinity to hydroxyl groups on the IONP surface.[62,63]

2.3.1 Synthesis of the Bifunctional Coating Ligands

The bifunctional ligand design has to meet several requirements; strong binding to the gold surface, strong chelation of the $[^{99m}Tc(CO)_3]^+$ moiety, high colloidal stability and facile syntheses. It has been shown in various studies that LA in its reduced form meets the criteria of strong gold-thiol binding and allows coupling to a linker *via* amide bond formation.[138] As a linker, we chose tetraethylene glycol because it is water soluble, cheap and the terminal hydroxyl groups are easily convertible into amines in a three step synthesis (Scheme 9).[139,140]

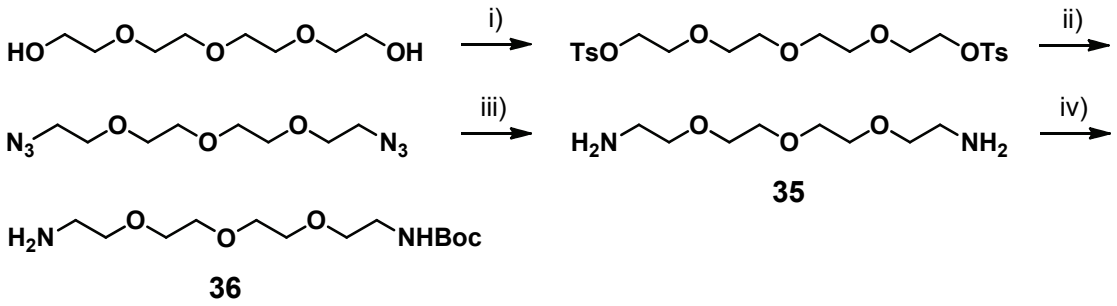

Scheme 9. Synthesis of the basic linker precursor **36**. i) TsCl, KOH, THF, 0-25 °C, 4 h, 99%; ii) NaN_3, MeCN, reflux, 18 h, 95%; iii) PPh_3, H_2O, THF, 25 °C, 5 h, 85%; iv) $(Boc)_2O$, CH_2Cl_2, 0-25 °C, 24 h, 99% (calculated for $(Boc)_2O$).

One terminal amine of compound **35** was protected with Boc to obtain compound **36**.[141] The chelators were generated at the second terminal amine through direct reductive *N*-alkylations with the aldehydes 2-pyridinecarboxaldehyde or ethyl glyoxylate (Scheme 10).[142]

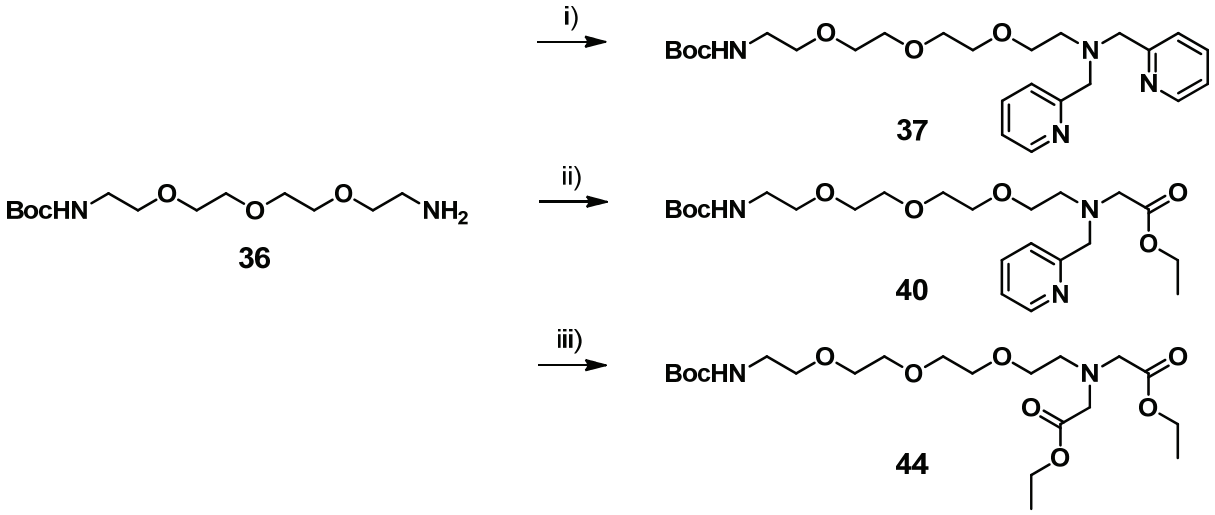

Scheme 10. Syntheses of the different chelator precursors **37**, **40** and **44**. i) $NaBH(OAc)_3$, 2-pyridinecarboxaldehyde, DCE, 0-25 °C, 4 h, 81%; ii) 2-pyridinecarboxaldehyde, $NaBH(OAc)_3$, ethyl glyoxylate, DCE, reflux-25 °C, 4 h, 70%; iii) $NaBH(OAc)_3$, ethyl glyoxylate, DCE, 0-25 °C, 4 h, 81%.

After deprotection of the Boc-group, the intermediates were conjugated to *in situ* produced mesyl-LA.[143] Ligand **39** was directly obtained after this step, whereas **43** and **47** required basic hydrolysis of the ethyl ester (Scheme 11). Since we did not intend to coat the NPs quantitatively with the chelator containing ligands, we synthesised compound **48** as a basic coating ligand with a terminal methyl ether, which is known to provide high colloidal stability (Scheme 12).[50] Moreover, we covalently attached the LA-PEG-NH_2 **49** moiety to *N*-hydroxysuccinimide activated d-biotin in order to introduce a biomolecule (Scheme 13). We

emphasize that basically any bioactive molecule or targeting function with a free carboxylic acid can be introduced at this point.

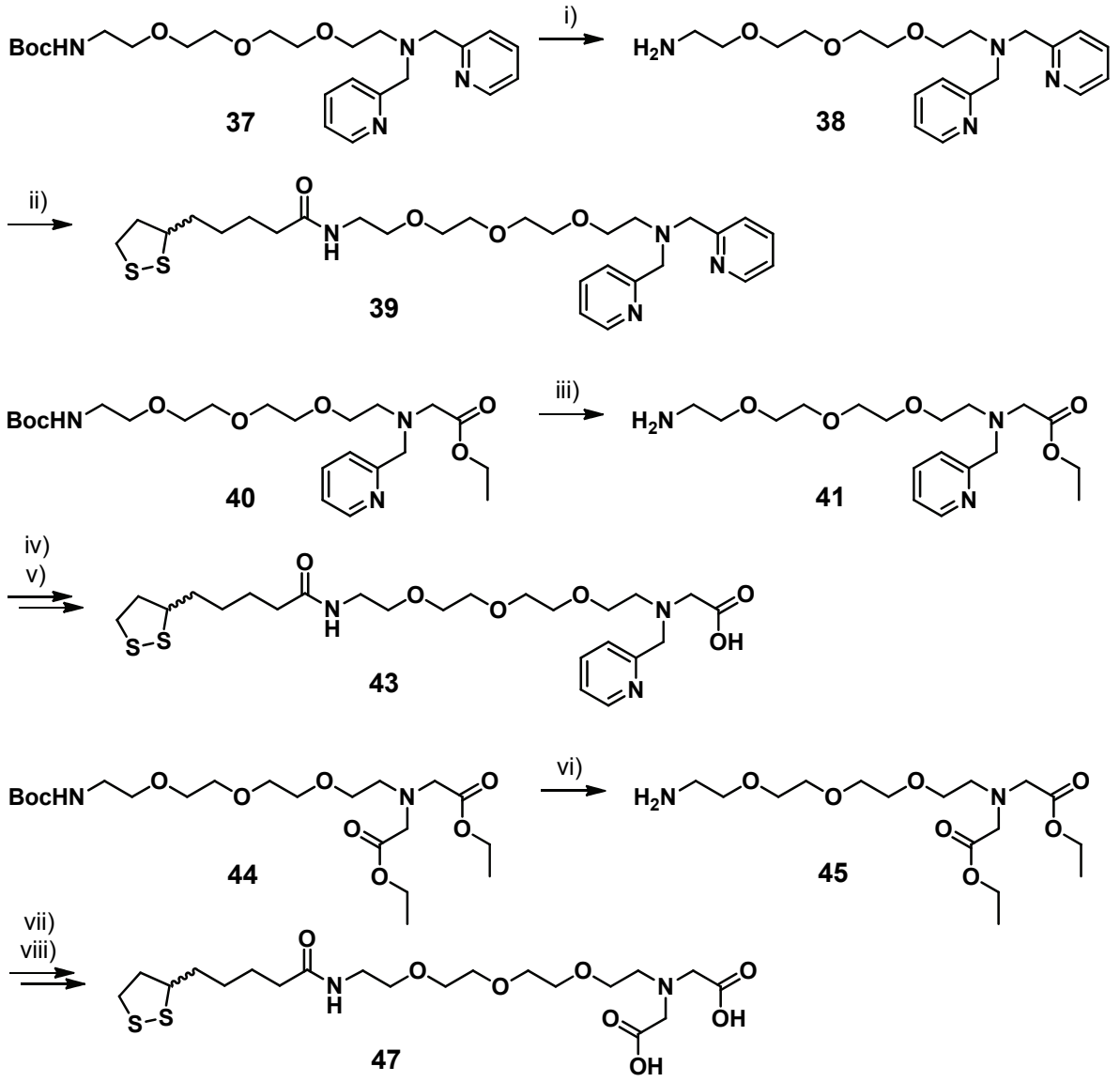

Scheme 11. Synthesis of the bifunctional coating ligands **39**, **43** and **47**. i) HCl sat. Et_2O, 25 °C, 0.5 h, 99%; ii) mesyl-LA (*in situ* produced), TEA, CH_2Cl_2, 25 °C, 19 h, 45%; iii) HCl sat. Et_2O, 25 °C, 0.5 h, 99%; iv) mesyl-LA (*in situ* produced), TEA, CH_2Cl_2, 25 °C, 17 h, 74%; v) MeOH / 1 M LiOH (1:1), 25 °C, 0.5 h, 92%; vi) HCl sat. Et_2O, 25 °C, 0.5 h, 99%; vii) mesyl-LA (*in situ* produced), TEA, CH_2Cl_2, 25 °C, 17 h, 74%; viii) MeOH / 1 M LiOH (1:1), 25 °C, 1.5 h, 86%.

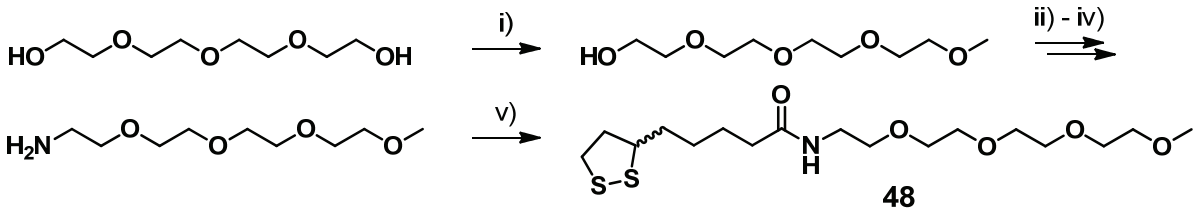

Scheme 12. Synthesis of the basic coating ligand **48**. i) CH_3I, NaH (60% suspension in oil), THF, 0-25 °C, 10 h, 23%; ii) TsCl, NaH, THF, 0-25 °C, 2 h, 99%, iii) NaN_3, MeCN, reflux, 18 h, 95%; vi) PPh_3, H_2O, THF, 25 °C, 5 h, 88%; v) LA, DCCI, DMAP, CH_2Cl_2, 0-25 °C, 18 h, 84%.

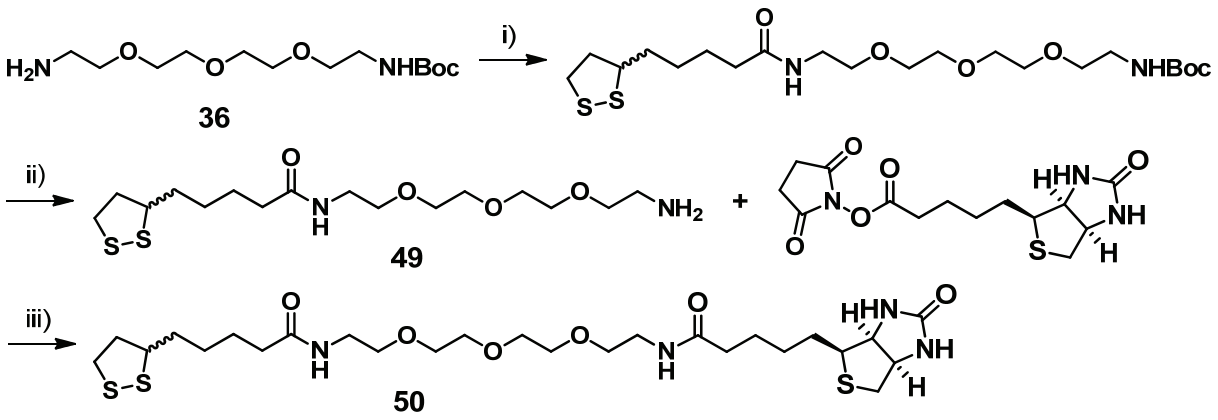

Scheme 13. Synthesis of the coating ligand **50** with the bioactive molecule d-biotin. i) LA, DCCI, DMAP, CH_2Cl_2, 0-25 °C, 21 h, 79%; ii) CH_2Cl_2 / TFA (1:1), 25 °C, 1 h, 99%; iii) TEA, DMF, H_2O, 25 °C, 48 h, 30%.

For the experiments with Au-Fe_3O_4 Dumbbell NPs we additionally synthesized the DAP based coating ligand **51** with a mono-thiol anchor for the gold surface, the ligand system that is described in section 2.2.1 (Scheme 14).

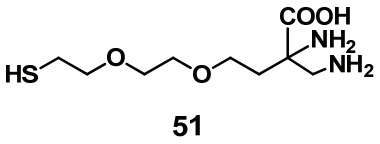

Scheme 14. The DAP based coating ligand **51** for the experiments with Au-Fe_3O_4 Dumbbell-like NPs.

The dopamine derivative **52** was synthesized as a coating ligand for the iron oxide surface of heterostructured Au-Fe_3O_4 Dumbbell-like NPs (Scheme 15). It is well known that catechols are excellent ligands for Fe_3O_4 surfaces and conjugation to PEG yields in highly stable probes while maintaining the magnetic properties.[144,145]

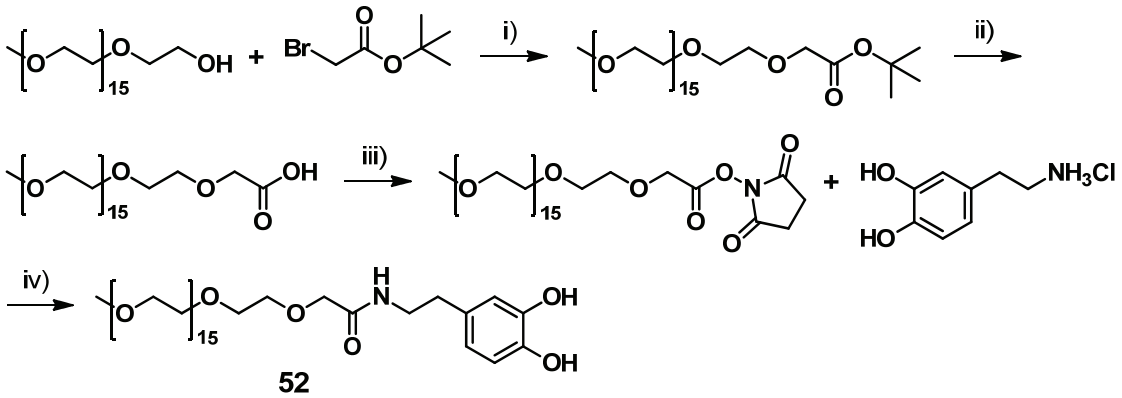

Scheme 15. Synthesis of the dopamine derivative **52**. i) NaH (60% suspension in oil), THF, 25 °C, 8 h, 91%; ii) CH_2Cl_2 / TFA (2:1), 25 °C, 3 h, 99%; iii) NHS, DCCI, CH_2Cl_2, DMF, 25 °C, 17 h, 64%; iv) TEA, DMF, 25 °C, 48 h, 30%.

2.3.2 Synthesis and Phase Transfer of Fe_3O_4-Au Core-Shell NPs

Gold shells around the IONP core can be formed along two approaches; directly on the IONP surface[28,146-150] or onto a middle layer, consisting of silica or a polymer which serves as a bridge between the IONP core and the gold shell.[136,151-155] We synthesized NPs with the gold shell directly on the IONP core according to a reported procedure.[156] TEM analysis of the as-synthesized IONPs showed an average diameter of 5.2 ± 0.4 nm. After addition of a gold shell, the average diameter was measured to be 7.9 ± 0.4 nm, suggesting an average Au shell thickness of ~1.4 nm, which is comparable to the values described in literature (Figure 21).[156] The hydrophobic NPs were further analyzed with EDX. The spectrum exhibited the characteristic peaks for Fe and Au (Figure 22). The Fe and Au concentrations (16 mM and 42 mM) in the hexane solution of hydrophobic core-shell NPs were determined with inductively coupled plasma mass spectrometry (ICP-MS) and the Fe/Au ratio is in the range of the data in literature.[157]

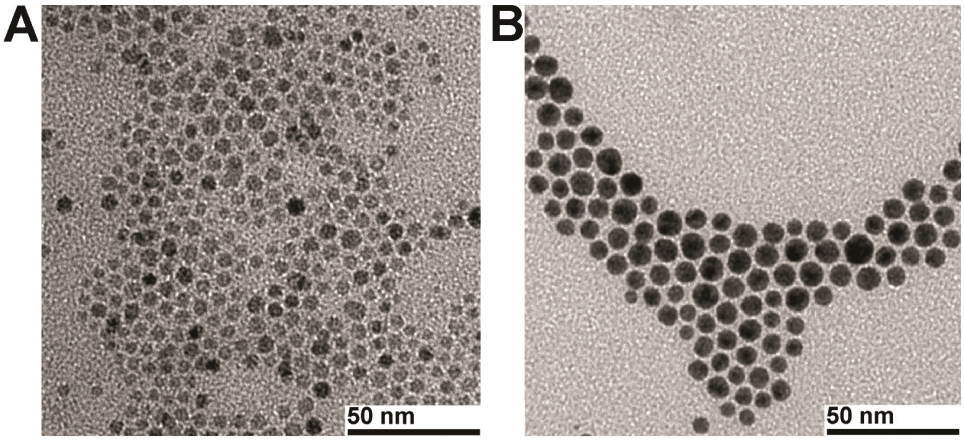

Figure 21. Representative TEM micrographs of (A) Fe_3O_4 NPs of 5.2 ± 0.4 nm and (B) Fe_3O_4-Au core-shell NPs of 7.9 ± 0.4 nm.

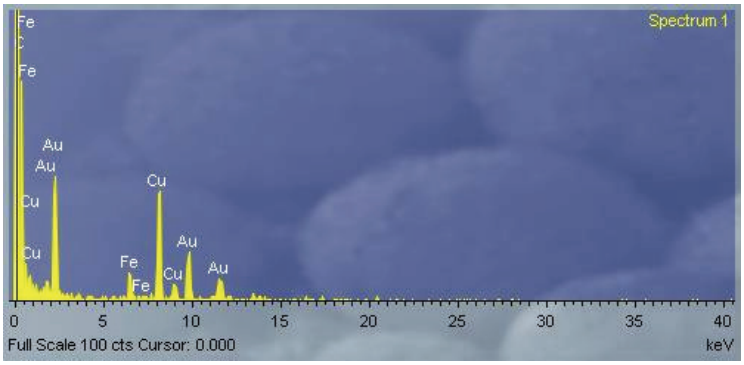

Figure 22. EDX spectrum of hydrophobic Fe_3O_4-Au core-shell NPs (Cu peaks originate from the formvar-coated copper grid).

A crucial step towards water soluble NPs is the transfer from the organic into the aqueous phase by replacing the hydrophobic coating with the LA-based ligands. We pursued for this a biphasic approach with the NPs in hexane on the top of a methanol phase containing the hydrophilic ligands. Before addition of the hexane phase, the disulfide of the LA moiety was reduced upon vortexing a mixture of the reducing agent tris(2-carboxyethyl)phosphine (TCEP) and the ligands in methanol. After vigorous stirring for 20 min, the hexane phase became completely colorless, indicating a successful functionalization. The hydrophilic core-shell NPs were redispersed in PBS pH 7.4 after evaporation of methanol. A threefold excess of the basic coating ligand **48** relative to the other ligands resulted in highly water soluble NP conjugates. NPs coated with **48** and **39** (3:1 ratio) or **48**, **39** and **50** (3:1:1 ratio) started to precipitate after 1 h, indicating not sufficiently high hydrophilicity of these particular NPs with the pyridine groups. However, once carboxylic acids are part of the coating ligands, the derivatized NPs remained highly soluble. In order to remove excess coating ligand and oxidized TCEP the NPs were purified with a PD-10 size exclusion column (Sephadex G-25 medium, PBS as mobile phase). This purification step is necessary for radiolabeling experiments since free ligand would compete with ligands attached to the NPs and, hence, lower the RCYs. DLS measurements of the purified NP conjugates showed a HDD of 11 nm when coated with **48** and **43** (3:1 ratio), as well as with **48** and **47** (3:1 ratio). With the coating layer containing ligand **50**, both HDDs increased to 13 nm. The HDD values did not change after storage at 4 °C for two weeks, demonstrating the high colloidal stability of these NPs. The SPR band was found to be at 547 nm for hydrophobic and hydrophilic NPs, which is consistent with the values described in literature (Figures 23 and 24).[156]

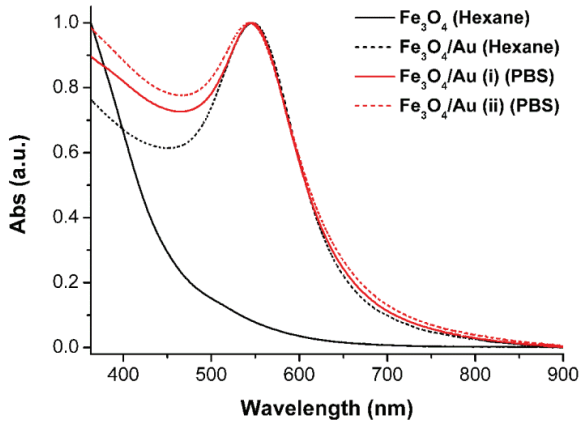

Figure 23. UV-Vis spectra of hydrophobic and hydrophilic Fe_3O_4-Au core-shell NPs, coated with (i) ligand **48** and **43** (ratio 3:1); (ii) ligand **48**, **43** and **50** (ratio 3:1:1).

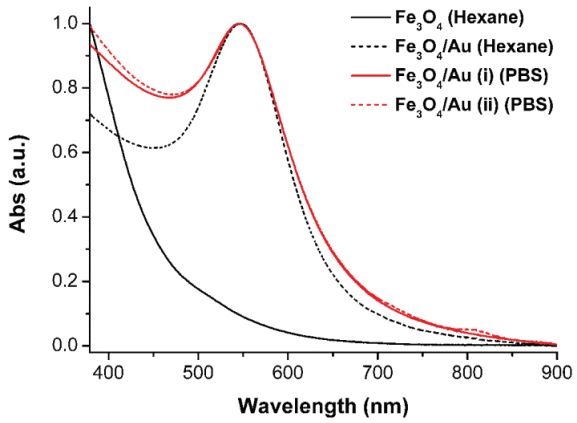

Figure 24. UV-Vis spectra of hydrophobic and hydrophilic Fe_3O_4-Au core-shell NPs, coated with (i) ligand **48** and **47** (ratio 3:1); (ii) ligand **48**, **47** and **50** (ratio 3:1:1).

2.3.3 Synthesis and Phase Transfer of Au-Fe_3O_4 Dumbbell-Like NPs

Heterostructured Dumbbell-like NPs were synthesized according to a procedure developed by Sun and co-workers, comprising the formation of AuNPs in a first step and the decomposition of iron pentacarbonyl on the AuNP surface in a second step.[158] AuNP cores had an average diameter of 10.1 ± 0.6 nm and the as-synthesized Au-Fe_3O_4 Dumbbell-like NPs 26.1 ± 1.6 nm (Figure 25). ICP-MS analysis of the NPs dispersed in hexane revealed an Fe concentration of 38 mM and 29 mM for Au. The SPR band of AuNPs was at 524 nm, whereas Dumbbell-like NPs showed a red-shift of 16 nm and a significantly lower absorbance, similarly as reported in literature (Figure 26).[158]

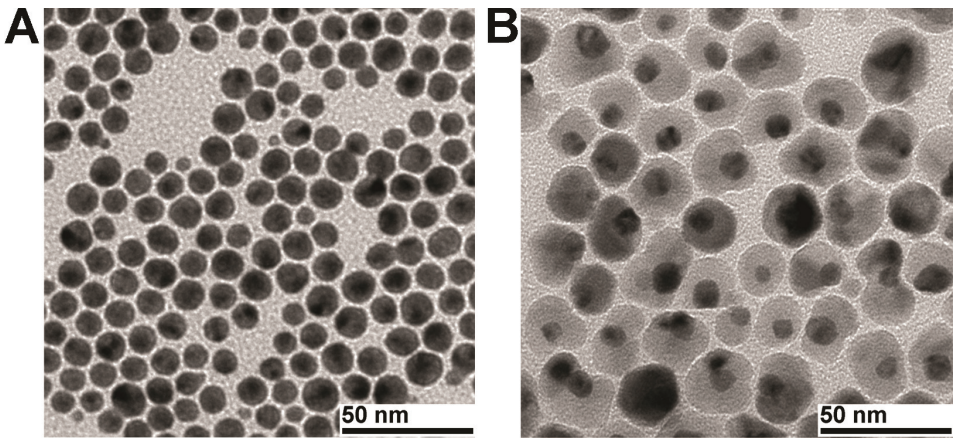

Figure 25. Representative TEM micrographs of (A) AuNPs of 10.1 ± 0.6 nm and (B) Au-Fe_3O_4 Dumbbell-like NPs of 26.1 ± 1.6 nm (AuNP component appears dark because of the heavy atom effect).

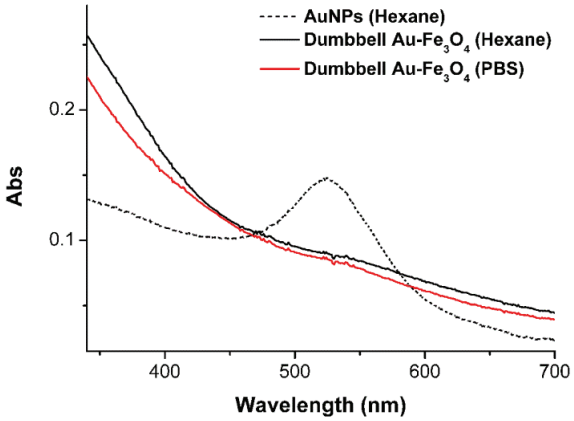

Figure 26. UV-Vis spectra of hydrophobic and hydrophilic Au-Fe_3O_4 Dumbbell-like NPs.

For the phase transfer, several methods were carried out; mixing hydrophobic NPs with ligand **52** in $CHCl_3$/DMF under basic conditions[145] or generating a water soluble intermediate coated with 1,2-dihydroxybenzoic acid followed by substitution with **52**.[159] These attempts gave only poorly soluble NP conjugates, assuming that the hydrophobic oleylamine coating on the AuNP surface was still intact and subsequently caused aggregation in aqueous media. Therefore, we used tetramethylammonium hydroxide (TMAOH) which stabilizes the IONP surface *via* interactions between $[NMe_4]^+$ cations and adsorbed hydroxide anions.[145] With this method extremely stable Au-Fe_3O_4 Dumbbell-like NPs can be obtained.[160] We observed, however, that these NPs did not run through the PD-10 column, a prerequisite for the radiolabeling experiments. Therefore, we synthesized compound **52** and coating with this ligand was successfully achieved by adding **52** directly after the phase transfer with TMAOH. These NP-conjugates can be readily purified with PD-10 columns. The derivatized Dumbbell-like NPs exhibited a HDD of 35 nm and the NPs showed high colloidal stability at 4 °C for two weeks. Particularly noteworthy is the fact that the AuNP surface was not coated with a specific thiol-containing ligand at this stage. This allowed us to evaluate a so-called pre-labeling, which means the labeling of the ligands **39**, **43**, **47** and **51** with the $[^{99m}Tc(CO)_3]^+$ fragment, followed by the attachment on the AuNP surface.

2.3.4 ^{99m}Tc Radiolabeling of Fe_3O_4-Au Core-Shell NPs

For the labeling of the core-shell NP conjugates, $[^{99m}Tc(OH_2)_3(CO)_3]^+$ was prepared with the commercially available IsoLink™ kit.[124] The three water ligands in $[^{99m}Tc(OH_2)_3(CO)_3]^+$ are labile and can be exchanged with the chelators attached to the NP surface (Figures 27 & 28).

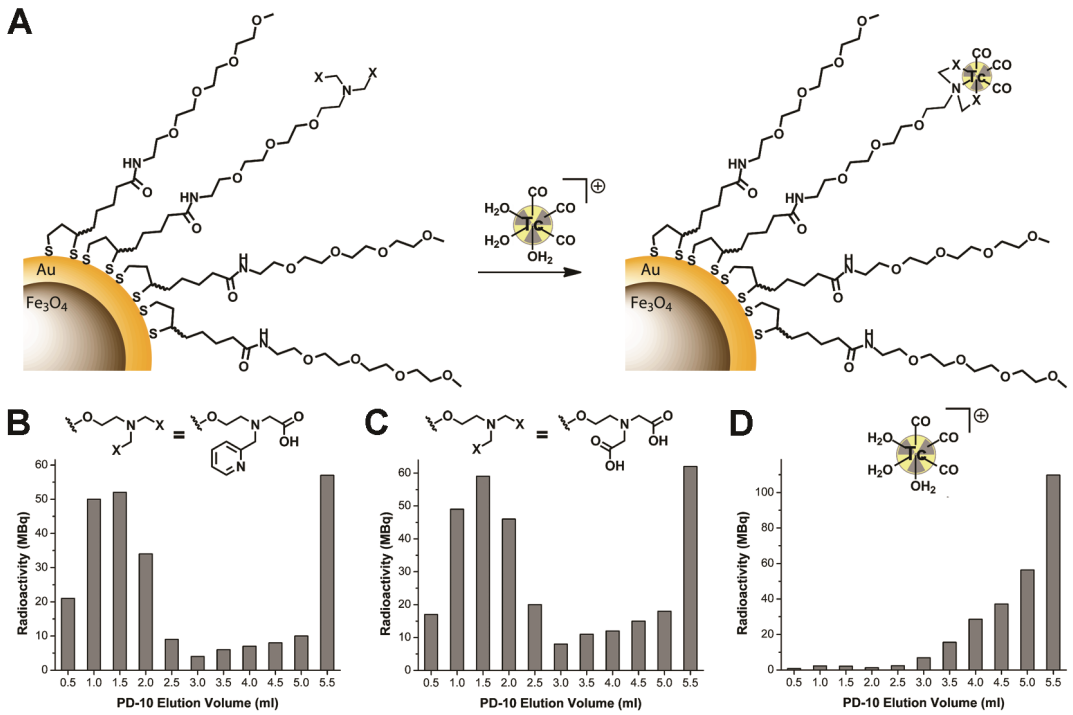

Figure 27. Radiolabeling of Fe_3O_4-Au core-shell NPs with an illustrative scheme of the labeling procedure (A) and the PD-10 size exclusion chromatograms after incubation at 50 °C for 2 h of NPs containing chelator **43** (B), **47** (C) and a control chromatogram with $[^{99m}Tc(OH_2)_3(CO)_3]^+$ only (D). Please note that 0.5 ml fractions were collected and the last fraction was the remainder activity in the PD-10 column. The very first 0.5 ml fraction is not shown in any of the chromatograms since it always was mobile phase only.

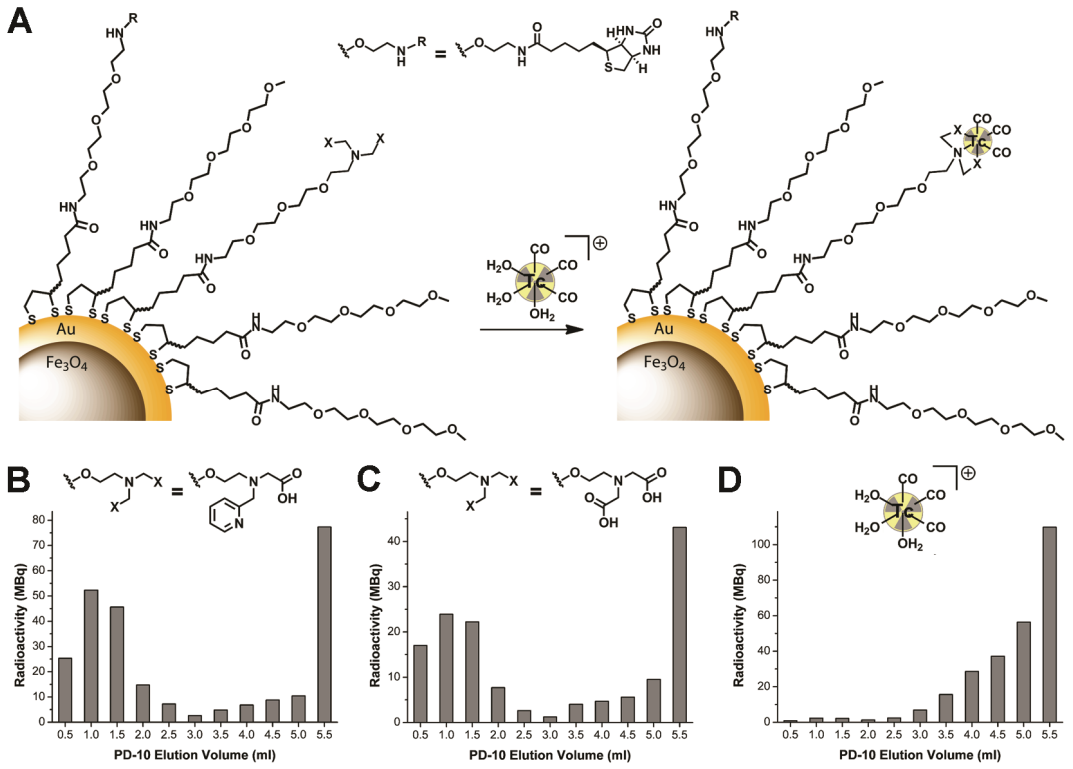

Figure 28. Radiolabeling of Fe_3O_4-Au core-shell NPs with an illustrative scheme of the labeling procedure (A) and the PD-10 size exclusion chromatograms after incubation at 50 °C for 2 h of NPs containing chelator **43** (B), **47** (C) and a control chromatogram with $[^{99m}Tc(OH_2)_3(CO)_3]^+$ only (D).

Typically, $[^{99m}Tc(OH_2)_3(CO)_3]^+$ in saline was added to NP solutions in PBS (final NP concentration ~1 mg/ml). As described in section 2.2.3, we monitored the labeling progress by HPLC, equipped with a size-exclusion column and two detectors (UV-Vis and γ-counter). Since the radio flow monitors in the γ-counter contain magnetic components interacting with the magnetic core-shell NPs, we could not follow this method since the NPs literally got stuck to the detector and the equipment could not be used anymore until the activity decayed. To avoid this problem, we had to analyze labeling yields with a PD-10 column by collecting 0.5 ml fractions and measuring the activity in the fractions with a dose calibrator, a similar analysis as recently described by Torres and co-workers with radiolabeled IONPs.[50] NPs were typically found in the first four purple colored fractions (0.5 – 2.0 ml) when the column was loaded with 1.5 ml reaction mixture (Figures 27B, 27C, 28B, 28C). The overall RCY varied from 24% to 52%. NPs coated with ligand **47** showed generally a lower RCY since it is a weaker chelator for the $[^{99m}Tc(CO)_3]^+$ fragment than ligand **43**.[161] A significant loss of activity during the transfer to the PD-10 column was observed, likely due to non-specific interactions with the glass wall and syringe material (Table 3). The d-biotin containing NPs exhibited a lower RCY compared to NPs coated only with ligand **48** and chelators **43** or **47**, consistent with the fact that the Au surface is coated with less chelator in the biotin-coating (20%) than the non-biotin coating (25%). Loading a PD-10 column with 1.5 ml $[^{99m}Tc(OH_2)_3(CO)_3]^+$ solution yields only 2% of the activity in the first four fractions, indicating a significantly longer retention of free $[^{99m}Tc(OH_2)_3(CO)_3]^+$ as compared to NPs labeled with the $[^{99m}Tc(CO)_3]^+$ fragment.

Table 3. Activity measurements of Fe_3O_4-Au core-shell NP labeling experiments.

Coating	*Reaction Vial[a] [MBq]*	*PD-10[b] [MBq]*	*NPs[c] [MBq]*	*RCY[d]*
48, **43**	302	262	157	52%
48, **47**	391	338	174	45%
48, **43**, **50**	324	263	138	43%
48, **47**, **50**	296	146	71	24%
Control[e]	427	274	6	2%

[a] Activity after incubation at 50 °C for 2 h; [b] Activity loaded on PD10 column; [c] Combined activity from the fractions 0.0 – 2.0 ml; [d] Radiochemical yield; [e] Control experiment, 1.5 ml $[^{99m}Tc(OH_2)_3(CO)_3]^+$ loaded on a PD-10 column.

2.3.5 ^{99m}Tc Radiolabeling of Au-Fe_3O_4 Dumbbell-Like NPs

As aforementioned, the Dumbbell-like NPs were labeled along a pre-labeling approach. In a first step, ^{99m}Tc complexes of ligands **39**, **43**, **47** and **51** were quantitatively obtained after reacting $[^{99m}Tc(OH_2)_3(CO)_3]^+$ with 0.1 mM ligand solutions at 70 °C for 30 min (Figure 29).

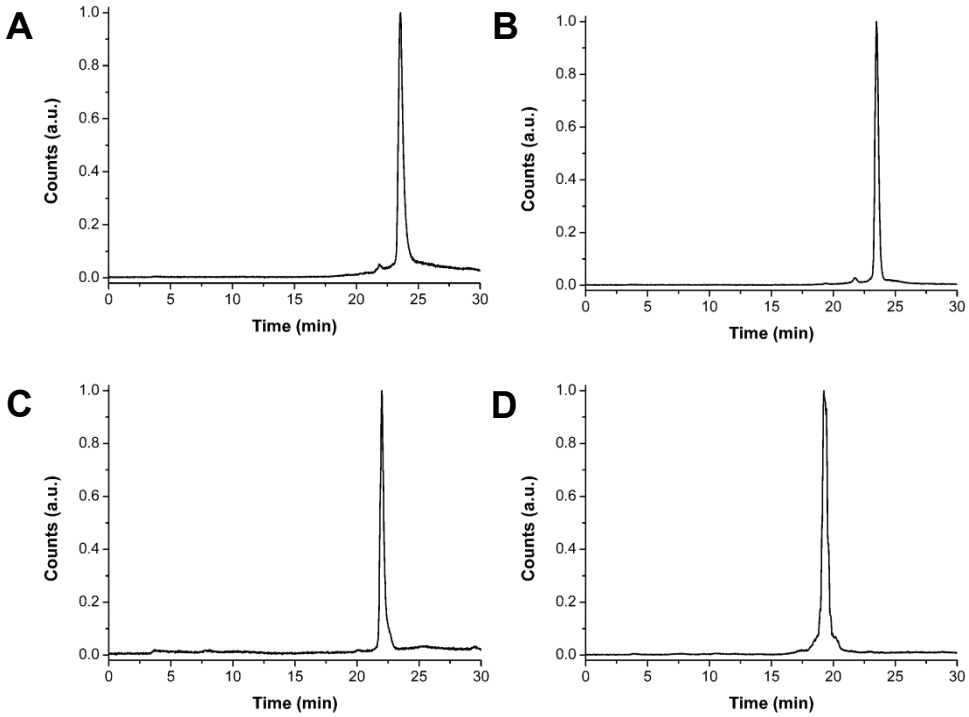

Figure 29. Normalized HPLC analysis of (A) ^{99m}Tc labeled ligand **39** (retention time 23.57 min), (B) ^{99m}Tc labeled ligand **43** (retention time 23.48 min), (C) ^{99m}Tc labeled ligand **47** (retention time 22.00 min) and (D) ^{99m}Tc labeled ligand **51** (retention time 19.23 min).

In the as-synthesized ^{99m}Tc complexes the disulfides of the LA moieties were reduced by the addition of excess TCEP. Then, the ^{99m}Tc complexes with a mono- or dithiol-anchor for the Au surface were incubated with Dumbbell-like NP solution at 50 °C for 60 min (Figure 30A). Analyses were performed with PD-10 separation and activity measurements of the collected fractions. The RCYs, ranging from 35% to 59%, confirm the ^{99m}Tc pre-labeling approach to be very convenient for Dumbbell-like NPs (Figures 30B-30E). The monothiol ligand **51** gave higher yields than the dithiol ligands **39**, **43** and **47** (Table 4). This difference might be caused by rather quick reoxidation of the dithiol ligands and the concomitant lower affinity to the Au surface. When the ^{99m}Tc complexes are incubated with Dumbbell-like NPs without the TCEP-reduction, the RCYs were in average 20% lower (Figure 31 and Table 5).

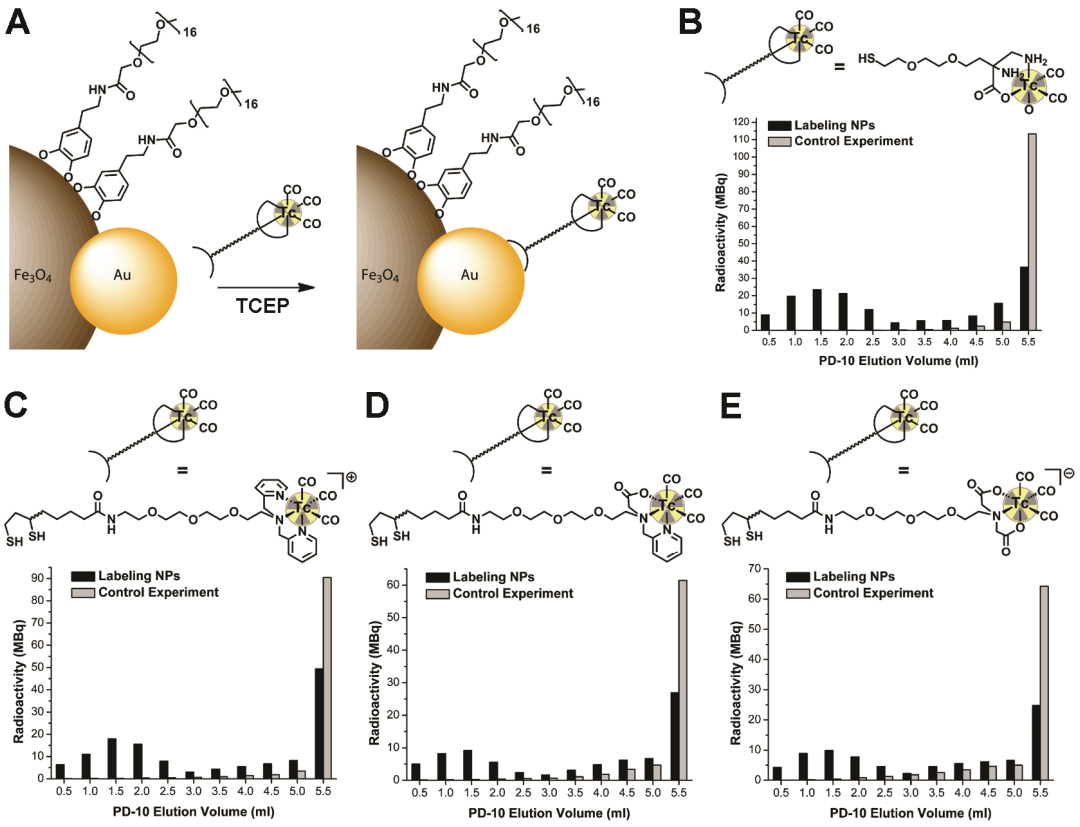

Figure 30. Radiolabeling of Au-Fe_3O_4 Dumbbell-like NPs with an illustrative scheme of the labeling procedure (A) and the PD-10 size exclusion chromatograms after incubation at 50 °C for 60 min of NPs and ^{99m}Tc complexes containing chelator **51** (B), **39** (C), **43** (D), **47** (E) and the corresponding control chromatograms (including reduction with TCEP).

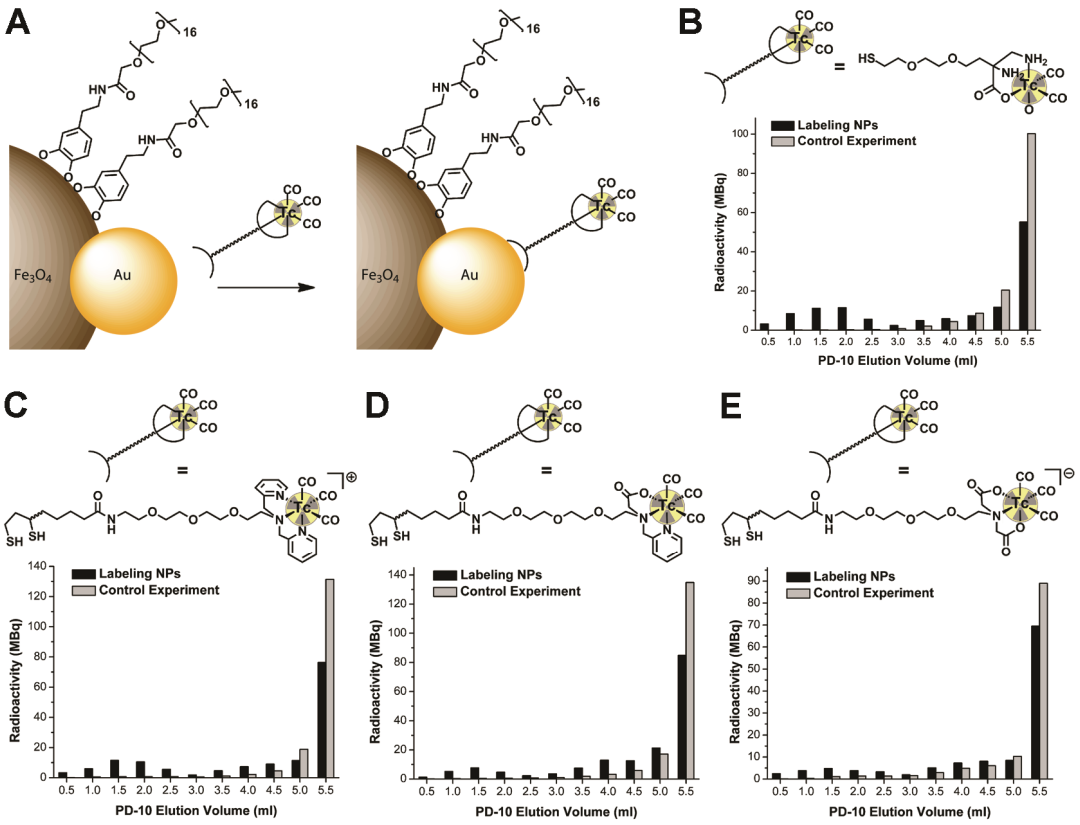

Figure 31. Analoguous radiolabeling procedure as in Figure 30, but without the use of TCEP.

Table 4. Activity measurements of Au-Fe_3O_4 Dumbbell-like NP labeling experiments (**including** reduction with TCEP).

Coating	*Reaction Vial*[a] *[MBq]*	*PD-10*[b] *[MBq]*	*NPs*[c] *[MBq]*	*RCY*[d]
39, **52**	157	141	59	38%
Control[e]	120	109	1	1%
43, **52**	87	77	30	35%
Control[e]	84	75	1	1%
47, **52**	86	79	35	41%
Control[e]	92	81	2	2%
51, **52**	144	130	85	59%
Control[e]	131	124	1	1%

[a] Activity after incubation at 50 °C for 2 h; [b] Activity loaded on PD-10 column; [c] Combined activity from the fractions 0.0 – 2.0 ml; [d] Radiochemical yield; [e] Control experiments, 1.5 ml ^{99m}Tc complex loaded on a PD-10 column.

Table 5. Activity measurements of Au-Fe_3O_4 Dumbbell-like NP labeling experiments (**without** reduction with TCEP).

Coating	*Reaction Vial*[a] *[MBq]*	*PD-10*[b] *[MBq]*	*NPs*[c] *[MBq]*	*RCY*[d]
39, **52**	168	150	37	22%
Control[e]	185	163	3	1%
43, **52**	172	158	21	12%
Control[e]	176	159	2	1%
47, **52**	119	109	18	15%
Control[e]	117	106	4	3%
51, **52**	172	163	40	23%
Control[e]	146	137	1	1%

[a] Activity after incubation at 50 °C for 2 h; [b] Activity loaded on PD-10 column; [c] Combined activity from the fractions 0.0 – 2.0 ml; [d] Radiochemical yield; [e] Control experiments, 1.5 ml ^{99m}Tc complex loaded on a PD-10 column.

We also observed that TCEP is necessary for the NP-labeling with the complex containing the monothiol ligand **51**, resulting in 26% higher RCY as compared to labeling without TCEP-reduction. This indicates the presence or formation of disulfides in the absence of TCEP,

however, reoxidation seem to be less of a problem for monothiol ligand **51**. Moreover, compound **51** is less bulky than the LA-derivatives, which in turn might lead to a higher RCY. In control experiments the ^{99m}Tc complexes only were loaded on the PD-10 column. As shown in Figures 30 and 31, free ^{99m}Tc complexes have distinctly different retention times than ^{99m}Tc labeled NPs.

2.3.6 Conclusion

With this work we demonstrated the feasibility to radiolabel gold-containing magnetic nanoparticles with the $[^{99m}Tc(CO)_3]^+$ fragment. On the one hand, Fe_3O_4-Au core-shell NPs were labeled in a direct approach, in which the gold surface was coated with bifunctional ligands, consisting of a anchor for the metal surface and chelators for the $[^{99m}Tc(CO)_3]^+$ moiety. Au-Fe_3O_4 Dumbbell-like NPs, on the other hand, were radiolabeled *via* a pre-labeling strategy, where the ^{99m}Tc complexes were firstly synthesized and then coated on the gold surface. Both approaches resulted in average to good radiochemical yields. These experiments can form the basis for the development of potential, NP-based SPECT/MRI dual-modality imaging agents.

2.4 Conjugation of a DAP-Based Chelator to the *para*-OH of L-Tyrosine and Biological Evaluation of the Corresponding *fac*-[^{99m}Tc(CO)$_3$]$^+$ Complex

One of the intermediates along the syntheses of the bifunctional coating ligands HS-PEG-DAP (**26** and **51**) comprises a terminal hydroxyl group, a PEG spacer and the fully protected DAP chelator. We were very much interested in conjugating this intermediate to the *para*-OH of L-Tyrosine to obtain a ^{99m}Tc labeled amino acid (Scheme 16).

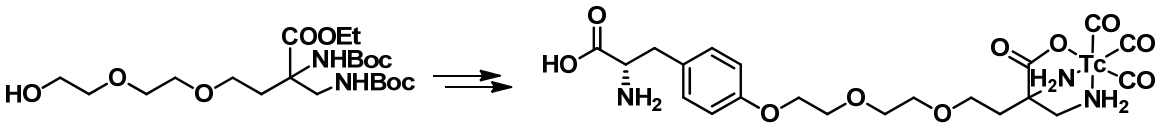

Scheme 16. ^{99m}Tc labeled L-tyrosine, using HO-PEG-DAP as starting compound.

Our interest arose from the fact that radiolabeling of amino acids is an important strategy to obtain highly sensitive and specific radiopharmaceuticals for cancer imaging.[162] A widely used neuroimaging agent with excellent performance for the diagnosis of brain tumors is *O*-^{18}F-fluoroethyl-L-tyrosine (^{18}F-FET).[163] The key characteristics of this tracer are low accumulation in cortical normal tissue, relatively slow blood clearance and high uptake into tumor tissue due to enhanced amino acid metabolism and protein synthesis in tumors compared to normal peripheral tissue.[164] It has been shown that the uptake of ^{18}F-FET in tumor cells occurs *via* the L-amino acid transport (LAT) system and the stereochemistry is absolutely essential since the D-isomer showed significantly lower accumulation in tumor tissue.[165] Another crucial feature of ^{18}F-FET is its high *in vivo* stability and lack of metabolite formation which could lead to accumulation of activity in non-tumor tissue.[166] Based on this fact it appears that conjugation of a radiolabel to the *para*-OH group of L-tyrosine is a reasonable approach to obtain metabolically stable tracers. This concept has also been applied for ^{99m}Tc compounds, whereas a chelator for the ^{99m}Tc core is required as compared to ^{18}F tracers. Following this approach, Yang and co-workers attached 1,4,8,11-tetra-azacyclotetradecane as a chelator to the *para*-OH moiety, yielding the ^{99m}Tc^V dioxo complex.[167] They observed moderate tumor uptake in breast tumor bearing rats, however, a metabolite analysis was not carried out throughout this study. Another example of a ^{99m}Tc labeled L-tyrosine derivative was published by Rösch and co-workers. In their work, they synthesized the tridentate ligand bearing *O*-(*N*,*N*-bis(carboxymethyl)aminoethyl)-L-tyrosine

for the labeling with the *fac*-[^{99m}Tc(CO)$_3$]$^+$ fragment.[168] Nevertheless, *in vitro* and *in vivo* studies have not been published with this compound. To the best of our knowledge, these are the only examples described in literature in context with ^{99m}Tc labeled L-tyrosine derivatives. Therefore, we developed a synthetic pathway to synthesize the aforementioned ^{99m}Tc labeled L-tyrosine derivative and we evaluated this compound in C6-xenograft bearing mice. A particular focus lied on the investigation of the metabolic stability. Due to an unexpected uptake in the gallbladder, further studies with healthy mice were performed.

2.4.1 Synthesis of the Ligand Tyr-PEG-DAP

The most important step in the synthesis of the target compound Tyr-PEG-DAP **55** is the coupling between the free hydroxyl group of **53** with the *para*-OH of the protected L-tyrosine derivative. A very powerful reaction for this type of coupling is the Mitsunobu methodology. In a first attempt we used diisopropyl azodicarboxylate (DIAD) and triphenylphosphine in tetrahydrofuran.[169] Further experiments showed that performing the reaction with DIAD led to a higher yield of **54** than with diethyl azodicarboxylate (DEAD) (58% compared to 49%). An explanation for this observation could be that less hydrazide byproducts are formed since DIAD is sterically more hindered than DEAD. After linking **53** to enantiomerically pure L-tyrosine precursor, compound **54** is no longer a racemate, it becomes a diastereomeric mixture. Nevertheless, the two diastereomers of **54** could not be separated with silica gel column chromatography and we continued the work without further separation, assuming that the distant chelator does not interfere with the bioactivity of enantiopure L-tyrosine. Compound **55** was finally obtained in 62% yield by basic ester hydrolysis of the ethyl- and methyl esters and subsequent deprotection of the Boc-groups under acidic conditions (Scheme 17).

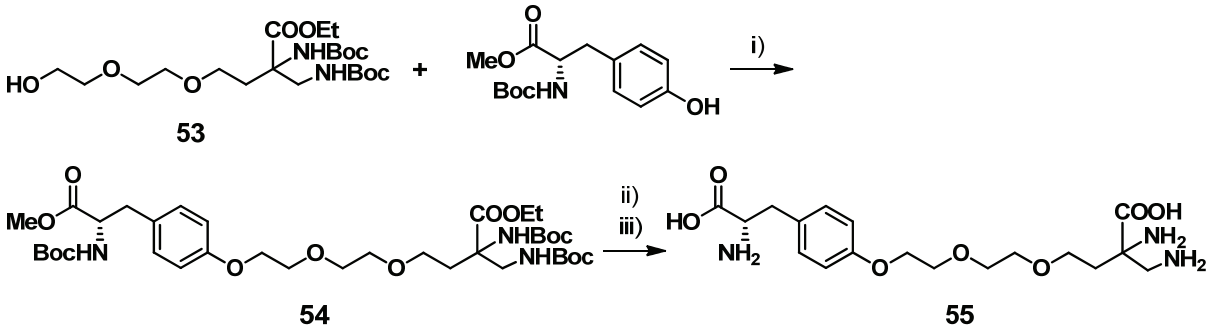

Scheme 17. Synthesis of the ligand Tyr-PEG-DAP **55**. i) DIAD, PPh_3, THF, 0-20°C, 24 h, 58%; ii) 1 M NaOH / MeOH, 85 °C, 11 h; iii) 1 M HCl, 90 °C, 12 h, 62% (ii and iii together). The stereochemistry of the DAP chelating moiety is omitted for simplicity.

2.4.2 Synthesis of the Complexes *fac*-[(Tyr-PEG-DAP)-M(CO)$_3$] (M = Re, ^{99m}Tc)

Due to the fact that analytical HPLC equipped with a γ-detector is the only method to characterize ^{99m}Tc compounds, the Re^{I} complex **56** was synthesized in order to compare the HPLC retention times after radiolabeling. Firstly, the common precursor *fac*-[Re(OH$_2$)$_3$(CO)$_3$]$^+$ was obtained quantitatively in a microwave reaction in water, starting from [ReBr(CO)$_5$]. Secondly, the tripodal ligand **55** was added and the mixture was stirred at 110 °C for 12 min under microwave irradiation (Scheme 18).

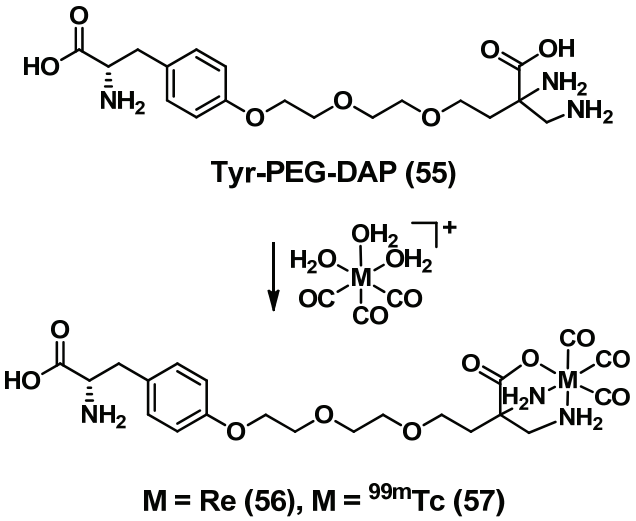

Scheme 18. Complexation of the ligand Tyr-PEG-DAP **55** with *fac*-[M(OH$_2$)$_3$(CO)$_3$]$^+$ (M = Re **56**, ^{99m}Tc **57**). The stereochemistry of the DAP chelating moiety is omitted for simplicity).

Purification with preparative HPLC afforded **56** in 45% yield as a diastereomeric mixture. HPLC analysis of **56** revealed mainly one peak at 17.5 min retention time (Figure 33). The IR spectrum of **56** showed two distinct CO vibrations at 2027 and 1908 cm^{-1}, which are characteristic for the *fac*-[Re(CO)$_3$]$^+$ core. The HR-ESI-MS spectra showed one dominant peak with the expected isotopic pattern at [M-H]$^-$ = 668.1254 m/z. NMR analysis of **56**, especially its ^{1}H NMR spectrum as compared to the one of compound **55**, uncovered some interesting features that underpin the expected coordination mode of the *fac*-[Re(CO)$_3$]$^+$ core (Figure 32). While the two diastereotopic 2H^a protons in **55** appear as a sharp singlet at δ 3.28, the signals of the two protons are clearly split and shifted to higher field (δ 2.56 and δ 2.28) upon coordination of the DAP moiety to the metal center. A reason for this observation is the increased rigidity of the chelator due to the coordination and, therefore, a reduced dynamic symmetry. The splitting of the signal for the 2H^d protons is additional evidence for

this rigidity. Furthermore, the coordination of the DAP ligand to the metal leads to a high field shift of the amine proton signals.

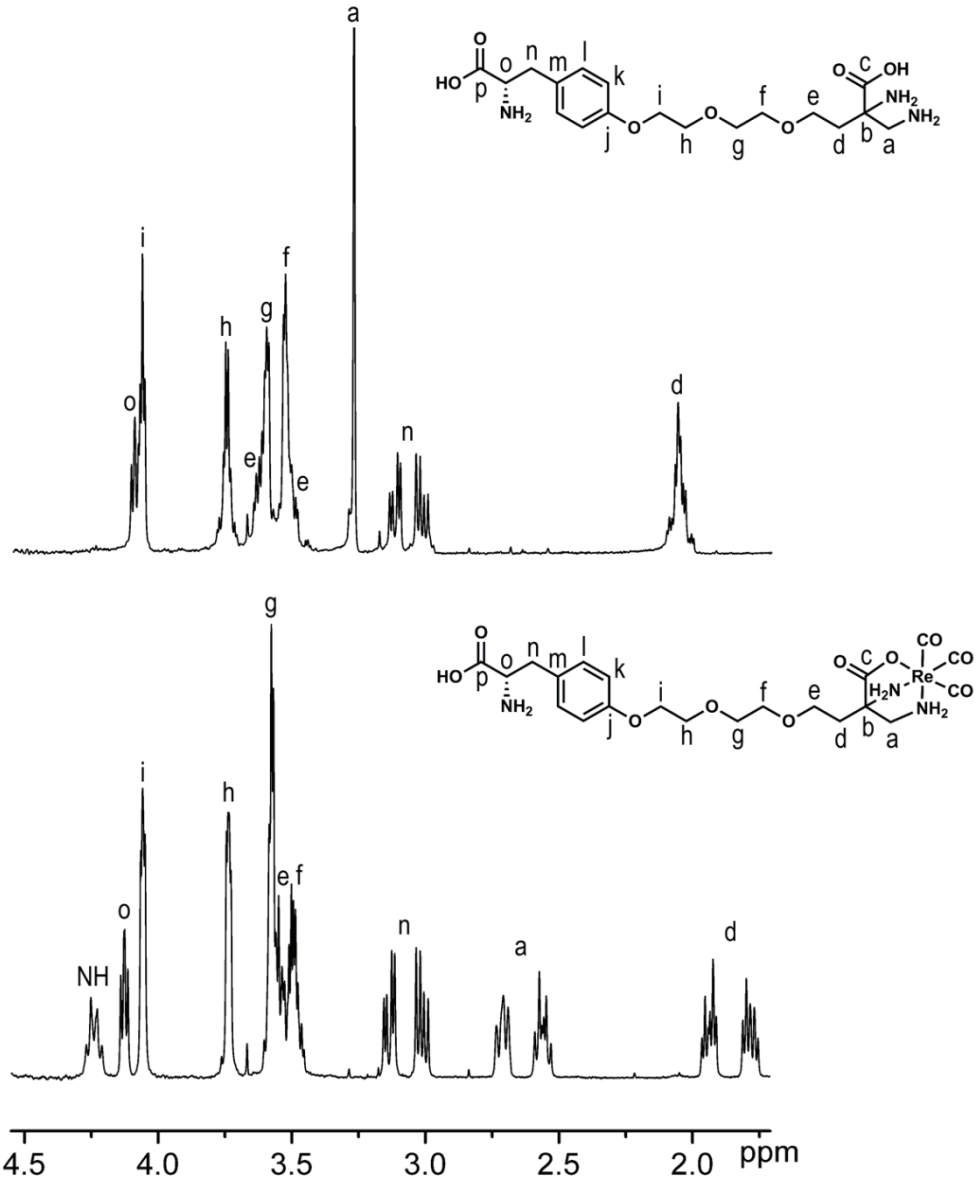

Figure 32. ^{1}H NMR spectra of the ligand **55** and the Re complex **56** (both measured in D_2O).

The $^{99m}Tc^{I}$ complex **57** was obtained *via* three different methods, whereas all of the syntheses yielded RCPs ≥95%. For two procedures the well-known precursor complex *fac*-$[^{99m}Tc(OH_2)_3(CO)_3]^+$ was prepared according to a reported procedure.[124] Compound **57** was generated by the reaction of **55** at 10^{-4} M with *fac*-$[^{99m}Tc(OH_2)_3(CO)_3]^+$ after either 11 min at 110 °C under microwave irradiation or after 20 min at 95 °C with thermal heating. It was also possible to synthesize **57** in a one-pot reaction by adding $Na[^{99m}TcO_4]$ in 0.9% saline and 10^{-4}

M ligand **55** solution to an Isolink™ kit. For this procedure the mixture was stirred at 95 °C for 30 min and HPLC with γ-detection revealed a single peak at 18.0 min retention time (Figure 33). In comparison with the HPLC retention time of the macroscopic Re^{I} homologue **56**, there is a difference of 0.4 min which is due to the HPLC setup where the γ-detector is located after the UV-detector in the HPLC setup. The two HPLC traces evidenced the successful synthesis of the target compound **57**, even though the two diastereomers could not be separated with the HPLC system used for this work.

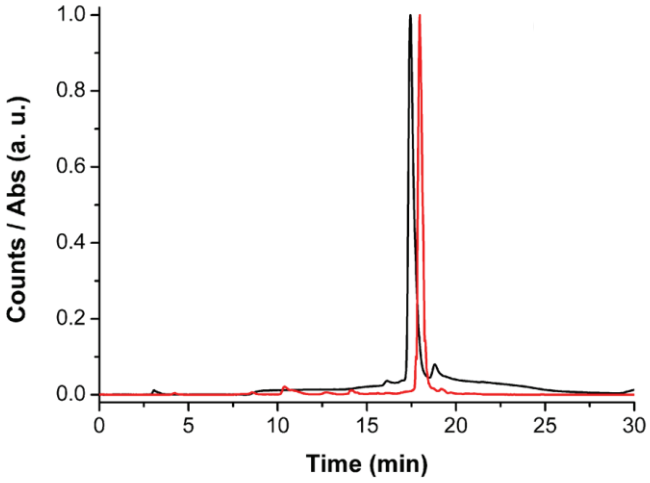

Figure 33. Normalized HPLC analysis of the Re complex **56** (black line) and the ^{99m}Tc compound **57** (red line, after one-pot synthesis). Please note that the difference of 0.4 min between the absorbance and γ-counts is due to the detector setup in which the γ-detector is located after the UV-detector.

2.4.3 Biological Evaluation

In order to have an injectable sterile solution of **57** after the aforementioned synthesis, the pure compound was extracted with a C18ec-SepPak cartridge. Subsequent rinsing with water and elution with ethanol led to an overall RCY of 81% and RCP ≥95%. The solvent was evaporated and the compound was dissolved in physiological saline (0.9%) solution. *In vivo* evaluation was carried out with five male nude NMRI mice bearing a C6-tumor xenograft in the region of the left shoulder. The injection of **57** occurred *via* the tail vein and three mice were used for microSPECT imaging. The data of the biodistribution studies of the tumor mice are summarized in Table 6 and Figure 34. At the first glance, the studies revealed negligible tumor (0.12 ± 0.05 %ID/g) and pancreas (0.07 ± 0.03 %ID/g) uptake, indicating that **57** was not recognized as an amino acid analogue. In particular the pancreas has normally an

increased amino acid requirement for the synthesis of several hormones and enzymes.[165] The reasons for the failure of tracer **57** as an amino acid analogue might lie in its lipophilic nature. Additionally, conjugation *via* a PEG-linker to the chelator makes the compound probably too bulky for recognition and transportation through the LAT system. Further evidence for the lipophilicity of **57** was partial hepatobiliary clearance, and hence accumulation in the liver (17.12 ± 3.82 %ID/g) and intestines (9.47 ± 3.09 %ID/g). However, uptake in the kidneys at 60 min p.i. (26.07 ± 6.37 %ID/g) pointed out that compound **57** was also excreted *via* the renal-urinary pathway.

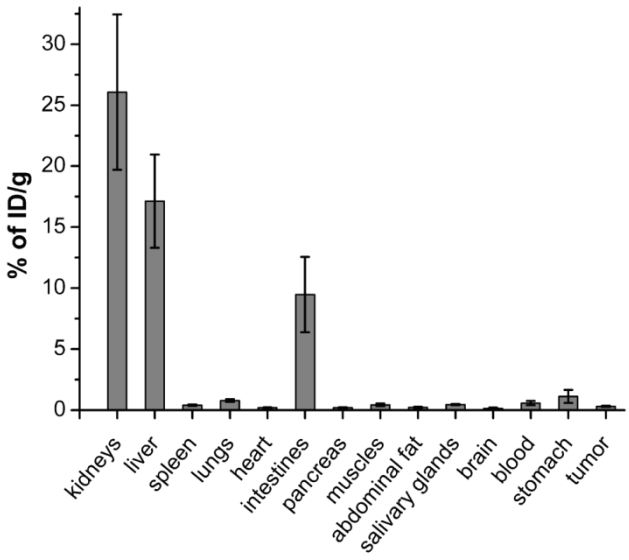

Figure 34. *Ex vivo* biodistribution of compound **57** in nude NMRI mice bearing a C6-tumor xenograft at 1 h p.i. (data expressed as %ID/g ± SEM).

HPLC analysis of urine samples at 60 min p.i. showed that a maximum of 30% of the parent compound **57** was still intact (Figure 35). However, the metabolites have retention times similar to the parent compound and little to none polar metabolites, indicating the effective *in vivo* stability of the *fac*-[DAP-^{99m}Tc(CO)$_3$]-moiety in **57**. The lack of polar metabolites (such as *fac*-[^{99m}Tc(OH$_2$)$_3$(CO)$_3$]$^+$ or [^{99m}TcO$_4$]$^-$) is confirmed by the lack of blood pool retention (a typical characteristic of *fac*-[^{99m}Tc(OH$_2$)$_3$(CO)$_3$]$^+$) and the lack of significant thyroid and stomach uptake (a typical property of [^{99m}TcO$_4$]$^-$). HPLC analysis of the blood plasma was also carried out, but the low amount of radioactivity remaining in the blood at 60 min p.i. did not allow a quantitative interpretation. Nevertheless, the main species in the blood was identified to be the parent compound.

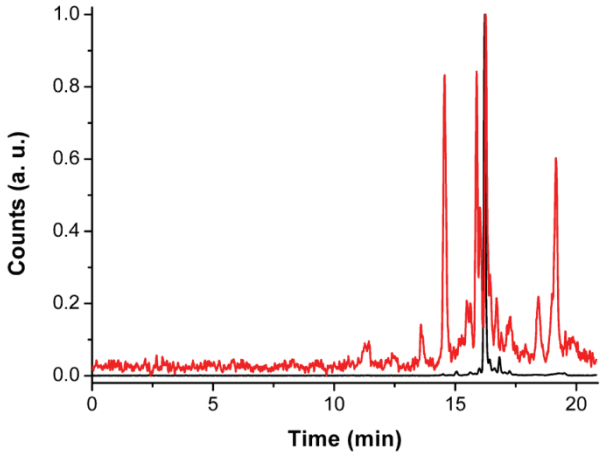

Figure 35. Normalized HPLC analysis of a representative urine sample at 1 h p.i. (red line) and the ^{99m}Tc compound **57** (black line, after one-pot synthesis) as a reference.

The microSPECT images at 20 min p.i. indicated a rapid clearance from the blood pool since the activity can mainly be seen in the liver and bladder. Interestingly, the gallbladder appeared as a bright spot, which implies excretion predominantly from the liver *via* the gallbladder into the intestines (Figure 36A).

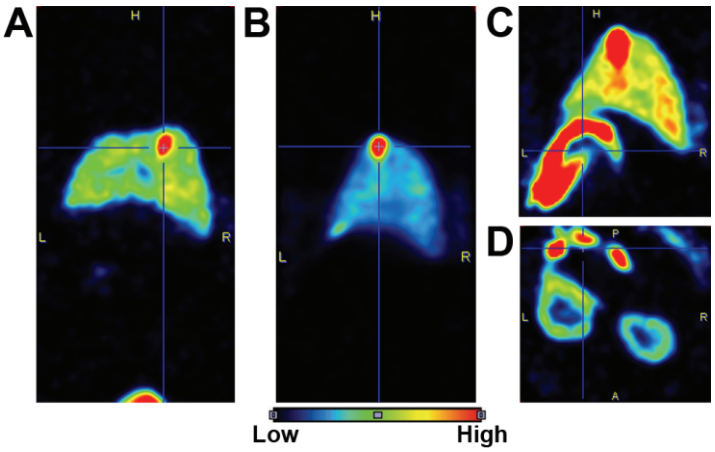

Figure 36. Representative microSPECT images of a C6-xenograft bearing NMRI mouse at 20 min p.i. (A) and images of a healthy NMRI mouse at 15 min p.i. (B, C and D). All the images are focusing on the gallbladder (A and B, both coronal plane) or the upper intestines part (C, coronal, and D, transversal plane) to point out the fast hepatobiliary clearance. D shows also the accumulation of activity in the corona of the kidneys.

This uptake and clearance behavior is similar to ^{99m}Tc-mebrofenin (Choletec®, Bracco Diagnostics Inc.), an imaging agent to evaluate hepatobiliary dysfunction associated with the gallbladder.[170] In order to gain more insights about the radiolabeled tyrosine-derivative and its uptake into the gallbladder, we performed additional experiments with three healthy male NMRI mice. The microSPECT images at 15 min p.i. showed a high uptake in the

gallbladder (Figure 36B) and clearance into the small intestines (Figure 36C). Moreover, the corona of the kidneys was also visible in the microSPECT images at 15 min p.i. (Figure 36D) due to partial renal clearance. The high uptake in the gallbladder (4.98 ± 1.85 %ID/g) at 60 min p.i. was confirmed with *ex vivo* biodistribution studies (Figure 37 and Table 6). Based on the fast uptake into the gallbladder and the fact, that the gallbladder can be visualized over an extended period, compound **57** might have potential to be used for gallbladder imaging and associated dysfunctions.

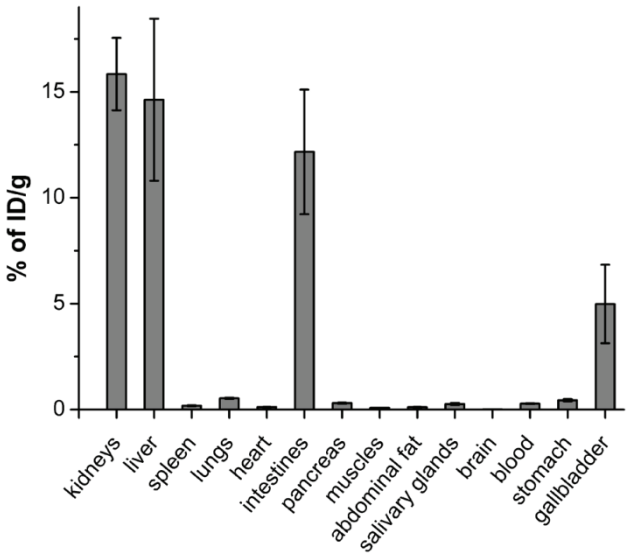

Figure 37. *Ex vivo* biodistribution of compound **57** in healthy NMRI mice at 1 h p.i. (data expressed as %ID/g ± SEM).

Table 6. *Ex vivo* biodistribution studies of compound **57** in nude NMRI mice bearing a C6-tumor xenograft and in healthy NMRI mice at 1 h p.i. (data expressed as %ID/g ± SEM).

organ / tissue	***tumor mice (n=5)***	***healthy mice (n=3)***
kidneys	26.07 ± 6.37	15.84 ± 1.71
liver	17.12 ± 3.82	14.62 ± 3.82
spleen	0.40 ± 0.06	0.18 ± 0.02
lungs	0.78 ± 0.12	0.53 ± 0.03
heart	0.19 ± 0.03	0.11 ± 0.01
intestines	9.47 ± 3.09	12.16 ± 2.94
pancreas	0.07 ± 0.03	0.31 ± 0.03
muscles	0.43 ± 0.11	0.08 ± 0.01
salivary glands	0.45 ± 0.05	0.26 ± 0.05
brain	0.12 ± 0.08	0.02 ± 0.01
blood	0.57 ± 0.18	0.28 ± 0.01
stomach	1.12 ± 0.53	0.44 ± 0.05
tumor	0.12 ± 0.05	-
gallbladder	-	4.98 ± 1.85

2.4.4 Conclusion

We synthesized an L-tyrosine derivative, which is conjugated *via* the *para*-OH moiety to a PEG-linker and DAP-chelator. The synthesis of the ^{99m}Tc complex was carried out in a one pot reaction and subsequent purification with a C18ec-SepPak cartridge lead to high RCY and RCP. Biological evaluation in mice showed rapid hepatobiliary clearance *via* the gallbladder into the intestines and partial renal-urinary clearance. However, tumor uptake in nude mice harboring C6-xenografts was low, indicating that the ^{99m}Tc labeled L-tyrosine derivative was not taken up by the LAT system. Nevertheless, the compound exhibited interesting features with regard to gallbladder imaging. In addition, derivatization of L-tyrosine at its *para*-OH position with a PEG-containing chelator seems to be a feasible approach and efforts to radiolabel peptides with this procedure are currently underway in our laboratories.

2.5 The Thiol-Disulfide Exchange Reaction as a Platform for the ^{99m}Tc Labeling of Biomolecules Containing a Thiol Group

As the preceding sections have shown, the bifunctional ligands with the basic structure HS-spacer-DAP (**9**, **26** and **51**) are versatile coating ligands for thiophilic NP surfaces. Moreover, we have demonstrated that compound **51** can first be labeled with the $[^{99m}Tc(CO)_3]^+$ fragment and then attached on the gold surface of Fe_3O_4-Au Dumbbell-like NPs (see section 2.3.5). The fact that the ^{99m}Tc labeled compound **51** contains an unprotected thiol group inspired us to test the radiolabeled complex in thiol-disulfide exchange reactions. These rearrangement reactions have been widely explored in proteins, in this context known as disulfide shuffling.[171] Thiol-disulfide exchange is essential for oxidative folding processes of proteins and typically involves two sequential exchanges.[172] In a first step, the thiol of a Cys residue attacks a disulfide, leading to the formation of a mixed disulfide species:

R''SH + RS–SR' ↔ R''S–SR + R'SH

The rate of this reaction is determined primarily by the accessibility of the disulfide, the reactivity of the attacking thiol and the concentration, whereas the reactivity depends on the pK_a of the thiol-group and, therefore, the pH of the media. Exchange reactions occur rapidly at pH 9 and become slower at lower pH values. However, such reactions are often catalyzed in proteins by an enzyme called thioredoxin.[107] In a second step, a nucleophilic attack from a second Cys thiolate takes place on the asymmetric disulfide **R''S–SR**:

R'''SH + R''S–SR ↔ R''S–SR''' + RSH

Consequently, a new disulfide bond **R''S–SR'''** is established and the second thiol-disulfide exchange reaction depends highly on the thermodynamic stability of mixed disulfide, associated with conformational features of the peptide or protein.[172]

Disulfides are not only important for the tertiary structure of proteins, but also for the formation of drug conjugates or prodrugs. Thereby, the disulfide bonds serve as covalently reversible linkages which can be cleaved after entering the strongly reducing environment of the cell. In tumor cells, most notably, the concentrations of the reducing molecule glutathione (GSH) are much higher than in blood plasma (2-8 mM versus 1-2 µM).[173] Liu and co-workers have impressively made use of this fact by conjugating the four first-line

chemotherapy drugs (Paclitaxel, Doxorubicin, Fluorouracil and Gemcitabine) to vitamin E *via* a cleavable disulfide linker.[174] Moreover, the chemotherapy drug derivatives self-assemble into nanomedicines in aqueous media, having the hydrophobic vitamin E part in the interior and the hydrophilic chemotherapy drug part at the outside. Additional PEGylation resulted in nanomedicines with improved pharmacokinetics and anticancer efficacy as compared to the chemotherapy drug alone. In their work, they conjugated a disulfide containing vitamin E derivative to the drugs in order to introduce the cleavable disulfide function in their prodrugs. Another possibility to synthesize disulfide-linked conjugates is carried out by using a sulfenyl-activated molecule (e.g. with 2-pyridinesulfenyl or 3-nitro-2-pyridinesulfenyl) that can be coupled with a molecule or peptide bearing a free thiol group (Scheme 19).[172]

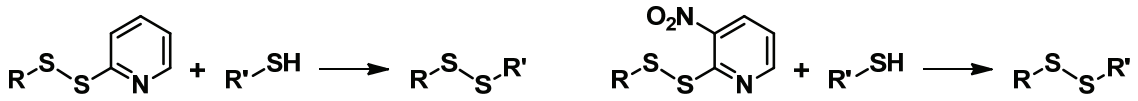

Scheme 19. The formation of disulfide bonds *via* a 2-pyridinesulfenyl-activated thiol (left) or a 3-nitro-2-pyridinesulfenyl-activated thiol (right).

Typically, these reactions are performed under acidic conditions (pH 4.5-7.0) to prevent oxidation of the molecule with the free thiol group (R'-SH in Scheme 19), leading to the undesired homodimer. Disulfide formation with sulfenyl-activated molecules is a very elegant method to insert the disulfide functionality. It has been applied for a variety of applications, a few examples are listed below:

Weissleder and co-workers synthesized an NHS-activated linker (*N*-succinimidyl 3-(2-pyridyldithio)propionate, SPDP), which they coupled to IONPs, functionalized with amine groups.[175] The IONPs with the 2-pyridinesulfenyl-activated thiol-group on the outermost layer was further conjugated to alkanethio-substituted oligonucleotides through a disulfide exchange reaction to obtain magnetic nanosensors.[176] Using the same principle, Cheon and co-workers attached the SPDP linker to the primary amine groups of bovine serum albumin coated IONPs (Mn-doped) *via* amide bond formation.[177] The SPDP-activated NPs were further treated with HS-PEG-RGD (targeting function), HS-siGFP-Cy5 (fluorescence label) and HS-siRNA (therapeutic function). It was shown that the disulfide bonds of the functionalized NPs were readily cleaved in the reductive intracellular environment. Reductive cleavage was also taken advantage of by Hubbell and co-workers for the intracellular delivery of

thioguanine, which induced a repair-resistant DNA damage upon incorporation into DNA.[178] They prepared thioguanine prodrug micelles as polymeric carriers *via* disulfide exchange of 2-pyridinesulfenyl-activated polymers with thioguanine. Disulfide exchange reactions with 2-pyridinesulfenyl-activated compounds are also interesting for analytical purposes, for instance to capture Cys-containing peptides on a resin[179] or to detect thiol-containing substances in highly selective and sensitive mass spectrometry experiments.[180]

Our focus was on the preformed ^{99m}Tc complex **60** with an orthopyridyl disulfide for the radiolabeling of biomolecules containing a free thiol group (Scheme 20).

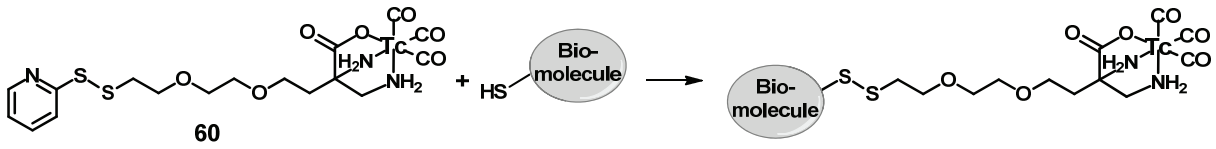

Scheme 20. Representative depiction of the aspired ^{99m}Tc labeling strategy of biomolecules based on a thiol-disulfide exchange reaction.

Such a radiolabeling procedure is particularly interesting because the only requirement is a free thiol group in a biomolecule, for instance a Cys residue in a peptide. This is a big advantage over the conventional $^{99m}Tc^{I}$ labeling strategies, which usually necessitate major chemical modifications of the bioactive molecule. A very prominent example is the addition of a histidine-tag to a recombinant protein for efficient and selective labeling with $[^{99m}Tc(OH_2)_3(CO)_3]^+$ (Figure 38A).[181] Another approach to make use of $[^{99m}Tc(OH_2)_3(CO)_3]^+$ for radiolabeling of a biomolecule is the so-called [2+1] mixed ligand concept in which the three water ligands are substituted by one bidentate and one monodentate ligand (Figure 38B).[182] However, the bioactive molecule has to be linked either to the monodentate ([2+1_B] concept) or to the bidentate ligand ([2_B+1] concept). Alternatively, an artificial amino acid bearing a tripodal chelator can directly be incorporated during the peptide synthesis and labeled with the $[^{99m}Tc(OH_2)_3(CO)_3]^+$ precursor (Figure 38C).[98] Other methods to combine a preformed ^{99m}Tc complex with a biomolecule are based on bioorthogonal chemistry (Figure 38D),[183,184] amide bond formation applied in peptide chemistry (Figure 38E)[185] or maleimide-thiol coupling (Figure 38F).[186] Nevertheless, these methods often include moisture-sensitive reagents and are therefore less suitable for the aqueous ^{99m}Tc labeling reactions.

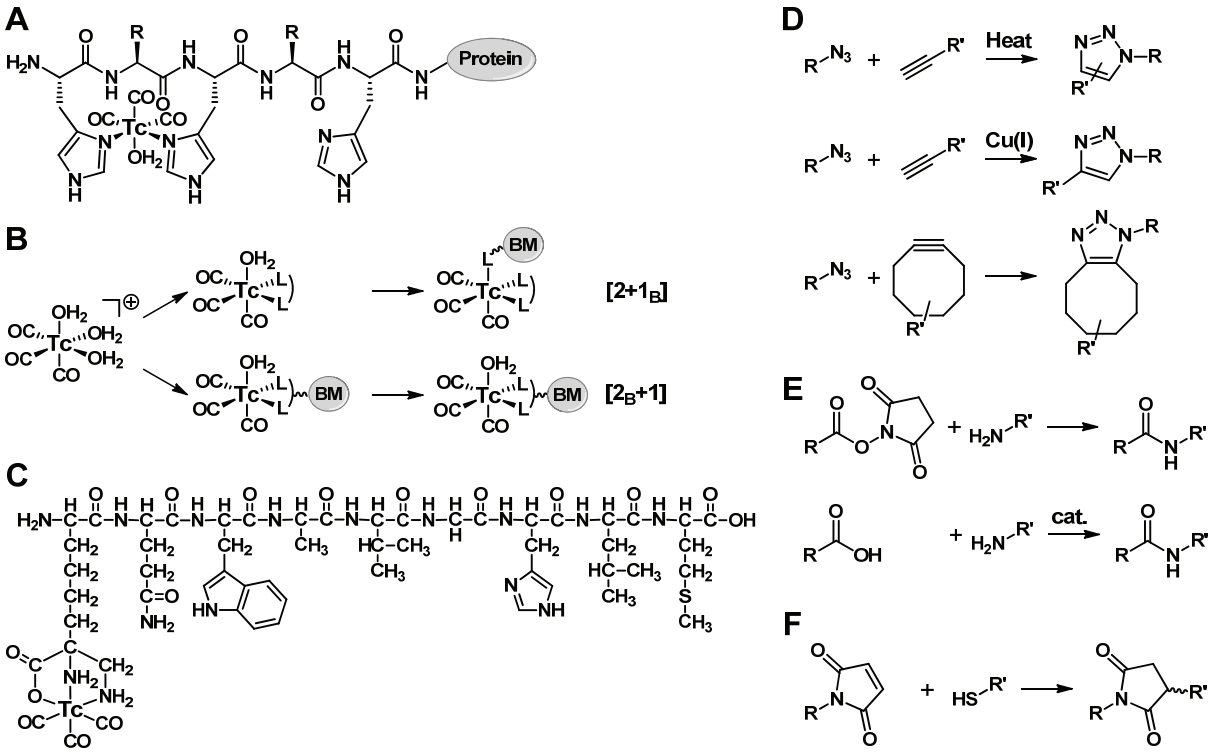

Figure 38. Overview of different methods to radiolabel bioactive molecules (BM) with the $[^{99m}Tc(CO)_3]^+$ fragment: (A) Addition of a histidine-tag to a recombinant protein, (B) the [2+1] mixed ligand concept, (C) incorporation of an artificial amino acid with a tripodal chelator into a peptide, (D) bioorthogonal chemistry; (E) amide bond formation; (F) maleimide-thiol conjugations. The radiolabel can be either part of R or R'.

2.5.1 Labeling of HS-PEG-DAP and Activation with 2,2'-Dithiodipyridine

The key step of the labeling strategy illustrated in Scheme 20 is the activation of the terminal thiol with 2,2'-Dithiodipyridine (DTDP) to obtain the orthopyridyl disulfide. There are two possibilities for that, either by activating ligand **51** before radiolabeling or by activating the ^{99m}Tc complex **58** with DTDP. In a preliminary experiment ligand **51** and DTDP were mixed in aqueous solution at neutral pH, leading to multiple peaks in the HPLC analysis. Before performing preparative HPLC purification, we carried out some initial labeling experiments to evaluate the approach with DTDP-activation of the ^{99m}Tc complex **58**. Firstly, labeling of ligand **51** with the $[^{99m}Tc(CO)_3]^+$ fragment was rendered by mixing the $[^{99m}Tc(OH_2)_3(CO)_3]^+$ precursor with an aqueous solution of **51** at 60 °C for 30 min at neutral pH (Scheme 21). HPLC analysis with a γ-detector revealed multiple minor peaks in the region of the main peak at 18.5 min (Figure 39). We decided to add a solution of DTDP in methanol and stirred the mixture at 60 °C for additional 30 min. Only one main peak at 20.9 min in 87% yield was unexpectedly observed, whereas the peak at 18.5 min almost disappeared (Figure 39). Based

on these results, which were notably fully reproducible, we hypothesized that all peaks between 16 and 22 min in Figure 39 are associated with the target complex **58**. The multiple peaks might be associated with the presence of a free thiol group, possibly leading to various interactions and hence different retention times in the HPLC analysis. However, upon addition of DTDP to the reaction mixture containing **58**, the main species is orthopyridyl disulfide **60** (Figure 39).

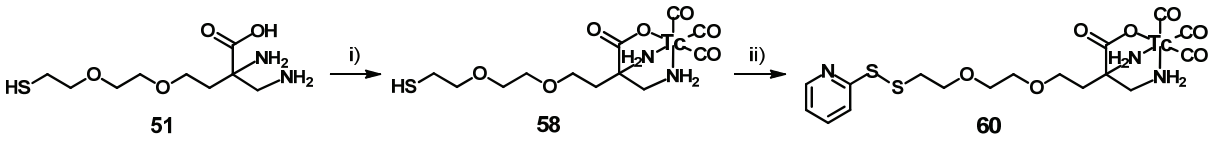

Scheme 21. Synthesis of the ^{99m}Tc complex **60** with the orthopyridyl disulfide. i) $[^{99m}Tc(OH_2)_3(CO)_3]^+$, H_2O, pH 7.4, 60 °C, 30 min; ii) DTDP, H_2O / MeOH 2:1, pH 7.4, 60 °C, 30 min.

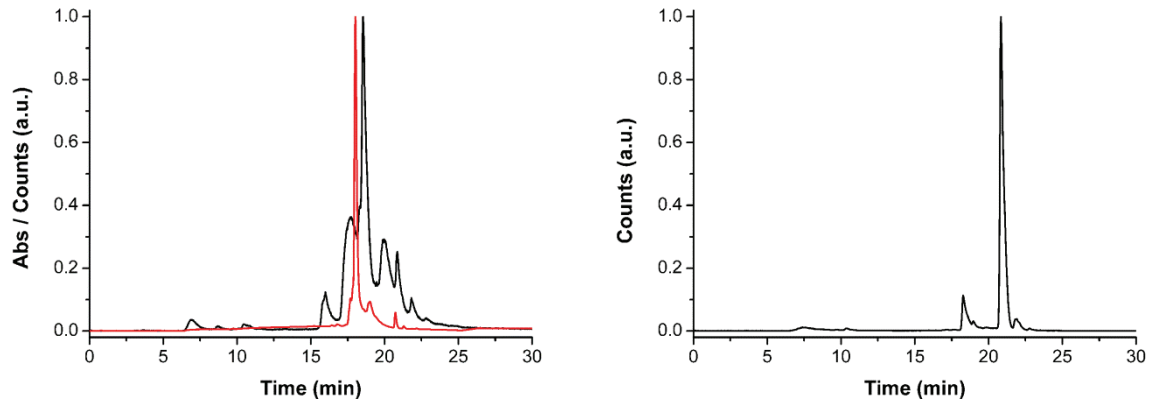

Figure 39. Normalized HPLC analysis after the synthesis of compound **58** (black line, left), the purified Re analog **59** (red line, left) and activated ^{99m}Tc complex **60** (black line, right). Please note that the difference of 0.5 min between the absorbance (red line) and γ-counts (black line) is due to the detector setup in which the γ-detector is located after the UV-detector.

The Re congener **59** of **58** was synthesized, purified with preparative HPLC and fully characterized. HPLC analysis of the isolated Re complex **59** exhibited one major peak at 18.0 min, which is in accordance with the main peak observed in the HPLC trace after the synthesis of **58** (Figure 39). The HPLC trace showed tailing of the main peak, which might be due to the presence of a free thiol. Additional peaks like in the spectrum of the corresponding ^{99m}Tc compound **58** were not evidenced. Therefore, the main peak after the synthesis of **58** (18.5 min retention time) was collected by means of semi-preparative HPLC. The solution with the isolated peak (an HPLC analysis thereof is presented in Figure 29D) was subsequently mixed with a solution of DTDP. The result was the same as with the unpurified

reaction solution after the synthesis of **58**, conversion to a new peak at 20.9 min. The only difference was more product **60** formation as compared to the experiment without semi-preparative purification (4% versus 9%). These findings led to the conclusion that DTDP-activation of **58** on tracer level is a feasible approach to obtain the desired compound **60**.

2.5.2 Labeling of Thiol-containing Biomolecules with the Pyridyl Disulfide ^{99m}Tc Tracer 60

The potential of the ^{99m}Tc complex **60** to radiolabel biomolecules with a thiol group was evaluated with thioglucose, Cys and GSH. The first target to label was thioglucose **61**, which is synthesized in three steps starting from 2,3,4,6-tetra-*O*-acetyl-α-D-glucopyranosyl bromide (Scheme 22).[187] Stenzel and co-workers showed that thioglucose can readily be converted to the pyridyl disulfide **62**.[188] This compound was interesting for radiolabeling experiments with **58** (^{99m}Tc complex with a free thiol group) since the activated thiol is located at the biomolecule and not at the radiolabel. It also serves as a control reaction for the labeling of **61** with the ^{99m}Tc complex **60**.

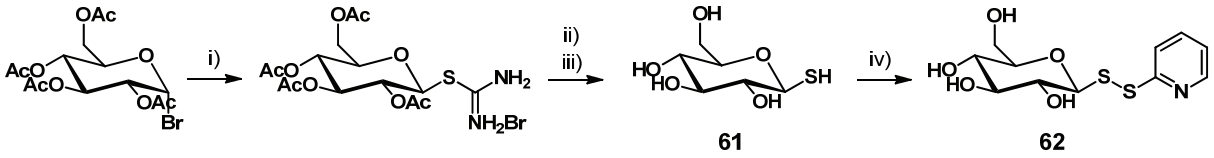

Scheme 22. Synthesis of thioglucose **61** and its pyridyl disulfide derivative **62**. i) Thiourea, acetone, 70 °C, 20 min, 52%; ii) $Na_2S_2O_5$, CH_2Cl_2 / H_2O 2:1, 60 °C, 90 min, 99%; iii) NaOMe, MeOH, 25 °C, 30 min, 98%; iv) DTDP, MeOH, 25 °C, 30 min, 62%.

The addition of an aqueous solution of **61** to the pyridyl disulfide complex **60** resulted in a new peak at 16.5 min (Scheme 23A and Figure 40A). The yield was only 15% after 30 min at 60 °C and prolonging the reaction time did not cause an increase of the peak. The main species after the reaction was the educt **60**. The temperature was kept at 60 °C to avoid hydrolysis of the sugar or disulfide bond cleavage. In order to make sure that the new peak at 16.5 min corresponds to the ^{99m}Tc labeled sugar derivative **63**, compound **62** was added to the complex **51** (Scheme 23B). After the same reaction time at 60 °C the peak at 16.5 min was observed as well, but in a higher yield (48%). The fact that both reactions generated the peak at 16.5 min corroborates the successful synthesis of the tracer **63**. After all, the low yields of **63** and the formation of compound **60** during the second reaction (peak at 20.9 min in Figure 38B) required further investigations.

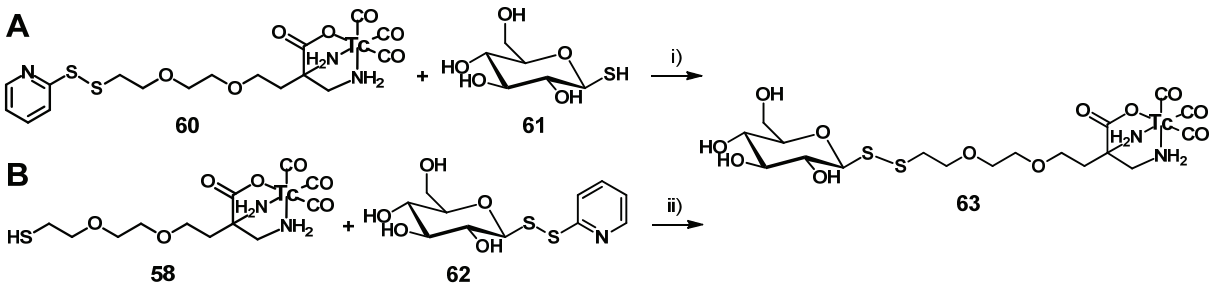

Scheme 23. Synthesis of the ^{99m}Tc labeled glucose derivative **63** *via* two different routes. i) H_2O, pH 7.4, 60 °C, 30 min; ii) H_2O / MeOH 1:2, pH 7.4, 60 °C, 30 min.

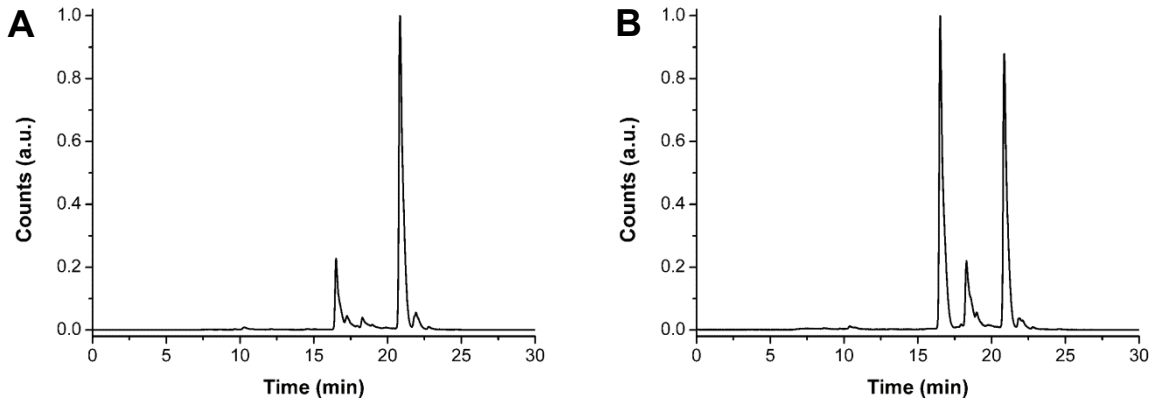

Figure 40. Normalized HPLC analyses after the syntheses of compound **63**; (A) addition of thioglucose **61** to **60** after 30 min at 60 °C and (B) addition of the pyridyl disulfide **62** to **58** after 30 min at 60 °C.

The answer to the aforementioned observation lies in the concentration differences between the reactions occurring at tracer level (10^{-9}-10^{-8} M) and the simultaneous reactions of the unlabeled ligands (10^{-3} M). When the ^{99m}Tc complex **58** is activated with DTDP, thiopyridine is not only formed through this reaction, but also excess ligand **51** reacts with DTDP, leading to thiopyridine concentrations in the mM range (Scheme 24A). Thioglucose **61**, which was used in a fivefold excess as compared to DTDP, can react with the activated complex **60** and the activated ligand **51** (Scheme 24B). Both reactions, in turn, potentially increase the thiopyridine concentration in the reaction mixture. Finally, the produced thiopyridine can attack complex **63** and, therefore, lower the yield (Scheme 24C). It should be emphasized that all these reactions are influenced by various factors, such as the reactivity of the thiol-groups, the accessibility of the disulfide bond and the thermodynamic stability of the disulfides, respectively. However, it was not part of this study to finetune the different parameters, because the easiest solution to this problem would be prevention of the formation of thiopyridine. The presence of thiopyridine is also the reason why complex **60** was formed during the reaction between **58** and **62** (Figure 40B). In addition to complex

58, the unlabeled ligand **51** reacts with the pyridyl disulfide as well (Scheme 25A). As a consequence, thiopyridine is produced in mM concentrations and attacks the ^{99m}Tc labeled glucose derivative **63**, generating complex **60** (Scheme 25B).

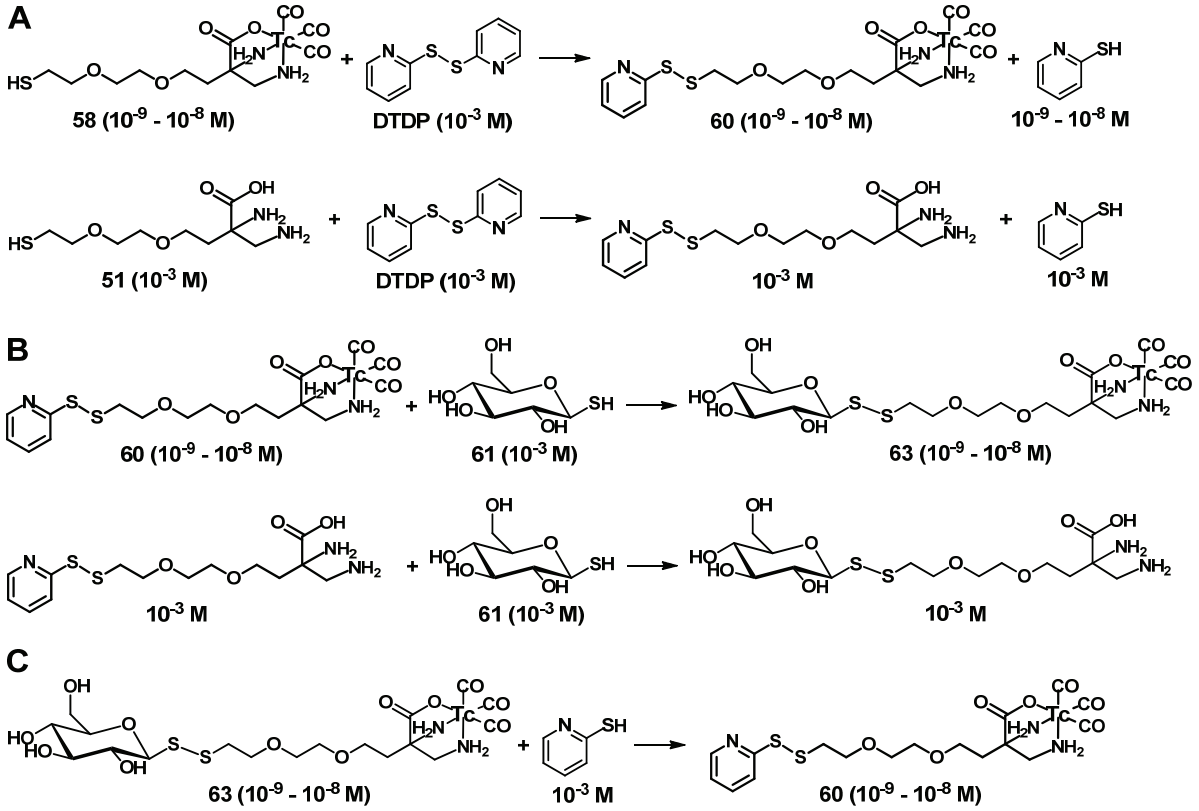

Scheme 24. Reactions occurring in the first attempt to synthesize the ^{99m}Tc labeled glucose derivative **63**.

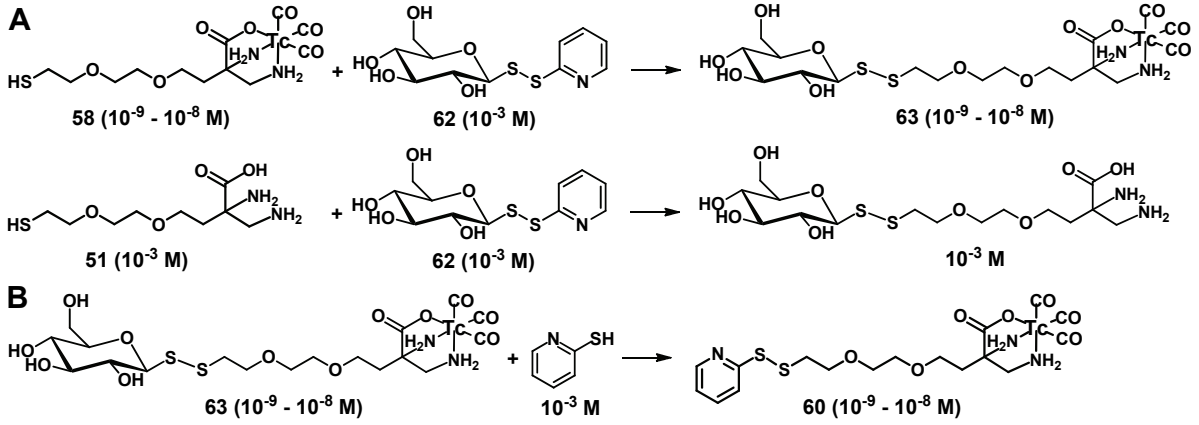

Scheme 25. Reactions occurring in the second attempt to synthesize the ^{99m}Tc labeled glucose derivative **63**.

Apart from thioglucose, the feasibility to radiolabel thiol-containing biomolecules with **60** was also exploited with Cys and GSH (Scheme 26). The reaction of the pyridyl disulfide complex **60** with Cys and GSH exhibited product formation according to HPLC analyses at 17.2 min (**64**) and 16.4 min (**65**) retention time (Figure 41). In line with the thioglucose-experiments, the limiting component of these reactions is the emerging thiopyridine, resulting in yields of 50% for **64** and 32% for **65**. The yield of **65** is probably lower due to steric effects since GSH is bulkier than Cys and, therefore, the thiol group less accessible.

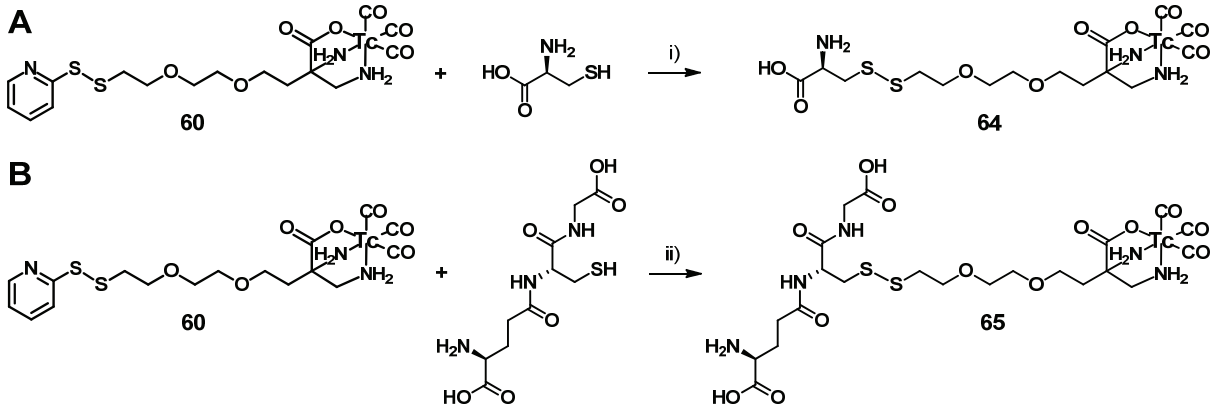

Scheme 26. Synthesis of the ^{99m}Tc labeled Cys derivative **64** (A) and GSH derivative **65**. i) H_2O / MeOH 2:1, pH 7.4, 60 °C, 30 min; ii) H_2O / MeOH 2:1, pH 7.4, 60 °C, 30 min.

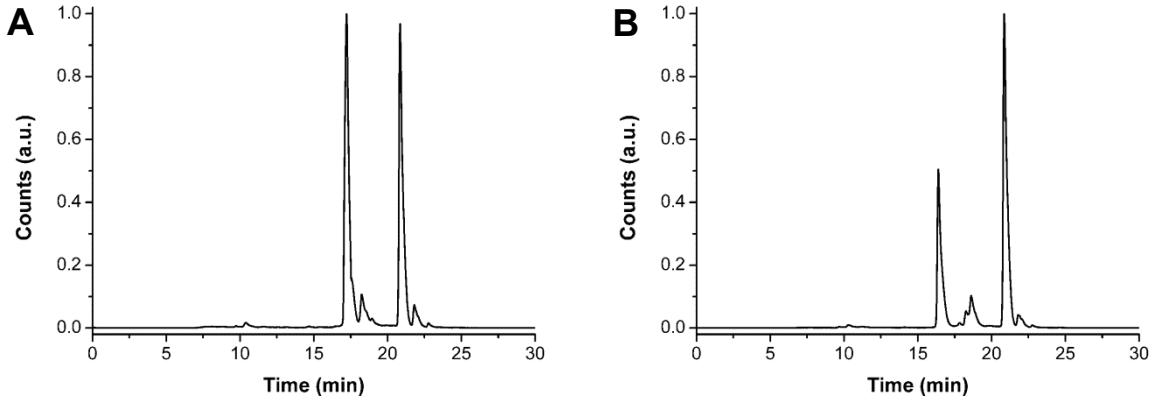

Figure 41. Normalized HPLC analyses after the syntheses of compound **64** (A) and **65** (B).

Based on the insights gained from the experiments, the focus was on finding a strategy which prevents or minimizes the formation of thiopyridine. It is obvious from the reactions shown in Scheme 24 that unlabeled ligand **51** is the driving force behind the generation of thiopyridine. Consequently, it was attempted to get rid off excess ligand **51** by means of a C18-SepPak cartridge. Compound **58** was synthesized as described above and purified by

loading the cartridge with the reaction mixture, washing it with water to elute the hydrophilic components (e.g. free ligand **51**) and, finally, extraction of the ^{99m}Tc complex **58** with methanol. The HPLC trace after SepPak purification is comparable to the one displayed in Figure 39 (reaction mixture after the labeling of ligand **51**) and the same three major peaks were present. Purified **58** was directly activated with DTDP to obtain the pyridyl disulfide complex **60** in 90% yield (Figure 42).

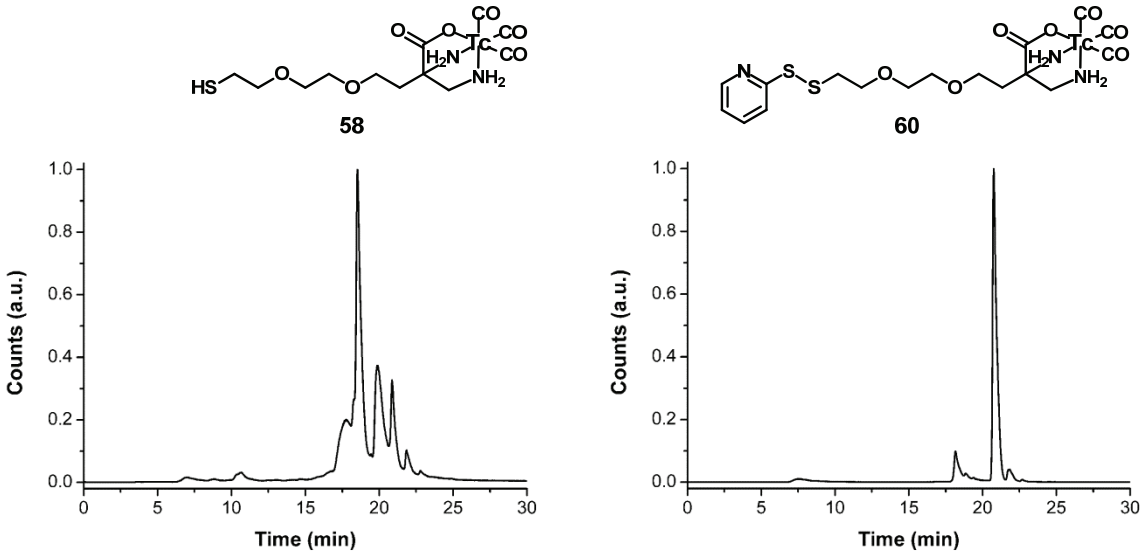

Figure 42. Normalized HPLC analyses of SepPak-purified compound **58** (left) and subsequent activation to the pyridyl disulfide **60** with DTDP (right).

The reaction mixture containing compound **60** was used without further purification and incubated with thioglucose **61** at 60 °C for 30 min. The desired product **63** was obtained in 88% yield, indicating that removal of excess ligand **51** is a successful approach to increase the yield of **63** as compared to the synthesis shown in Scheme 23. The same holds true for the reaction of purified **58** with pyridyl disulfide glucose **62**, generating the radiolabeled glucose derivative **63** in 90% yield (Figure 43). For both reactions, the ^{99m}Tc complex **58** was observed in the HPLC analyses, originating from either unactivated compound **58** in the first case or incomplete reaction with the pyridyl disulfide glucose **62** in the second case. Nonetheless, the experiments can be considered as major improvement and the SepPak-purification strategy was further evaluated with Cys and GSH (Figure 44). In comparison to the labeling experiments with unpurified complex **58**, the yield can significantly be increased with purified and DTDP activated **58** (79% vs. 50% for the reaction with Cys and 72% vs. 32% for the reaction with GSH).

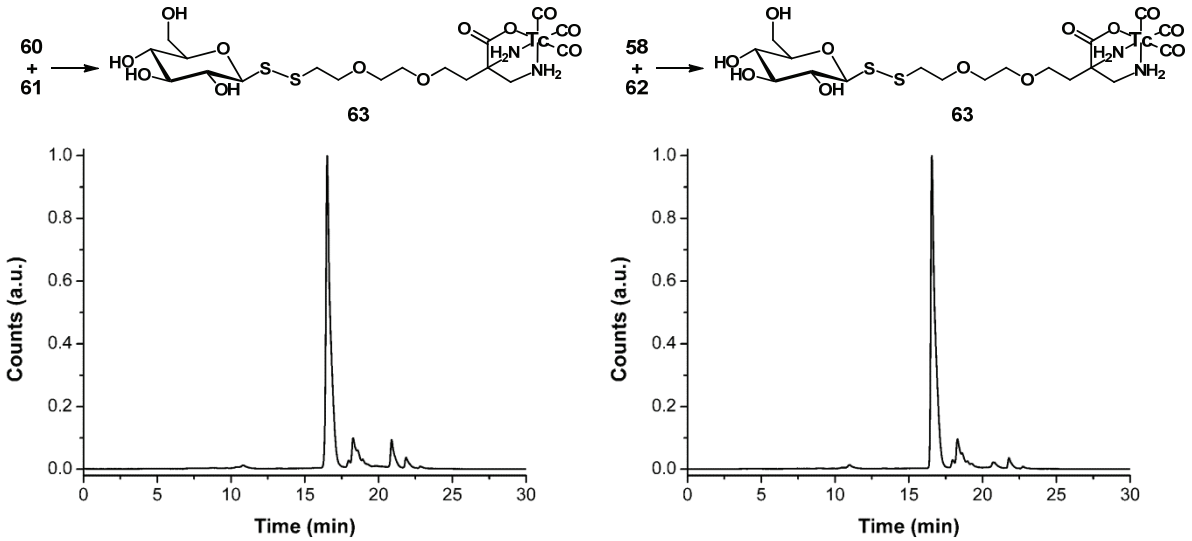

Figure 43. Normalized HPLC analyses of the ^{99m}Tc labeled glucose derivative **63**, synthesized *via* the pyridyl disulfide complex **60** and thioglucose **61** (left) or *via* the reaction of SepPak-purified compound **58** and activated thioglucose **62** (right).

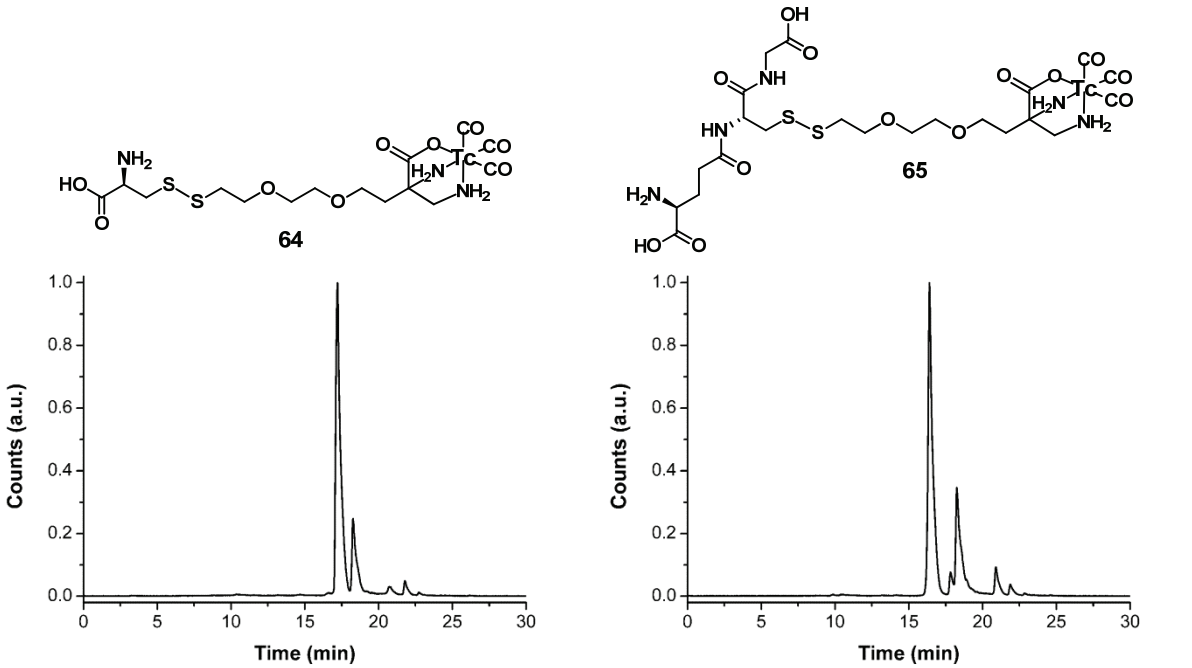

Figure 44. Normalized HPLC analyses after the syntheses of compound **64** (left) and **65** (right) by using SepPak-purified complex **58**, which was activated with DTDP.

The major side product of the labeling experiments with Cys and GSH was complex **58** with a terminal thiol group. The reason why complex **58** is formed is exemplified for the reaction with Cys (Scheme 27). For the synthesis of compound **60**, complex **58** is incubated with a 1 mM solution of DTDP. It is assumed that the excess DTDP reacts with Cys and forms its pyridyl disulfide conjugate. Therefore, Cys was added in a fivefold excess as compared to DTDP in order to have Cys with the free thiol group available for the reaction with **60**.

However, the excess Cys can further react with **64**, generating **58**, or pyridyl disulfide Cys. Both reactions lead to Cys in its oxidized form (cystine), which can be considered as the thermodynamically favored disulfide.

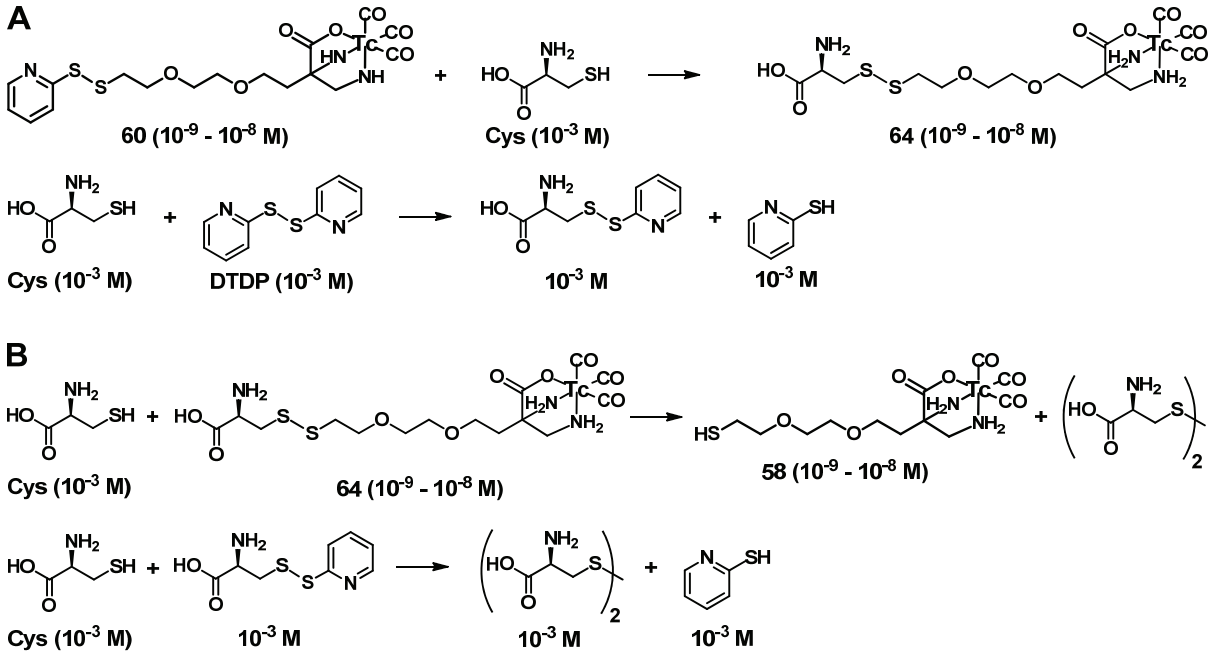

Scheme 27. Reactions occurring during the synthesis of ^{99m}Tc labeled Cys **64**.

The preparation of the pyridyl disulfide complex **60** was additionally investigated with microwave-assisted synthesis. Firstly, compound **58** was obtained upon addition of $[^{99m}Tc(OH_2)_3(CO)_3]^+$ to ligand **51** and stirred at 110 °C for 4 min under microwave irradiation. As shown in Figure 43, the product peak is more distinct after SepPak purification as compared to the HPLC analysis of the thermal reaction (Figure 45). Secondly, complex **58** was converted to the activated complex **60** and best yields (85%) were achieved after 4 min at 90 °C under microwave irradiation. We also evaluated the conjugation of **60** to the thiol-containing biomolecules, whereas the yields were in all cases lower than the thermal reactions. From these results we concluded that microwave-assisted synthesis is suitable for the formation of compound **60** and the overall reaction time can be reduced from 1 h to 8 min. However, thermal heating turned out to be better for the coupling to biomolecules, most likely due to the milder reaction conditions.

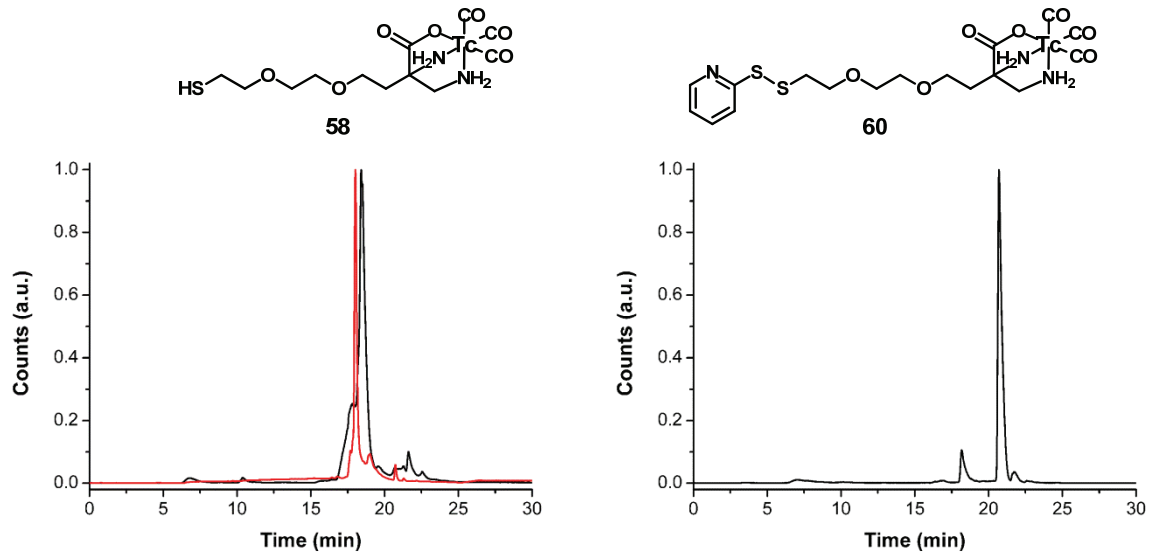

Figure 45. Normalized HPLC analysis of the microwave-assisted syntheses of compounds **58** (left) and **60** (right). The red line indicates the absorbance of the Re-compound **59** and the black lines correspond to the ^{99m}Tc complexes.

2.5.3 Activation of HS-PEG-DAP-^{99m}Tc(CO)$_3$ with Ellman's Reagent

A well known compound to quantify the number or concentration of thiol groups in a sample is 5,5'-dithiobis-(2-nitrobenzoic acid) (DTNB), also known as Ellman's reagent because it was introduced in 1959 by George Ellman.[189] Its chemistry is very similar to DTDP. We therefore tested this compound as activating reagent of the terminal thiol group in the ^{99m}Tc complex **58** (Scheme 28). In a first attempt DTNB was added to SepPak-purified **58** and stirred at 90 °C for 4 min under microwave irradiation (analogously to DTDP activation). HPLC analysis revealed only 59% product formation at 21.3 min retention time and the second peak (41%) was assigned as educt (Figure 46). During the labeling optimization a better yield was achieved at slightly alkaline conditions and the reaction worked best (85% yield) upon addition of borate buffer (pH 8.3). In contrast to the experiments with DTDP a buffer is needed for these reactions, which might originate from the presence of the carboxylate function in DTNB.

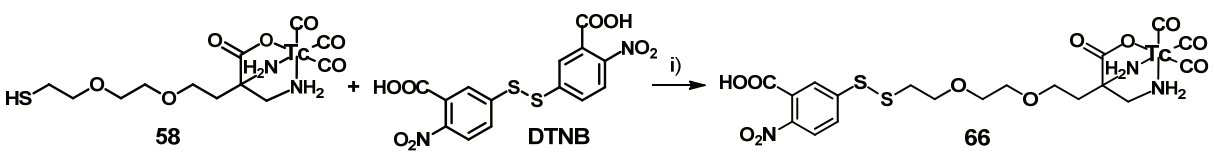

Scheme 28. Synthesis of the ^{99m}Tc complex **66** with the activated thiol group. i) DTNB, borate buffer (10 mM, pH 8.3) / MeOH 2:1, 90 °C, 4 min.

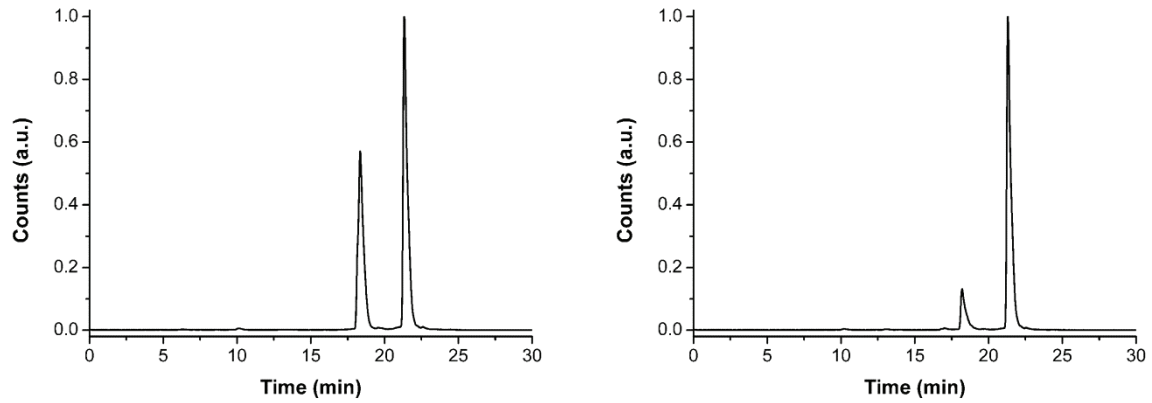

Figure 46. Normalized HPLC analyses of the microwave-assisted synthesis of compounds **66** without (left) and with the use of borate buffer pH 8.3 (right).

The ability to radiolabel thiol-containing biomolecules with the activated ^{99m}Tc complex **66** was investigated with thioglucose **61**, Cys and GSH. In all three cases the desired product was observed, although the yields were substantially lower as compared to the conversion with pyridyl disulfide **60**. As a consequence, we decided at this point to focus on DTNP for future experiments and we did not further evaluate the work with DTNB.

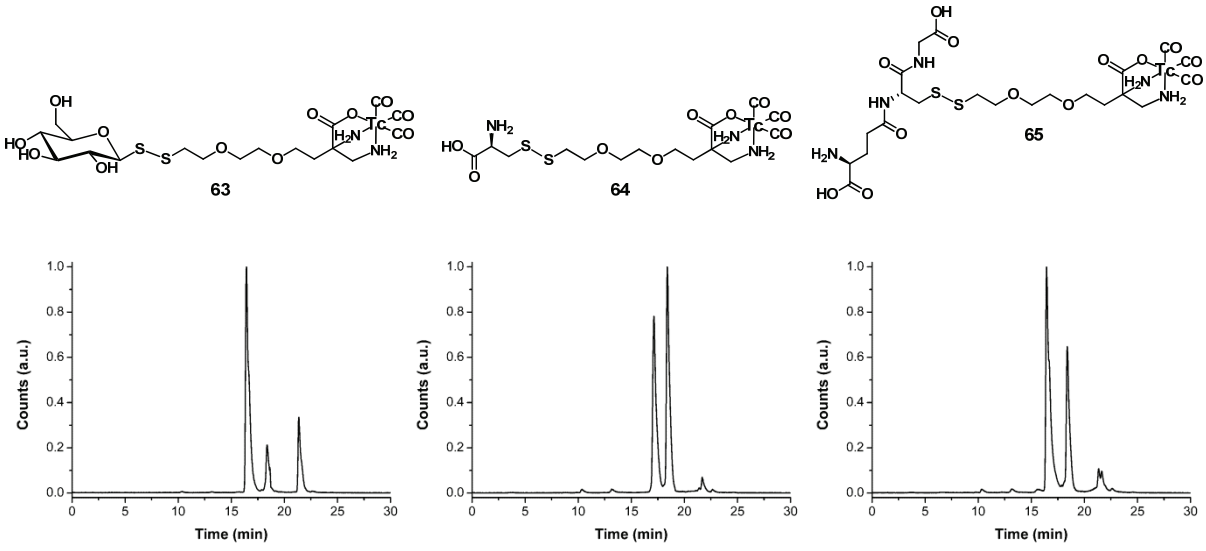

Figure 47. Normalized HPLC analyses after the conjugation of compound **66** with thioglucose **61**, Cys and GSH to obtain the ^{99m}Tc labeled biomolecues **63** (left), **64** (middle) and **65** (right).

2.5.4 Conclusion

The performed experiments have demonstrated that the bifunctional ligand system HS-PEG-DAP is not only interesting as a coating ligand for NPs, but also for the labeling of

biomolecules with a free thiol group. Therefore, the complex HS-PEG-DAP-^{99m}Tc(CO)$_3$ (**58**) was activated with DTDP to form the pyridyl disulfide derivative **60**. This compound can be attacked nucleophilically by a thiol-functionality (e.g. thioglucose, Cys or GSH) to form a new disulfide bond. We envision that this novel labeling strategy allows the conjugation of the activated ^{99m}Tc complex to peptides or proteins bearing a free thiol group. Experiments in this direction and kinetic studies are currently underway in our laboratories.

3. Experimental Procedures & Analytical Data

3.1 Materials

All reagents were purchased from commercial sources and used without further purification. Ethyl cyanoacetate (98%), di-*tert*-butyl dicarbonate (97%) and sodium borohydride (>96%) were acquired from ABCR (Germany). Glacial acetic acid (100%), tellurium powder, dichloromethane, ethanol, ethyl acetate, acetone, hexane, tetrahydrofuran, butanol, toluene, methanol, chloroform, dimethylformamide and 1,2-dichloroethane (all reagent grade) were purchased from Merck (Switzerland). Sodium nitrite (≥97%), sodium bicarbonate (99%), diethyl ether (≥97%), sodium dithionite (technical grade, 85%), *p*-toluenesulfonic acid monohydrate (≥98.5%), magnesium sulfate (97%), *N,N'*-diisopropylethylamine (≥99%), 1,2-dibromoethane (98%), potassium *tert*-butoxide (98%), sodium iodide (99%), sodium chloride (97%), diphenyl sulfoxide (96%), methyltrichlorosilane (99%), 2-benzyloxyethanol (98%), 2-sulfanylethanol (≥99%), potassium bicarbonate (99.7%), bromine (reagent grade), hydrobromic acid (48 wt. % in H_2O, ≥99%), sodium carbonate (≥99%), L-cysteine (≥97%), L-cystine, cadmium perchlorate hexahydrate (reagent grade), zinc perchlorate hexahydrate (reagent grade), triethylene glycol (99%), tetraethylene glycol (99%), sodium hydride (60% dispersion in mineral oil), benzyl bromide (98%), tetrabromomethane (99%), triphenylphosphine (≥98.5%), sodium (cubes), nickel(II) chloride hexahydrate (≥98%), diethylenetriamine (99%), palladium on carbon (10 wt. % loading), triphenylmethanethiol (97%), triethylsilane (97%), triphosgene (98%), triethylamine (≥99%), sodium hydrogen sulfate (technical grade), 6-aminohexanoic acid (≥98.5%), *N,N'*-dicyclohexylcarbodiimide (99%), dimethylaminopyridine (≥99%), sodium phosphate monobasic dihydrate (≥99%), sodium phosphate dibasic dodecahydrate (≥99%), trioctylphosphine oxide (99%), hexadecylamine (98%), cadmium acetylacetonate (≥99.9%), 1,2-hexadecanediol (technical grade, 90%), trioctylphosphine (97%), hexamethyldisilathiane (synthesis grade), diethylzinc (1 M in hexane), oleylamine (technical grade, 70%), hydroxyapatite (nanopowder, <200 nm particle size, ≥99%), fetal bovine serum (FBS), *p*-toluenesulfonyl chloride (97%), potassium hydroxide (flakes, 90%), sodium azide (≥99%), sodium triacetoxyborohydride (97%), 2-pyridinecarboxaldehyde (99%), DL-α-lipoic acid (≥98%), methanesulfonyl chloride (≥99.7%), ethyl glyoxylate (50% solution in toluene), lithium hydroxide (98%), amberlite IR120 H, *N*-hydroxysuccinimide (≥97%), d-biotin (≥99%),

N,N'-dicyclohexylcarbodiimide (99%), dimethylaminopyridine (≥99%), iodomethane (≥99%), methoxypolyethylene glycol 750, *tert*-butyl bromoacetate (98%), dopamine hydrochloride, iron(III) acetylacetonate (≥97%), oleylamine (tech. grade, 70%), 1,2-hexadecanediol (tech. grade 90%), iron pentacarbonyl, sodium phosphate monobasic dehydrate (≥99%), sodium phosphate dibasic dodecahydrate (≥99%), tris(2-carboxyethyl)phosphine hydrochloride (≥98%), tetramethylammonium hydroxide solution (25 wt. % in water), 2,2'-dithiodipyridine (≥99%), 2,3,4,6-tetra-O-acetyl-α-D-glucopyranosyl bromide (97%), thiourea (≥99%), sodium pyrosulfite (≥99%), sodium methoxide (≥97%), glutathione (≥97%), 5,5'-dithiobis-(2-nitrobenzoic acid) (≥98%) and HPLC solvents were purchased from Sigma Aldrich (Switzerland). Phenylmethanethiol (96%), trifluoroacetic acid (99%), diphenyl ether (99%), oleic acid (tech. grade 90%), 1,2,3,4-tetrahydronaphthalene (97%), 1-octadecene (tech. grade 90%), gold(III) acetate (99.9%) and hydrogen tetrachloroaurate(III) hydrate (99.9%) were obtained from Alfa Aesar (Germany). The amino acid derivatives L-glutamic acid di-*tert*-butyl ester hydrochloride, N(ε)-benzoyloxycarbonyl-L-lysine *tert*-butyl ester hydrochloride and *N*-(*tert*-butoxycarbonyl)-L-tyrosine methyl ester (99%) were purchased from Bachem (Switzerland). Deuterated NMR solvents were obtained from Armar Chemicals (Switzerland). Water was doubly distilled before use. PD-10 size exclusion columns (Sephadex G-25 medium) were purchased from GE Healthcare (Switzerland). C18ec-SepPak cartridges were purchased from Machery-Nagel (Switzerland). Isolink™ kits were a gift from Mallinckrodt Medical B.V. (Netherlands). $Na^{99m}TcO_4$ in 0.9% saline was eluted from a $^{99}Mo/^{99m}Tc$ UTK FM generator form Mallinckrodt Medical B.V. (Netherlands).

3.2 Characterization

The UV-Vis measurements were collected on a Perkin Elmer Lambda 35 UV-Vis spectrophotometer between 200 and 900 nm. The luminescence measurements were performed on a Perkin Elmer LS50 B spectrophotometer. The luminescence quantum yield was calculated based on a relative method reported in literature with Rhodamine 6G or methylene blue as a reference dye.[54] FT-IR spectra were acquired on a Perkin Elmer Spectrum Two spectrophotometer equipped with a Specac Golden Gate single reflection diamond accessory. ^1H NMR and ^{13}C NMR spectra were recorded on a BrukerDRX 400 MHz or BrukerDRX 500 MHz spectrometer. ^1H and ^{13}C chemical shifts were referenced with the

residual solvent resonances relative to TMS. The spectra were fully assigned with the help of various experiments (1D NOE, ^{1}H COSY, C,H Correlation and ^{13}C DEPT). Electronspray-ionisation mass spectrometry (ESI-MS) was performed on a Bruker esquire^{TM}/LC spectrometer or on a Bruker esquire^{TM}/HCT^{TM} spectrometer. High-resolution mass spectrometry (HR-MS) was performed on a Thermo DFS double-focusing system (ThermoFisher Scientific, Germany). Inductively coupled plasma mass spectrometry (ICP-MS) was measured on an Agilent QQQ8800 Triple Quad, equipped with a standard x-lens setting, nickel cones and a "micro-mist" quartz nebulizer. Tune settings were based on the Agilent General Purpose method and only slightly modified by an autotune procedure. Iron was measured as isotope ^{56}Fe, gold as isotope ^{197}Au and the values are reported as the average of 50 sweeps with five replicates. DLS measurements were carried out on a Malvern Zetasizer Nano Series instrument utilizing 90° backscatter at 25 °C. The concentration of stock NPs solutions were 0.5 mg/ml in PBS pH 7.4 and all NPs were filtered through a 0.2 µm filter before analysis. Typical count rates were 150-300 kHz. Hydrodynamic size data are reported as the mean of triplicate measurements. Zeta-potential measurements were performed on the same instrument using a Malvern folded U-shaped capillary cuvette. TEM was done on a FEI Tecnai G2 Spirit operated at 120 kV (NP analysis after synthesis). One drop of a dilute sample of NPs in hexane or PBS pH 7.4 was placed onto a formvar-coated copper grid, allowing the solvent to evaporate. Size analysis was performed on captured digital images using ImageJ V.1.47m, the size was determined from an average of 50 measurements and expressed as mean value ± standard deviation. Preparative HPLC was performed on a Varian Pro Star system, using a Macherey-Nagel RP 250/40 Nucleosil Gravity 7 µm C18 column. The solvents were 0.1% trifluoroacetic acid (solvent A) and methanol or acetonitrile (solvent B). The HPLC gradient used is as follows: 0-6 minutes: 95% A, 5% B; 6-20 minutes: linear gradient from 95% A (5% B) to 66% A (34% B); 20-60 minutes: linear gradient from 66% A (34% B) to 0% A (100% B). The flow rate was 30ml/min. Detection was performed at 254 nm. Analytical HPLC was performed on a Merck L7000 system, using a Macherey-Nagel Nucleosil C18 column. HPLC solvents were 0.1% TFA (solvent A) and methanol HPLC grade (solvent B). The HPLC gradient used is as follows: 0-3 minutes: 100% A; 3.1-9 minutes: 75% A, 25% B; 9.1-20 minutes: linear gradient from 66% A (34% B) to 0% A (100% B); 20-28 minutes: 100% B; 28.1-30: 100% A. The flow rate was 0.5 ml/min. Detection was performed at 254 nm. Size exclusion analytical HPLC in Zurich was performed on a Merck Hitachi L7000

system, using a RP-HPLC on a 8 x 300 mm, 200 Å Diol YMC size exclusion column. The system was equipped with the UV-detector L-7400, the luminescence-detector L-7485 and the radio-detector Berthold FlowStar LB513. The flow rate was 1.0 ml/min using PBS (pH 6.9) as a mobile phase. UV-detection was performed at 365 nm and luminescence-detection at 650 nm (excitation at 365 nm), equipped with the UV-detector L-7400 and the radio-detector Berthold FlowStar LB513. Activity measurements were carried out with a VDC-304 dose calibrator (Veenstra Instruments). Quality control in Maastricht was performed by analytical HPLC, using an LC apparatus that consisted of a solvent pump (Shimadzu, 20-AT) and a RP-HPLC on a 8 x 300 mm, 200 Å Diol YMC size exclusion column. The system was equipped with a diode array detector (Shimadzu, 20-AT) and a 3-inch radiometric NaI(Tl) detector in series. The flow rate was 1.0 ml/min using PBS (pH 6.9) as a mobile phase.

Microwave synthesis was carried out with a Biotage Initiator+ system.

3.3 Synthetic Part of the Section 2.1

3.3.1 The Synthesis of HS-CH_2-CH_2-DAP

Ethyl 2-cyano(hydroxyimino)ethanoate (1)[99]

A mixture of ethyl cyanoacetate (10.6 ml, 0.1 mol) and aqueous acetic acid (45%, 45 ml) was stirred at 0 °C. Sodium nitrite (21.0 g, 0.3 mol) was added portionwise during a period of 90 min. After the addition the reaction mixture was stirred at room temperature for another 4 h. The crude product was extracted with diethyl ether (2 x 200 ml). The solvent was removed under reduced pressure and the yellow solid dried in vacuum. Yield: 13.9 g (97%). ^{1}H NMR (300 MHz, $CDCl_3$, ppm) δ 4.38 (q, 2H, *J*=7.2 Hz), 1.40 (t, 3H, *J*=7.2 Hz).

1-Cyano-2-ethoxy-2-oxoethanaminium 4-methylbenzenesulfonate (2)[100]

Water (60 ml) was added to **1** (10.0 g, 70.0 mmol) and the suspension was carefully treated with a saturated sodium hydrogen carbonate solution (30 ml). To the yellow solution sodium dithionite (34.0 g, 0.2 mol) was added portionwise over a period of one hour. The temperature was kept below 20 °C during the addition. After stirring for another 30 min, extraction with dichloromethane (4 x 60 ml) was carried out. The combined organic phases were dried with magnesium sulfate and the solvent was removed under reduced pressure. The resulting yellow oil was dried under vacuum. Yield: 6.1 g (67%). This oil was immediately diluted with diethyl ether (50 ml) and a solution of *p*-toluenesulfonic acid monohydrate (10.1 g, 53.1 mmol) in ethanol (30 ml) was added. After stirring at room temperature for 15 min, the mixture was diluted with diethyl ether (100 ml) to induce crystallization. The flask was kept overnight at -20 °C and the precipitated white crystals were collected *via* filtration. Yield: 7.8 g (37%).

Ethyl *N*-(*tert*-butoxycarbonyl)-3-nitriloalaninate (3)[101]

To a solution of di-*tert*-butyl dicarbonate (8.0 g, 36.6 mmol) in toluene (25 ml) was added **2** (6.4 g, 20.9 mmol) and *N,N'*-diisopropylethylamine (3.6 ml, 20.9 mmol). The reaction mixture was refluxed at 100 °C for 6 h. After cooling to room temperature, water (25 ml) was added and the resulting suspension was poured into ethyl acetate (300 ml). The organic layer was extracted with 1:1 water / saturated aqueous sodium hydrogen carbonate (200 ml), water (200 ml) and brine (200 ml). The organic phase was dried over sodium sulfate, filtered and concentrated in vacuum. The residue was purified by silica gel column chromatography (4:1

hexane / ethyl acetate) to give the product as a white solid. Yield: 3.2 g (70%). ^{1}H NMR (400 MHz, $CDCl_3$, ppm) δ 5.37 (s, 1H), 5.26 (d, 1H, *J*=7.8 Hz), 4.36 (q, 2H, *J*=7.2 Hz), 1.48 (s, 9H), 1.36 (t, 3H, *J*=7.2 Hz). R_f = 0.35 (4:1 hexane / ethyl acetate).

{[(2-Bromoethyl)sulfanyl]methyl}benzene (4)[102]

Potassium *tert*-butoxide (3.4 g, 30 mmol) was dissolved in dry ethanol (30 ml) and stirred at room temperature for 10 min. Phenylmethanethiol (3.5 ml, 30 mmol) and 1,2-dibromoethane (5.17 ml, 60 mmol) were added and the mixture was stirred at room temperature for 13 h, whereas a colorless precipitate was formed over time. After adding diethyl ether (200 ml), the mixture was filtered and concentrated under reduced pressure. The residue was purified by silica gel column chromatography (ethyl acetate) to give a colorless oil. Yield: 5.3 g (77%). ^{1}H NMR (300 MHz, $CDCl_3$, ppm) δ 7.26 – 7.39 (m, 5H), 3.79 (s, 2H), 3.39 (t, 2H, *J*=8.3 Hz), 2.88 (t, 2H, *J*=8.3 Hz). ESI-MS (MeOH): m/z = 253 $[M+Na]^+$. R_f = 0.70 (ethyl acetate).

{[(2-Iodoethyl)sulfanyl]methyl}benzene (5)[102]

4 (4.0 g, 17 mmol) was dissolved in acetone (100 ml) and sodium iodide (5.2 g, 35 mmol) was added. The mixture was stirred at room temperature for 14 h, whereas a colorless precipitate was formed over time. The precipitate was filtered and the filtrate was concentrated under reduced pressure. The residue was dissolved in diethyl ether (150 ml), washed with aqueous sodium dithionite solution and dried with magnesium sulfate. After filtration, the solvent was removed under reduced pressure and the product as a colorless oil was used without further purification. Yield: 4.3 g (90%). ^{1}H NMR (300 MHz, $CDCl_3$, ppm) δ 7.26 – 7.37 (m, 5H), 3.78 (s, 2H), 3.19 (t, 2H, *J*=8.4 Hz), 2.90 (t, 2H, *J*=8.4 Hz). ESI-MS (MeOH): m/z = 301 $[M+Na]^+$. R_f = 0.57 (3:1 hexane / ethyl acetate).

Ethyl 4-(benzylsulfanyl)-*N*-(*tert*-butoxycarbonyl)-2'-nitriloisovalinate (6)

Potassium *tert*-butoxide (224 mg, 2.0 mmol) was dissolved in dry *tert*-butanol (15 ml) and **3** (228 mg, 1.0 mmol) was added. The mixture was stirred at 50 °C for 20 min and cooled to room temperature. **5** (160 µl, 1.0 mmol) was added to the solution and the reaction mixture was stirred at 80 °C for 14 h while it became red. The solvent was removed under reduced pressure and the resulting residue was treated with water (50 ml) and extracted with ethyl acetate (3 x 100 ml). The organic phase was washed with brine, dried over magnesium

sulfate and filtered. The solvent was removed under reduced pressure and the resulting crude was purified by silica gel column chromatography (3:1 hexane / ethyl acetate) to give a yellow oil. Yield: 182 mg (50%). ^{1}H NMR (300 MHz, $CDCl_3$, ppm) δ 7.24 – 7.37 (m, 5H), 5.60 (s, 1H), 4.28 (q, 2H, *J*=7.2 Hz), 3.74 (s, 2H), 2.55 (t, 2H, *J*=7.7 Hz), 2.31 – 2.43 (m, 1H), 2.15 – 2.25 (m, 1H), 1.45 (s, 9H), 1.32 (t, 3H, *J*=7.2 Hz). ^{13}C NMR (75 MHz, $CDCl_3$, ppm) δ 137.41, 128.97, 128.83, 127.51, 63.93, 36.44, 28.30, 28.37, 28.27, 27.90, 25.17, 14.07. ESI-MS (MeOH): m/z = 401 $[M+Na]^+$. R_f = 0.25 (3:1 hexane / ethyl acetate).

Ethyl 4-(benzylsulfanyl)-*N*-(*tert*-butoxycarbonyl)-2'-[(*tert*-butoxycarbonyl)amino]isovalinate (7)

6 (320 mg, 0.9 mmol) was dissolved in dry methanol (20 ml) and cooled to 0 °C. Di-*tert*-butyldicarbonat (371 mg, 1.7 mmol) and nickel(II) chloride hexahydrate (20 mg, 0.09 mmol) were added. Afterwards sodium borohydride (257 mg, 6.8 mmol) was added portionwise during a time period of 30 min. The black mixture was stirred at room temperature for 16 h. Diethylenetriamine (0.1 ml, 0.9 mmol) was added and the mixture was stirred at room temperature for an additional 60 min. The solvent was evaporated and the residue was partitioned between ethyl acetate and saturated sodium hydrogen carbonate. The organic phase was dried over magnesium sulfate and the resulting colorless oil was purified by silica gel column chromatography (1:2 hexane / ethyl acetate). Yield: 340 mg (82%). ^{1}H NMR (300 MHz, $CDCl_3$, ppm) δ 7.28 – 7.33 (m, 5H), 5.66 (s, 1H), 5.05 (s, 1H), 4.26 (q, 2H, *J*=7.0 Hz), 3.84 (s, 2H), 3.74 (s, 2H), 2.55 (t, 2H, *J*=7.7 Hz), 2.18 – 2.24 (m, 1H), 1.99 – 2.09 (m, 1H), 1.48 (s, 18H), 1.32 (t, 3H, *J*=7.0 Hz). ^{13}C NMR (75 MHz, $CDCl_3$, ppm) δ 155.49, 148.22, 128.84, 128.68, 127.36, 57.85, 36.22, 28.36, 28.22, 28.11, 26.72, 24.99, 14.20. ESI-MS (MeOH): m/z = 505 $[M+Na]^+$. R_f = 0.22 (1:2 hexane / ethyl acetate).

2'-Amino-4-(benzylsulfanyl)isovaline hydrochloride (8)

7 (338 mg, 0.7 mmol) was dissolved in a mixture of MeOH and 1 M NaOH (1:1, 5 ml). The hydrolysis of the ester occurred at 80 °C during 12 h. After neutralization with 1 M HCl, the solvent was removed under reduced pressure and the residue was dissolved in 1 M HCl (4 ml). Stirring at 90 °C for 12 h led to complete removal of the amine protection groups. After cooling to room temperature, the pH was adjusted to 7 and the solvent was evaporated. The mixture was redissolved in methanol (1ml) and the product was separated from sodium chloride *via* decantation of the methanol phase. This procedure was repeated four times. Yield: 108 mg (53%). ^{1}H NMR (500 MHz, MeOD, ppm) δ 7.19 – 7.32 (m, 5H), 4.16 – 4.19 (m,

2H), 3.72 (s, 2H), 2.50 (t, 2H, *J*=7.3 Hz), 1.99 – 2.07 (m, 1H), 1.84 – 1.91 (m, 1H). ^{13}C NMR (125 MHz, MeOD, ppm) δ 130.18, 129.64, 128.14, 58.81, 36.62, 32.37, 27.51. ESI-MS (MeOH): m/z = 253 $[M-H]^-$.

4,4'-Disulfanediylbis[2-amino-2-(aminomethyl)butanoic acid] dihydrochloride (9)

8 (68 mg, 0.24 mmol) was dissolved in a solution of 0.4 M diphenyl sulfoxide and 1 M methyltrichlorosilane in TFA. The mixture was stirred at 0 °C for 4 h while a colorless precipitate was formed over time. After warming up to room temperature, the solvent was removed under reduced pressure and the resulting residue was washed five times with diethyl ether to remove unreacted diphenyl sulfoxide. The residue was dissolved in water and lyophilized to give the product as a colorless solid. Yield: 40 mg (53%). ^{1}H NMR (300 MHz, D_2O, ppm) δ 4.81 (t, 2H, *J*=5.7 Hz), 3.12 (t, 2H, *J*=6.6 Hz), 2.54 – 2.68 (m, 2H). ^{13}C NMR (75 MHz, D_2O, ppm) δ 178.37, 58.55, 32.80, 30.24. ESI-MS (MeOH): m/z = 325 $[M-H]^-$.

[(2-Bromoethoxy)methyl]benzene (10)

2-Benzyloxyethanol (2.9 g, 19.1 mmol) was dissolved in dry dichloromethane (100 ml) and cooled to 0 °C. Tetrabromomethane (7.3 g, 22.0 mmol) was added and the mixture was stirred for 5 min. Afterwards triphenylphosphine (5.8 g, 22.0 mmol) was added portionwise during 30 min. The mixture was stirred at room temperature for additional 5 h. After concentration to half of its volume, hexane (250 ml) was added and a white precipitate was filtered. The solvent was removed under reduced pressure and the resulting crude was purified by silica gel column chromatography (1:1 hexane / ethyl acetate) to give the product as a colorless oil. Yield: 3.4 g (82%). ^{1}H NMR (400 MHz, $CDCl_3$, ppm) δ 7.30 – 7.37 (m, 5H), 4.60 (s, 2H), 3.80 (t, 2H, *J*=6.3 Hz), 3.50 (t, 2H, *J*=6.3 Hz). ESI-MS (MeOH): m/z = 237 $[M+Na]^+$. R_f = 0.73 (1:1 hexane / ethyl acetate).

Ethyl 4-(benzyloxy)-*N*-(tert-butoxycarbonyl)-2'-nitriloisovalinate (11)

Sodium (0.26 g, 11.1 mmol) was dissolved in dry ethanol (100 ml) and **3** (2.54 g, 11.1 mmol) was added. The mixture was stirred at 60 °C for 45 min and then cooled to room temperature. **10** (2.39 g, 9.4 mmol) was added to the solution and the reaction mixture was refluxed overnight while it became red. The solvent was removed under reduced pressure and the resulting residue was treated with water (100 ml) and extracted with ethyl acetate (2 x 300 ml). The organic phase was washed with brine, dried over magnesium sulfate and

filtered. The solvent was removed under reduced pressure and the resulting crude was purified by silica gel column chromatography (2:1 hexane / ethyl acetate) to give a yellowish oil. Yield: 1.72 g (42%). ^{1}H NMR (400 MHz, $CDCl_3$, ppm) δ 7.29 – 7.38 (m, 5H), 6.63 (s, 1H), 4.48 – 4.57 (m, 2H), 4.26 (q, 2H, *J*=7.3 Hz), 3.82 – 3.88 (m, 1H), 3.72 – 3.73 (m, 1H), 2.30 – 2.39 (m, 2H), 1.46 (s, 9H) 1.29 (t, 3H, *J*=7.3 Hz). ^{13}C NMR (100 MHz, $CDCl_3$, ppm) δ 166.52, 153.99, 136.89, 129.62, 128.53, 128.09, 126.86, 73.66, 66.14, 64.06, 63.41, 35.97, 28.11, 13.87. ESI-MS (MeOH): m/z = 385 $[M+Na]^+$. R_f = 0.32 (2:1 hexane / ethyl acetate).

Ethyl 4-(benzyloxy)-*N*-(*tert*-butoxycarbonyl)-2'-[(*tert*-butoxycarbonyl)amino]isovalinate (12)

10 (1.70 g, 4.7 mmol) was dissolved in dry methanol (75 ml) and cooled to 0 °C. Di-*tert*-butyldicarbonat (2.03 g, 9.3 mmol) and nickel(II) chloride hexahydrate (0.01 g, 0.5 mmol) were added. Afterwards sodium borohydride (1.41 g, 37.2 mmol) was added portionwise during a time period of 1 h. The black mixture was stirred at room temperature for 14 h. Diethylenetriamine (0.55 ml, 5.1 mmol) was added and the mixture was stirred at room temperature for 60 min. The solvent was evaporated and the residue was partitioned between ethyl acetate and saturated sodium hydrogen carbonate. The organic phase was dried over magnesium sulfate and the resulting colorless oil was purified by silica gel column chromatography (1:1 hexane / ethyl acetate). Yield: 1.69 g (78%). ^{1}H NMR (400 MHz, $CDCl_3$, ppm) δ 7.27 – 7.35 (m, 5H), 6.13 (s, 1H), 5.03 (s, 1H), 4.44 (s, 2H), 4.11 (q, 2H, *J*=7.3 Hz), 3.67 – 3.73 (m, 2H), 3.52 – 3.58 (m, 2H), 2.26 – 2.33 (m, 1H), 2.09 – 2.16 (m, 1H), 1.41 (s, 18H), 1.21 (t, 3H, *J*=7.3 Hz). ^{13}C NMR (100 MHz, $CDCl_3$, ppm) δ 172.69, 156.86, 154.65, 137.81, 129.72, 128.32, 127.74, 127.67, 79.54, 73.27, 66.04, 62.35, 61.65, 44.61, 32.88, 23.30, 13.96. ESI-MS (MeOH): m/z = 489 $[M+Na]^+$. R_f = 0.63 (2:1 hexane / ethyl acetate).

Ethyl *N*-(*tert*-butoxycarbonyl)-2'-[(*tert*-butoxycarbonyl)amino]-4-hydroxyisovalinate (13)

12 (1.69 g, 3.6 mmol) was dissolved in methanol (25 ml). Palladium on carbon (10%) (65 mg) was added and the benzyl protecting group was cleaved under atmospheric hydrogen pressure overnight at room temperature. The reaction mixture was filtered and the volatile part was removed to give a colorless oil. Yield: 1.13 g (83%). ^{1}H NMR (400 MHz, $CDCl_3$, ppm) δ 5.96 (s, 1H), 5.00 (s, 1H), 4.20 (q, 2H, *J*=7.3 Hz), 3.64 – 3.76 (m, 4H), 2.18 – 2.28 (m, 1H), 2.02 – 2.11 (m, 1H), 1.42 (s, 18H), 1.27 (t, 3H, *J*=7.3 Hz). ^{13}C NMR (100 MHz, $CDCl_3$, ppm) δ 173.00, 156.02, 154.65, 79.51, 62.25, 61.86, 44.63, 28.29, 14.01. ESI-MS (MeOH): m/z = 399 $[M+Na]^+$. R_f = 0.27 (1:1 hexane / ethyl acetate).

Ethyl 4-bromo-*N*-(*tert*-butoxycarbonyl)-2'-[(*tert*-butoxycarbonyl)amino]isovalinate (14)

13 (1.72 g, 4.56 mmol) was dissolved in dry dichloromethane (50 ml) and cooled to 0 °C. Tetrabromomethane (1.66 g, 5.02 mmol) was added and the mixture was stirred for 5 min. Afterwards triphenylphosphine (1.32 g, 5.02 mmol) was added portionwise during 30 min. The mixture was stirred at room temperature for additional 3 h. After concentration to half of its volume, hexane (100 ml) was added and the white precipitate was filtered. The solvent was removed under reduced pressure and the resulting crude was purified by silica gel column chromatography (1:1 hexane / ethyl acetate). Yield: 1.50 g (75%). ^{1}H NMR (400 MHz, $CDCl_3$, ppm) δ 5.67 (s, 1H), 4.76 (s, 1H), 4.23 (q, 2H, *J*=7.3 Hz), 3.62 – 3.75 (m, 2H), 3.32 – 3.38 (m, 1H), 3.22 – 3.28 (m, 1H), 2.70 – 2.79 (m, 1H), 2.39 – 2.46 (m, 1H), 1.45 (s, 9H), 1.42 (s, 9H), 1.28 (t, 3H, *J*=7.3 Hz). ^{13}C NMR (100 MHz, $CDCl_3$, ppm) δ 171.75, 155.64, 154.10, 79.75, 63.43, 62.47, 44.82, 35.83, 28.30, 13.98. ESI-MS (MeOH): m/z = 439 $[M+H]^+$. R_f = 0.77 (1:1 hexane / ethyl acetate).

1,1',1''-{[(2-Bromoethyl)sulfanyl]methanetriyl}tribenzene (15)

Potassium *tert*-butoxide (0.50 g, 4.4 mmol) was dissolved in dry methanol (20 ml) and stirred for 10 min at room temperature. Triphenylmethanethiol (1.11 g, 4.0 mmol) and 1,2-dibromoethane (0.70 ml, 8.0 mmol) were added and the mixture was stirred at room temperature for 13 h, whereas a colorless precipitate was formed over time. After adding diethyl ether (200 ml), the mixture was filtered and concentrated under reduced pressure. The residue was purified by silica gel column chromatography (ethyl acetate) to give a yellow solid. Yield: 1.07 g (70%). ^{1}H NMR (400 MHz, $CDCl_3$, ppm) δ 7.46 – 7.50 (m, 6H), 7.25 – 7.35 (m, 9H), 2.92 (t, 2H, *J*=6.8 Hz), 2.77 (t, 2H, *J*=6.8 Hz). ESI-MS (MeOH): m/z = 383 $[M+H]^+$. R_f = 0.74 (ethyl acetate).

2,2'-Disulfanediyldiethanol (16)[108]

2-Sulfanylethanol (12.0 ml, 0.17 mol) was dissolved in dichloromethane (160 ml) and an aqueous potassium bicarbonate solution (10%, 160 ml). Bromine (8 ml) was added dropwise at 0°C and after addition the mixture was stirred for additional 60 min at room temperature. The organic phase was separated and the aqueous phase was extracted with dichoromethane (3 x 100 ml). The combined organic phases were dried with sodium sulfate and the solvent was removed under reduced pressure. The resulting crude was purified by silica gel column chromatography (10:1 dichloromethane / methanol) to give a colorless oil.

Yield: 3.1 g (12%). ^{1}H NMR (400 MHz, $CDCl_3$, ppm) δ 3.88 (t, 2H, *J*=5.7 Hz), 2.86 (t, 2H, *J*=5.7 Hz). ESI-MS (MeOH): m/z = 177 $[M+H]^+$. R_f = 0.46 (10:1 dichloromethane / methanol).

1-Bromo-2-[(2-bromoethyl)disulfanyl]ethane (17)[108]

To a solution of hydrobromic acid (48%, 52 ml) was added dropwise to concentrated sulfuric acid (34 ml) at 0 °C. Afterwards 2,2'-disulfanediyldiethanol (1.5 g, 9.6 mmol) was added dropwise and the mixture was stirred at room temperature for 20 h and at 80 °C for 3 h. After cooling to room temperature, dichloromethane (10 ml) was added, the upper layer was taken and washed with aqueous sodium carbonate solution (10%). The solvent was removed under reduced pressure and the product as a colorless oil was used without further purification. Yield: 1.0 g (37%). ^{1}H NMR (400 MHz, $CDCl_3$, ppm) δ 3.61 (t, 2H, *J*=7.9 Hz), 3.10 (t, 2H, *J*=7.9 Hz).

3.3.2 The Synthesis of CdTe/ZnTe Core-Shell QDs

This synthesis was performed according to a literature procedure, but L-cystine was used instead of L-cysteine and the entire synthesis was downscaled.[109] L-cystine (121.4 mg, 0.51 mmol) and $NaBH_4$ (38.2 mg (1.0 mmol) were mixed in nitrogen-saturated water (10 ml) and stirred at room temperature for 4 h. In the meantime, tellurium powder (15 mg), sodium borohydride (9 mg) and nitrogen-saturated water (2 ml) were mixed and stirred at room temperature for 30 min, whereas the mixture became slightly pink. In a three-neck round bottom flask cadmium perchlorate hexahydrate (0.5 g), zinc perchlorate hexahydrate (1.33 g) and nitrogen-saturated water (20 ml) were mixed and the reduced L-cystine containing aqueous solution was added. 10 M sodium hydroxide solution (0.5 ml) was added dropwise to obtain an optically clear mixture. The solution with NaHTe precursor was added and the mixture was heated to 100 °C over a period of 20 min and stirred at this temperature for 60 min. After cooling to room temperature, ethanol (150 ml) was added to precipitate the quantum dots. After centrifugation and removal of the supernatant, the quantum dots were washed with ethanol and dried under vacuum.

3.3.3 The Functionalization of CdTe/ZnTe Core-Shell QDs with HS-CH_2-CH_2-DAP

The disulfide **9** (70 mg, 0.23 mmol) and $NaBH_4$ (9.6 mg (0.25 mmol) were dissolved in nitrogen-saturated water (10 ml) and the solution was stirred at room temperature for 2 h. CdTe/ZnTe core-shell QDs (5 mg) were dispersed in 0.8 ml of the reduced disulfide solution

and stirred at room temperature for 5 h. To remove excess coating ligand, ethanol (10 ml) was added and the precipitated QDs were isolated by centrifugation and removal of the surfactant. This procedure was repeated three times and the purified QDs were dispersed in water (2.5 ml).

3.4 Synthetic Part of the Section 2.2

3.4.1 The Synthesis of HS-PEG-DAP (26)

1-Phenyl-2,5,8,11-tetraoxatridecan-13-ol (18)[106]

Tetraethylene glycol (9.7 g, 50 mmol) was dissolved in tetrahydrofurane (50 ml) and cooled to 0 °C. Sodium hydride (60% dispersion in mineral oil, 2.08 g) was added and the resulting mixture was stirred at room temperature for 30 min. Afterwards benzyl bromide (5.12 g, 43.4 mmol) was added and the mixture was stirred at room temperature overnight. The reaction was quenched with water (50 ml) and the mixture was extracted with ethyl acetate (3 x 80 ml). The combined organic phases were dried over magnesium sulfate, filtered and concentrated under reduced pressure. The residue was purified by silica gel column chromatography (ethyl acetate) to give **18** as a colorless oil. Yield: 7.32 g (86%). ^{1}H NMR (400 MHz, $CDCl_3$, ppm) δ 7.27 – 7.37 (m, 5H), 4.58 (s, 2H), 3.60 – 3.74 (m, 16H), 2.76 (s, 1H). ESI-MS (MeOH): m/z = 307 $[M+Na]^+$. R_f = 0.12 (ethyl acetate).

13-Bromo-1-phenyl-2,5,8,11-tetraoxatridecane (19)[116]

18 (3.7 g, 13.0 mmol) was dissolved in dry dichloromethane (70 ml) and cooled to 0 °C. Tetrabromomethane (5.1 g, 15.2 mmol) was added and the mixture was stirred for 5 min. Afterwards triphenylphosphine (4.0 g, 15.2 mmol) was added portionwise during 30 min. The mixture was stirred at room temperature for an additional 3 h. After concentration to half of its volume, hexane (200 ml) was added and the white precipitate was filtered. The solvent was removed under reduced pressure and the resulting crude was purified by silica gel column chromatography (1:1 hexane / ethyl acetate) to give **19** as a colorless oil. Yield: 4.4 g (98%). ^{1}H NMR (400 MHz, $CDCl_3$, ppm) δ 7.25 – 7.35 (m, 5H), 4.57 (s, 2H), 3.80 (t, 2H, *J*=6.3 Hz), 3.62 – 3.69 (m, 12H), 3.45 (t, 2H, *J*=6.3 Hz). ESI-MS (MeOH): m/z = 349 $[M+Na]^+$. R_f = 0.30 (1:1 hexane / ethyl acetate).

Ethyl 4-(2-{2-[2-(benzyloxy)ethoxy]ethoxy}ethoxy)-*N*-(*tert*-butoxycarbonyl)-2'-nitriloisovalinate (20)

Sodium (0.15 g, 6.4 mmol) was dissolved in dry ethanol (55 ml) and **3** (1.46 g, 6.4 mmol) was added. The mixture was stirred at 60 °C for 40 min and then cooled to room temperature. **19** (2.22 g, 6.4 mmol) was added to the solution and the reaction mixture was refluxed overnight while it became red. The solvent was removed under reduced pressure and the

resulting residue was treated with water (80 ml) and extracted with ethyl acetate (3 x 150 ml). The combined organic phases were washed with brine, dried over magnesium sulfate and filtered. The solvent was removed under reduced pressure and the resulting crude was purified by silica gel column chromatography (2:1 hexane / ethyl acetate) to give the product **20** as a yellow oil. Yield: 2.03 g (64%). ^{1}H NMR (400 MHz, $CDCl_3$, ppm) δ 7.24 – 7.35 (m, 5H), 6.61 (s, 1H), 4.56 (s, 2H), 4.29 (q, 2H, *J*=7.0 Hz), 3.59 – 3.79 (m, 14H), 2.19 – 2.35 (m, 1H), 1.95 – 2.12 (m, 1H), 1.45 (s, 9H) 1.32 (t, 3H, *J*=7.0 Hz). ^{13}C NMR (100 MHz, $CDCl_3$, ppm) δ 171.07, 166.59, 138.21, 128.29, 127.67, 127.54, 116.93, 81.24, 73.16, 70.63, 70.59, 70.54, 70.40, 70.25, 69.03, 67.03, 63.29, 60.32, 32.10, 28.24, 28.14, 15.10, 13.89. ESI-MS (MeOH): m/z = 517 $[M+Na]^+$. HR-ESI-MS (3:2 MeOH / $CHCl_3$) for $C_{25}H_{38}N_2NaO_8$ $[M+Na]^+$: calculated, 517.2520; found, 517.2519. R_f = 0.16 (2:1 hexane / ethyl acetate).

Ethyl 4-(2-{2-[2-(benzyloxy)ethoxy]ethoxy}ethoxy)-*N*-(*tert*-butoxycarbonyl)-2'-[(*tert*-butoxycarbonyl)amino]isovalinate (21)

20 (2.03 g, 4.1 mmol) was dissolved in dry methanol (40 ml) and cooled to 0 °C. Di-*tert*-butyldicarbonat (1.79 g, 8.2 mmol) and nickel(II) chloride hexahydrate (0.10 g, 0.4 mmol) were added. Afterwards sodium borohydride (1.24 g, 32.8 mmol) was added portionwise during a period of 1 h. The black mixture was stirred at room temperature for 14 h. Diethylenetriamine (0.49 ml, 4.5 mmol) was added and the mixture was stirred at room temperature for additional 90 min. The solvent was evaporated and the residue was partitioned between ethyl acetate and a saturated sodium hydrogen carbonate solution. The organic phase was dried over magnesium sulfate and the resulting colorless oil was purified by silica gel column chromatography (1:1 hexane / ethyl acetate). Yield: 1.91 g (77%). ^{1}H NMR (400 MHz, $CDCl_3$, ppm) δ 7.24 – 7.35 (m, 5H), 6.04 (s, 1H), 5.08 (s, 1H), 4.56 (s, 2H), 4.17 (q, 2H, *J*=7.0 Hz), 3.48 – 3.68 (m, 16H), 2.25 – 2.30 (m, 1H), 2.06 – 2.13 (m, 1H), 1.42 (s, 9H), 1.41 (s, 9H), 1.26 (t, 3H, *J*=7.0 Hz). ^{13}C NMR (100 MHz, $CDCl_3$, ppm) δ 172.69, 155.91, 154.64, 138.25, 128.32, 127.70, 127.56, 79.53, 79.24, 73.21, 70.64, 70.63, 70.57, 70.36, 70.27, 69.41, 66.91, 62.27, 61.60, 44.62, 32.73, 31.89, 29.66, 28.30, 22.66, 14.02. ESI-MS (MeOH): m/z = 621 $[M+Na]^+$. HR-ESI-MS (3:2 MeOH / $CHCl_3$) for $C_{30}H_{51}N_2O_{10}$ $[M+H]^+$: calculated, 599.3538; found, 599.3536. R_f = 0.35 (1:1 hexane / ethyl acetate).

Ethyl *N*-(*tert*-butoxycarbonyl)-2'-[(*tert*-butoxycarbonyl)amino]-4-{2-[2-(2-hydroxyethoxy)ethoxy]ethoxy}isovalinate (22)

21 (1.21 g, 2.0 mmol) was dissolved in dry methanol (25 ml). Palladium on carbon (10%) (35 mg) was added and the benzyl protecting group was cleaved under atmospheric hydrogen pressure overnight at room temperature. The reaction mixture was filtered and the volatile part was removed to give the product as a colorless oil. Yield: 1.02 g (98%). ^{1}H NMR (400 MHz, $CDCl_3$, ppm) δ 6.06 (s, 1H), 5.13 (s, 1H), 4.17 (q, 2H, *J*=7.0 Hz), 3.50 – 3.73 (m, 16H), 2.24 – 2.28 (m, 1H), 2.07 – 2.14 (m, 1H), 1.42 (s, 9H), 1.41 (s, 9H), 1.26 (t, 3H, *J*=7.0 Hz). ^{13}C NMR (100 MHz, $CDCl_3$, ppm) δ 172.70, 155.92, 154.64, 79.27, 72.56, 70.58, 70.38, 70.32, 70.21, 66.91, 62.19, 61.69, 61.61, 50.72, 44.64, 32.67, 28.30, 14.01. ESI-MS (MeOH): m/z = 531 $[M+Na]^+$. R_f = 0.11 (1:1 hexane / ethyl acetate).

Ethyl 4-{2-[2-(2-bromoethoxy)ethoxy]ethoxy}-*N*-(*tert*-butoxycarbonyl)-2'-[(*tert*-butoxycarbonyl)amino]isovalinate (23)

22 (1.02 g, 2.0 mmol) was dissolved in dry dichloromethane (30 ml) and cooled to 0 °C. Tetrabromomethane (0.78 g, 2.4 mmol) was added and the mixture was stirred for 5 min. Afterwards triphenylphosphine (0.62 g, 2.4 mmol) was added portionwise during 30 min. The mixture was stirred for at room temperature for additional 4 h. After concentration to half of its volume, hexane (80 ml) was added and the white precipitate was filtered. The solvent was removed under reduced pressure and the resulting crude was purified by silica gel column chromatography (1:1 hexane / ethyl acetate) to give the product as a colorless oil. Yield: 0.93 g (71%). ^{1}H NMR (400 MHz, $CDCl_3$, ppm) δ 6.04 (s, 1H), 5.07 (s, 1H), 4.17 (q, 2H, *J*=7.0 Hz), 3.80 (t, 2H, *J*=6.3 Hz), 3.51 – 3.68 (m, 12H), 3.47 (t, 2H, *J*=6.3 Hz), 2.24 – 2.30 (m, 1H), 2.06 – 2.13 (m, 1H), 1.42 (s, 9H), 1.41 (s, 9H), 1.26 (t, 3H, *J*=7.0 Hz). ^{13}C NMR (100 MHz, $CDCl_3$, ppm) δ 172.70, 155.91, 154.62, 79.55, 79.28, 71.21, 70.54, 70.44, 70.28, 66.95, 62.27, 61.62, 44.62, 32.74, 30.21, 28.31, 14.17. ESI-MS (MeOH): m/z = 595 $[M+Na]^+$. HR-ESI-MS (3:2 MeOH / $CHCl_3$) for $C_{23}H_{44}BrN_2O_9$ $[M+H]^+$: calculated, 571.2220; found, 571.2219. R_f = 0.56 (1:1 hexane / ethyl acetate).

Ethyl *N*-(*tert*-butoxycarbonyl)-2'-[(*tert*-butoxycarbonyl)amino]-4-(2-{2-[2-(tritylsulfanyl)ethoxy]ethoxy}ethoxy)isovalinate (24)

Triphenylmethanethiol (0.37 g, 1.34 mmol) was dissolved in dry tetrahydrofurane (12 ml) and sodium hydride (60% dispersion in mineral oil, 53.6 mg) was added. The yellow solution was stirred at room temperature for 20 min. Afterwards **23** (0.73 g, 1.28 mmol), dissolved in dry THF (7 ml), was added and the mixture was refluxed for 3 h. The solvent was removed

under reduced pressure and the resulting residue was treated with water (20 ml) and extracted with ethyl acetate (3 x 60 ml). The organic phase was washed with brine, dried over magnesium sulfate and filtered. The solvent was removed under reduced pressure and the resulting crude was purified by silica gel column chromatography (1:1 hexane / ethyl acetate) to give the product as a colorless oil. Yield: 0.89 g (90%). ^{1}H NMR (400 MHz, $CDCl_3$, ppm) δ 7.39 – 7.42 (m, 6H), 7.24 – 7.29 (m, 6H), 7.18 – 7.22 (m, 3H), 6.03 (s, 1H), 5.07 (s, 1H), 4.16 (q, 2H, *J*=7.0 Hz), 3.65 – 3.70 (m, 2H), 3.43 – 3.57 (m, 10H), 3.29 (t, 2H, *J*=7.0 Hz), 2.42 (t, 2H, *J*=7.0 Hz), 2.24 – 2.28 (m, 1H), 2.05 – 2.12 (m, 1H), 1.42 (s, 18H), 1.25 (t, 3H, *J*=7.0 Hz). ^{13}C NMR (100 MHz, $CDCl_3$, ppm) δ 172.73, 155.95, 154.66, 144.85, 129.64, 127.88, 126.66, 79.29, 70.45, 70.40, 70.30, 70.20, 69.65, 66.61, 62.30, 61.65, 44.66, 32.76, 31.65, 28.36, 14.06. ESI-MS (MeOH): m/z = 789 $[M+Na]^+$. HR-ESI-MS (3:2 MeOH / $CHCl_3$) for $C_{42}H_{58}N_2NaO_9S$ $[M+Na]^+$: calculated, 789.3755; found, 789.3750. R_f = 0.59 (1:1 hexane / ethyl acetate).

_N_-(_tert_-Butoxycarbonyl)-2'-[(_tert_-butoxycarbonyl)amino]-4-(2-{2-[2-(tritylsulfanyl)ethoxy]ethoxy}ethoxy)isovaline (25)

24 (0.587 g, 0.76 mmol) was dissolved in a 1:1 mixture of 1 M NaOH (4 ml) and methanol (4 ml). The solution was stirred for 16 h at 80 °C. Afterwards, the solution was allowed to cool to room temperature and the pH was adjusted to pH ~ 7 with 2 M HCl. The solvent was removed under reduced pressure and the resulting residue was washed with water (4 x 7 ml) to remove the sodium chloride. The product was obtained as a colorless oil. Yield: 0.544 g (97%). ^{1}H NMR (400 MHz, $CDCl_3$, ppm) δ 7.42 – 7.45 (m, 6H), 7.27 – 7.31 (m, 6H), 7.21 – 7.24 (m, 3H), 6.40 (s, 1H), 5.14 (s, 1H), 3.42 – 3.60 (m, 12H), 3.31 (t, 2H, *J*=6.8 Hz), 2.45 (t, 2H, *J*=6.8 Hz), 2.28 – 2.30 (m, 1H), 2.05 – 2.08 (m, 1H), 1.44 (s, 9H), 1.41 (s, 9H). ^{13}C NMR (100 MHz, $CDCl_3$, ppm) δ 178.06, 156.78, 154.96, 145.04, 129.85, 128.11, 126.88, 79.47, 70.11, 70.02, 69.90, 69.72, 67.71, 66.87, 62.07, 31.66, 28.76, 28.66. ESI-MS (MeOH): m/z = 737 $[M-H]^-$, m/z = 783 $[M-H+2Na]^+$. HR-ESI-MS (3:2 MeOH / $CHCl_3$) for $C_{40}H_{53}N_2Na_2O_9S$ $[M-H+2Na]^+$: calculated, 783.3261; found, 783.3254.

2'-Amino-4-{2-[2-[2-sulfanylethoxy]ethoxy}ethoxy)isovaline (26)

25 (150 mg, 0.20 mmol) was dissolved in dichloromethane (1.2 ml, 19.2 mmol). Trifluoroacetic acid (0.61 ml, 7.8 mmol) and triethylsilane (0.24 ml, 1.5 mmol) was added and the solution was stirred at room temperature for 2 h. The solvent was removed under reduced pressure and the resulting residue was washed with diethylether (4 x 10 ml) to give the product as a colorless, sticky solid. Yield: 58 mg (98%). ^{1}H NMR (400 MHz, D_2O, ppm) δ 3.81 – 3.86 (m, 2H), 3.68 – 3.76 (m, 12H), 3.48 (s, 2H), 2.78 (t, 2H, *J*=6.0 Hz). ^{13}C NMR (100 MHz, D_2O, ppm) δ 171.98, 72.12, 69.65, 69.46, 69.24, 69.15, 66.15, 60.19, 42.27, 32.56, 23.07. ESI-MS (MeOH): m/z = 295 $[M-H]^-$, m/z = 297 $[M+H]^+$. HR-ESI-MS (3:2 MeOH / $CHCl_3$) for $C_{25}H_{38}N_2NaO_8$ $[M+H]^+$: calculated, 297.1478; found, 297.1481.

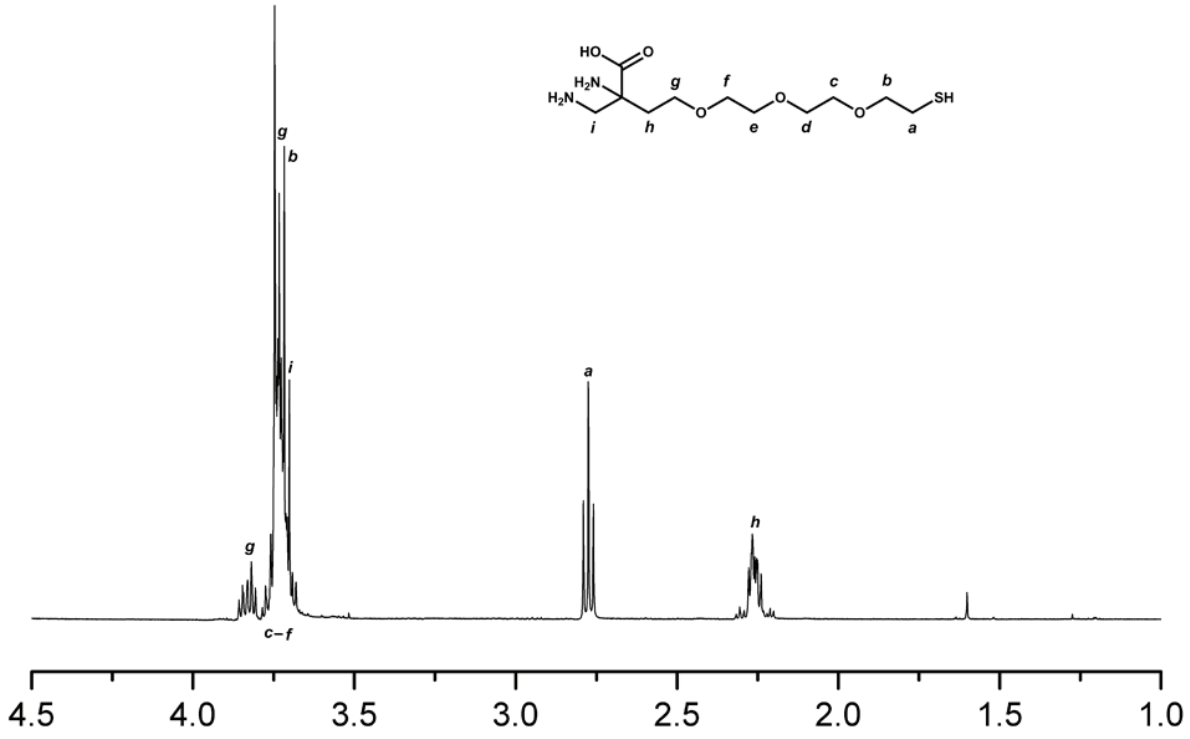

Figure 48. ^{1}H NMR (400 MHz) of compound **26**, measured in D_2O (chemical shifts in ppm).

3.4.2 The Synthesis of HS-PEG-DAP-TF (34)

Di-*tert*-butyl *N*-{[(2*S*)-6-{[(benzyloxy)carbonyl]amino}-1-*tert*-butoxy-1-oxohexan-2-yl]carbamoyl}-L-glutamate (27)[190]

Triphosgene (0.83 g, 2.8 mmol) was dissolved in dry dichloromethane (10 ml) and cooled to 0 °C. To this solution a mixture of L-glutamic acid di-*tert*-butyl ester hydrochloride (2.24 g, 7.6 mmol), triethylamine (2.1 ml, 15.2 mmol) and dry dichloromethane (30 ml) was added

dropwise at 0 °C during 2 h. After stirring for additional 40 min, a solution of N(ε)-benzoyloxycarbonyl-L-lysine *tert*-butyl ester hydrochloride (2.82 g, 7.6 mmol), triethylamine (2.1 ml, 15.2 mmol) and dry dichloromethane (25 ml) was added and the mixture was stirred at room temperature for 2 h. Afterwards the solution was concentrated and ethyl acetate (50 ml) was added. The organic phase was washed with 2 M $NaHSO_4$ (2 x 50 ml), brine (40 ml) and dried over magnesium sulfate. The solvent was removed under reduced pressure and the residue was purified by silica gel column chromatography (1:1 ethyl acetate / hexane) to give the product as a colorless oil which solidified after a while. Yield: 2.56 g (69%). ^{1}H NMR (400 MHz, $CDCl_3$, ppm) δ 7.28 – 7.35 (m, 5H), 5.13 – 5.23 (m, 3H), 5.09 (d, 2H, *J*=5.7 Hz), 4.29 – 4.37 (m, 2H), 3.14 – 3.20 (m, 2H), 2.22 – 2.33 (m, 2H), 1.49 – 1.85 (m, 8H), 1.42 – 1.46 (m, 27H). ESI-MS (MeOH): m/z = 644 $[M+Na]^+$. R_f = 0.47 (1:1 ethyl acetate / hexane).

Di-*tert*-butyl *N*-{[(2*S*)-6-amino-1-*tert*-butoxy-1-oxohexan-2-yl]carbamoyl}-L-glutamate (28)[190]

27 (630 mg, 1.0 mmol) was dissolved in dry methanol (15 ml). Palladium on carbon (10%) (40 mg) was added and the benzyloxycarbonyl protecting group was cleaved under atmospheric hydrogen pressure at room temperature overnight. The reaction mixture was filtered and the volatile part was removed to give a colorless oil. Yield: 480 mg (98%). ^{1}H NMR (400 MHz, $CDCl_3$, ppm) δ 5.16 – 5.20 (m, 2H), 4.29 – 4.35 (m, 2H), 2.66 (t, 2H, *J*=6.8 Hz), 2.21 – 2.37 (m, 2H), 2.01 – 2.10 (m, 1H), 1.71 – 1.86 (m, 2H), 1.48 – 1.64 (m, 6H), 1.44 (s, 18H), 1.42 (m, 9H). ESI-MS (MeOH): m/z = 488 $[M+H]^+$.

6-[(*tert*-Butoxycarbonyl)amino]hexanoic acid (29)[191]

6-Aminohexanoic acid (1.27 g, 9.7 mmol) was dissolved in tetrahydrofurane (25 ml) and 1 M sodium hydroxide solution (10 ml). The solution was cooled to 0 °C and di-*tert*-butyldicarbonate (2.8 g, 12.6 mmol) was added. The mixture was stirred at room temperature for 3 h. The solvent was removed under reduced pressure and the crude was dissolved in water (20 ml). The water phase was washed with diethyl ether and afterwards adjusted to pH = 1 with 1 M hydrochloride solution. The product was extracted with diethyl ether (2 x 40 ml) and the combined organic phases were dried over magnesium sulfate. The solvent was removed under reduced pressure and the waxy oil was dried under high vacuum. Yield: 2.0 g (89%). ^{1}H NMR (500 MHz, $CDCl_3$, ppm) δ 4.54 (s, 1H), 3.09 – 3.14 (m,

2H), 2.35 (t, 2H, *J*=7.6 Hz), 1.81 (quin, 2H, *J*=7.6 Hz), 1.47 – 1.52 (m, 2H), 1.44 (s, 9H), 1.34 – 1.40 (m, 2H). ESI-MS (MeOH): m/z = 254 $[M+Na]^+$. R_f = 0.41 (diethyl ether).

Di-*tert*-butyl *N*-{[(17*S*)-2,2,20,20-tetramethyl-4,11,18-trioxo-3,19-dioxa-5,12-diazahenicosan-17-yl]carbamoyl}-L-glutamate (30)

28 (778 mg, 1.6 mmol) and **29** (370 mg, 1.6 mmol) were dissolved in dry dichloromethane (25 ml). *N,N'*-dicyclohexylcarbodiimide (362 mg, 1.8 mmol) and dimethylaminopyridine (22 mg, 0.2 mmol) were added and the suspension was stirred at 0 °C for 30 min and at room temperature for 42 h. The white precipitate was separated from the reaction solution *via* decantation. The solvent was removed under reduced pressure and the residue was purified by silica gel column chromatography (ethyl acetate / hexane 1:1) to give the product as a waxy oil. Yield: 766 mg (69%). ^{1}H NMR (500 MHz, $CDCl_3$, ppm) δ 6.03 (s, 1H), 5.34 (s, 1H), 4.67 (s, 1H), 4.29 – 4.33 (m, 2H), 3.29 – 3.34 (m, 1H), 3.08 – 3.17 (m, 3H), 2.26 – 2.38 (m, 2H), 2.29 (t, 2H, *J*=7.0 Hz), 2.05 – 2.11 (m, 1H), 1.77 – 1.88 (m, 2H), 1.56 – 1.70 (m, 5H), 1.48 – 1.54 (m, 3H), 1.46 (s, 9H), 1.45 (s, 9H), 1.43 (s, 18H), 1.30 – 1.38 (m, 4H). ^{13}C NMR (125 MHz, $CDCl_3$, ppm) δ 173.34, 172.54, 157.33, 82.16, 81.80, 80.71, 79.27, 53.33, 53.25, 40.58, 39.00, 36.65, 34.08, 32.68, 31.82, 29.79, 28.87, 28.60, 28.36, 28.24, 28.17, 26.42, 25.76, 25.48, 22.40. ESI-MS (MeOH): m/z = 723 $[M+Na]^+$. HR-ESI-MS (MeOH + NaOH) for $C_{35}H_{64}N_4NaO_{10}$ $[M+Na]^+$: calculated, 723.4514; found, 723.4508. R_f = 0.42 (ethyl acetate / hexane 1:1).

***N*-({(1*S*)-5-[(6-Aminohexanoyl)amino]-1-carboxypentyl}carbamoyl)-L-glutamic acid (31)**

30 (511 mg, 0.73 mmol) was dissolved in dichloromethane (6 ml, 93 mmol). Trifluoroacetic acid (2.9 ml, 38 mmol) and triethylsilane (1.2 ml, 7.3 mmol) was added and the solution was stirred at room temperature for 2 h. The solvent was removed under reduced pressure and the resulting residue was washed with diethylether (4 x 10 ml) to give the product as a waxy oil. Yield: 309 mg (99%). ^{1}H NMR (500 MHz, D_2O, ppm) δ 4.28 – 4.31 (m, 1H), 4.20 – 4.23 (m, 1H), 3.21 (t, 2H, *J*=6.9 Hz), 3.01 (t, 2H, *J*=7.6 Hz), 2.54 (t, 2H, *J*=7.3 Hz), 2.27 (t, 2H, *J*=7.6 Hz), 2.19 – 2.23 (m, 1H), 1.97 – 2.04 (m, 1H), 1.84 – 1.91 (m, 1H), 1.72 – 1.78 (m, 1H), 1.69 (t, 2H, *J*=7.6 Hz), 1.64 (t, 2H, *J*=7.6 Hz), 1.53 – 1.59 (m, 2H), 1.36 – 1.45 (m, 4H). ^{13}C NMR (125 MHz, D_2O, ppm) δ 177.26, 177.12, 176.57, 176.27, 159.34, 53.20, 52.57, 39.28, 38.91, 35.48, 30.56, 30.04, 27.73, 26.42, 26.22, 25.05, 24.85, 22.24**.** ESI-MS (MeOH): m/z = 431 $[M-H]^-$. HR-ESI-MS (MeOH + HCOOH) for $C_{18}H_{33}N_4O_8$ $[M+H]^+$: calculated, 433.2293; found, 433.2293.

2,5-Dioxopyrrolidin-1-yl *N*-(*tert*-butoxycarbonyl)-2'-[(*tert*-butoxycarbonyl)amino]-4-(2-{2-[2-(tritylsulfanyl)ethoxy]ethoxy}ethoxy)isovalinate (32)

25 (561 mg, 0.76 mmol), *N*-hydroxysuccinimide (91 mg, 0.79 mmol) and *N,N'*-dicyclohexylcarbodiimide (204 mg, 1.00 mmol) were dissolved in *N,N'*-dimethylformamide (15 ml). The mixture was stirred at room temperature for 17 h, while a white precipitate was formed. The precipitate was separated from the solution with the help of centrifugation. The solvent was removed under reduced pressure and the residue was purified by silica gel column chromatography (10:1 dichloromethane / methanol) to give the product as a colorless oil. Yield: 457 mg (72%). ^{1}H NMR (400 MHz, $CDCl_3$, ppm) δ 7.39 – 7.42 (m, 6H), 7.25 – 7.29 (m, 6H), 7.18 – 7.22 (m, 3H), 6.34 (s, 1H), 5.57 (s, 1H), 3.96 – 4.02 (m, 1H), 3.69 (t, 2H, *J*=5.5 Hz), 3.55 – 3.59 (m, 7H), 3.45 (t, 2H, *J*=4.5 Hz), 3.30 (t, 2H, *J*=7.0 Hz), 2.81 (s, 4H), 2.43 (t, 2H, *J*=7.0 Hz), 1.44 (s, 18H). ^{13}C NMR (100 MHz, $CDCl_3$, ppm) δ 157.01, 145.07, 129.85, 128.10, 126.87, 70.64, 70.57, 70.53, 70.42, 69.84, 66.99, 66.82, 63.53, 33.19, 34.19, 31.86, 28.54, 25.80. ESI-MS (MeOH): m/z = 858 $[M+Na]^+$. HR-ESI-MS (MeOH) for $C_{44}H_{57}N_3NaO_{11}S$ $[M+Na]^+$: calculated, 858.3606; found, 858.3603. R_f = 0.24 (10:1 dichloromethane / methanol).

***N*-({(1*S*)-5-[(6-{[*N*-(*tert*-butoxycarbonyl)-2'-[(*tert*-butoxycarbonyl)amino]-4-(2-{2-[2-(tritylsulfanyl)ethoxy]ethoxy}ethoxy)isovalyl]amino}hexanoyl)amino]-1-carboxypentyl}carbamoyl)-L-glutamic acid (33)**

32 (732 mg, 0.88 mmol), **31** (315 mg, 0.73 mmol) and triethylamine (1.90 ml, 14.01 mmol) were dissolved in *N,N*-dimethylformamide (8 ml) and water (2 ml). The mixture was stirred at room temperature for 48 h. After evaporation of the solvent the resulting residue was purified by preparative HPLC to give the product as a colorless solid. Yield: 690 mg (82%). ^{1}H NMR (500 MHz, MeOD, ppm) δ 7.39 – 7.41 (m, 6H), 7.27 – 7.30 (m, 6H), 7.20 – 7.23 (m, 3H), 4.30 – 4.33 (m, 1H), 4.25 – 4.28 (m, 1H), 3.48 – 3.60 (m, 10H), 3.44 (t, 2H, *J*=5.0 Hz), 3.27 (t, 2H, *J*=6.6), 3.16 (t, 4H, *J*=6.9 Hz), 2.38 – 2.43 (m, 4H), 2.17 (t, 2H, *J*=7.3 Hz), 2.05 – 2.08 (m, 2H), 1.80 – 1.93 (m, 2H), 1.65 – 1.70 (m, 1H), 1.60 (t, 2H, *J*=7.3 Hz), 1.49 – 1.56 (m, 5H), 1.43 (s, 9H), 1.42 (s, 9H), 1.29 – 1.36 (m, 2H). ^{13}C NMR (125 MHz, MeOD, ppm) δ 176.41, 176.36, 176.09, 175.80, 160.10, 158.41, 156.21, 146.27, 130.79, 128.92, 127.82, 80.27, 71.45, 71.41, 71.30, 71.23, 70.63, 67.94, 67.73, 63.23, 53.96, 53.50, 49.85, 44.94, 40.54, 40.12, 37.01, 34.30, 33.21, 32.80, 31.11, 29.97, 28.93, 29.80, 27.56, 26.70, 23.96. ESI-MS (MeOH): m/z = 1151 $[M-H]^-$. HR-ESI-MS (MeOH) for $C_{58}H_{84}N_6O_{16}S$ $[M+H]^+$: calculated, 1153.5743; found,

1153.5751. HPLC (TFA / MeOH, C18rp): 25.0 min. Preparative HPLC (TFA / MeOH, C18rp): 60 min.

N-{[(1*S*)-5-({6-[(2'-amino-4-{2-[2-(2-sulfanylethoxy)ethoxy]ethoxy}isovalyl)amino]-hexanoyl}amino)-1-carboxypentyl]carbamoyl}-L-glutamic acid (34)

33 (242 mg, 0.21 mmol), was dissolved in dichloromethane (1.3 ml). Trifluoroacetic acid (0.63 ml) and triethylsilane (0.25 ml) were added and the solution was stirred at room temperature for 2 h. The solvent was removed under reduced pressure and the resulting residue was washed with diethylether (5 x 10 ml). Yield: 145 mg (97%). ^{1}H NMR (500 MHz, D_2O, ppm) δ 4.25 – 4.28 (m, 1H), 4.16 – 4.19 (m, 1H), 3.76 – 3.80 (m, 1H), 3.62 – 3.69 (m, 13H), 3.38 – 3.44 (m, 1H), 3.17 (t, 2H, *J*=6.6 Hz), 3.12 – 3.15 (m, 1H), 2.72 (t, 2H, *J*=6.3 Hz), 2.50 (t, 2H, *J*=7.3 Hz), 2.30 – 2.41 (m, 2H), 2.22 (t, 2H, *J*=7.3 Hz), 2.15 – 2.19 (m, 1H), 1.94 – 2.00 (m, 1H), 1.80 – 1.87 (m, 1H), 1.66 – 1.74 (m, 1H), 1.49 – 1.62 (m, 6H), 1.37 – 1.44 (m, 2H), 1.29 – 1.34 (m, 2H). ^{13}C NMR (125 MHz, D_2O, ppm) δ 177.16, 177.01, 176.60, 176.14, 166.59, 159.24, 72.10, 69.82, 69.49, 69.21, 69.10, 69.21, 65.41, 61.26, 53.18, 52.52, 43.49, 40.28, 38.91, 35.58, 32.57, 30.58, 30.00, 27.76, 26.25, 25.63, 25.00, 23.06, 22.31. ESI-MS (MeOH): m/z = 709 $[M-H]^-$. HR-ESI-MS (MeOH) for $C_{29}H_{55}N_6O_{12}S$ $[M+H]^+$: calculated, 711.3593; found, 711.3586.

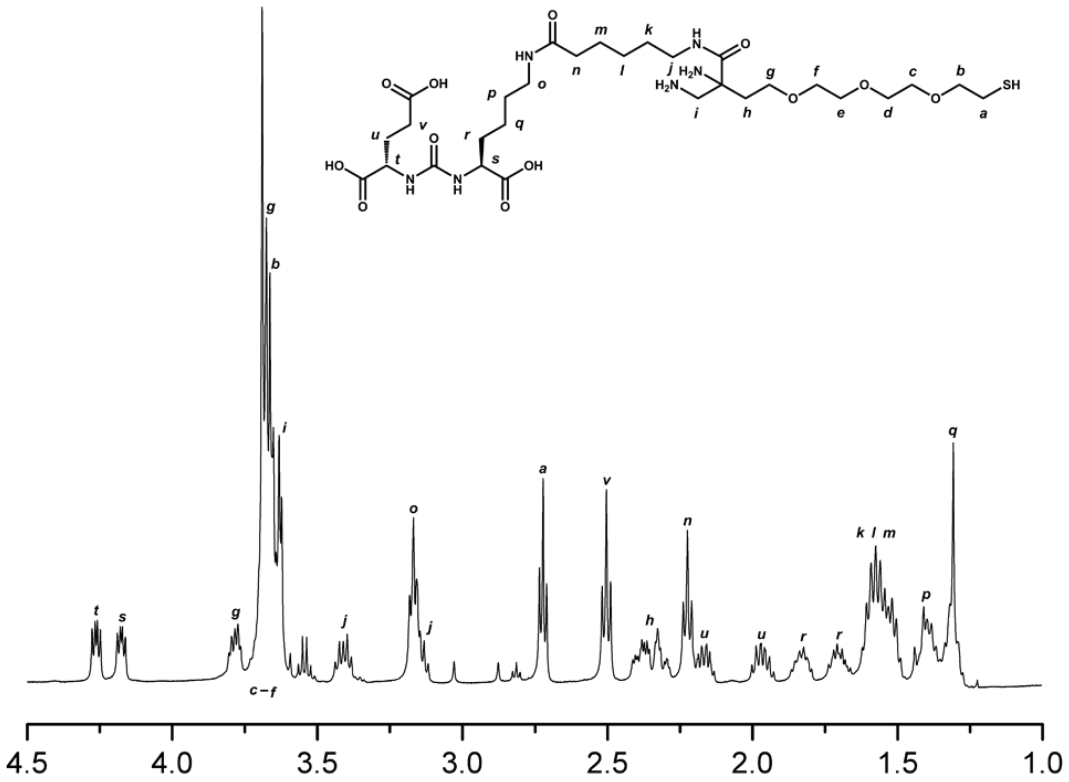

Figure 49. ^{1}H NMR (400 MHz) of compound **34**, measured in D_2O (chemical shifts in ppm).

3.4.3 The Synthesis, Functionalization and Radiolabeling of NPs

Synthesis of CdSe/ZnS core-shell QDs

CdSe/ZnS core-shell nanocrystals were prepared according to a reported procedure.[123] Briefly, trioctylphosphine oxide (5 g), hexadecylamine (2.5 g) and trioctylphosphine (1.25 ml) were kept under vacuum at 130 °C for 1 h. Under atmospheric pressure the temperature was elevated to 350 °C. In a separate flask, cadmium acetylacetonate (155 mg), 1,2-hexadecanediol (300 mg) and trioctylphosphine (2.5 ml) were heated under vacuum to 100 °C until the solution became homogeneous. After cooling to 80 °C under atmospheric pressure, 2.5 ml of a 1 M solution of selenium powder in trioctylphosphine (2.5 ml) was added. This mixture with the cadmium and selenium precursors was immediately injected into the 350 °C hot flask and then cooled to 270 °C. At this temperature the mixture was stirred for 60 min and after cooling to room temperature, butanol (50 ml) was added to precipitate the QDs. After centrifugation and removal of the supernatant, the QDs were dispersed in hexane (5 ml) and the precipitation procedure was repeated twice. For the overcoating, trioctylphosphine oxide (30 g) was kept under vacuum at 120 °C for 2 h. The purified CdSe quantum dots from step 1 were dispersed in 10 ml hexane and 1 ml of this solution was added to the trioctylphosphine oxide at atmospheric pressure. The solvent was removed under vacuum. At atmospheric pressure, the mixture was heated to 180 °C. In a separate two-neck round-bottom flask trioctylphosphine (4 ml), diethylzinc (1 M in hexane; 1.0 ml) and hexamethyldisilathiane (180 mg) were mixed and loaded into a syringe. This solution was slowly added to the QD solution and afterwards the temperature was lowered to 80 °C. The mixture was stirred at 80 °C for 2 h and the overcoated QDs were isolated *via* precipitation with butanol (30 ml) and centrifugation.

Synthesis of AuNPs

AuNPs were prepared according to a reported procedure.[122] Briefly, a solution of toluene (49 ml) and oleylamine (2.9 ml) was heated to 115 °C. In a separate flask tetrachloroauric acid trihydrate (60 mg) were dissolved in oleylamine (1.2 ml, 3.7 mmol) and toluene (1 ml). The gold precursor solution was injected in one portion to the boiling solution and the mixture was refluxed for 9 min (6.6 nm AuNPs) or 130 min (13.8 nm AuNPs). The particle growth was quenched by the addition of methanol (100 ml) and the precipitate was isolated by

centrifugation. The product as a black solid was washed three times with methanol and dried *in vacuo*.

Functionalization of QDs and AuNPs

The photoinduced phase transfer was adapted from a reported procedure with modifications.[110] Briefly, a mixture of HS-PEG-DAP (7.4 mg, 25 µmol) and HS-PEG-DAP-TF (17.1 mg, 25 µmol) was dissolved in methanol (0.8 ml) and transferred in a nitrogen flushed glass vial with a magnetic stir bar, sealed with a aluminum crimp cap with a butyl septa. NPs (ca. 1.0 mg) were dispersed in hexane (0.8 ml) and overlayed on the methanol phase. The glass vial was placed in front of a UV lamp (365 nm) and irradiated under vigorous stirring for 50 min. During this procedure, the originally purple hexane phase became completely transparent while the as-functionalized NPs precipitated and the free ligands stayed dispersed in the solvent. The supernatant with excess ligands was removed *via* decantation. The precipitated NPs were washed with methanol and dispersed in PBS pH 7.4 (0.5 ml). A further purification step was performed with a PD-10 size exclusion column and PBS pH 7.4 as a mobile phase. The colored fraction was collected and TEM, UV-Vis, IR, DLS and ζ-Pot. analyses were carried out.

Labeling of functionalized QDs with *fac*-$[^{99m}Tc(OH_2)_3(CO)_3]^+$

An aqueous solution of $[^{99m}Tc(OH_2)_3(CO)_3]^+$ (0.5 ml, pH=7-8) was added to QDs in PBS pH 7.4 (0.5 ml). The mixture was stirred using a temperature gradient (50 – 60 °C) over 60 min and additional stirring at 60 °C for 60 min. Radiolabeled QDs were purified with a PD-10 column, whereas only the reddish colored fraction was collected and analyzed with size-exclusion HPLC.

Labeling of functionalized AuNPs with *fac*-$[^{99m}Tc(OH_2)_3(CO)_3]^+$

An aqueous solution of $[^{99m}Tc(OH_2)_3(CO)_3]^+$ (0.5 ml, pH=7-8) was added to purified AuNPs in PBS pH 7.4 (0.5 ml). The mixture was stirred using a temperature gradient (50 – 70 °C) over 60 min and additional stirring at 70 °C for 60 min. The radiolabeled AuNPs were purified with a PD-10 column, whereas only the purple colored fraction was collected and analyzed with size-exclusion HPLC.

3.4.4 *In Vitro* and *In Vivo* Studies

Cellular Uptake Studies

LNCaP (ATCC® CRL-1740™) and Cos-7 (ATCC® CRL-1651™) cell lines were purchased from ATCC (France). Both cell lines were cultured according to the guidelines of ATCC and seeded on glass coverslips which were placed in 24-well plates. The cells were incubated with 400 µl AuNP solution (PBS pH 7.4 / medium 1:4) for 30 s and 90 min at 37 °C under 5% CO_2 atmosphere. The concentration of 7 nm AuNPs was 179 µg/ml and of 14 nm AuNPs it was 189 µg/ml (determined by ICP-MS). Control experiments for both incubation times were carried out under the same conditions, but without using AuNP solution. After incubation the AuNP solutions were removed, the glass coverslips were washed with PBS and transferred into well plates containing 2.5% glutaraldehyde in 0.1 M PB solution. After fixation at 4 °C for 1 h the samples were washed with PBS and incubated in 1% osmium tetroxide in 0.1 M PB at room temperature for 30 min. After washing with water, the cells were dehydrated in an increasing concentration of ethanol (70%, 96% and 100%). The cells were infiltrated in a mixture of Epon 812 resin and ethanol (2:1) and finally embedded in pure resin at 60 °C for 60 h. Ultrathin sections (65 nm) were cut with a Reichert Ultracut and collected on electron microscopy grids. Transmission electron microscopy (TEM) was performed on a Philips CM100.

***In Vivo* Studies and *ex Vivo* Biodistribution Analysis**

All animal experiments were conducted according to the Dutch code of practice for the care and use of animals, after approval from the local animal ethics committee. Animals were male nude NMR mice, both purchased from Harlan (Netherlands) and 12 weeks old at the start of the experiment. For the tumor inoculation LNCaP cells (ATCC® CRL-1740™) were cultured according to the guidelines of ATCC and 1 million cells in 200 µl volume were subcutaneously injected in the left shoulder. Tumors were allowed to grow for 4 weeks, and reached a volume of 0.2 – 1.0 cm^3. The xenograft-bearing mice were anesthetized using isoflurane gas in oxygen (induction 2.5%, maintenance 1.5%) flowing at 2 L/min prior and during the injection of the compounds. The mice were injected via the tail vein with 10 – 70 MBq radiolabeled AuNPs in 200 µl of PBS pH 7.4. After each study, the mice were sacrificed by intraperitoneal injection of pentobarbital. Blood was collected immediately after sacrifice by cardiac puncture and the other organs/tissues were harvested, weighted and counted in

an automated gamma counter (Perkin Elmer Wallac Wizard 1480 automatic gamma). The data are expressed as mean percentage injected dose per gram (%ID/g) ± standard error of the mean.

MicroSPECT Imaging

Single photon emission computed tomography (SPECT) images were obtained on a U-SPECT-II scanner (MILabs) equipped with three gamma detectors. MicroSPECT studies were performed right after i.v. of the radiolabeled AuNPs and the mice were kept anesthetized with 1% isoflurane gas in oxygen flowing at 0.25 L/min. The length of the scan was set to 20 min in order to obtain three sets of data, corresponding to 0 – 20, 20 – 40 and 40 – 60 min p.i. of the tracer. The SPECT data were acquired and reconstructed with the software that is provided with the U-SPECT-II scanner (MILabs). Image analysis was performed with PMOD software (version 2.9, PMOD Inc.).

Metabolite Analysis

Blood samples were withdrawn and immediately transferred into heparinized centrifugation tubes. After centrifugation for 5 min at 2000g, the separated plasma was directly injected into size-exclusion HPLC. Urine samples were injected directly after isolation without any additional preparation.

3.5 Synthetic Part of the Section 2.3

3.5.1 The Synthesis of the Bifunctional Coating Ligands

Oxybis(ethane-2,1-diyloxyethane-2,1-diyl) bis(4-methylbenzenesulfonate)[140]

Tetraethylene glycol (5.0 g, 25.7 mmol) and *p*-toluenesulfonyl chloride (14.7 g, 77.2 mmol) were dissolved in tetrahydrofurane (100 ml) and cooled to 0 °C. Potassium hydroxide (10.1 g, 180.2 mmol) in water (25 ml) was added dropwise over a period of 60 min. The mixture was stirred at room temperature for additional 3 h and afterwards poured in a 2:1 diethyl ether / water mixture (150 ml). The water phase was extracted with diethyl ether (2 x 100 ml). The combined ether phases were washed with brine (100 ml), dried over magnesium sulfate, filtered and concentrated under reduced pressure. The residue was purified by silica gel column chromatography (95:5 ethyl acetate / methanol) to give a colorless oil. Yield: 12.9 g (99%). ^{1}H NMR (400 MHz, $CDCl_3$, ppm) δ 7.78 (d, 4H, *J*=8.5 Hz), 7.33 (d, 4H, *J*=8.0 Hz), 4.15 (t, 4H, *J*=4.6 Hz), 3.67 (t, 4H, *J*=5.0 Hz), 3.52 – 3.57 (m, 8H), 2.44 (s, 6H). ESI-MS (MeOH): m/z = 525 $[M+Na]^+$. R_f = 0.46 (95:5 ethyl acetate / methanol).

1-Azido-2-{2-[2-(2-azidoethoxy)ethoxy]ethoxy}ethane[140]

Oxybis(ethane-2,1-diyloxyethane-2,1-diyl) bis(4-methylbenzenesulfonate) (12.9 g, 25.7 mmol) was dissolved in acetonitrile (200 ml) and sodium azide (5.0 g, 77.0 mmol) was added. The suspension was refluxed for 18 h. After cooling to room temperature, water (100 ml) was added and the aqueous phase was extracted with dichloromethane (4 x 70 ml). The combined organic phases were dried over magnesium sulfate, filtered and concentrated under reduced pressure. The resulting yellow oil was dried under vacuum and used directly for the next step without further purification. Yield: 6.0 g (95%). ^{1}H NMR (400 MHz, $CDCl_3$, ppm) δ 3.64 – 3.68 (m, 12H), 3.37 (t, 4H, *J*=5.0 Hz). ESI-MS (MeOH): m/z = 267 $[M+Na]^+$.

2,2'-[Oxybis(ethane-2,1-diyloxy)]diethanamine (35)[141]

1-Azido-2-{2-[2-(2-azidoethoxy)ethoxy]ethoxy}ethane (6.0 g, 24.4 mmol) was dissolved in tetrahydrofurane (100 ml) and triphenylphosphine (14.1 g, 53.6 mmol) and water (1.32 ml) was added. The mixture was stirred at room temperature for 5 h. The solvent was removed under reduced pressure and the residue was purified by silica gel column chromatography (10:1:0.03 dichloromethane / methanol / 25% ammonia solution) to give a yellow oil. Yield: 4.0 g (85%). ^{1}H NMR (400 MHz, $CDCl_3$, ppm) δ 4.73 (s, 4H), 3.59 – 3.66 (m, 8H), 3.50 (t, 4H,

J=5.0 Hz), 2.85 (t, 4H, *J*=5.3 Hz). ESI-MS (MeOH): m/z = 193 $[M+H]^+$. R_f = 0.09 (10:1:0.03 dichloromethane / methanol / 25% ammonia solution).

tert-Butyl (2-{2-[2-(2-aminoethoxy)ethoxy]ethoxy}ethyl)carbamate (36)[142]

35 (2.4 g, 12.6 mmol) was dissolved in dry dichloromethane (80 ml) and cooled to 0 °C. Di-*tert*-butyl dicarbonate (0.4 g, 1.9 mmol), dissolved in dichloromethane (10 ml), was slowly added to the diamine and the mixture was stirred at 0 °C for 5 h and at room temperature for 18 h. The organic phase was washed with water (3 x 150 ml) and dried over magnesium sulfate. The solvent was removed under reduced pressure and the residue was used without further purification. Yield: 0.6 g (99%, calculated for di-*tert*-butyl dicarbonate). ^{1}H NMR (400 MHz, $CDCl_3$, ppm) δ 5.24 (s, 1H), 3.59 – 3.67 (m, 8H), 3.50 – 3.55 (m, 4H), 3.29 – 3.32 (m, 2H), 2.86 (t, 2H, *J*=5.3 Hz), 1.51 (s, 2H), 1.44 (s, 9H). ESI-MS (MeOH): m/z = 293 $[M+Na]^+$.

tert-Butyl [1-(pyridin-2-yl)-2-(pyridin-2-ylmethyl)-5,8,11-trioxa-2-azatridecan-13-yl]carbamate (37)

36 (415 mg, 1.4 mmol) was dissolved in dry 1,2-dichloroethane (8 ml) and sodium triacetoxyborohydride (752 mg, 3.6 mmol) was added at 0 °C. 2-Pyridinecarboxaldehyde (280 µl, 3 mmol) was dissolved in 1,2-dichloroethane (3 ml) and added to the suspension. The mixture was stirred at room temperature for 4 h and afterwards quenched with water (10 ml). The mixture was extracted with chloroform (3 x 50 ml) and the combined organic phases were washed with water, brine and dried over magnesium sulfate. The solvent was removed under reduced pressure and the residue was purified by silica gel column chromatography (10:1 dichloromethane / methanol) to give a yellow oil. Yield: 545 mg (81%). ^{1}H NMR (400 MHz, $CDCl_3$, ppm) δ 8.51 (d, 2H, *J*=4.8 Hz), 7.63 (t, 2H, *J*=7.5 Hz), 7.55 (d, 2H, *J*=7.8 Hz), 7.13 (t, 2H, *J*=6.0 Hz), 5.07 (s, 1H), 3.90 (s, 4H), 3.53 – 3.64 (m, 10H), 3.50 (t, 2H, *J*=5.0 Hz), 3.26 – 3.30 (m, 2H), 2.83 (t, 2H, *J*=5.8 Hz), 1.42 (s, 9H). ^{13}C NMR (100 MHz, $CDCl_3$, ppm) δ 159.93, 156.15, 149.08, 136.54, 123.07, 122.05, 70.77, 70.69, 70.50, 70.41, 70.36, 69.77, 61.00, 53.72, 50.87, 40.51, 28.56. ESI-MS (MeOH): m/z = 475 $[M+H]^+$. HR-ESI-MS (MeOH + NaI) for $C_{25}H_{38}N_4NaO_5$ $[M+Na]^+$: calculated, 497.2734; found, 497.2729. R_f = 0.17 (10:1 dichloromethane / methanol).

1-(Pyridin-2-yl)-2-(pyridin-2-ylmethyl)-5,8,11-trioxa-2-azatridecan-13-amine (38)

37 (545 mg, 1.2 mmol) was dissolved in dichloromethane (5 ml) and added dropwise to a diethyl ether solution, saturated with hydrochloric acid (15 ml). An immediate precipitation

was observed and the mixture was stirred at room temperature for additional 30 min. The solvent was removed under reduced pressure and the product as a colorless solid was dried under high vacuum. Yield: 555 mg (99%, product · 3 HCl). ^{1}H NMR (500 MHz, MeOD, ppm) δ 8.91 (d, 2H, *J*=5.7 Hz), 8.62 (t, 2H, *J*=7.9 Hz), 8.19 (d, 2H, *J*=7.9 Hz), 8.05 (t, 2H, *J*=6.6 Hz), 4.50 (s, 4H), 3.72 (t, 2H, *J*=5.0 Hz), 3.66 – 3.68 (m, 6H), 3.62 (t, 2H, *J*=4.7 Hz), 3.52 (t, 2H, *J*=4.7 Hz), 3.12 (t, 2H, *J*=4.7 Hz), 2.93 (t, 2H, *J*=4.4 Hz). ^{13}C NMR (125 MHz, $CDCl_3$, ppm) δ 153.56, 146.93, 141.31, 127.03, 126.04, 69.99, 69.94, 69.82, 68.29, 66.46, 56.25, 53.83, 39.22. ESI-MS (MeOH): m/z = 375 $[M+H]^+$.

5-(1,2-Dithiolan-3-yl)-*N*-[1-(pyridin-2-yl)-2-(pyridin-2-ylmethyl)-5,8,11-trioxa-2-azatridecan-13-yl]pentanamide (39)

DL-α-Lipoic acid (297 mg, 1.4 mmol) was dissolved in dry dichloromethane (5 ml) and triethylamine (200 µl, 1.4 mmol) was added. The mixture was cooled to 0 °C and stirred for 30 min. Methanesulfonyl chloride (111 µl, 1.4 mmol) was added dropwise. After addition, the mixture was warmed up to room temperature and stirred for 5 h. In the meantime, **38** (· 3 HCl; 555 mg, 1.2 mmol) was dissolved in dry dichloromethane (10 ml) and triethylamine (478 µl, 3.5 mmol). The amine solution was added dropwise to the mixture with the activated lipoic acid, followed by stirring at room temperature for 19 h. The reaction mixture was washed with water (2 x 15 ml) and saturated sodium carbonate solution (2 x 15 ml). The organic phase was dried over magnesium sulfate. The solvent was reduced under reduced pressure and the residue was purified by silica gel column chromatography (10:1 dichloromethane / methanol) to give a yellow oil. Yield: 291 mg (45%). ^{1}H NMR (400 MHz, $CDCl_3$, ppm) δ 8.51 (d, 2H, *J*=4.8 Hz), 7.64 (t, 2H, *J*=7.8 Hz), 7.54 (d, 2H, *J*=7.8 Hz), 7.13 (t, 2H, *J*=7.3 Hz), 6.22 (s, 1H), 3.90 (s, 4H), 3.51 – 3.63 (m, 13H), 3.42 (q, 2H, *J*=5.3 Hz), 3.06 – 3.19 (m, 2H), 2.83 (t, 2H, *J*=6.0 Hz), 2.39 – 2.47 (m, 1H), 2.15 (t, 2H, *J*=7.3 Hz), 1.84 – 1.92 (m, 1H), 1.59 – 1.70 (m, 4H), 1.38 – 1.49 (m, 2H). ^{13}C NMR (100 MHz, $CDCl_3$, ppm) δ 172.89, 159.92, 149.09, 136.55, 123.06, 122.08, 70.72, 70.68, 70.48, 70.38, 70.05, 69.76, 60.98, 56.55, 53.67, 40.35, 39.28, 38.58, 36.46, 34.78, 29.04, 25.49. ESI-MS (MeOH): m/z = 563 $[M+H]^+$. HR-ESI-MS (MeOH + NaI) for $C_{28}H_{43}N_4O_4S_2$ $[M+H]^+$: calculated, 563.2720; found, 563.2716. R_f = 0.12 (10:1 dichloromethane / methanol).

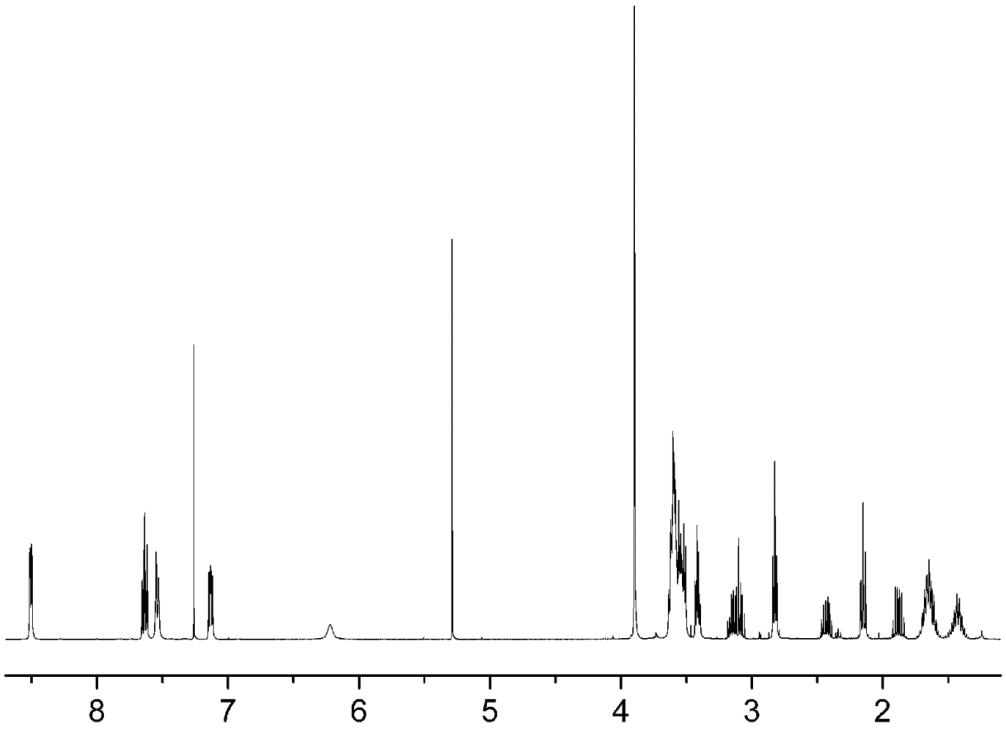

Figure 50. ^{1}H NMR (400 MHz) of compound **39**, measured in $CDCl_3$ (chemical shifts in ppm).

Ethyl *N*-(2,2-dimethyl-4-oxo-3,8,11,14-tetraoxa-5-azahexadecan-16-yl)-*N*-(pyridin-2-ylmethyl)glycinate (40)

A solution of **36** (558 mg, 1.9 mmol) and 2-pyridinecarboxaldehyde (182 µl, 1.9 mmol) was refluxed in dry 1,2-dichloroethane (10 ml) for 10 min. After cooling to 0 °C, sodium triacetoxyborohydride (1.0 g, 4.8 mmol) and ethyl glyoxylate (50% solution in toluene, 0.39 ml, 1.9 mmol) were sequentially added. The mixture was stirred at room temperature for 3.5 h and afterwards quenched with water (25 ml). The mixture was extracted with chloroform (4 x 50 ml). The combined organic phases were washed with water, brine and dried over magnesium sulfate. The solvent was removed under reduced pressure and the residue was purified by silica gel column chromatography (10:1 dichloromethane / methanol) to give a yellow oil. Yield: 625 mg (70%). ^{1}H NMR (400 MHz, $CDCl_3$, ppm) δ 8.52 (d, 1H, *J*=4.8 Hz), 7.65 (t, 1H, *J*=7.5 Hz), 7.53 (d, 1H, *J*=7.8 Hz), 7.14 (t, 1H, *J*=6.0 Hz), 5.05 (s, 1H), 4.15 (q, 2H, *J*=7.0 Hz), 4.00 (s, 2H), 3.51 – 3.60 (m, 14H), 3.27 – 3.31 (m, 2H), 2.94 (t, 2H, *J*=5.8 Hz), 1.43 (s, 9H), 1.25 (t, 3H, *J*=7.0 Hz). ^{13}C NMR (100 MHz, $CDCl_3$, ppm) δ 171.70, 159.76, 156.14, 149.14, 136.65, 123.19, 122.14, 70.72, 70.69, 70.47, 70.42, 70.38, 70.19, 60.85, 60.45, 55.86, 53.62, 40.52, 28.56, 14.43. ESI-MS (MeOH): m/z = 470 $[M+H]^+$. HR-ESI-MS (MeOH + NaI) for $C_{23}H_{39}N_3NaO_7$ $[M+Na]^+$: calculated, 492.2680; found, 492.2678. R_f = 0.47 (10:1 dichloromethane / methanol).

Ethyl *N*-(2-{2-[2-(2-aminoethoxy)ethoxy]ethoxy}ethyl)-*N*-(pyridin-2-ylmethyl)glycinate (41)

40 (530 mg, 1.1 mmol) was dissolved in dichloromethane (5 ml) and added dropwise to a diethyl ether solution, saturated with hydrochloric acid (15 ml). An immediate precipitation was observed and the mixture was stirred at room temperature for additional 30 min. The solvent was removed under reduced pressure and the product was dried under high vacuum to give a yellow oil. Yield: 538 mg (99%, product · 3 HCl). ^{1}H NMR (500 MHz, MeOD, ppm) δ 8.76 (d, 1H, *J*=4.7 Hz), 8.31 (t, 1H, *J*=7.6 Hz), 7.84 (d, 1H, *J*=7.9 Hz), 7.78 (t, 1H, *J*=6.6 Hz), 4.59 (s, 2H), 4.24 (q, 2H, *J*=7.0 Hz), 4.04 (s, 2H), 3.74 (t, 2H, *J*=4.7 Hz), 3.71 (t, 2H, *J*=5.0 Hz), 3.68 (s, 6H), 3.63 – 3.65 (m, 2H), 3.58 – 3.60 (m, 2H), 3.12 (t, 2H, *J*=5.0 Hz), 1.29 (t, 3H, *J*=7.0 Hz). ^{13}C NMR (125 MHz, MeOD, ppm) δ 170.53, 154.35, 145.59, 144.21, 126.63, 126.42, 71.41, 71.34, 71.30, 71.20, 68.40, 67.87, 62.88, 58.16, 56.35, 55.99, 40.64, 14.43. ESI-MS (MeOH): m/z = 370 $[M+H]^{+}$.

Ethyl *N*-[17-(1,2-dithiolan-3-yl)-13-oxo-3,6,9-trioxa-12-azaheptadec-1-yl]-*N*-(pyridin-2-ylmethyl)glycinate (42)

DL-α-Lipoic acid (291 mg, 1.4 mmol) was dissolved in dry dichloromethane (5 ml) and triethylamine (196 µl, 1.4 mmol) was added. The mixture was cooled to 0 °C and stirred for 30 min. Methanesulfonyl chloride (1095 µl, 1.4 mmol) was added dropwise, then the mixture was warmed up to room temperature and stirred for 5 h. In the meantime **41** (· 3 HCl; 538 mg, 1.1 mmol) was dissolved in dry dichloromethane (10 ml) and triethylamine (548 µl, 4.0 mmol). Afterwards the amine solution was added dropwise to the mixture with activated lipoic acid, followed by stirring at room temperature for 17 h. The reaction mixture was washed with water (2 x 20 ml) and saturated sodium carbonate solution (2 x 20 ml). The organic phase was dried over magnesium sulfate. The solvent was reduced under reduced pressure and the residue was purified by silica gel column chromatography (10:1 dichloromethane / methanol) to give a yellow oil. Yield: 464 mg (74%). ^{1}H NMR (400 MHz, $CDCl_3$, ppm) δ 8.53 (d, 1H, *J*=4.8 Hz), 7.65 (t, 1H, *J*=7.8 Hz), 7.52 (d, 1H, *J*=7.8 Hz), 7.15 (t, 1H, *J*=4.8 Hz), 6.16 (s, 1H), 4.15 (q, 2H, *J*=7.0 Hz), 4.00 (s, 2H), 3.51 – 3.63 (m, 15H), 3.44 (t, 2H, *J*=5.0 Hz), 3.07 – 3.20 (m, 2H), 2.94 (t, 2H, *J*=6.0 Hz), 2.41 – 2.48 (m, 1H), 2.17 (t, 2H, *J*=7.8 Hz), 1.85 – 1.94 (m, 1H), 1.61 – 1.72 (m, 4H), 1.40 – 1.51 (m, 2H), 1.26 (t, 3H, *J*=7.0 Hz). ^{13}C NMR (100 MHz, $CDCl_3$, ppm) δ 172.90, 171.71, 159.73, 149.18, 136.66, 123.17, 122.19, 70.69, 70.49, 70.46, 70.41, 70.21, 70.08, 60.85, 60.50, 56.57, 55.90, 53.62, 40.37, 39.31,

38.60, 36.49, 34.81, 29.06, 25.52, 14.44. ESI-MS (MeOH): m/z = 558 $[M+H]^+$. HR-ESI-MS (MeOH + NaI) for $C_{26}H_{44}N_3O_6S_2$ $[M+H]^+$: calculated, 558.2666; found, 558.2662. R_f = 0.44 (10:1 dichloromethane / methanol).

N-[17-(1,2-Dithiolan-3-yl)-13-oxo-3,6,9-trioxa-12-azaheptadec-1-yl]-*N*-(pyridin-2-ylmethyl)glycine (43)

42 (386 mg, 0.7 mmol) was dissolved in methanol (1.5 ml) and 1 M aqueous lithium hydroxide solution (1.5 ml) was added. The mixture was stirred at room temperature for 1.5 h and neutralized with Amberlite IR120 H to reach pH 7. The suspension was filtered and the solvent was removed under reduced pressure to give a yellow oil. Yield: 337 mg (92%). ^{1}H NMR (500 MHz, MeOD, ppm) δ 8.64 (d, 1H, *J*=5.0 Hz), 7.89 (t, 1H, *J*=7.6 Hz), 7.52 (d, 1H, *J*=7.6 Hz), 7.43 (t, 1H, *J*=5.0 Hz), 4.57 (s, 2H), 3.85 (t, 2H, *J*=4.7 Hz), 3.78 (s, 2H), 3.60 – 3.67 (m, 9H), 3.53 (t, 2H, *J*=5.7 Hz), 3.45 (t, 2H, *J*=5.0 Hz), 3.34 (t, 2H, *J*=5.7 Hz), 3.15 – 3.18 (m, 1H), 3.07 – 3.12 (m, 1H), 2.42 – 2.49 (m, 1H), 2.20 (t, 2H, *J*=7.6 Hz), 1.85 – 1.92 (m, 1H), 1.59 – 1.74 (m, 4H), 1.42 – 1.49 (m, 2H). ^{13}C NMR (125 MHz, MeOD, ppm) δ 175.93, 170.54, 152.83, 150.34, 138.91, 125.12, 125.01, 71.46, 71.39, 71.32, 71.15, 70.44, 66.73, 59.50, 57.77, 57.44, 55.17, 41.16, 40.17, 39.17, 36.64, 35.57, 29.68, 26.53. ESI-MS (MeOH): m/z = 530 $[M+H]^+$. HR-ESI-MS (MeOH + NaI) for $C_{24}H_{38}N_3O_6S_2$ $[M-H]^-$: calculated, 528.2208; found, 528.2214.

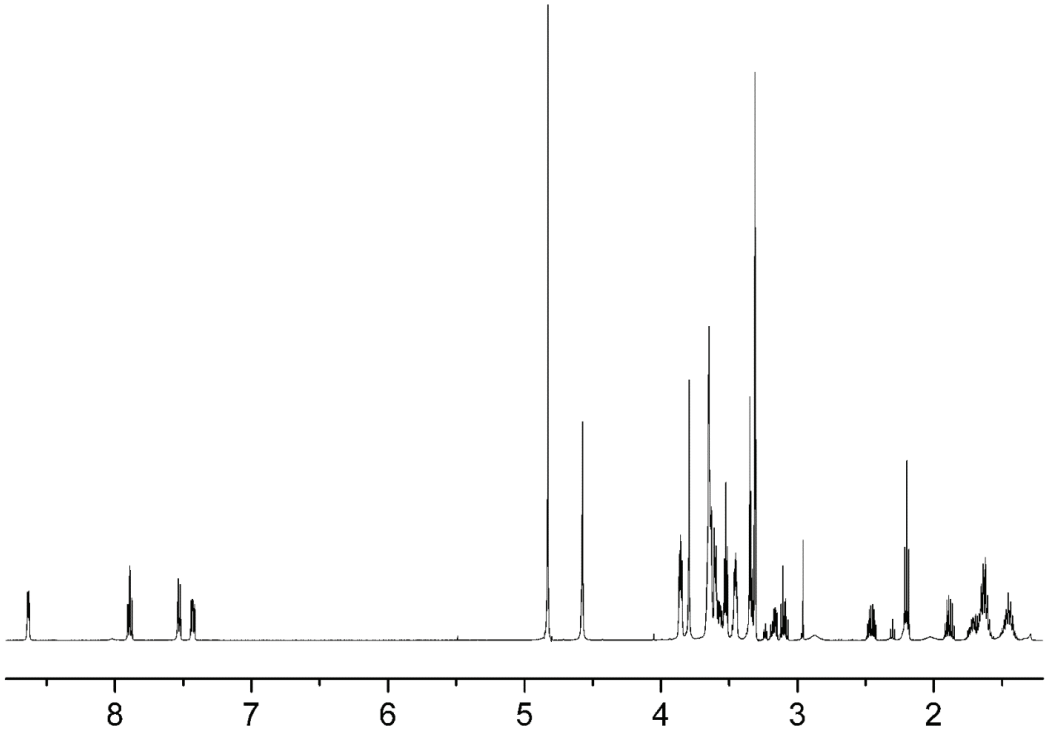

Figure 51. ^{1}H NMR (500 MHz) of compound **43**, measured in MeOD (chemical shifts in ppm).

Ethyl 17-(2-ethoxy-2-oxoethyl)-2,2-dimethyl-4-oxo-3,8,11,14-tetraoxa-5,17-diazanonadecan-19-oate (44)

36 (400 mg, 1.4 mmol) was dissolved in dry 1,2-dichloroethane (10 ml) and sodium triacetoxyborohydride (726 g, 3.4 mmol) was added at 0 °C. Ethyl glyoxylate (50% solution in toluene, 0.59 ml, 2.9 mmol) was added to the suspension. The mixture was stirred at room temperature for 4 h and afterwards quenched with water (15 ml). The mixture was extracted with chloroform (3 x 50 ml). The combined organic phases were washed with water, brine and dried over magnesium sulfate. The solvent was removed under reduced pressure and the residue was purified by silica gel column chromatography (10:1 dichloromethane / methanol) to give the product as a colorless oil. Yield: 515 mg (81%). ^{1}H NMR (400 MHz, $CDCl_3$, ppm) δ 5.05 (s, 1H), 4.15 (q, 4H, *J*=7.0 Hz), 3.58 – 3.65 (m, 14H), 3.52 (t, 2H, *J*=5.3 Hz), 3.28 – 3.32 (m, 2H), 2.96 (t, 2H, *J*=5.5 Hz), 1.43 (s, 9H), 1.25 (t, 6H, *J*=7.0 Hz). ^{13}C NMR (100 MHz, $CDCl_3$, ppm) δ 171.55, 156.15, 70.69, 70.65, 70.53, 70.47, 70.42, 70.39, 60.74, 60.56, 56.02, 53.78, 28.56, 14.39. ESI-MS (MeOH): m/z = 487 $[M+H]^+$. HR-ESI-MS (MeOH + NaI) for $C_{21}H_{40}N_2NaO_9$ $[M+Na]^+$: calculated, 487.2626; found, 487.2627. R_f = 0.52 (10:1 dichloromethane / methanol).

Ethyl 1-amino-12-(2-ethoxy-2-oxoethyl)-3,6,9-trioxa-12-azatetradecan-14-oate (45)

44 (515 mg, 1.1 mmol) was dissolved in dichloromethane (5 ml) and added dropwise to a diethyl ether solution, saturated with hydrochloric acid (15 ml). An immediate precipitation was observed and the mixture was stirred at room temperature for additional 30 min. The solvent was removed under reduced pressure and the product was dried under high vacuum to give a colorless oil. Yield: 460 mg (99%, product · 2 HCl). ^{1}H NMR (400 MHz, MeOD, ppm) δ 4.40 (s, 4H), 4.33 (q, 4H, *J*=7.0 Hz), 3.90 (t, 2H, *J*=4.8 Hz), 3.65 – 3.77 (m, 12H), 3.15 (t, 2H, *J*=4.8 Hz), 1.33 (t, 6H, *J*=7.0 Hz). ^{13}C NMR (125 MHz, MeOD, ppm) δ 167.21, 71.49, 71.46, 71.34, 71.25, 67.90, 66.40, 63.95, 57.12, 56.12, 40.69, 14.33. ESI-MS (MeOH): m/z = 365 $[M+H]^+$.

Ethyl 20-(1,2-dithiolan-3-yl)-3-(2-ethoxy-2-oxoethyl)-16-oxo-6,9,12-trioxa-3,15-diazaicosan-1-oate (46)

DL-α-Lipoic acid (279 mg, 1.4 mmol) was dissolved in dry dichloromethane (5 ml) and triethylamine (187 µl, 1.35 mmol) was added. The mixture was cooled to 0 °C and stirred for 30 min. Methanesulfonyl chloride (105 µl, 1.4 mmol) was added dropwise, then the mixture

was warmed up to room temperature and stirred for 5 h. In the meantime **45** (· 2 HCl; 460 mg, 1.1 mmol) was dissolved in dry dichloromethane (10 ml) and triethylamine (374 µl, 2.7 mmol). Afterwards the amine solution was added dropwise to the mixture with activated lipoic acid, followed by stirring at room temperature for 17 h. The reaction mixture was washed with water (2 x 15 ml) and saturated sodium carbonate solution (2 x 15 ml). The organic phase was dried over magnesium sulfate. The solvent was reduced under reduced pressure and the residue was purified by silica gel column chromatography (10:1 dichloromethane / methanol) to give a yellow oil. Yield: 443 mg (74%). ^{1}H NMR (400 MHz, $CDCl_3$, ppm) δ 6.20 (s, 1H), 4.15 (q, 4H, *J*=7.0 Hz), 3.58 – 3.64 (m, 16H), 3.55 (t, 2H, *J*=5.3 Hz), 3.07 – 3.20 (m, 2H), 2.96 (t, 2H, *J*=5.8 Hz), 2.41 – 2.49 (m, 1H), 2.19 (t, 2H, *J*=7.5 Hz), 1.86 – 1.94 (m, 1H), 1.62 – 1.72 (m, 4H), 1.41 – 1.52 (m, 2H), 1.26 (t, 6H, *J*=7.0 Hz). ^{13}C NMR (100 MHz, $CDCl_3$, ppm) δ 176.29, 173.00, 171.54, 70.66, 70.62, 70.45, 70.39, 70.33, 70.11, 60.63, 56.58, 56.01, 53.79, 40.36, 39.31, 38.61, 36.47, 34.78, 33.63, 29.05, 25.40, 14.28. ESI-MS (MeOH): m/z = 553 $[M+H]^+$. HR-ESI-MS (MeOH + NaI) for $C_{24}H_{44}N_2NaO_8S_2$ $[M+Na]^+$: calculated, 575.2431; found, 575.2429. R_f = 0.48 (10:1 dichloromethane / methanol).

3-(Carboxymethyl)-20-(1,2-dithiolan-3-yl)-16-oxo-6,9,12-trioxa-3,15-diazaicosan-1-oic acid (47)

46 (158 mg, 0.3 mmol) was dissolved in methanol (1.5 ml) and 1 M aqueous lithium hydroxide solution (1.5 ml) was added. The mixture was stirred for 1.5 h at room temperature and neutralized with Amberlite IR120 H to reach pH 7. The suspension was filtered and the solvent was removed under reduced pressure to give a yellow oil. Yield: 119 mg (86%). ^{1}H NMR (500 MHz, MeOD, ppm) δ 3.92 (s, 2H), 3.83 (t, 1H, *J*=5.0 Hz), 3.56 – 3.67 (m, 12H), 3.55 (t, 2H, *J*=5.4 Hz), 3.45 (t, 1H, *J*=4.3 Hz), 3.36 (t, 2H, *J*=5.4 Hz), 3.15 – 3.20 (m, 1H), 3.08 – 3.13 (m, 1H), 2.43 – 2.50 (m, 1H), 2.22 (t, 2H, *J*=7.3 Hz), 1.86 – 1.93 (m, 1H), 1.71 – 1.76 (m, 1H), 1.61 – 1.67 (m, 4H), 1.42 – 1.51 (m, 2H). ^{13}C NMR (125 MHz, MeOD, ppm) δ 176.05, 170.28, 71.49, 71.45, 71.42, 71.30, 71.15, 70.49, 57.57, 57.43, 55.74, 41.16, 40.17, 39.17, 36.63, 35.57, 29.68, 26.54. ESI-MS (MeOH): m/z = 495 $[M-H]^-$. HR-ESI-MS (MeOH + NaI) for $C_{20}H_{35}N_2O_8S_2$ $[M-H]^-$: calculated, 495.1840; found, 495.1848.

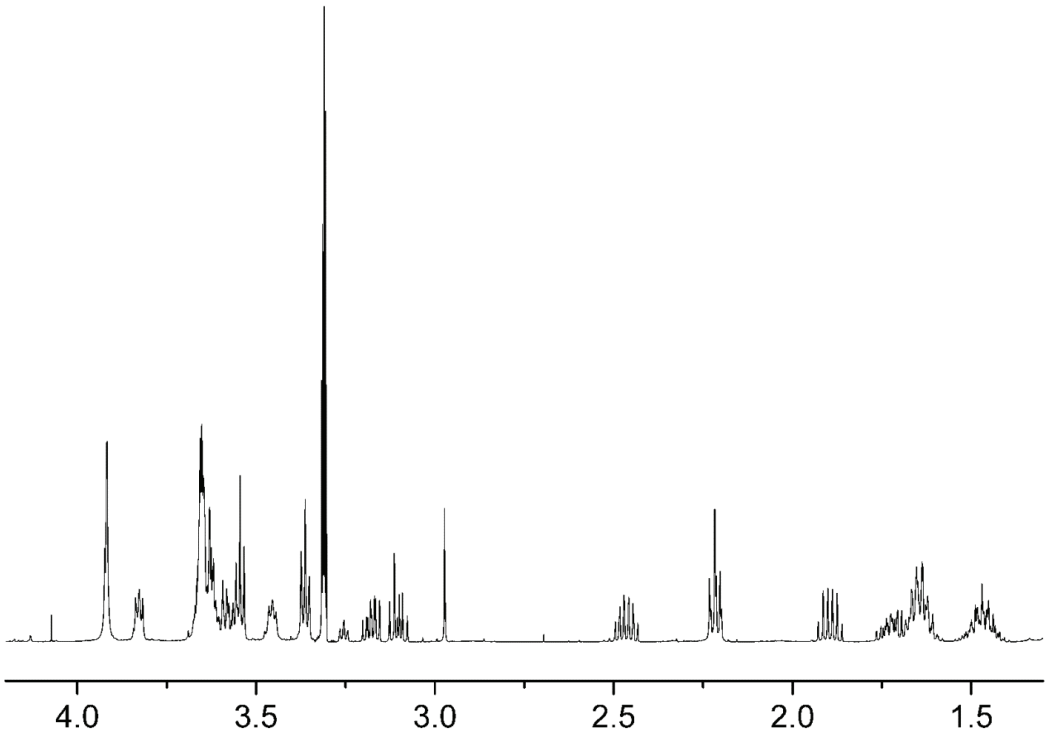

Figure 52. ^{1}H NMR (500 MHz) of compound **47**, measured in MeOD (chemical shifts in ppm).

2,5,8,11-Tetraoxatridecan-13-ol

Tetraethylene glycol (10.0 g, 51.4 mmol) was dissolved in dry tetrahydrofurane (35 ml) and sodium hydride (60% dispersion in mineral oil, 2.08 g) was added at 0 °C. The mixture was stirred at 0 °C for 30 min and iodomethane (3.2 ml, 51.4 mmol) was added. After stirring at room temperature for 9 h, the reaction mixture was extracted with dichloromethane (2 x 200 ml). The combined organic phases were washed with water, brine and dried over magnesium sulfate. The solvent was removed under reduced pressure and the residue was purified by silica gel column chromatography (10:1 dichloromethane / methanol) to give a colorless oil. Yield: 2.5 g (23%). ^{1}H NMR (400 MHz, $CDCl_3$, ppm) δ 3.67 (t, 2H, *J*=4.3 Hz), 3.59 – 3.65 (m, 10H), 3.56 (t, 2H, *J*=4.3 Hz), 3.50 (t, 2H, *J*=4.7 Hz), 3.33 (s, 3H), 2.76 (s, 1H). ESI-MS (MeOH): m/z = 231 $[M+Na]^+$. R_f = 0.23 (10:1 dichloromethane / methanol).

2,5,8,11-Tetraoxatridecan-13-yl 4-methylbenzenesulfonate

2,5,8,11-Tetraoxatridecan-13-ol (1.1 g, 5.4 mmol) was dissolved in dry tetrahydrofurane (5 ml) and cooled to 0 °C. Sodium hydride (60% dispersion in mineral oil, 0.23 g) was added and the mixture was stirred at 0 °C for 10 min. Afterwards a solution of *p*-toluenesulfonyl chloride (1.1 g, 5.9 mmol) in dry tetrahydrofurane (12 ml) was added dropwise. After stirring at room temperature for 2 h, the reaction mixture was quenched with water (50 ml) and

extracted with dichloromethane (3 x 50 ml). The combined organic phases were washed with water, brine and dried over magnesium sulfate. The solvent was removed under reduced pressure and the residue was purified by silica gel column chromatography (2:1 ethyl acetate / hexane) to give a colorless oil. Yield: 1.9 g (99%). ^{1}H NMR (500 MHz, $CDCl_3$, ppm) δ 7.79 (d, 2H, *J*=8.2 Hz), 7.31 (d, 2H, *J*=8.2 Hz), 4.15 (t, 2H, *J*=4.7 Hz), 3.68 (t, 2H, *J*=4.7 Hz), 3.60 – 3.64 (m, 6H), 3.57 (s, 4H), 3.52 – 3.55 (m, 2H), 3.36 (s, 3H), 2.44 (s, 3H). ESI-MS (MeOH): m/z = 385 $[M+Na]^+$. R_f = 0.20 (2:1 ethyl acetate / hexane).

13-Azido-2,5,8,11-tetraoxatridecane

2,5,8,11-Tetraoxatridecan-13-yl 4-methylbenzenesulfonate (1.9 g, 5.2 mmol) was dissolved in acetonitrile (40 ml) and sodium azide (0.5 g, 7.8 mmol) was added. The suspension was refluxed for 18 h. After cooling to room temperature, water (100 ml) was added and the aqueous phase was extracted with dichloromethane (3 x 50 ml). The combined organic phases were dried over magnesium sulfate, filtered and concentrated under reduced pressure. The resulting yellow oil was dried under vacuum and used directly for the next step without further purification. Yield: 1.2 g (95%). ^{1}H NMR (400 MHz, $CDCl_3$, ppm) δ 3.58 – 3.67 (m, 10H), 3.63 (t, 2H, *J*=5.0 Hz), 3.54 (t, 2H, *J*=5.0 Hz), 3.36 – 3.38 (m, 5H). ESI-MS (MeOH): m/z = 256 $[M+Na]^+$.

2,5,8,11-Tetraoxatridecan-13-amine

13-Azido-2,5,8,11-tetraoxatridecane (2.3 g, 10.0 mmol) was dissolved in tetrahydrofurane (50 ml) and triphenylphosphine (2.9 g, 11.0 mmol) and water (0.3 ml) was added. The mixture was stirred at room temperature for 5 h. The solvent was removed under reduced pressure and the residue was purified by silica gel column chromatography (10:1:0.03 dichloromethane / methanol / 25% ammonia solution) to give a colorless oil. Yield: 1.8 g (88%). ^{1}H NMR (400 MHz, $CDCl_3$, ppm) δ 3.60 – 3.66 (m, 10H), 3.47 – 3.53 (m, 4H), 3.35 (s, 3H), 2.84 (t, 2H, *J*=5.1 Hz), 1.67 (s, 2H). ESI-MS (MeOH): m/z = 208 $[M+H]^+$. R_f = 0.06 (10:1:0.03 dichloromethane / methanol / 25% ammonia solution).

5-(1,2-Dithiolan-3-yl)-*N*-(2,5,8,11-tetraoxatridecan-13-yl)pentanamide (48)

2,5,8,11-Tetraoxatridecan-13-amine (940 mg, 4.5 mmol) was dissolved in dry dichloromethane (20 ml) and cooled to 0 °C. DL-α-Lipoic acid (932 mg, 4.5 mmol), *N,N'*-dicyclohexylcarbodiimide (1.0 g, 5.0 mmol) and dimethylaminopyridine (50 mg, 0.5 mmol)

were added and the suspension was stirred at 0 °C for 15 min and at room temperature for 18 h. The white precipitate was separated from the reaction solution *via* decantation. The solvent was removed under reduced pressure and the residue was purified by silica gel column chromatography (ethyl acetate) to give a yellow oil. Yield: 1.5 g (84%). ^{1}H NMR (400 MHz, $CDCl_3$, ppm) δ 6.16 (s, 1H), 3.57 – 3.64 (m, 10H), 3.51 – 3.55 (m, 5H), 3.42 (q, 2H, *J*=5.3 Hz), 3.34 (s, 3H), 3.05 – 3.17 (m, 2H), 2.39 – 2.46 (m, 1H), 2.16 (t, 2H, *J*=7.2 Hz), 1.83 – 1.92 (m, 1H), 1.60 – 1.70 (m, 4H), 1.38 – 1.48 (m, 2H). ^{13}C NMR (125 MHz, $CDCl_3$, ppm) δ 172.93, 72.00, 70.67, 70.62, 70.57, 70.30, 70.01, 59.08, 56.52, 40.33, 39.28, 38.55, 36.39, 34.75, 29.01, 25.48. ESI-MS (MeOH): m/z = 418 $[M+Na]^+$. HR-ESI-MS (MeOH + NaI) for $C_{17}H_{34}NO_5S_2$ $[M+H]^+$: calculated, 396.1873; found, 396.1870. R_f = 0.28 (ethyl acetate).

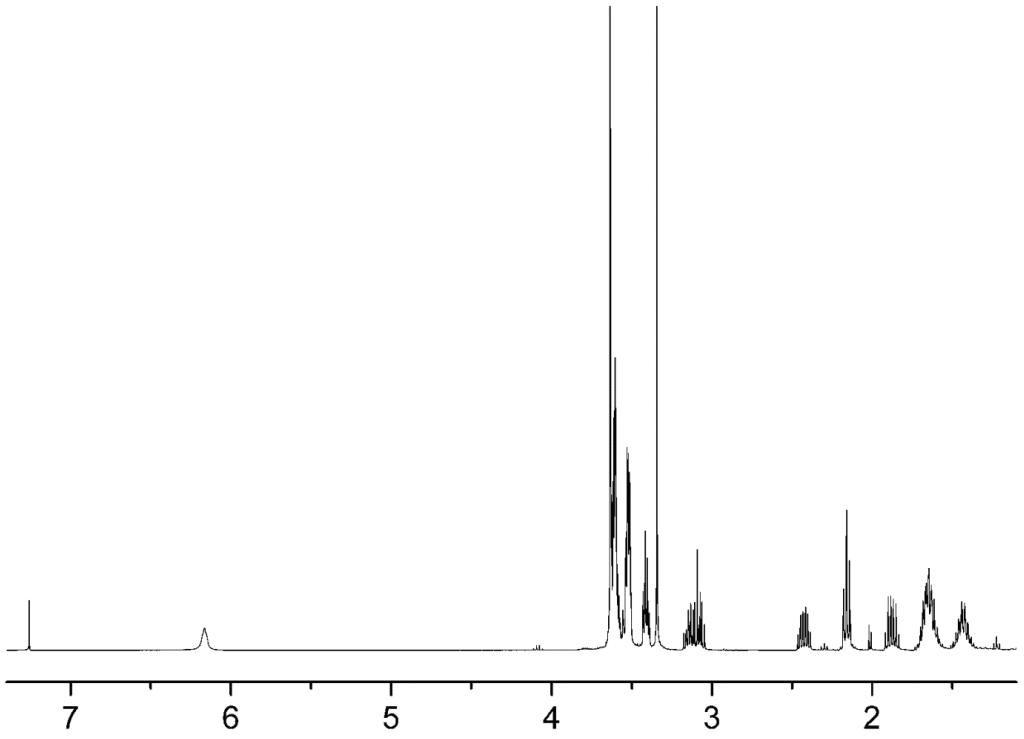

Figure 53. ^{1}H NMR (400 MHz) of compound **48**, measured in $CDCl_3$ (chemical shifts in ppm).

tert-Butyl [17-(1,2-dithiolan-3-yl)-13-oxo-3,6,9-trioxa-12-azaheptadec-1-yl]carbamate

36 (847 mg, 2.9 mmol) was dissolved in dry dichloromethane (80 ml) and cooled to 0 °C. DL-α-Lipoic acid (598 mg, 2.9 mmol), *N,N'*-dicyclohexylcarbodiimide (643 mg, 3.1 mmol) and dimethylaminopyridine (35 mg, 0.3 mmol) were added and the suspension was stirred at 0 °C for 15 min and at room temperature for 21 h. The white precipitate was separated from the reaction solution *via* decantation. The solvent was removed under reduced pressure and the residue was purified by silica gel column chromatography (ethyl acetate) to give a yellow

oil. Yield: 1.1 g (79%). ^{1}H NMR (400 MHz, $CDCl_3$, ppm) δ 6.07 (s, 1H), 5.04 (s, 1H), 3.60 – 3.66 (m, 8H), 3.53 – 3.58 (m, 5H), 3.45 (q, 2H, *J*=5.3 Hz), 3.29 – 3.33 (m, 2H), 3.07 – 3.20 (m, 2H), 2.41 – 2.49 (m, 1H), 2.19 (t, 2H, *J*=7.3 Hz), 1.86 – 1.94 (m, 1H), 1.62 – 1.73 (m, 4H), 1.41 – 1.50 (m, 11H). ESI-MS (MeOH): m/z = 503 $[M+Na]^+$. HR-ESI-MS (MeOH + NaI) for $C_{21}H_{40}N_2NaO_6S_2$ $[M+Na]^+$: calculated, 503.2220; found, 503.2220. R_f = 0.29 (ethyl acetate).

_N_-(2-{2-[2-(2-aminoethoxy)ethoxy]ethoxy}ethyl)-5-(1,2-dithiolan-3-yl)pentanamide (49)

tert-Butyl [17-(1,2-dithiolan-3-yl)-13-oxo-3,6,9-trioxa-12-azaheptadec-1-yl]carbamate (615 mg, 1.3 mmol) was dissolved in dichloromethane (2 ml) and trifluoroacetic acid (2 ml) was added. The mixture was stirred at room temperature for 1 h. The solvent was removed under reduced pressure and the residue was used without further purification. Yield: 779 mg (99%, product · 2 TFA). ^{1}H NMR (400 MHz, MeOD, ppm) δ 3.64 – 3.77 (m, 10H), 3.56 (t, 2H, *J*=5.5 Hz), 3.39 (t, 2H, *J*=5.8 Hz), 3.12 – 3.18 (m, 2H), 2.84 – 2.94 (m, 2H), 2.43 – 2.51 (m, 1H), 2.25 (t, 2H, *J*=7.3 Hz), 2.00 – 2.06 (m, 1H), 1.86 – 1.94 (m, 1H), 1.61 – 1.72 (m, 4H), 1.44 – 1.53 (m, 2H). ESI-MS (MeOH): m/z = 381 $[M+H]^+$.

Biotinyl-*N*-hydroxysuccinimide[17]

d-Biotin (1.0 g, 4.1 mmol) was dissolved in 60 °C warm dimethylformamide (30 ml). *N*-Hydroxysuccinimide (0.5 g, 4.1 mmol) and *N,N'*-dicyclohexylcarbodiimide (1.1 g, 5.3 mmol) were added and the mixture was stirred at room temperature for 18 h. The formed precipitate was filtered and washed with ethanol to afford the product as a white solid. Yield: 1.4 g (98%). ^{1}H NMR (400 MHz, DMSO, ppm) δ 6.40 (s, 1H), 6.34 (s, 1H), 4.31 (t, 1H, *J*=5.7 Hz), 4.15 (t, 1H, *J*=5.3 Hz), 3.33 – 3.36 (m, 1H), 3.08 – 3.13 (m, 1H), 2.81 (s, 4H), 2.67 (t, 2H, *J*=7.5 Hz), 2.57 – 2.60 (m, 1H), 1.60 – 1.73 (m, 4H), 1.43 – 1.53 (m, 2H). ESI-MS (MeOH): m/z = 364 $[M+Na]^+$.

5-(1,2-dithiolan-3-yl)-*N*-{13-oxo-17-[d-biotin]-3,6,9-trioxa-12-azaheptadec-1-yl}pentanamide (50)

49 (· 2 TFA, 780 mg, 1.3 mmol) was dissolved in *N,N*-dimethylformamide (4 ml) and water (1 ml). Triethylamine (887 µl, 6.4 mmol) and biotinyl-*N*-hydroxysuccinimide (437 mg, 1.3 mmol) were added and the mixture was stirred at room temperature for 48 h. The formed precipitate was filtered and washed with ethanol. The solvent was removed under reduced pressure and the residue was purified by silica gel column chromatography (10:1

dichloromethane / methanol) to give the product as a yellow oil. Yield: 224 mg (30%). ^{1}H NMR (400 MHz, $CDCl_3$, ppm) δ 6.65 (s, 1H), 6.53 (s, 1H), 4.52 (t, 1H, *J*=5.8 Hz), 4.34 (t, 1H, *J*=5.8 Hz), 3.53 – 3.64 (m, 12H), 3.40 – 3.48 (m, 4H), 3.08 – 3.21 (m, 4H), 2.88 – 2.92 (m, 1H), 2.71 – 2.77 (m, 1H), 2.42 – 2.50 (m, 1H), 2.17 – 2.24 (m, 4H), 1.86 – 1.95 (m, 1H), 1.58 – 1.76 (m, 8H), 1.41 – 1.51 (m, 4H), 1.37 (t, 2H, *J*=7.3 Hz). ^{13}C NMR (100 MHz, $CDCl_3$, ppm) δ 173.72, 173.53, 164.32, 70.48, 70.22, 64.25, 62.19, 60.65, 56.65, 55.63, 50.95, 45.85, 0.52, 40.41, 39.29, 38.62, 36.40, 35.89, 34.77, 29.84, 29.69, 29.06, 25.51, 8.70. ESI-MS (MeOH): m/z = 629 $[M+Na]^+$. HR-ESI-MS (MeOH + NaI) for $C_{26}H_{46}N_4NaO_6S_3$ $[M+Na]^+$: calculated, 629.2472; found, 629.2465. R_f = 0.10 (10:1 dichloromethane / methanol).

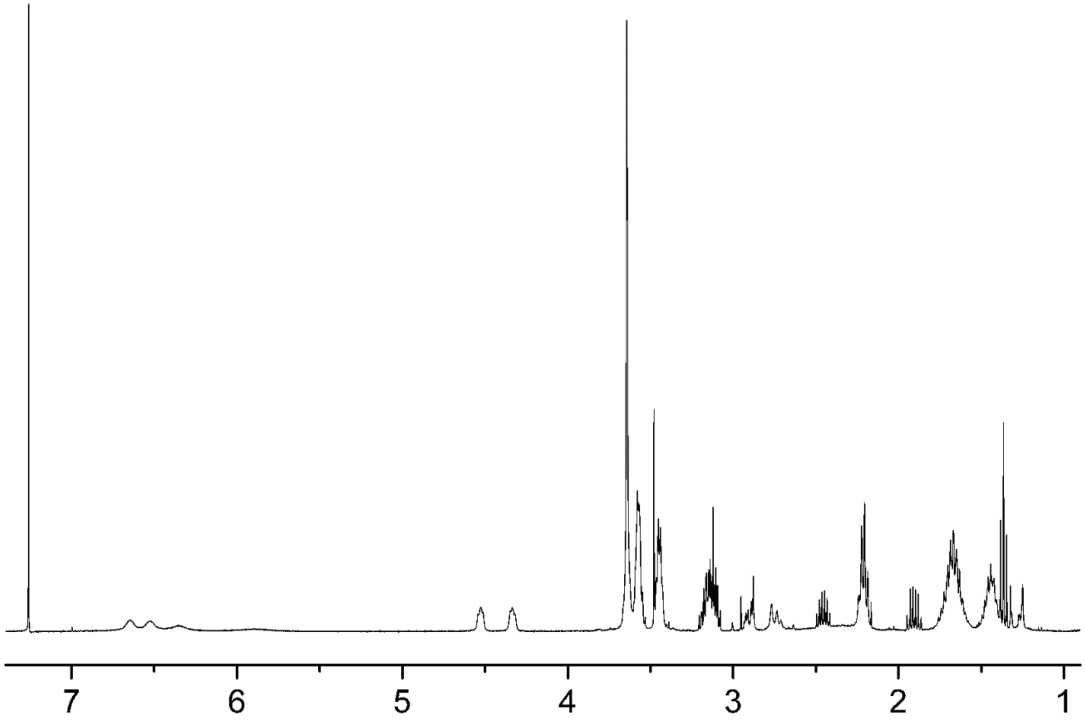

Figure 54. ^{1}H NMR (400 MHz) of compound **50**, measured in $CDCl_3$ (chemical shifts in ppm).

2-{2-[2-(Benzyloxy)ethoxy]ethoxy}ethanol[192]

Triethylene glycol (5.5 ml, 41.3 mmol) was dissolved in 50% aqueous sodium hydroxide solution and stirred at room temperature for 10 min. Benzyl chloride (5.0 ml, 43.4 mmol) was added and the mixture was refluxed at 105 °C for 15 h. After cooling to room temperature, extraction with dichloromethane (3 x 200 ml) was carried out and the organic layer was washed with water (150 ml) and brine (150 ml). The organic phase was dried over magnesium sulfate, filtered and concentrated under reduced pressure. The residue was purified by silica gel column chromatography (ethyl acetate) to give a colorless oil. Yield: 4.2

g (43%). ^{1}H NMR (400 MHz, $CDCl_3$, ppm) δ 7.28 – 7.38 (m, 5H), 4.61 (s, 2H), 3.62 – 3.75 (m, 12H), 2.67 (s, 1H). ESI-MS (MeOH): m/z = 263 $[M+Na]^+$. R_f = 0.25 (ethyl acetate).

({2-[2-(2-Bromoethoxy)ethoxy]ethoxy}methyl)benzene

Synthesized analogously to compound **19** with the following chemicals: 2-{2-[2-(Benzyloxy)ethoxy]ethoxy}ethanol (4.2 g, 17.4 mmol), tetrabromomethane (6.4 g, 19.2 mmol) and triphenylphosphine (5.0 g, 19.2 mmol). Yield: 4.2 g (80%). ^{1}H NMR (400 MHz, $CDCl_3$, ppm) δ 7.27 – 7.36 (m, 5H), 4.58 (s, 2H), 3.82 (t, 2H, *J*=8.0 Hz), 3.64 – 3.72 (m, 8H), 3.47 (t, 2H, *J*=8.0 Hz). ESI-MS (MeOH): m/z = 325 $[M+Na]^+$. R_f = 0.63 (ethyl acetate).

Ethyl 4-{2-[2-(benzyloxy)ethoxy]ethoxy}-*N*-(*tert*-butoxycarbonyl)-2'-nitriloisovalinate

Synthesized analogously to compound **20** with the following chemicals: Sodium (0.22 g, 9.4 mmol), **3** (1.94 g, 8.5 mmol) and ({2-[2-(2-bromoethoxy)ethoxy]ethoxy}methyl)benzene (2.51 g, 9.4 mmol). Yield: 1.92 g (50%). ^{1}H NMR (400 MHz, $CDCl_3$, ppm) δ 7.25 – 7.34 (m, 5H), 6.61 (s, 1H), 4.56 (s, 2H), 4.29 (q, 2H, *J*=7.0 Hz), 3.61 – 3.90 (m, 10H), 2.23 – 2.36 (m, 1H), 1.95 – 2.13 (m, 1H), 1.45 (s, 9H) 1.32 (t, 3H, *J*=7.0 Hz). ^{13}C NMR (100 MHz, $CDCl_3$, ppm) δ 166.81, 154.32, 138.35, 129.83, 128.53, 127.89, 127.79, 81.48, 73.41, 70.77, 70.49, 69.67, 67.26, 66.77, 63.52, 62.62, 32.32, 29.84, 28.44, 28.34, 14.09. ESI-MS (MeOH): m/z = 473 $[M+Na]^+$. HR-ESI-MS (MeCN) for $C_{23}H_{34}N_2NaO_7$ $[M+Na]^+$: calculated, 473.2258; found, 473.2252. R_f = 0.15 (2:1 hexane / ethyl acetate).

Ethyl 4-{2-[2-(benzyloxy)ethoxy]ethoxy}-*N*-(*tert*-butoxycarbonyl)-2'-[(*tert*-butoxycarbonyl)amino]isovalinate

Synthesized analogously to compound **21** with the following chemicals: Ethyl 4-{2-[2-(benzyloxy)ethoxy]ethoxy}-*N*-(*tert*-butoxycarbonyl)-2'-nitriloisovalinate (1.21 g, 2.7 mmol), di-*tert*-butyldicarbonat (1.17 g, 5.4 mmol), nickel(II) chloride hexahydrate (0.06 g, 0.3 mmol), sodium borohydride (0.81 g, 21.4 mmol) and diethylenetriamine (0.32 ml, 3.0 mmol). Yield: 1.12 g (78%). ^{1}H NMR (400 MHz, $CDCl_3$, ppm) δ 7.25 – 7.35 (m, 5H), 6.05 (s, 1H), 5.08 (s, 1H), 4.56 (s, 2H), 4.17 (q, 2H, *J*=7.3 Hz), 3.51 – 3.68 (m, 12H), 2.25 – 2.29 (m, 1H), 2.07 – 2.13 (m, 1H), 1.42 (s, 9H), 1.41 (s, 9H), 1.25 (t, 3H, *J*=7.3 Hz). ^{13}C NMR (100 MHz, $CDCl_3$, ppm) δ 172.91, 156.16, 154.87, 138.41, 129.88, 128.56, 127.93, 127.81, 79.51, 73.44, 70.66, 70.61, 69.64, 69.43, 67.14, 62.49, 61.85, 44.85, 32.95, 29.88, 28.52, 14.23. ESI-MS (MeOH): m/z =

577 $[M+Na]^+$. HR-ESI-MS (MeCN) for $C_{28}H_{46}N_2NaO_9$ $[M+Na]^+$: calculated, 577.3095; found, 577.3092. R_f = 0.28 (2:1 hexane / ethyl acetate).

Ethyl *N*-(*tert*-butoxycarbonyl)-2'-[(*tert*-butoxycarbonyl)amino]-4-[2-(2-hydroxyethoxy)ethoxy]isovalinate (53)

Synthesized analogously to compound **22** with the following chemicals: Ethyl 4-{2-[2-(benzyloxy)ethoxy]ethoxy}-*N*-(*tert*-butoxycarbonyl)-2'-[(*tert*-butoxycarbonyl)amino]isovalinate (1.01 g, 1.8 mmol) and palladium on carbon (10%) (50 mg). Yield: 0.74 g (90%). ^{1}H NMR (400 MHz, $CDCl_3$, ppm) δ 6.08 (s, 1H), 5.07 (s, 1H), 4.19 (q, 2H, *J*=7.0 Hz), 3.54 – 3.75 (m, 12H), 2.25 – 2.29 (m, 1H), 2.07 – 2.13 (m, 1H), 1.43 (s, 9H), 1.42 (s, 9H), 1.28 (t, 3H, *J*=7.0 Hz). ^{13}C NMR (100 MHz, $CDCl_3$, ppm) δ 173.10, 156.16, 154.87, 79.92, 79.64, 72.73, 70.42, 67.07, 62.52, 62.01, 44.77, 29.91, 28.55, 14.25. ESI-MS (MeOH): m/z = 487 $[M+Na]^+$. HR-ESI-MS (MeCN) for $C_{21}H_{40}N_2NaO_9$ $[M+Na]^+$: calculated, 487.2626; found, 487.2624. R_f = 0.29 (ethyl acetate).

Ethyl 4-[2-(2-bromoethoxy)ethoxy]-*N*-(*tert*-butoxycarbonyl)-2'-[(*tert*-butoxycarbonyl)amino]isovalinate

Synthesized analogously to compound **23** with the following chemicals: Ethyl *N*-(*tert*-butoxycarbonyl)-2'-[(*tert*-butoxycarbonyl)amino]-4-[2-(2-hydroxyethoxy)-ethoxy]isovalinate (1.09 g, 2.4 mmol), tetrabromomethane (0.94 g, 2.8 mmol) and triphenylphosphine (0.79 g, 2.8 mmol). Yield: 0.95 g (77%). ^{1}H NMR (400 MHz, $CDCl_3$, ppm) δ 6.04 (s, 1H), 5.07 (s, 1H), 4.18 (q, 2H, *J*=7.1 Hz), 3.79 (t, 2H, *J*=6.3Hz), 3.52 – 3.69 (m, 8H), 3.47 (t, 2H, *J*=6.3Hz), 2.26 – 2.29 (m, 1H), 2.07 – 2.14 (m, 1H), 1.43 (s, 9H), 1.42 (s, 9H), 1.28 (t, 3H, *J*=7.1 Hz). ^{13}C NMR (100 MHz, $CDCl_3$, ppm) δ 172.97, 156.18, 154.86, 79.56, 71.39, 70.53, 70.43, 67.26, 62.52, 61.89, 44.83, 32.97, 30.36, 28.56, 14.28. ESI-MS (MeOH): m/z = 549 $[M+Na]^+$. HR-ESI-MS (MeOH+HCOOH) for $C_{21}H_{39}BrN_2NaO_8$ $[M+Na]^+$: calculated, 549.1782; found, 549.1776. R_f = 0.55 (1:1 hexane / ethyl acetate).

Ethyl *N*-(*tert*-butoxycarbonyl)-2'-[(*tert*-butoxycarbonyl)amino]-4-{2-[2-(tritylsulfanyl)-ethoxy]ethoxy}isovalinate

Synthesized analogously to compound **24** with the following chemicals: Triphenylmethanethiol (0.51 g, 1.8 mmol), sodium hydride (60% dispersion in mineral oil, 78 mg), and Ethyl 4-[2-(2-bromoethoxy)ethoxy]-*N*-(*tert*-butoxycarbonyl)-2'-[(*tert*-

butoxycarbonyl)amino]isovalinate (0.85 g, 1.6 mmol). Yield: 1.04 g (91%). ^{1}H NMR (400 MHz, $CDCl_3$, ppm) δ 7.40 – 7.44 (m, 6H), 7.25 – 7.31 (m, 6H), 7.18 – 7.22 (m, 3H), 6.01 (s, 1H), 5.06 (s, 1H), 4.15 (q, 2H, *J*=7.2 Hz), 3.63 – 3.71 (m, 2H), 3.35 – 3.55 (m, 6H), 3.28 (t, 2H, *J*=7.0 Hz), 2.41 (t, 2H, *J*=7.0 Hz), 2.23 – 2.27 (m, 1H), 2.05 – 2.11 (m, 1H), 1.42 (s, 18H), 1.24 (t, 3H, *J*=7.2 Hz). ^{13}C NMR (100 MHz, $CDCl_3$, ppm) δ 172.87, 156.11, 154.80, 145.00, 130.28, 129.79, 128.05, 126.83, 79.47, 71.21, 70.31, 70.05, 67.09, 62.45, 61.82, 44.81, 32.89, 31.76, 28.51, 14.21. ESI-MS (MeOH): m/z = 745 $[M+Na]^+$. HR-ESI-MS (MeOH+NaOH) for $C_{40}H_{54}N_2NaO_8S$ $[M+Na]^+$: calculated, 745.3493; found, 745.3483. R_f = 0.29 (2:1 hexane / ethyl acetate).

_N_-(*tert*-Butoxycarbonyl)-2'-[(*tert*-butoxycarbonyl)amino]-4-{2-[2-(tritylsulfanyl)ethoxy]ethoxy}isovaline

Synthesized analogously to compound **25**. Yield: 0.981 g (98%). ^{1}H NMR (400 MHz, $CDCl_3$, ppm) δ 7.41 – 7.44 (m, 6H), 7.26 – 7.31 (m, 6H), 7.20 – 7.24 (m, 3H), 6.37 (s, 1H), 5.11 (s, 1H), 3.63 – 3.68 (m, 2H), 3.31 – 3.56 (m, 6H), 3.25 (t, 2H, *J*=7.0 Hz), 2.44 (t, 2H, *J*=7.0 Hz), 2.23 – 2.27 (m, 1H), 1.99 – 2.04 (m, 1H), 1.39 (s, 9H), 1.37 (s, 9H). ^{13}C NMR (100 MHz, $CDCl_3$, ppm) δ 156.61, 154.89, 144.86, 129.65, 127.89, 126.66, 79.46, 69.81, 69.61, 69.49, 67.55, 66.67, 61.88, 45.87, 31.32, 29.74, 28.54, 28.43. ESI-MS (MeOH): m/z = 693 $[M-H]^-$, m/z = 717 $[M+Na]^+$. HR-ESI-MS (MeOH+NaOH) for $C_{38}H_{50}N_2NaO_8S$ $[M+Na]^+$: calculated, 717.3180; found, 717.3177.

2'-Amino-4-[2-(2-sulfanylethoxy)ethoxy]isovaline (51)

Synthesized analogously to compound **26** with the following chemicals: *N*-(*tert*-Butoxycarbonyl)-2'-[(*tert*-butoxycarbonyl)amino]-4-{2-[2-(tritylsulfanyl)ethoxy]ethoxy}-isovaline (150 mg, 0.21 mmol), dichloromethane (1.3 ml, 20.2 mmol), trifluoroacetic acid (0.63 ml, 8.2 mmol) and triethylsilane (0.25 ml, 1.6 mmol). Yield: 52 mg (98%). ^{1}H NMR (400 MHz, D_2O, ppm) δ 3.82 – 3.87 (m, 2H), 3.68 – 3.76 (m, 6H), 2.78 (t, 2H, *J*=6.0 Hz), 2.24 – 2.29 (m, 2H). ^{13}C NMR (100 MHz, D_2O, ppm) δ 171.85, 72.00, 69.65, 68.89, 66.26, 60.31, 42.32, 32.53. ESI-MS (MeOH): m/z = 249 $[M-H]^-$, m/z = 253 $[M+H]^+$. HR-ESI-MS (MeOH+HCOOH) for $C_9H_{21}N_2O_4S$ $[M+H]^+$: calculated, 253.1217; found, 253.1211.

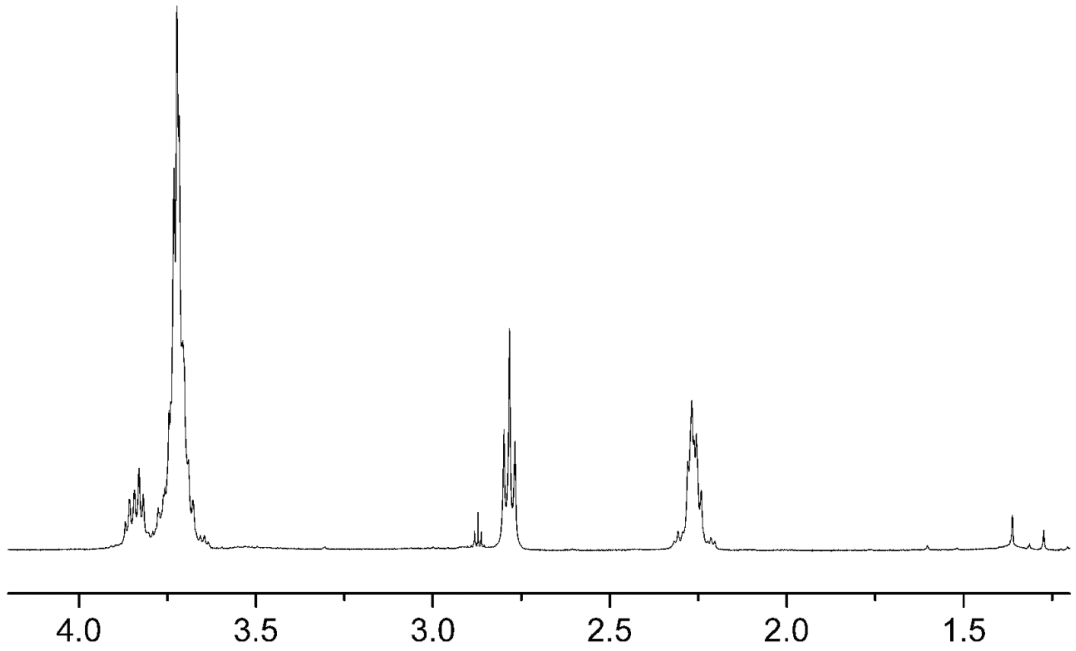

Figure 55. ^{1}H NMR (400 MHz) of compound **51**, measured in D_2O (chemical shifts in ppm).

tert-Butyl 2-methoxypolyethylene glycol(750) acetate

Methoxypolyethylene glycol 750 (6.84 g, 9.1 mmol) was dissolved in tetrahydrofurane (20 ml) and cooled to 0 °C. Sodium hydride (60% dispersion in mineral oil, 0.73 g) was added portionwise. Afterwards *tert*-butyl bromoacetate (3.4 ml, 22.8 mmol) was added and the reaction mixture was stirred at room temperature for 8 h. Then methanol (1 ml) was added and the solvent was removed under reduced pressure. The residue was purified by silica gel column chromatography (10:1 dichloromethane / methanol). Yield: 7.05 g (91%). ^{1}H NMR (400 MHz, $CDCl_3$, ppm) δ 4.00 (s, 2H), 3.66 – 3.70 (m, 4H), 3.61 – 3.64 (m, 58), 3.51 – 3.54 (m, 2H), 3.36 (s, 3H), 1.45 (s, 9H). ESI-MS (MeOH): m/z = 873 $[M+Na]^+$. R_f = 0.43 (10:1 dichloromethane / methanol).

2-Methoxypolyethylene glycol(750) acetic acid

tert-Butyl 2-methoxypolyethylene glycol(750) acetate (2.0 g, 2.48 mmol) was dissolved in dichloromethane (10 ml) and trifluoroacetic acid (5 ml). The mixture was stirred at room temperature for 3 h. The solvent was removed under vacuum and the residue was used directly for the next step without further purification. Yield: 1.96 g (99%). ^{1}H NMR (400 MHz, $CDCl_3$, ppm) δ 4.16 (s, 2H), 3.74 – 3.76 (m, 2H), 3.63 – 3.69 (m, 60), 3.55 – 3.57 (m, 2H), 3.38 (s, 3H). ESI-MS (MeOH): m/z = 817 $[M+Na]^+$.

2,5-Dioxopyrrolidin-1-yl-2-methoxypolyethylene glycol(750) acetate

2-Methoxypolyethylene glycol(750) acetic acid (1.97 g, 2.5 mmol), *N*-hydroxysuccinimide (0.30 g, 2.6 mmol) and *N,N'*-dicyclohexylcarbodiimide (0.61 g, 3.0 mmol) were dissolved in dichloromethane (20 ml) and *N,N*-dimethylformamid (3 ml). The mixture was stirred at room temperature for 19 h, while a white precipitate was formed. The precipitate was separated from the solution with the help of centrifugation. The solvent was removed under reduced pressure and the residue was purified by silica gel column chromatography (10:1 dichloromethane / methanol). Yield: 1.36 g (64%). ^{1}H NMR (400 MHz, $CDCl_3$, ppm) δ 4.14 (s, 2H), 3.67 – 3.69 (m, 2H), 3.52 – 3.56 (m, 60), 3.42 – 3.44 (m, 2H), 3.35 (s, 3H), 2.67 (s, 4H). ESI-MS (MeOH): m/z = 848 $[M+Na]^+$. R_f = 0.46 (10:1 dichloromethane / methanol).

***N*-(3,4-Dihydroxyphenethyl)-2-methoxypolyethylene glycol(750) acetamide (52)**

2,5-Dioxopyrrolidin-1-yl-2-methoxypolyethylene glycol(750) acetate (1.15 g, 1.3 mmol), dopamine hydrochloride (0.24 g, 1.3 mmol) and triethylamine (0.36 ml, 2.6 mmol) were dissolved in *N,N*-dimethylformamid (10 ml). The mixture was stirred at room temperature for 48 h. After evaporation of the solvent the resulting residue was purified by silica gel column chromatography (10:1 dichloromethane / methanol). Yield: 496 mg (44%). ^{1}H NMR (500 MHz, MeOD, ppm) δ 6.74 (d, 1H, *J*=7.9 Hz), 6.70 (s, 1H), 6.58 (d, 1H, *J*=7.9 Hz), 3.73 (s, 2H), 3.69 – 3.71 (m, 2H), 3.62 – 3.67 (m, 60), 3.53 – 3.55 (m, 2H), 3.36 (s, 3H), 3.13 (t, 2H, *J*=7.9 Hz), 2.81 (t, 2H, *J*=7.9 Hz). ESI-MS (MeOH): m/z = 885 $[M-H]^-$. R_f = 0.41 (10:1 dichloromethane / methanol).

3.5.2 The Synthesis, Functionalization and Radiolabeling of NPs

Synthesis of Fe_3O_4-Au Core-Shell NPs

Fe_3O_4-Au NPs were prepared in two steps according to a reported procedure with slight modifications.[156] Briefly, a mixture of iron acetylacetonate (0.18 g, 0.50 mmol), diphenyl ether (6 ml), oleic acid (0.5 ml, 1.57 mmol) and oleylamine (0.5 ml, 1.00 mmol) was stirred under nitrogen at room temperature for 5 min. 1,2-Hexadecanediol (0.65 g, 2.52 mmol) was added and the temperature was increased to 210 °C over the course of 30 min. The black mixture was stirred at this temperature for 120 min and cooled to room temperature. Half of this suspension (3.5 ml) was loaded into a syringe and added to a mixture of gold acetate (0.21 g, 0.55 mmol), oleic acid (0.13 ml, 0.41 mmol), 1,2-hexadecanediol (0.78 g, 3.02 mmol)

and oleylamine (0.75 ml, 1.50 mmol) in diphenyl ether (7.5 ml). The temperature was increased to 190 °C over the course of 35 min and the mixture was stirred at 190 °C for 90 min. After cooling to room temperature, ethanol (60 ml) was added and the dark purple precipitate was isolated by centrifugation. The NPs were finally dried in vacuum, redispersed in hexane (~15 mg/ml NPs) and stored at 4 °C.

Phase Transfer of Fe_3O_4-Au Core-Shell NPs

In a typical procedure basic coating ligand **48** (25.3 µmol), chelator containing ligand (**39**, **43** or **47**; 8.4 µmol), biotin containing ligand (**50**; 8.4 µmol) and TCEP (12 mg, 42.1 µmol) were dissolved in methanol (800 µl) and water (50 µl). The mixture was vortexed for 5 min and transferred in a nitrogen flushed glass vial with a magnetic stir bar, sealed with a butyl septa and an aluminium-butyl crimp cap. Fe_3O_4-Au NPs (100 µl of the native hexane solution) were diluted with hexane (700 µl) and overlayed on the methanol phase. The mixture was vigorously stirred at room temperature for 20 min. Over the course of the phase transfer, the originally purple hexane phase became completely transparent while the as-functionalized Fe_3O_4-Au NPs were dispersed in the methanol phase. The hexane supernatant with the hydrophobic coating ligands was removed *via* decantation. After evaporation of methanol, the derivatized Fe_3O_4-Au NPs were dispersed in PBS (1 ml). The purification was performed with a PD-10 column and PBS as mobile phase. The samples were purified for three times, whereas only the purple colored fractions were collected and the volume was concentrated to 1 ml.

^{99m}Tc Radiolabeling of Fe_3O_4-Au Core-Shell NPs

In general, an aqueous solution of $[^{99m}Tc(OH_2)_3(CO)_3]^+$ (0.5 ml, pH=7-8, 300-390 MBq) was added to purified Fe_3O_4-Au NPs (1 ml in PBS). The mixture was incubated at 50 °C for 120 min. Radiolabelled NPs were purified with a PD-10 column, whereas 12 fractions (each 0.5 ml) were collected directly after loading the column. The activities of the different fractions were measured with a dose calibrator, the NP containing fractions were combined and the radiochemical yield determined.

Synthesis of Au-Fe_3O_4 Dumbbell-Like NPs

Au-Fe_3O_4 Dumbbell-like NPs were prepared in two steps according to a reported procedure with slight modifications.[158] Briefly, 1,2,3,4-tetrahydronaphthalene (100 ml) was added to

tetrachloroauric acid trihydrate (1.0 g, 2.5 mmol), followed by oleylamine (10 ml, 30 mmol). The orange mixture was stirred at room temperature for 5 min and heated at 65 °C for 5 h. Due to the fact that the orange mixture did not change to an intense red solution, the temperature was elevated to 115 °C for 10 min and cooled to room temperature. Ethanol (100 ml) was added to the solution and the participated AuNPs were separated by centrifugation, washed with ethanol, dried and redispersed in hexane (~20 mg/ml). For the synthesis of Dumbbell-like NPs, oleic acid (1.0 ml, 3.0 mmol) in 1-octadecene (20 ml) was heated at 120 °C for 20 min under a flow of N_2. Iron pentacarbonyl (0.15 ml, 1.1 mmol) was added and the yellow solution was stirred at 120 °C for 5 min. Oleylamine (0.5 ml, 1.5 mmol) was added, followed by 1.4 ml of the above AuNP solution in hexane. The temperature was increased to 310 °C over the course of 20 min and the solution was stirred at 310 °C for additional 45 min. After cooling to room temperature, the particles were separated by adding iso-propanol, centrifuged and washed with iso-propanol. Dried NPs were finally dispersed in hexane (~10 mg/ml) and stored at 4 °C.

Phase Transfer of Au-Fe_3O_4 Dumbbell-Like NPs

In a typical procedure, NPs in hexane (500 µl of the native solution) were transferred to a test tube and the solvent was removed under a stream of nitrogen. A solution of water (2.5 ml), 0.01 M acetic acid (1.5 ml) and 25% tetramethylammonium hydroxide solution (120 µl) was added to the NPs and the mixture was sonicated at 37 °C for 30 min. Coating ligand **52** (80 mg) was added and the mixture was sonicated for additional 30 min. After evaporation of the solvent, the black crude was redispersed in PBS (1.5 ml) and purified with a PD-10 column (PBS as mobile phase) to remove unbound coating ligand. Purified NPs were kept in PBS at 4 °C.

^{99m}Tc Radiolabeling of Au-Fe_3O_4 Dumbbell-Like NPs

In a first step, chelator containing ligands (**39**, **43**, **47** or **51**) were radiolabelled. An aqueous solution of $[^{99m}Tc(OH_2)_3(CO)_3]^+$ (0.5ml, pH=7-8, 170-350 MBq) was added to a ligand solution (0.5 mL, 0.1 mM in H_2O) and the mixture was stirred at 70 °C for 30 min. Reaction control was carried out with HPLC (TFA/MeOH, C18rp). In a second step, NP solution in PBS (0.5 ml) was mixed with ^{99m}Tc complex solution (0.5 ml) and aqueous TCEP solution (0.5 ml, 1 mg/ml). The mixture was incubated for 60 min at 50 °C. Radiolabelled NPs were purified with a PD-10 column, whereas 12 fractions (each 0.5 ml) were collected directly after loading the

column. The activities of the different fractions were measured with a dose calibrator, the NP containing fractions were combined and the radiochemical yield determined.

3.6 Synthetic Part of the Section 2.4

3.6.1 The Synthesis of Tyr-PEG-DAP

Methyl *N*-(*tert*-butoxycarbonyl)-*O*-{7-[(*tert*-butoxycarbonyl)amino]-7-(ethoxycarbonyl)-2,2-dimethyl-4-oxo-3,10,13-trioxa-5-azapentadecan-15-yl}-L-tyrosinate (54)

53 (744 mg, 1.6 mmol) and *N*-(*tert*-butoxycarbonyl)-L-tyrosine methyl ester (434 mg, 1.5 mmol) were dissolved in dry THF (20 ml) and cooled to 0 °C. Triphenylphosphine (465 mg, 1.8 mmol) was added portionwise during a period of 30 min. Afterwards diisopropyl azodiformate (0.35 ml, 1.8 mmol) was added dropwise and the yellow reaction mixture was allowed to reach room temperature and stirred for 24 h. The reaction was quenched with water and the product was extracted with diethyl ether (2 x 150 ml). The combined organic phases were washed with brine, dried over magnesium sulfate and the solvent was removed under reduced pressure. The resulting oil was purified by silica gel column chromatography to give the product as a colorless oil (1:1 hexane / ethyl acetate). Yield: 687 mg (58%). ^{1}H NMR (500 MHz, $CDCl_3$) δ 6.98 (d, 2H, *J*=8.5 Hz), 6.80 (d, 2H, *J*=8.8 Hz), 6.05 (s, 1H), 5.09 (s, 1H), 4.91 – 4.98 (m, 1H), 4.48 (t, 1H, *J*=5.9 Hz), 4.14 (q, 2H, *J*=6.9 Hz), 4.06 (t, 2H, *J*=4.9 Hz), 3.79 (t, 2H, *J*=4.9 Hz), 3.67 (s, 3H), 3.63 – 3.64 (m, 4H), 3.50 – 3.57 (m, 4H), 2.93 – 3.02 (m, 2H), 2.23 – 2.26 (m, 1H), 2.05 – 2.09 (m, 1H), 1.39 (s, 18H), 1.38 (s, 9H), 1.22 (t, 3H, *J*=6.9 Hz). ^{13}C NMR (125 MHz, $CDCl_3$) δ 172.67, 172.40, 157.75, 130.18, 128.09, 114.56, 79.87, 79.56, 79.29, 70.53, 70.22, 69.66, 67.27, 66.90, 62.20, 61.62, 54.38, 52.14, 44.41, 37.34, 32.59, 28.25, 13.97. ESI-MS (MeOH): m/z = 764 $[M+Na]^+$. HR-ESI-MS (MeCN) for $C_{36}H_{60}N_3O_{13}$ $[M+H]^+$: calculated, 742.4121; found, 742.4119. R_f = 0.35 (1:1 hexane / ethyl acetate)

***O*-{2-[2-(3,4-Diamino-3-carboxybutoxy)ethoxy]ethyl}-L-tyrosine (Tyr-PEG-DAP 55)**

54 (281 mg, 0.4 mmol) was dissolved in a mixture of MeOH and 1 M NaOH (1:1, 6 ml). The hydrolysis of the esters occurred at 80 °C during 11 h. After neutralization with 2 M HCl, the solvent was removed under reduced pressure and the residue was dissolved in 2 M HCl (4 ml). Stirring at 90 °C for 12 h led to the complete removal of the amine protection groups. After cooling to room temperature, the pH was adjusted to a value of 4 and the water was evaporated. The mixture was redissolved in methanol (0.7 ml) and the product was separated from sodium chloride *via* decantation of the methanol phase. This procedure was repeated four times to give the product as a colorless solid. Yield: 94 mg (62%). ^{1}H NMR (500 MHz, D_2O, ppm) δ 7.11 (d, 2H, *J*=8.5 Hz), 6.86 (d, 2H, *J*=8.5 Hz), 4.10 (t, 1H, *J*=6.1 Hz), 4.07 (t,

2H, *J*=4.9 Hz), 3.72 – 3.79 (m, 2H), 3.58 – 3.65 (m, 3H), 3.51 – 3.54 (m, 3H), 3.27 (s, 2H), 3.10 – 3.13 (m, 1H), 3.00 – 3.04 (m, 1H), 2.01 – 2.10 (m, 2H). ^{13}C NMR (125 MHz, D_2O, ppm) δ 172.28, 157.95, 131.22, 127.40, 115.79, 70.06, 69.77, 69.49, 67.61, 66.60, 60.50, 54.89, 42.67, 35.32, 33.02. ESI-MS (MeOH): m/z = 400 $[M+H]^+$, m/z = 422 $[M+Na]^+$. HR-ESI-MS (H_2O) for $C_{18}H_{28}N_3O_7$ $[M-H]^-$: calculated, 398.1933; found, 398.1927.

3.6.2 The Synthesis of *fac*-[(Tyr-PEG-DAP)-Re(CO)$_3$] (56)

To the precursor $[ReBr(CO)_5]$ (54 mg, 0.13 mmol) water (1.4 ml) was added and the mixture was stirred at 180 °C for 20 min under microwave irradiation to obtain *fac*-$[Re(OH_2)_3(CO)_3]Br$. The completion of the reaction was checked with HPLC (TFA / MeOH, C18rp, retention time R_T=5.6 min). To the *fac*-$[Re(OH_2)_3(CO)_3]^+$-solution (pH adjusted to 9 with 1 M NaOH) compound **55** (58 mg, 0.14 mmol) was added and the mixture was stirred at 110 °C for 12 min under microwave irradiation. After evaporation of the solvent the resulting residue was purified by preparative HPLC. The neutral complex **56** was obtained as a colorless powder. Yield: 40 mg (45%). ^{1}H NMR (500 MHz, D_2O) δ 7.11 (d, 2H, *J*=8.5 Hz), 6.86 (d, 2H, *J*=8.8 Hz), 4.88 (d, 1H, *J*=11.3 Hz) 4.58 – 4.64 (m, 2H), 4.24 (q, 1H, *J*=11.3 Hz), 4.13 (t, 1H, *J*=7.3 Hz), 4.06 (t, 2H, *J*=4.3 Hz), 3.74 (t, 2H, *J*=5.2 Hz), 3.58 (t, 1H, *J*=4.0 Hz), 3.46 – 3.55 (m, 4H), 3.12 – 3.16 (m, 1H), 2.99 – 3.03 (m, 1H), 2.69 – 2.73 (m, 1H), 2.53 – 2.59 (m, 1H), 1.91 – 1.96 (m, 1H), 1.76 – 1.81 (m, 1H). ^{13}C NMR (125 MHz, D_2O) δ 197.72, 196.20, 196.18, 181.47, 172.00, 158.10, 131.23, 127.19, 115.81, 115.60, 70.15, 69.73, 69.50, 67.68, 66.69, 65.78, 54.68, 45.35, 35.23, 32.94. ESI-MS (MeOH): m/z = 670 $[M+H]^+$, m/z = 692 $[M+Na]^+$. HR-ESI-MS (H_2O) for $C_{21}H_{27}N_3O_{10}Re$ $[M-H]^-$: calculated, 668.1260; found, 668.1254. IR (KBr): ν_{CO} = 2027 (s), 1908 (s). HPLC (TFA / MeOH, C18rp): 17.6 min. Preparative HPLC (TFA / MeOH, C18rp): 38 min.

3.6.3 The Synthesis of *fac*-[(Tyr-PEG-DAP)-^{99m}Tc(CO)$_3$] (57) and its Formulation for *in vivo* Experiments

Method A) To ligand **55** (0.7 ml, $1.15\cdot10^{-4}$ M in H_2O) was added $[^{99m}Tc(OH_2)_3(CO)_3]^+$ (1.0 ml, pH=7-8, 980 MBq). The mixture was stirred at 95 °C for 20 min. HPLC (TFA / MeOH, C18rp, γ-detection): 18.0 min, radiochemical purity (RCP) ≥95%.

Method B) An aqueous solution of $[^{99m}Tc(OH_2)_3(CO)_3]^+$ (0.5ml, pH=7-8, 750 MBq) was added to a ligand **55** solution (0.5 mL, $1.15\cdot10^{-4}$ M in H_2O) and the mixture was stirred at 110 °C for

11 min under microwave irradiation. HPLC (TFA / MeOH, C18rp, γ-detection): 18.0 min, RCP ≥95%.

Method C) A ligand **55** solution (0.5 mL, $1.15 \cdot 10^{-4}$ M in H_2O) and Na[$^{99m}TcO_4$] in 0.9% saline (0.5 ml, 710 MBq) was added to an Isolink™ kit. The mixture was stirred at 95 °C for 30 min. HPLC (TFA / MeOH, C18rp, γ-detection): 18.0 min, RCP ≥95%.

Formulation: To obtain an injectable sterile solution for *in vivo* evaluation, the product was extracted from the reaction mixture using a C18-SepPak cartridge. The loaded cartridge was rinsed with sterile water (3 ml) and eluted with ethanol (1.5 ml). The solvent was evaporated and physiological saline solution (0.9%) was finally added. HPLC (TFA / MeOH, C18rp, γ-detection): 18.0 min, RCP ≥95%. RCY: 81%.

3.6.4 *In vivo* Studies and *ex vivo* Biodistribution Analysis

All animal experiments were conducted according to the Dutch code of practice for the care and use of animals, after approval from the local animal ethics committee. Animals were male NMRI mice and male nude NMRI mice, purchased from Harlan (Netherlands) and 12 weeks old at the start of the experiment. For tumor inoculation C6 cells (ATCC® CCL-107) were cultured according to the guidelines of ATCC and 1 million cells in 200 µl volume were subcutaneously injected in the left shoulder. Tumors were allowed to grow for 2 weeks, and reached a volume of 0.5 – 1.0 cm^3. The healthy and xenograft-bearing mice were anesthetized using isoflurane gas in oxygen (induction 2.5%, maintenance 1.5%) flowing at 2 L/min prior and during the injection of the compounds. The mice were injected via the tail vein with 10 – 55 MBq *fac*-[(Tyr-PEG-DAP)-$^{99m}Tc(CO)_3$] in 200 µl physiological saline solution. After each study, the mice were killed by intraperitoneal injection of pentobarbital. Blood was collected immediately after sacrifice by cardiac puncture and the other organs/tissues were harvested, weighted and counted in an automated gamma counter (Perkin Elmer Wallac Wizard 1480 automatic gamma). The data are expressed as mean percentage injected dose per gram (%ID/g) ± standard error of the mean.

3.6.5 MicroSPECT Imaging

Single photon emission computed tomography images were obtained on a U-SPECT-II scanner (MILabs, Netherlands) equipped with three γ-detectors. MicroSPECT studies were performed right after i.v. of *fac*-[(Tyr-PEG-DAP)-$^{99m}Tc(CO)_3$] and the mice were kept

anesthetized with 1% isoflurane gas in oxygen flowing at 0.25 L/min. The length of the scan for the tumor mice was set to 20 min in order to obtain three sets of data, corresponding to 0 – 20, 20 – 40 and 40 – 60 min p.i. of the tracer. The length of the scan for the healthy mice was set to 15 min in order to obtain three sets of data, corresponding to 0 – 15, 15 – 30, 30 – 45 and 45 – 60 min p.i. of the tracer. The SPECT data were acquired and reconstructed with the software that is provided with the U-SPECT-II scanner (MILabs). Image analysis was performed with PMOD software (version 2.9, PMOD Inc.).

3.6.6 Metabolite Analysis

Blood samples were withdrawn and immediately transferred into heparinized centrifugation tubes. After centrifugation for 5 min at 2000g, the separated plasma was directly injected into analytical HPLC. Urine samples were injected directly after isolation without any additional preparation.

3.7 Synthetic Part of the Section 2.5

Labeling of Ligand 51 with $[^{99m}Tc(OH_2)_3(CO)_3]^+$ (58)

Method A) $[^{99m}Tc(OH_2)_3(CO)_3]^+$ (0.5 ml, pH=7-8) was added to ligand **51** (0.5 ml, $1.0 \cdot 10^{-3}$ M in water). The mixture was stirred for 30 min at 60 °C. HPLC (TFA / methanol, C18rp, γ-detection): 18.5 min and 53% yield.

Method B) An aqueous solution of $[^{99m}Tc(OH_2)_3(CO)_3]^+$ (0.5ml, pH=7-8) was added to a ligand **51** solution (0.5 ml, $1.0 \cdot 10^{-3}$ M in water) and the mixture was stirred for 4 min at 110 °C under microwave irradiation. HPLC (TFA / methanol, C18rp, γ-detection): 18.5 min and 85% yield.

The product **58** was extracted from excess ligand **51** using a C18-SepPak cartridge (activated with 1.0 ml ethanol). The loaded cartridge was rinsed with water (1.0 ml), flushed with air (1.0 ml) and eluted with methanol (1.0 ml).

Synthesis of the *fac*-$[Re(CO)_3]^+$ Complex with Ligand 51 (59)

To the precursor $[ReBr(CO)_5]$ (162 mg, 0.21 mmol) water (2.0 ml) was added and the mixture was stirred at 180 °C for 20 min under microwave irradiation to obtain *fac*-$[Re(OH_2)_3(CO)_3]Br$. The completion of the reaction was checked with HPLC (TFA / methanol, C18rp, retention time 5.6 min). To the *fac*-$[Re(OH_2)_3(CO)_3]^+$-solution (pH adjusted to 8 with 1 M NaOH) compound **51** (TFA salt, 73 mg, 0.21 mmol) was added and the mixture was stirred at 60 °C for 4 h. After evaporation of the solvent the residue was purified by preparative HPLC. The *fac*-$[Re(CO)_3]^+$ complex **59** was obtained as a colorless powder. Yield: 63 mg (58%). ^1H NMR (500 MHz, MeOD) δ 5.17 (d, 1H, *J*=11.0 Hz) 4.79 – 4.81 (m, 1H), 4.69 (d, 1H, *J*=11.0 Hz), 4.58 (q, 1H, *J*=11.0 Hz), 3.60 – 3.80 (m, 8Hz), 3.06 (t, 2H, *J*=6.9 Hz), 2.76 – 2.83 (m, 2H), 2.04 (t, 2H, *J*=5.7 Hz). ^{13}C NMR (125 MHz, MeOD) δ 198.09, 197.19, 196.91, 181.31, 74.15, 71.28, 71.00, 67.90, 66.63, 46.24, 35.04, 31.42. ESI-MS (MeOH): m/z = 670 $[M+H]^+$, m/z = 692 $[M+Na]^+$. IR (KBr): ν_{CO} = 2027 (s), 1908 (s). HPLC (TFA / MeOH, C18rp): 18.0 min. Preparative HPLC (TFA / MeOH, C18rp): 51.3 min.

Pyridyl Disulfide ^{99m}Tc Complex (60)

Method A) Compound **58** in methanol (1.0 ml) was added to a DTDP solution (0.5 ml, $5 \cdot 10^{-3}$ M in methanol). The mixture was stirred at 60 °C for 30 min. HPLC (TFA / MeOH, C18rp, γ-detection): 20.8 min and 88% yield.

Method B) Compound **58** in methanol (1.0 ml) was added to a DTDP solution (0.5 ml, $5 \cdot 10^{-3}$ M in methanol) and the mixture was stirred at 90 °C for 4 min under microwave irradiation. HPLC (TFA / MeOH, C18rp, γ-detection): 20.8 min and 85% yield.

(2,3,4,6-Tetra-O-acetyl-β-D-glucopyranosyl)-1-isothiouronium bromide[187]

2,3,4,6-Tetra-O-acetyl-α-D-glucopyranosyl bromide (2.2 g, 5.35 mmol) and thiourea (0.62 g, 8.14 mmol) were dissolved in acetone (11 ml) and heated to 70 °C. After 15 min a white solid precipitated, which was filtered, washed with acetone and the filtrated was heated to 80 °C for 15 min. Another batch of the white solid precipitated and this procedure was repeated twice. The combined white solid was dried under vacuum for 4 h. Yield: 1.37 g (52%). ^{1}H NMR (400 MHz, DMSO, ppm) δ 9.21 (s, 2H), 9.09 (s, 2H), 5.67 (d, 1H, *J*=9.8 Hz), 5.31 (t, 1H, *J*=9.4 Hz), 5.11 (t, 2H, *J*=9.4 Hz), 4.15 – 4.23 (m, 2H), 4.07 – 4.10 (m, 1H), 2.05 (s, 3H), 2.02 (s, 3H), 2.00 (s, 3H), 1.97 (s, 3H). ESI-MS (MeOH): m/z = 407 $[M\text{-}Br]^+$.

1-Thio-2,3,4,6-tetra-O-acetyl-β-D-glucopyranose[187]

(2,3,4,6-Tetra-O-acetyl-β-D-glucopyranosyl)-1-isothiouronium bromide (1.37 g, 2.80 mmol) and sodium pyrosulfite (0.75 g, 3.95 mmol) were added to a mixture of dichloromethane (23 ml) and water (11 ml). The mixture was heated to 60 °C for 90 min. After cooling to room temperature, the product was extracted with dichloromethane (3 x 80 ml) and dried over magnesium sulfate. The solvent was removed under reduced pressure and the product as a white solid was dried under vaccum for 3 h. Yield: 1.03 g (99%). ^{1}H NMR (400 MHz, $CDCl_3$, ppm) δ 5.18 (t, 1H, *J*=9.4 Hz), 5.09 (t, 1H, *J*=9.8 Hz), 4.96 (t, 1H, *J*=9.4 Hz), 4.54 (t, 1H, *J*=9.8), 4.22 – 4.26 (m, 2H), 4.10 – 4.26 (m, 1H), 3.69 – 3.74 (m, 1H), 2.30 (d, 1H, *J*=10.2 Hz), 2.09 (s, 3H), 2.07 (s, 3H), 2.01 (s, 3H), 2.00 (s, 3H). ESI-MS (MeOH): m/z = 387 $[M+Na]^+$.

1-Thio -β-D-glucopyranosyl-2-thiopyridine disulfide (61 and 62)[188]

1-Thio-2,3,4,6-tetra-O-acetyl-β-D-glucopyranose (0.25 g, 0.70 mmol) was added to a sodium methoxide solution (30% in methanol, 0.76 ml), diluted with methanol (10 ml). The mixture was stirred at room temperature for 45 min and then neutralized with glacial acetic acid (0.25 ml). Thioglucose was either isolated at this stage by evaporation of the solvent after neutralization or directly used for the activation reaction. A solution of 2,2'-dithiopyridine (0.40 g, 1.82 mmol) in methanol (5 ml) was prepared and 2.5 ml of the thiopyranose was added dropwise. The solution was stirred at room temperature for 4 h. The solvent was

removed under reduced pressure and the resulting crude was purified by silica gel column chromatography (9:1 ethyl acetate / methanol) to give the product as a white solid. Yield: 0.13 g (62%). ^{1}H NMR (400 MHz, D_2O, ppm) δ 8.44 – 8.46 (m, 1H), 7.84 – 7.92 (m, 2H), 7.35 – 7.38 (m, 2H), 4.65 (d, 1H, *J*=9.0 Hz), 4.17 (q, 1H, *J*=7.2 Hz), 3.82 – 3.85 (m, 1H), 3.57 – 3.67 (m, 3H), 3.48 – 3.52 (m, 1H), 3.38 – 3.43 (m, 1H), 2.11 (d, 1H, *J*=6.4 Hz), 1.28 (t, 1H, *J*=7.2). ESI-MS (MeOH): m/z = 328 $[M+Na]^+$. R_f = 0.19 (9:1 ethyl acetate / methanol).

^{99m}Tc Labeled Thioglucose (63)

Method A) Compound **60** in methanol (1.0 ml) was added to a thioglucose **61** solution (0.5 ml, $5\cdot10^{-3}$ M in water). The mixture was stirred at 60 °C for 30 min. HPLC (TFA / MeOH, C18rp, γ-detection): 16.5 min and 88% yield.

Method B) Compound **58** in methanol (1.0 ml) was added to the thioglucose derivative **62** (0.5 ml, $5\cdot10^{-3}$ M in methanol) and the mixture was stirred at 60 °C for 30 min. HPLC (TFA / MeOH, C18rp, γ-detection): 16.5 min and 85% yield.

^{99m}Tc Labeled Cysteine (64)

Compound **60** in methanol (1.0 ml) was added to a cysteine solution (0.5 ml, $5\cdot10^{-3}$ M in water). The mixture was stirred at 60 °C for 30 min. HPLC (TFA / MeOH, C18rp, γ-detection): 17.2 min and 79% yield.

^{99m}Tc Labeled Glutathione (65)

Compound **60** in methanol (1.0 ml) was added to a glutathione solution (0.5 ml, $5\cdot10^{-3}$ M in water). The mixture was stirred at 60 °C for 30 min. HPLC (TFA / MeOH, C18rp, γ-detection): 16.4 min and 72% yield.

The ^{99m}Tc Complex 58 Activated with Ellman's Reagent (66)

Compound **58** in methanol (1.0 ml) was added to a mixture of borate buffer (10 mM, pH 8.3, 0.5 ml) and DTNB solution (0.5 ml, $5\cdot10^{-3}$ M in water / methanol 1:1). The resulting mixture was stirred at 90 °C for 4 min under microwave irradiation. HPLC (TFA / MeOH, C18rp, γ-detection): 21.3 min and 85% yield.

4. References

(1) Sun, T.; Zhang, Y. S.; Pang, B.; Hyun, D. C.; Yang, M.; Xia, Y. *Angew. Chem. Int. Ed.* **2014**, *53*, 12320.
(2) Bai, C. L.; Liu, M. H. *Angew. Chem., Int. Ed.* **2013**, *52*, 2678.
(3) Barry, N. P. E.; Sadler, P. J. *ACS Nano* **2013**, *7*, 5654.
(4) Xia, Y. *Angew. Chem. Int. Ed.* **2014**, *53*, 12268.
(5) Svenson, S. *Mol. Pharmaceutics* **2013**, *10*, 848.
(6) Kim, D.; Jeong, Y. Y.; Jon, S. *ACS Nano* **2010**, *4*, 3689.
(7) Liu, Y. J.; Welch, M. J. *Bioconjugate Chem.* **2012**, *23*, 671.
(8) Marchesan, S.; Prato, M. *ACS Med. Chem. Lett.* **2013**, *4*, 147.
(9) Heister, E.; Brunner, E. W.; Dieckmann, G. R.; Jurewicz, I.; Dalton, A. B. *ACS Appl. Mater. Interfaces* **2013**, *5*, 1870.
(10) Tassa, C.; Shaw, S. Y.; Weissleder, R. *Acc. Chem. Res.* **2011**, *44*, 842.
(11) Luk, B. T.; Zhang, L. *ACS Appl. Mater. Interfaces* **2014**.
(12) Duncan, R.; Richardson, S. C. W. *Mol. Pharmaceutics* **2012**, *9*, 2380.
(13) Wang, H.; Wu, Y.; Zhao, R. F.; Nie, G. J. *Adv. Mater.* **2013**, *25*, 1616.
(14) Zhu, M. T.; Nie, G. J.; Xia, T.; Nel, A.; Zhao, Y. L. *Acc. Chem. Res.* **2013**, *46*, 622.
(15) Erathodiyil, N.; Ying, J. Y. *Acc. Chem. Res.* **2011**, *44*, 925.
(16) Palui, G.; Aldeek, F.; Wang, W.; Mattoussi, H. *Chem. Soc. Rev.* **2015**, *44*, 193.
(17) Susumu, K.; Uyeda, H. T.; Medintz, I. L.; Pons, T.; Delehanty, J. B.; Mattoussi, H. *J. Am. Chem. Soc.* **2007**, *129*, 13987.
(18) Tournebize, J.; Boudier, A.; Sapin-Minet, A.; Maincent, P.; Leroy, P.; Schneider, R. *ACS Appl. Mater. Interfaces* **2012**, *4*, 5790.
(19) Takeuchi, H.; Omogo, B.; Heyes, C. D. *Nano Lett.* **2013**, *13*, 4746.
(20) Zylstra, J.; Amey, J.; Miska, N. J.; Pang, L. S.; Hine, C. R.; Langer, J.; Doyle, R. P.; Maye, M. M. *Langmuir* **2011**, *27*, 4371.
(21) Zayed, G. M. S.; Tessmar, J. K. V. *Macromol. Biosci.* **2012**, *12*, 1124.
(22) Reddy, L. H.; Arias, J. L.; Nicolas, J.; Couvreur, P. *Chem. Rev.* **2012**, *112*, 5818.
(23) Liu, X.; Li, H.; Jin, Q.; Ji, J. *Small* **2014**, *10*, 4230.
(24) Garcia, K. P.; Zarschler, K.; Barbaro, L.; Barreto, J. A.; O'Malley, W.; Spiccia, L.; Stephan, H.; Graham, B. *Small* **2014**, *10*, 2516.
(25) Zeng, J. F.; Jing, L. H.; Hou, Y.; Jiao, M. X.; Qiao, R. R.; Jia, Q. J.; Liu, C. Y.; Fang, F.; Lei, H.; Gao, M. Y. *Adv. Mater.* **2014**, *26*, 2694.
(26) Wei, H.; Insin, N.; Lee, J.; Han, H. S.; Cordero, J. M.; Liu, W. H.; Bawendi, M. G. *Nano Lett.* **2012**, *12*, 22.
(27) Wang, W. T.; Ji, X.; Bin Na, H.; Safi, M.; Smith, A.; Palui, G.; Perez, J. M.; Mattoussi, H. *Langmuir* **2014**, *30*, 6197.
(28) Cho, S. J.; Jarrett, B. R.; Louie, A. Y.; Kauzlarich, S. M. *Nanotechnology* **2006**, *17*, 640.
(29) Chanda, N.; Kattumuri, V.; Shukla, R.; Zambre, A.; Katti, K.; Upendran, A.; Kulkarni, R. R.; Fent, G. M.; Casteel, S. W.; Smith, C. J.; Boote, E.; Robertson, J. D.; Cutler, C.; Lever, J. R.; Katti, K. V.; Kannan, R. *Proc. Natl. Acad. Sci. U. S. A.* **2010**, *107*, 8760.
(30) Jokerst, J. V.; Gambhir, S. S. *Acc. Chem. Res.* **2011**, *44*, 1050.
(31) Lee, D. E.; Koo, H.; Sun, I. C.; Kim, K.; Kwon, I. C. *Chem. Soc. Rev.* **2012**, *41*, 2656.
(32) Mieszawska, A. J.; Mulder, W. J. M.; Fayad, Z. A.; Cormode, D. P. *Mol. Pharmaceutics* **2013**, *10*, 831.
(33) Chen, F.; Hong, H.; Zhang, Y.; Valdovinos, H. F.; Shi, S. X.; Kwon, G. S.; Theuer, C. P.; Barnhart, T. E.; Cai, W. B. *ACS Nano* **2013**, *7*, 9027.

(34) Smith, N. B.; Webb, A. *Introduction to Medical Imaging*; 1st ed.; Cambridge University Press: New York, **2011**.
(35) Signore, A.; Mather, S. J.; Piaggio, G.; Malviya, G.; Dierckx, R. A. *Chem. Rev.* **2010**, *110*, 3112.
(36) Huang, W. Y.; Davis, J. J. *Dalton Trans.* **2011**, *40*, 6087.
(37) Jurisson, S. S.; Lydon, J. D. *Chem. Rev.* **1999**, *99*, 2205.
(38) Cutler, C. S.; Schwarz, S. W. *J. Nucl. Med.* **2014**, *55*, 1208.
(39) Pillai, M. R. A.; Dash, A.; Knapp, F. F. *J. Nucl. Med.* **2013**, *54*, 313.
(40) Peng, C. L.; Shih, Y. H.; Lee, P. C.; Hsieh, T. M. H.; Luo, T. Y.; Shieh, M. J. *ACS Nano* **2011**, *5*, 5594.
(41) Lammers, T.; Aime, S.; Hennink, W. E.; Storm, G.; Kiessling, F. *Acc. Chem. Res.* **2011**, *44*, 1029.
(42) Larson, S. M.; Nelp, W. B. *J. Nucl. Med.* **1966**, *7*, 817.
(43) Thorek, D. L. J.; Ulmert, D.; Diop, N. F. M.; Lupu, M. E.; Doran, M. G.; Huang, R. M.; Abou, D. S.; Larson, S. M.; Grimm, J. *Nat. Commun.* **2014**, *5*.
(44) Mitra, A.; Nan, A.; Papadimitriou, J. C.; Ghandehari, H.; Line, B. R. *Nucl. Med. Biol.* **2006**, *33*, 43.
(45) Schipper, M. L.; Cheng, Z.; Lee, S. W.; Bentolila, L. A.; Iyer, G.; Rao, J. H.; Chen, X. Y.; Wul, A. M.; Weiss, S.; Gambhir, S. S. *J. Nucl. Med.* **2007**, *48*, 1511.
(46) Hwang, D. W.; Ko, H. Y.; Kim, S. K.; Lee, D. S.; Kim, S. *Chem. Eur. J.* **2009**, *15*, 9387.
(47) Maldonado, C. R.; Gomez-Blanco, N.; Jauregui-Osoro, M.; Brunton, V. G.; Yate, L.; Mareque-Rivas, J. C. *Chem. Commun.* **2013**, *49*, 3985.
(48) Wang, Y. C.; Liu, Y. J.; Luehmann, H.; Xia, X. H.; Brown, P.; Jarreau, C.; Welch, M.; Xia, Y. N. *ACS Nano* **2012**, *6*, 5880.
(49) Frigell, J.; Garcia, I.; Gomez-Vallejo, V.; Llop, J.; Penades, S. *J. Am. Chem. Soc.* **2014**, *136*, 449.
(50) Sandiford, L.; Phinikaridou, A.; Protti, A.; Meszaros, L. K.; Cui, X. J.; Yan, Y.; Frodsham, G.; Williamson, P. A.; Gaddum, N.; Botnar, R. M.; Blower, P. J.; Green, M. A.; de Rosales, R. T. M. *ACS Nano* **2013**, *7*, 500.
(51) de Rosales, R. T. M.; Tavare, R.; Paul, R. L.; Jauregui-Osoro, M.; Protti, A.; Glaria, A.; Varma, G.; Szanda, I.; Blower, P. J. *Angew. Chem. Int. Ed.* **2011**, *50*, 5509.
(52) de Rosales, R. T. M.; Tavare, R.; Glaria, A.; Varma, G.; Protti, A.; Blower, P. J. *Bioconjugate Chem.* **2011**, *22*, 455.
(53) Morales-Avila, E.; Ferro-Flores, G.; Ocampo-Garcia, B. E.; De Leon-Rodriguez, L. M.; Santos-Cuevas, C. L.; Garcia-Becerra, R.; Medina, L. A.; Gomez-Olivan, L. *Bioconjugate Chem.* **2011**, *22*, 913.
(54) Choi, H. S.; Liu, W.; Misra, P.; Tanaka, E.; Zimmer, J. P.; Ipe, B. I.; Bawendi, M. G.; Frangioni, J. V. *Nat. Biotechnol.* **2007**, *25*, 1165.
(55) Choi, H. S.; Ipe, B. I.; Misra, P.; Lee, J. H.; Bawendi, M. G.; Frangioni, J. V. *Nano Lett.* **2009**, *9*, 2354.
(56) Xie, J.; Chen, K.; Huang, J.; Lee, S.; Wang, J. H.; Gao, J.; Li, X. G.; Chen, X. Y. *Biomaterials* **2010**, *31*, 3016.
(57) Zeng, J. F.; Jia, B.; Qiao, R. R.; Wang, C.; Jing, L. H.; Wang, F.; Gao, M. Y. *Chem. Commun.* **2014**, *50*, 2170.
(58) Zhao, Y. F.; Sultan, D.; Detering, L.; Cho, S. H.; Sun, G. R.; Pierce, R.; Wooley, K. L.; Liu, Y. J. *Angew. Chem. Int. Ed.* **2014**, *53*, 156.
(59) Goel, S.; Chen, F.; Ehlerding, E. B.; Cai, W. *Small* **2014**, *10*, 3825.

(60) Zhou, C.; Hao, G. Y.; Thomas, P.; Liu, J. B.; Yu, M. X.; Sun, S. S.; Oz, O. K.; Sun, X. K.; Zheng, J. *Angew. Chem. Int. Ed.* **2012**, *51*, 10118.
(61) Wang, Y. C.; Liu, Y. J.; Luehmann, H.; Xia, X. H.; Wan, D. H.; Cutler, C.; Xia, Y. N. *Nano Lett.* **2013**, *13*, 581.
(62) Blanco, N. G.; Jauregui-Osoro, M.; Cobaleda-Siles, M.; Maldonado, C. R.; Henriksen-Lacey, M.; Padro, D.; Clark, S.; Mareque-Rivas, J. C. *Chem. Commun.* **2012**, *48*, 4211.
(63) Cobaleda-Siles, M.; Henriksen-Lacey, M.; de Angulo, A. R.; Bernecker, A.; Vallejo, V. G.; Szczupak, B.; Llop, J.; Pastor, G.; Plaza-Garcia, S.; Jauregui-Osoro, M.; Meszaros, L. K.; Mareque-Rivas, J. C. *Small* **2014**, *10*, 5054.
(64) Chen, F.; Ellison, P. A.; Lewis, C. M.; Hong, H.; Zhang, Y.; Shi, S. X.; Hernandez, R.; Meyerand, M. E.; Barnhart, T. E.; Cai, W. B. *Angew. Chem. Int. Ed.* **2013**, *52*, 13319.
(65) Chakravarty, R.; Valdovinos, H. F.; Chen, F.; Lewis, C. M.; Ellison, P. A.; Luo, H.; Meyerand, M. E.; Nickles, R. J.; Cai, W. *Adv. Mater.* **2014**, *26*, 5119.
(66) Boros, E.; Bowen, A. M.; Josephson, L.; Vasdev, N.; Holland, J. P. *Chem. Sci.* **2015**, *6*, 225.
(67) Liu, J. B.; Yu, M. X.; Zhou, C.; Yang, S. Y.; Ning, X. H.; Zheng, J. *J. Am. Chem. Soc.* **2013**, *135*, 4978.
(68) Sun, X. L.; Huang, X. L.; Guo, J. X.; Zhu, W. L.; Ding, Y.; Niu, G.; Wang, A.; Kiesewetter, D. O.; Wang, Z. L.; Sun, S. H.; Chen, X. Y. *J. Am. Chem. Soc.* **2014**, *136*, 1706.
(69) Liu, H.; Zhang, X.; Xing, B.; Han, P.; Gambhir, S. S.; Cheng, Z. *Small* **2010**, *6*, 1087.
(70) Perez-Campana, C.; Gomez-Vallejo, V.; Puigivila, M.; Martin, A.; Calvo-Fernandez, T.; Moya, S. E.; Ziolo, R. F.; Reese, T.; Llop, J. *ACS Nano* **2013**, *7*, 3498.
(71) Cho, E. C.; Zhang, Q.; Xia, Y. N. *Nat. Nanotechnol.* **2011**, *6*, 385.
(72) Alric, C.; Miladi, I.; Kryza, D.; Taleb, J.; Lux, F.; Bazzi, R.; Billotey, C.; Janier, M.; Perriat, P.; Roux, S.; Tillement, O. *Nanoscale* **2013**, *5*, 5930.
(73) Longmire, M.; Choyke, P. L.; Kobayashi, H. *Nanomedicine* **2008**, *3*, 703.
(74) Wang, B.; He, X.; Zhang, Z. Y.; Zhao, Y. L.; Feng, W. Y. *Acc. Chem. Res.* **2013**, *46*, 761.
(75) Sharifi, S.; Behzadi, S.; Laurent, S.; Forrest, M. L.; Stroeve, P.; Mahmoudi, M. *Chem. Soc. Rev.* **2012**, *41*, 2323.
(76) Inai, T.; Mancuso, M.; Hashizume, H.; Baffert, F.; Haskell, A.; Baluk, P.; Hu-Lowe, D. D.; Shalinsky, D. R.; Thurston, G.; Yancopoulos, G. D.; McDonald, D. M. *Am. J. Pathol.* **2004**, *165*, 35.
(77) Alkilany, A. M.; Lohse, S. E.; Murphy, C. J. *Acc. Chem. Res.* **2013**, *46*, 650.
(78) Couvreur, P. *Adv. Drug Delivery Rev.* **2013**, *65*, 21.
(79) Ferrari, M. *Nat. Rev. Cancer* **2005**, *5*, 161.
(80) Herd, H.; Daum, N.; Jones, A. T.; Huwer, H.; Ghandehari, H.; Lehr, C. M. *ACS Nano* **2013**, *7*, 1961.
(81) Albanese, A.; Tang, P. S.; Chan, W. C. W. *Annu. Rev. Biomed. Eng.* **2012**, *14*, 1.
(82) Alexis, F.; Pridgen, E.; Molnar, L. K.; Farokhzad, O. C. *Mol. Pharmaceutics* **2008**, *5*, 505.
(83) Chouly, C.; Pouliquen, D.; Lucet, I.; Jeune, J. J.; Jallet, P. *J. Microencapsulation* **1996**, *13*, 245.
(84) Howes, P. D.; Chandrawati, R.; Stevens, M. M. *Science* **2014**, *346*, 53.
(85) Longmire, M. R.; Ogawa, M.; Choyke, P. L.; Kobayashi, H. *Bioconjugate Chem.* **2011**, *22*, 993.
(86) Li, W. Q.; Wang, F.; Liu, Z. M.; Wang, Y. C.; Wang, J.; Sun, F. *Small* **2013**, *9*, 1708.
(87) Hamad, I.; Al-Hanbali, O.; Hunter, A. C.; Rutt, K. J.; Andresen, T. L.; Moghimi, S. M. *ACS Nano* **2010**, *4*, 6629.

(88) Moyano, D. F.; Saha, K.; Prakash, G.; Yan, B.; Kong, H.; Yazdani, M.; Rotello, V. M. *ACS Nano* **2014**, *8*, 6748.
(89) Tonga, G. Y.; Saha, K.; Rotello, V. M. *Adv. Mater.* **2014**, *26*, 359.
(90) Han, H. S.; Martin, J. D.; Lee, J.; Harris, D. K.; Fukumura, D.; Jain, R. K.; Bawendi, M. *Angew. Chem. Int. Ed.* **2013**, *52*, 1414.
(91) Liu, J. B.; Yu, M. X.; Ning, X. H.; Zhou, C.; Yang, S. Y.; Zheng, J. *Angew. Chem. Int. Ed.* **2013**, *52*, 12572.
(92) Rivera-Gil, P.; De Aberasturi, D. J.; Wulf, V.; Pelaz, B.; Del Pino, P.; Zhao, Y. Y.; De La Fuente, J. M.; De Larramendi, I. R.; Rojo, T.; Liang, X. J.; Parak, W. J. *Acc. Chem. Res.* **2013**, *46*, 743.
(93) Liu, G.; Gao, J. H.; Ai, H.; Chen, X. Y. *Small* **2013**, *9*, 1533.
(94) Stark, W. J. *Angew. Chem. Int. Ed.* **2011**, *50*, 1242.
(95) Lu, X. F.; Liu, Y.; Kong, X. J.; Lobie, P. E.; Chen, C. Y.; Zhu, T. *Small* **2013**, *9*, 1654.
(96) Misra, P.; Humblet, V.; Pannier, N.; Maison, W.; Frangioni, J. V. *J. Nucl. Med.* **2007**, *48*, 1379.
(97) Liu, Y.; Oliveira, B. L.; Correia, J. D. G.; Santos, I. C.; Santos, I.; Spingler, B.; Alberto, R. *Org. Biomol. Chem.* **2010**, *8*, 2829.
(98) Shen, Y. J.; Schottelius, M.; Zelenka, K.; De Simone, M.; Pohle, K.; Kessler, H.; Wester, H. J.; Schmutz, P.; Alberto, R. *Bioconjugate Chem.* **2013**, *24*, 26.
(99) Yu, G.; Wang, S. Z.; Wang, K.; Hu, Y. F.; Hu, H. W. *Synthesis* **2004**, 1021.
(100) Demeester, J. W. G.; Vanderplas, H. C.; Middelhoven, W. J. *J. Heterocycl. Chem.* **1987**, *24*, 441.
(101) Balskus, E. P.; Jacobsen, E. N. *J. Am. Chem. Soc.* **2006**, *128*, 6810.
(102) Schollkopf, U.; Lonsky, R. *Synthesis* **1983**, 675.
(103) Caddick, S.; Judd, D. B.; Lewis, A. K. D.; Reich, M. T.; Williams, M. R. V. *Tetrahedron* **2003**, *59*, 5417.
(104) Greene, T. W.; Wuts, P. G. M. *Protective Groups in Organic Synthesis, Third Edition*; John Wiley & Sons, Inc.: New York, **1999**.
(105) Koide, T.; Otaka, A.; Suzuki, H.; Fujii, N. *Synlett* **1991**, 345.
(106) Jiang, Z. X.; Yu, Y. B. *Synthesis* **2008**, 215.
(107) Koval, I. V. *Russian Chem. Rev.* **1994**, *63*, 776.
(108) Rai, S. K.; Sharma, M.; Tiwari, M. *Bioorg. Med. Chem.* **2008**, *16*, 7301.
(109) Law, W. C.; Yong, K. T.; Roy, I.; Ding, H.; Hu, R.; Zhao, W. W.; Prasad, P. N. *Small* **2009**, *5*, 1302.
(110) Palui, G.; Avellini, T.; Zhan, N. Q.; Pan, F.; Gray, D.; Alabugin, I.; Mattoussi, H. *J. Am. Chem. Soc.* **2012**, *134*, 16370.
(111) Chaudhuri, R. G.; Paria, S. *Chem. Rev.* **2012**, *112*, 2373.
(112) Cai, W. B.; Chen, K.; Li, Z. B.; Gambhir, S. S.; Chen, X. Y. *J. Nucl. Med.* **2007**, *48*, 1862.
(113) Lu, W.; Zhang, G. D.; Zhang, R.; Flores, L. G.; Huang, Q.; Gelovani, J. G.; Li, C. *Cancer Res.* **2010**, *70*, 3177.
(114) Li, S. H.; Goins, B.; Zhang, L. J.; Bao, A. D. *Bioconjugate Chem.* **2012**, *23*, 1322.
(115) Ocampo-Garcia, B. E.; Ramirez, F. D.; Ferro-Flores, G.; De Leon-Rodriguez, L. M.; Santos-Cuevas, C. L.; Morales-Avila, E.; de Murphy, C. A.; Pedraza-Lopez, M.; Medina, L. A.; Camacho-Lopez, M. A. *Nucl. Med. Biol.* **2011**, *38*, 1.
(116) Baughman, T. W.; Sworen, J. C.; Wagener, K. B. *Tetrahedron* **2004**, *60*, 10943.
(117) Schulke, N.; Varlamova, O. A.; Donovan, G. P.; Ma, D. S.; Gardner, J. P.; Morrissey, D. M.; Arrigale, R. R.; Zhan, C. C.; Chodera, A. J.; Surowitz, K. G.; Maddon, P. J.; Heston, W. D. W.; Olson, W. C. *Proc. Natl. Acad. Sci. U. S. A.* **2003**, *100*, 12590.

(118) Hillier, S. M.; Maresca, K. P.; Lu, G.; Merkin, R. D.; Marquis, J. C.; Zimmerman, C. N.; Eckelman, W. C.; Joyal, J. L.; Babich, J. W. *J. Nucl. Med.* **2013**, *54*, 1369.
(119) Hrkach, J.; Von Hoff, D.; Ali, M. M.; Andrianova, E.; Auer, J.; Campbell, T.; De Witt, D.; Figa, M.; Figueiredo, M.; Horhota, A.; Low, S.; McDonnell, K.; Peeke, E.; Retnarajan, B.; Sabnis, A.; Schnipper, E.; Song, Y. H.; Summa, J.; Tompsett, D.; Troiano, G.; Hoven, T. V.; Wright, J.; LoRusso, P.; Kantoff, P. W.; Bander, N. H.; Sweeney, C.; Farokhzad, O. C.; Langer, R.; Zale, S. *Sci. Transl. Med.* **2012**, *4*.
(120) Barinka, C.; Rovenska, M.; Mlcochova, P.; Hlouchova, K.; Plechanovova, A.; Majer, P.; Tsukamoto, T.; Slusher, B. S.; Konvalinka, J.; Lubkowski, J. *J. Med. Chem.* **2007**, *50*, 3267.
(121) Banerjee, S. R.; Pullambhatla, M.; Byun, Y.; Nimmagadda, S.; Foss, C. A.; Green, G.; Fox, J. J.; Lupold, S. E.; Mease, R. C.; Pomper, M. G. *Angew. Chem. Int. Ed.* **2011**, *50*, 9167.
(122) Hiramatsu, H.; Osterloh, F. E. *Chem. Mater.* **2004**, *16*, 2509.
(123) Clapp, A. R.; Goldman, E. R.; Mattoussi, H. *Nat. Protoc.* **2006**, *1*, 1258.
(124) Alberto, R.; Ortner, K.; Wheatley, N.; Schibli, R.; Schubiger, A. P. *J. Am. Chem. Soc.* **2001**, *123*, 3135.
(125) Jadzinsky, P. D.; Calero, G.; Ackerson, C. J.; Bushnell, D. A.; Kornberg, R. D. *Science* **2007**, *318*, 430.
(126) Gravel, E.; Tanguy, C.; Cassette, E.; Pons, T.; Knittel, F.; Bernards, N.; Garofalakis, A.; Duconge, F.; Dubertret, B.; Doris, E. *Chem. Sci.* **2013**, *4*, 411.
(127) Zhan, N.; Palui, G.; Safi, M.; Ji, X.; Mattoussi, H. *J. Am. Chem. Soc.* **2013**, *135*, 13786.
(128) Ojea-Jimenez, I.; Garcia-Fernandez, L.; Lorenzo, J.; Puntes, V. F. *ACS Nano* **2012**, *6*, 7692.
(129) Oh, N.; Park, J.-H. *ACS Nano* **2014**, *8*, 6232.
(130) Qiu, Y.; Liu, Y.; Wang, L. M.; Xu, L. G.; Bai, R.; Ji, Y. L.; Wu, X. C.; Zhao, Y. L.; Li, Y. F.; Chen, C. Y. *Biomaterials* **2010**, *31*, 7606.
(131) Saha, K.; Kim, S. T.; Yan, B.; Miranda, O. R.; Alfonso, F. S.; Shlosman, D.; Rotello, V. M. *Small* **2013**, *9*, 300.
(132) Bolander, M. E.; Young, M. F.; Fisher, L. W.; Yamada, Y.; Termine, J. D. *Proc. Natl. Acad. Sci. U. S. A.* **1988**, *85*, 2919.
(133) Zhang, Z. Y.; Ross, R. D.; Roeder, R. K. *Nanoscale* **2010**, *2*, 582.
(134) Jessica, C. *Master Thesis, University of Zurich* **2013**.
(135) Hoskins, C.; Min, Y.; Gueorguieva, M.; McDougall, C.; Volovick, A.; Prentice, P.; Wang, Z. G.; Melzer, A.; Cuschieri, A.; Wang, L. J. *J. Nanobiotechnol.* **2012**, *10*.
(136) Wang, X. D.; Liu, H. Y.; Chen, D.; Meng, X. W.; Liu, T. L.; Fu, C. H.; Hao, N. J.; Zhang, Y. Q.; Wu, X. L.; Ren, J.; Tang, F. Q. *ACS Appl. Mater. Interfaces* **2013**, *5*, 4966.
(137) Patel, D.; Kell, A.; Simard, B.; Xiang, B.; Lin, H. Y.; Tian, G. H. *Biomaterials* **2011**, *32*, 1167.
(138) Aldeek, F.; Muhammed, M. A. H.; Palui, G.; Zhan, N. Q.; Mattoussi, H. *ACS Nano* **2013**, *7*, 2509.
(139) Cubberley, M. S.; Iverson, B. L. *J. Am. Chem. Soc.* **2001**, *123*, 7560.
(140) Schmidt, F.; Rosnizeck, I. C.; Spoerner, M.; Kalbitzer, H. R.; Konig, B. *Inorg. Chim. Acta* **2011**, *365*, 38.
(141) Favre, A.; Grugier, J.; Brans, A.; Joris, B.; Marchand-Brynaert, J. *Tetrahedron* **2012**, *68*, 10818.
(142) Levadala, M. K.; Banerjee, S. R.; Maresca, K. P.; Babich, J. W.; Zubieta, J. *Synthesis* **2004**, 1759.

(143) Zhan, N. Q.; Palui, G.; Grise, H.; Tang, H. L.; Alabugin, I.; Mattoussi, H. *ACS Appl. Mater. Interfaces* **2013**, *5*, 2861.
(144) Amstad, E.; Gillich, T.; Bilecka, I.; Textor, M.; Reimhult, E. *Nano Lett.* **2009**, *9*, 4042.
(145) Xu, C.; Xie, J.; Ho, D.; Wang, C.; Kohler, N.; Walsh, E. G.; Morgan, J. R.; Chin, Y. E.; Sun, S. *Angew. Chem. Int. Ed.* **2008**, *47*, 173.
(146) Lyon, J. L.; Fleming, D. A.; Stone, M. B.; Schiffer, P.; Williams, M. E. *Nano Lett.* **2004**, *4*, 719.
(147) Xu, C. J.; Wang, B. D.; Sun, S. H. *J. Am. Chem. Soc.* **2009**, *131*, 4216.
(148) Kim, D.; Kim, J. W.; Jeong, Y. Y.; Jon, S. *Bull. Korean Chem. Soc.* **2009**, *30*, 1855.
(149) Kumagai, M.; Sarma, T. K.; Cabral, H.; Kaida, S.; Sekino, M.; Herlambang, N.; Osada, K.; Kano, M. R.; Nishiyama, N.; Kataoka, K. *Macromol. Rapid Commun.* **2010**, *31*, 1521.
(150) Salado, J.; Insausti, M.; Lezama, L.; de Muro, I. G.; Moros, M.; Pelaz, B.; Grazu, V.; de la Fuente, J. M.; Rojo, T. *Nanotechnology* **2012**, *23*.
(151) Hu, Y.; Meng, L. J.; Niu, L. Y.; Lu, Q. H. *ACS Appl. Mater. Interfaces* **2013**, *5*, 4586.
(152) Wang, L. Y.; Bai, J. W.; Li, Y. J.; Huang, Y. *Angew. Chem. Int. Ed.* **2008**, *47*, 2439.
(153) Dong, W. J.; Li, Y. S.; Niu, D. C.; Ma, Z.; Gu, J. L.; Chen, Y.; Zhao, W. R.; Liu, X. H.; Liu, C. S.; Shi, J. L. *Adv. Mater.* **2011**, *23*, 5392.
(154) Li, J. C.; Zheng, L. F.; Cai, H. D.; Sun, W. J.; Shen, M. W.; Zhang, G. X.; Shi, X. Y. *ACS Appl. Mater. Interfaces* **2013**, *5*, 10357.
(155) He, X. X.; Liu, F. Y.; Liu, L.; Duan, T. C.; Zhang, H. M.; Wanq, Z. X. *Mol. Pharmaceutics* **2014**, *11*, 738.
(156) Robinson, I.; Tung, L. D.; Maenosono, S.; Walti, C.; Thanh, N. T. K. *Nanoscale* **2010**, *2*, 2624.
(157) Wang, L. Y.; Luo, J.; Fan, Q.; Suzuki, M.; Suzuki, I. S.; Engelhard, M. H.; Lin, Y. H.; Kim, N.; Wang, J. Q.; Zhong, C. J. *J. Phys. Chem. B* **2005**, *109*, 21593.
(158) Yu, H.; Chen, M.; Rice, P. M.; Wang, S. X.; White, R. L.; Sun, S. H. *Nano Lett.* **2005**, *5*, 379.
(159) Hao, R.; Yu, J.; Ge, Z. G.; Zhao, L. Y.; Sheng, F. G.; Xu, L. L.; Li, G. J.; Hou, Y. L. *Nanoscale* **2013**, *5*, 11954.
(160) Zhu, J.; Lu, Y. J.; Li, Y. G.; Jiang, J.; Cheng, L.; Liu, Z.; Guo, L.; Pan, Y.; Gu, H. W. *Nanoscale* **2014**, *6*, 199.
(161) Maresca, K. P.; Marquis, J. C.; Hillier, S. M.; Lu, G. L.; Femia, F. J.; Zimmerman, C. N.; Eckelman, W. C.; Joyal, J. L.; Babich, J. W. *Bioconjugate Chem.* **2010**, *21*, 1032.
(162) Huang, C. F.; McConathy, J. *J. Nucl. Med.* **2013**, *54*, 1007.
(163) Dunet, V.; Rossier, C.; Buck, A.; Stupp, R.; Prior, J. O. *J. Nucl. Med.* **2012**, *53*, 207.
(164) Lau, E. W. F.; Drummond, K. J.; Ware, R. E.; Drummond, E.; Hogg, A.; Ryan, G.; Grigg, A.; Callahan, J.; Hicks, R. J. *J. Clin. Neurosci.* **2010**, *17*, 43.
(165) Tsukada, H.; Sato, K.; Fukumoto, D.; Kakiuchi, T. *Eur. J. Nucl. Med. Mol. Imaging* **2006**, *33*, 1017.
(166) Wester, H. J.; Herz, M.; Weber, W.; Heiss, P.; Senekowitsch-Schmidtke, R.; Schwaiger, M.; Stocklin, G. *J. Nucl. Med.* **1999**, *40*, 205.
(167) Kong, F.-L.; Ali, M. S.; Rollo, A.; Smith, D. L.; Zhang, Y.; Yu, D.-F.; Yang, D. J. *J. Biomed. Biotechnol.* **2012**, *2012*, 671708.
(168) Schirrmacher, R.; Comagic, S.; Schirrmacher, E.; Rosch, F. *J. Labelled Compd. Radiopharm.* **2004**, *47*, 477.
(169) Arumugam, S.; Popik, V. V. *J. Am. Chem. Soc.* **2011**, *133*, 5573.

(170) Ghibellini, G.; Leslie, E. M.; Pollack, G. M.; Brouwer, K. L. R. *Pharma. Res.* **2008**, *25*, 1851.
(171) Gilbert, H. F. *Methods in Enzymology* **1995**, *251*, 8.
(172) Gongora-Benitez, M.; Tulla-Puche, J.; Albericio, F. *Chem. Rev.* **2014**, *114*, 901.
(173) Wang, C.; Wesener, S. R.; Zhang, H. L.; Cheng, Y. Q. *Chem. Biol.* **2009**, *16*, 585.
(174) Wang, Y.; Liu, D.; Zheng, Q.; Zhao, Q.; Zhang, H.; Ma, Y.; Fallon, J. K.; Fu, Q.; Haynes, M. T.; Lin, G.; Zhang, R.; Wang, D.; Yang, X.; Zhao, L.; He, Z.; Liu, F. *Nano Lett.* **2014**, *14*, 5577.
(175) Josephson, L.; Tung, C. H.; Moore, A.; Weissleder, R. *Bioconjugate Chem.* **1999**, *10*, 186.
(176) Josephson, L.; Perez, J. M.; Weissleder, R. *Angew. Chem. Int. Ed.* **2001**, *40*, 3204.
(177) Lee, J. H.; Lee, K.; Moon, S. H.; Lee, Y.; Park, T. G.; Cheon, J. *Angew. Chem. Int. Ed.* **2009**, *48*, 4174.
(178) van der Vlies, A. J.; Hasegawa, U.; Hubbell, J. A. *Mol. Pharmaceutics* **2012**, *9*, 2812.
(179) Kim, J. S.; Dai, Z. Y.; Aryal, U. K.; Moore, R. J.; Camp, D. G.; Baker, S. E.; Smith, R. D.; Qian, W. J. *Anal. Chem.* **2013**, *85*, 6826.
(180) Paulech, J.; Solis, N.; Edwards, A. V. G.; Puckeridge, M.; White, M. Y.; Cordwell, S. J. *Anal. Chem.* **2013**, *85*, 3774.
(181) Waibel, R.; Alberto, R.; Willuda, J.; Finnern, R.; Schibli, R.; Stichelberger, A.; Egli, A.; Abram, U.; Mach, J. P.; Pluckthun, A.; Schubiger, P. A. *Nat. Biotechnol.* **1999**, *17*, 897.
(182) Mundwiler, S.; Kundig, M.; Ortner, K.; Alberto, R. *Dalton Trans.* **2004**, 1320.
(183) Carroll, L.; Evans, H. L.; Aboagye, E. O.; Spivey, A. C. *Org. Biomol. Chem.* **2013**, *11*, 5772.
(184) Kasten, B. B.; Ma, X. W.; Liu, H. G.; Hayes, T. R.; Barnes, C. L.; Qi, S. B.; Cheng, K.; Bottorff, S. C.; Slocumb, W. S.; Wang, J.; Cheng, Z.; Benny, P. D. *Bioconjugate Chem.* **2014**, *25*, 579.
(185) Causey, P. W.; Besanger, T. R.; Schaffer, P.; Valliant, J. F. *Inorg. Chem.* **2008**, *47*, 8213.
(186) Banerjee, S. R.; Schaffer, P.; Babich, J. W.; Valliant, J. F.; Zubieta, J. *Dalton Trans.* **2005**, 3886.
(187) Gamblin, D. P.; Garnier, P.; van Kasteren, S.; Oldham, N. J.; Fairbanks, A. J.; Davis, B. G. *Angew. Chem. Int. Ed.* **2004**, *43*, 828.
(188) Pearson, S.; Scarano, W.; Stenzel, M. H. *Chem. Commun.* **2012**, *48*, 4695.
(189) Ellman, G. L. *Arch. Biochem. Biophys.* **1959**, *82*, 70.
(190) Babich, J. W.; Zimmerman, C. N.; Maresca, K. P. (Molecular Insight Pharmaceuticals), WO2008058192-A2; US2008193381-A1; WO2008058192-A3; TW200836765-A; IN200901787-P2; AU2007316391-A1; EP2097111-A2; CA2669127-A1; JP2010509358-W; CN101778910-A; US2012208988-A1; US2012269726-A1; US8487129-B2; AU2007316391-B2.
(191) Buchini, S.; Buschiazzo, A.; Withers, S. G. *Angew. Chem. Int. Ed.* **2008**, *47*, 2700.
(192) Andrus, M. B.; Turner, T. M.; Updegraff, E. P.; Sauna, Z. E.; Ambudkar, S. V. *Tetrahedron Lett.* **2001**, *42*, 3819.

5. Acknowledgment

Prof. Dr. Roger Alberto was a great mentor during my entire time at the University of Zurich and I am deeply grateful for that. The combination of his experience, enthusiastic attitude and creativity makes him a great supervisor. He supported me not only in scientific challenges, but also in activities which were not directly related to my PhD thesis. I cannot thank him enough for his commitment.

My permanent companion, both professionally as well as privately, is my very close friend Sebastian Imstepf. Our common path began during the "Grundlagenpraktikum" when we shared a fume hood and a wonderful friendship started to develop. I always highly appreciated his ideas, inspiration and permanent support. Thank you for everything Bro and I am excited where our journey takes us.

I am also very grateful to my collaboration partners. This includes Dr. Matthias Bauwens, Dr. Marijke De Saint-Hubert, Dr. Stefan Voo, Geert Hendrikx, Ivo Pooters, Rul Wierts and Prof. Dr. Felix M. Mottaghy from the Department of Nuclear Medicine at the Maastricht University Medical Center. The *in vivo* evaluations were always very interesting and I definitely learned a lot. It was always a pleasure to go to Maastricht because of the extremely friendly atmosphere, great infrastructure and the leisure activities. Special thanks go to Dr. José M. Mateos, Dr. Andres Käch, Dr. Urs Ziegler, Gery Barmettler, Therese Bruggmann und Ursula Lüthi from the Center for Microscopy and Image Analysis at the University of Zurich. Apart from learning how to perform TEM analysis, we also carried out fascinating *in vitro* studies.

Throughout the years as a PhD student I was regularly dependent on specialists operating various instruments. In particular, I would like to acknowledge Dr. Thomas Fox for his great help in measuring and analyzing challenging NMR spectra, Dr. Ferdinand Wild for his ICP-MS and ESI-MS measurements, as well as the team of PD Dr. Laurant Bigler for the HR-ESI-MS analyses.

It was always very pleasant and inspiring to work in the good old 34-G-40. Several persons have contributed to it, including Dr. Yunjun Shen who taught me a lot about organic synthesis and the Chinese culture, my good friend and former Master student Jessica Clavadetscher, Alois Degonda, Dr. Qaisar Nadeem and Angelo Frei. My second laboratory was in the radiochemistry section, where I had great company from Dr. Henrik Braband, Dr. Daniel Can and Michael Benz. At this point I would also like to thank all current and former Alberto group members, I always appreciated the good atmosphere, the unforgettable retreats and legendary Christmas dinners.

I would also like to thank the Graduate School of Chemical and Molecular Sciences Zurich for the very generous financial support for travelling and for the organization of the outstanding annual retreats. In this context, I would like to acknowledge Prof. Dr. Roland Sigel, Head of the Graduate School, for his efforts for the Graduate School and for being in the committee of my thesis. During the retreats we were constantly pampered with culinary delights from Bea and Andi Spichtig, thank you very much for that.

My biggest thanks go to my parents for their tireless support during my entire life and education. Without them it would never have been possible for me to study and I am extremely grateful for all you have done for me. I am also very thankful to the rest of my family, especially my brother Fabian, for all his contribution to my life.

The University of Zurich was not only a fantastic place to study, but it was also the place where I met the love of my life. Ever since we came together I am having the best time of my life and I am deeply grateful for everything Silvia. I would also like to thank your family and your friends in Brazil, whenever I am there they make me feel at home.

Finally, I want to thank all my friends in Switzerland and all over the world, you are a very important part of my life and I highly appreciate the time we had and will have together.

6. Curriculum Vitae

PERSONAL INFORMATION

Name	Michael
Surname	Felber
Date of Birth	18.07.1986
Nationality	Swiss
Place of Origin	Römerswil (LU)
Marital Status	Single

EDUCATION

University of Zurich, Switzerland

02/2011 - 02/2015
PhD in Chemistry - *"Bifunctional Ligand Systems for the Radiolabeling of Nanoparticles and Biomolecules with the fac-[^{99m}Tc(CO)$_3$]$^+$-Core"*
Advisor: Prof. Dr. Roger Alberto, Department of Chemistry

09/2009 - 08/2010
Master of Science in Chemistry - *"The Development of Model Systems for Dual Modality Imaging Agents and the Investigation of Self-Luminescence in Systems containing the fac-[^{99m}Tc(CO)$_3$]$^+$-Core"*
Advisor: Prof. Dr. Roger Alberto, Department of Chemistry

09/2006 - 01/2010
Bachelor of Science in Chemistry and Business Studies

ETH Zurich, Switzerland

09/2010 - 10/2012
Master of Advanced Studies in Medical Physics
Specialization in radiation therapy. Fundamental lectures in diverse areas such as medical imaging, biomedical engineering, bioimaging, biomechanics and biocompatible materials.

Paul Scherrer Institute, Switzerland

06/2012 - 06/2012
Radiation Protection Officer
Official certificate that is necessary to take on the responsibility in a radiolab type B and C.

High School (Gymnasium) Reussbühl, Switzerland

08/1999 - 06/2005
Matura
Major in chemistry, biology, geography and music.
Thesis in geology about the effect of global warming on the permafrost in Switzerland, exemplified on the "Schafberg".

AWARDS

2010, 2009, 2008 Award of the Alfred Werner-Legacy for good accomplishment during the master, bachelor and basic studies.

2006 Award for an outstanding Matura Thesis

PUBLICATIONS

Felber M., Alberto R., **The Thiol-Disulfide Exchange Reaction as a Platform for the ^{99m}Tc Labeling of Biomolecules Containing a Thiol Group**, *in preparation*.

Felber M., Bauwens M., Imstepf S., Fox T., Mottaghy F., Alberto R., **Conjugation of a 2,3-Diamino Propionic Acid-Based Chelator to the *Para*-OH of L-Tyrosine and Biological Evaluation of the Corresponding *fac*-[^{99m}Tc(CO)$_3$]$^+$ Complex**, *submitted*.

Felber M., Alberto R., **^{99m}Tc Radiolabeling of Fe_3O_4-Au Core-Shell and Au-Fe_3O_4 Dumbbell-Like Nanoparticles**, *Nanoscale* 2015, *7*, 6653-6660.

Felber M., Bauwens M., Mateos J. M., Imstepf S., Mottaghy F., Alberto R., **^{99m}Tc Radiolabeling and Biological Evaluation of Nanoparticles Functionalized with a Versatile Coating Ligand**, *Chemistry – A European Journal* 2015, *21*, 6090-6099.

Alberto R., Braband H., Benz M., Felber M., Imstepf S., **Organometallic Technetium Chemistry; Past, Present and Future**, *Nuclear Medicine and Biology* 2014, *41*, 613-613.

Nadeem Q., Can D., Shen Y., Felber M., Mahmood Z., Alberto R., **Synthesis of Tripeptide Derivatized Cyclopentadienyl Complexes of Technetium and Rhenium as Radiopharmaceutical Probes**, *Organic & Biomolecular Chemistry* 2014, *12*, 1966-1974.

Veron A. C., Felber M., Blacque O., Spingler B., **Conformational Flexibility of Palladium BINAP Complexes Explored by X-Ray Analyses and DFT Studies**, *Polyhedron* 2013, *52*, 102-105.

Braband H., Imstepf S., Felber M., Spingler B., Alberto R., **Triazacyclohexane (tach) Complexes of High-Valent Rhenium**, *Inorganic Chemistry* 2010, *49*, 1283-1285.

PRESENTATIONS

Oral NanoTracking 2nd Annual Meeting, Heidelberg, 2013.
2nd International Symposium on Functional Metal Complexes that Bind to Biomolecules, Barcelona, 2013.
Molecular Insight Pharmaceuticals Inc., Cambridge, USA, 2012.

Poster Swiss Chemical Society Fall Meeting, Switzerland:
ETH Lausanne 2009, ETH Zurich 2010 and University of Zurich 2014.

7. Appendix

7.1 Index of Synthesized Compounds

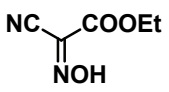

1

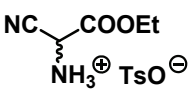

2

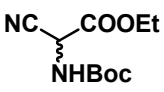

3

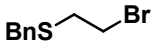

4

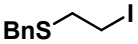

5

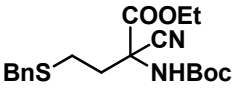

6

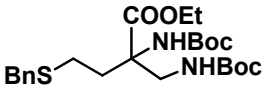

7

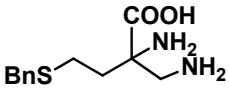

8

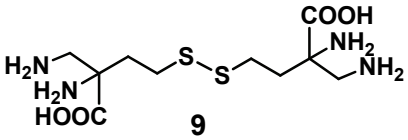

9

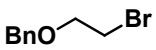

10

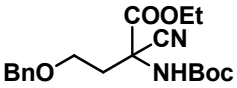

11

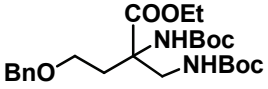

12

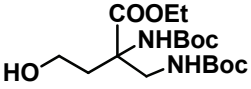

13

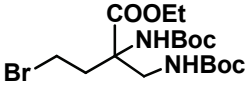

14

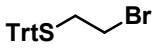

15

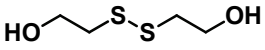

16

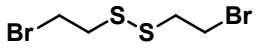

17

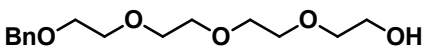

18

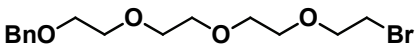

19

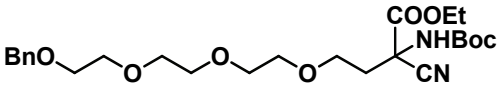

20

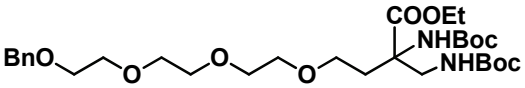

21

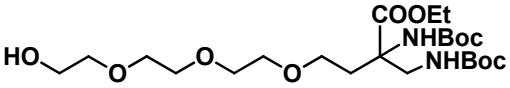

22

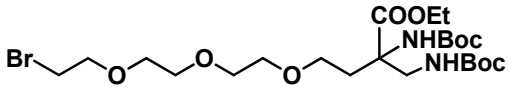

23

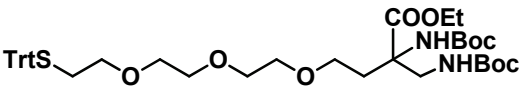

24

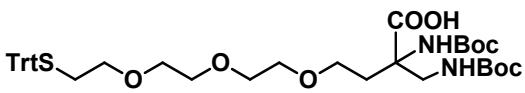

25

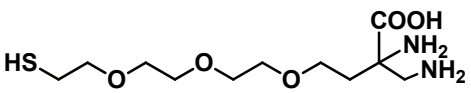

26

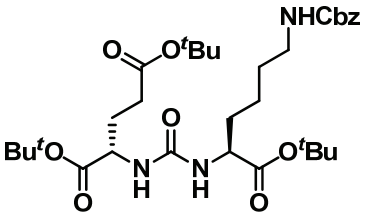

27

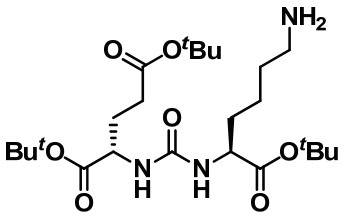

28

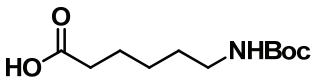

29

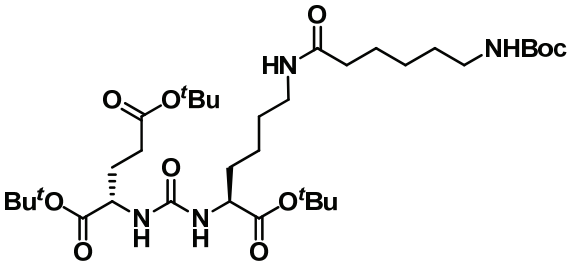

30

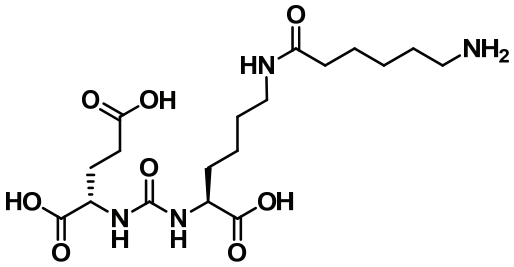

31

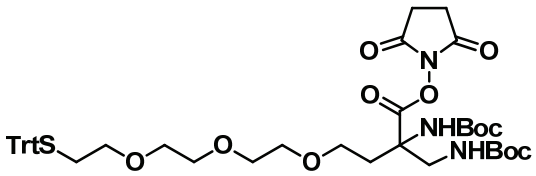

32

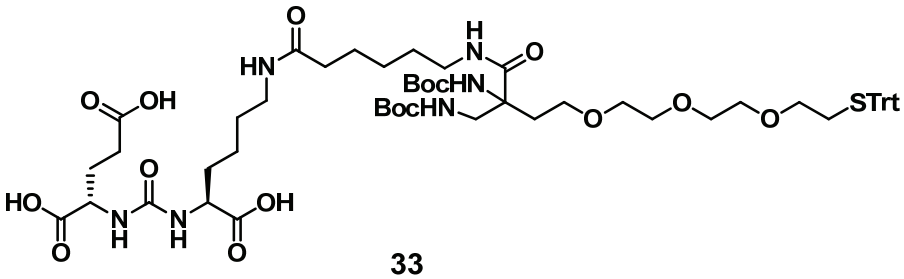

33

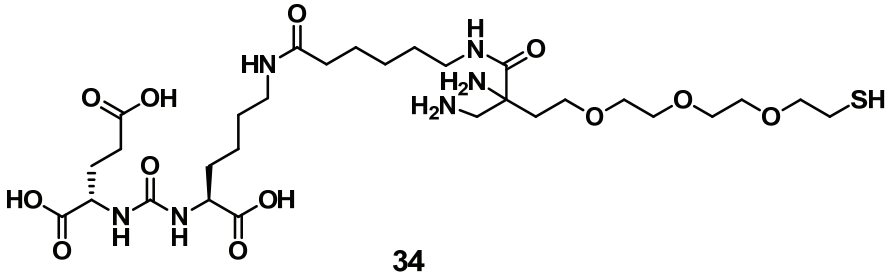

34

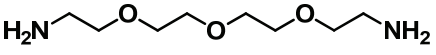

35

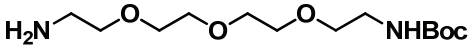

36

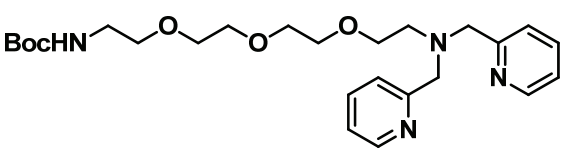

37

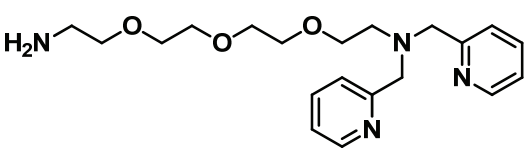

38

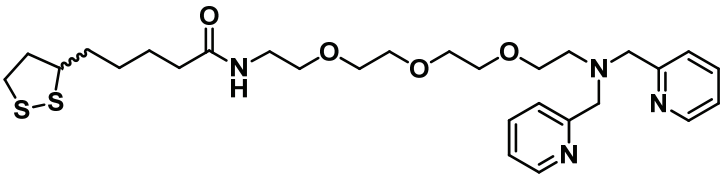

39

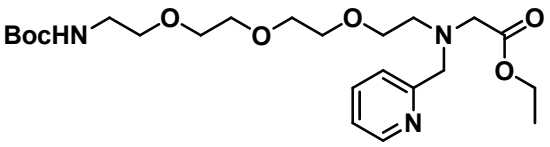

40

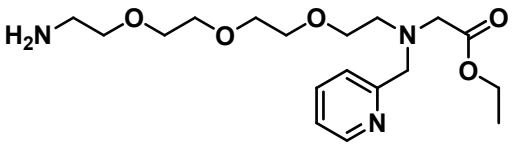

41

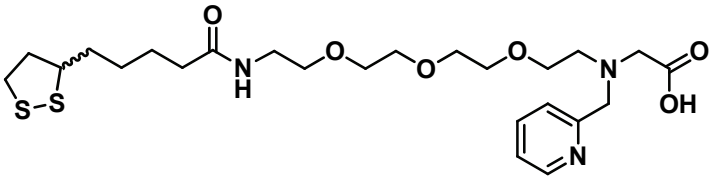

43

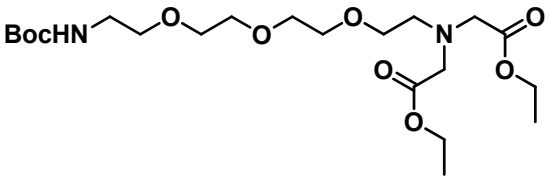

44

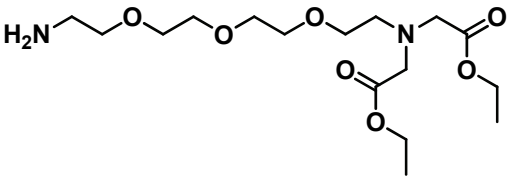

45

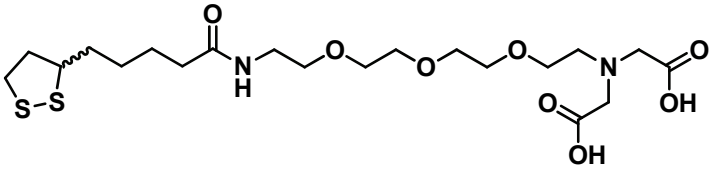

47

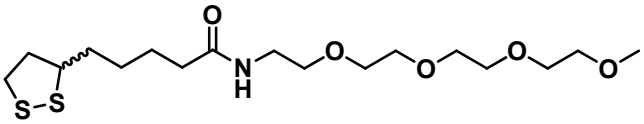

48

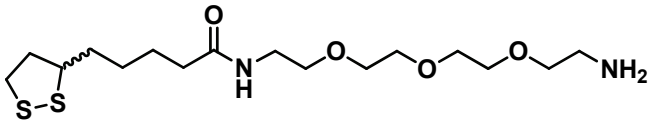

49

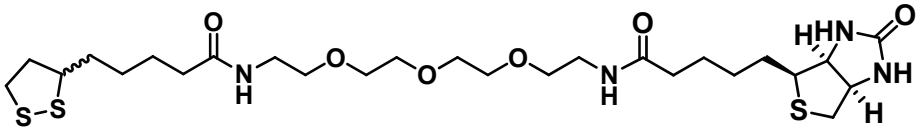

50

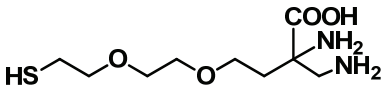

51

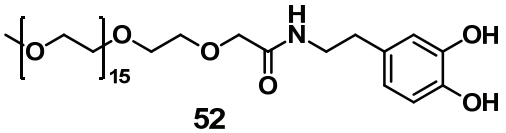

52

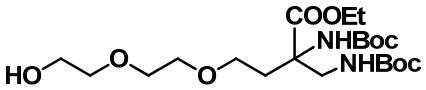

53

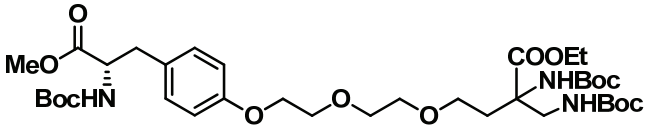

54

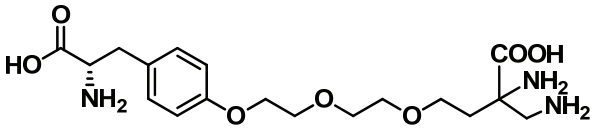

55

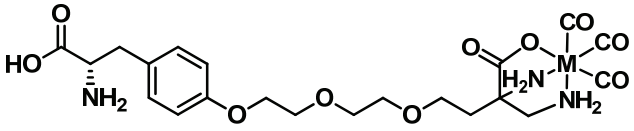

M = Re (56), ^{99m}Tc (57)

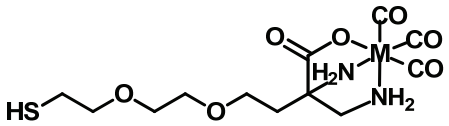

M = ^{99m}Tc (58), Re (59)

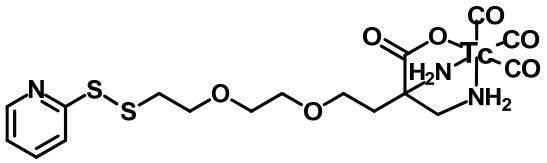

60

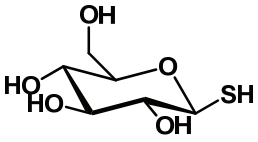

61

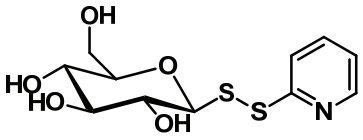

62

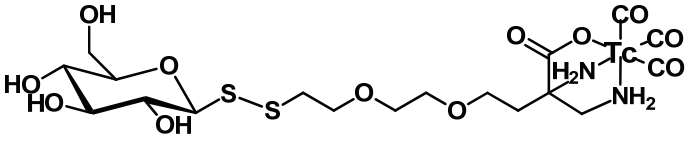

63

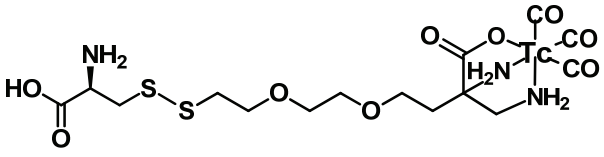

64

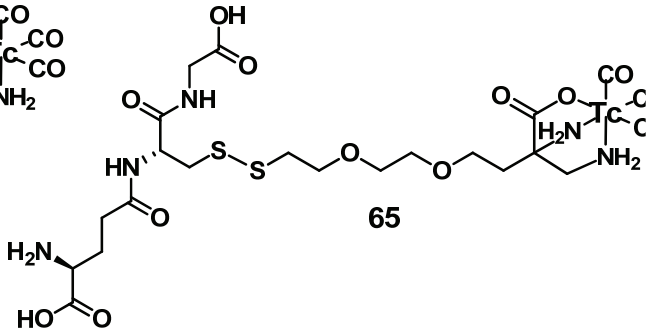

65

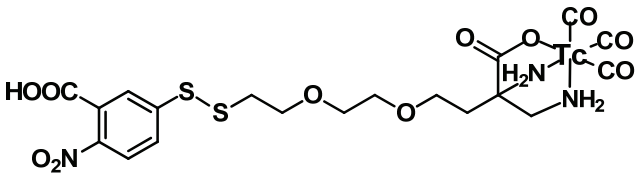

66

7.2 Abbreviations

AuNP(s)	Gold nanoparticle(s)
Bn	Benzyl
CNT(s)	Carbon nanotube(s)
Cys	Cysteine
DAP	2,3-diaminopropionic acid
DEAD	Diethyl azodicarboxylate
DFO	Desferrioxamine
DHLA	Dihydrolipoic acid
DIAD	Diisopropyl azodicarboxylate
DIEA	*N,N*-diisopropylethylamine
DOTA	1,4,7,10-tetraazacyclododecane-1,4,7,10-tetraacetic acid
DPA	Dipicolylamine
DTDP	2,2'-Dithiodipyridine
DTPA	Diethylenetriaminepentaacidic acid
DTNB	5,5'-Dithiobis-(2-nitrobenzoic acid)
DLS	Dynamic light scattering
EDC	1-ethyl-3-(3-dimethylaminopropyl)carbodiimide
EDDA	*N,N*-ethylene diamine diacetic acid
EDX	Energy dispersive X-ray spectroscopy
EPR	Enhanced permeability and retention effect
ESI-MS	Electronspray-ionization mass spectrometry
FBS	Fetal bovine serum
FET	Fluoroethyl-L-tyrosine
GSH	Glutathione
HDD	Hydrodynamic diameter
HPLC	high performance liquid chromatography
HPMA	*N*-(2-hydroxypropyl)methacrylamide
HYNIC	Hydrazinonicotinamide
HSA	Human serum albumin
ICP-MS	Inductively coupled plasma mass spectrometry
ID	Injected dose
IONP(s)	Iron oxide nanoparticle(s)
i.v.	intravenous
LA	Lipoic acid
LAT	L-amino acid transport
Mal	Maleimide
MAS_3	S-acetylmercaptoacetyltriserine
MNP(s)	Magnetic nanoparticle(s)
MPS	Mononuclear phagocyte system
MRI	Magnetic resonance imaging

mSiNP(s)	mesoporous silica nanoparticle(s)
NHS	N-hydroxysuccinimide
NIH	US National Institutes of Health
NIR	Near infrared
NMR	Nuclear magnetic resonance
NOTA	1,4,7-triazacyclononane-1,4,7-triacetic acid
NP(s)	Nanoparticle(s)
PBS	Phosphate buffered saline
PEG	Polyethylene glycol
PET	Positron emission tomography
p.i.	post injection
PSMA	Prostate specific membrane antigen
QD(s)	Quantum dot(s)
QY	Quantum yield
RCP	Radiochemical purity
RCY	Radiochemical yield
RES	Reticuloendothelial system
SCM	Succinimidyl carboxy methyl ester
SCN	Isothiocyanate
SPDP	*N*-succinimidyl 3-(2-pyridyldithio)propionate
SPECT	Single photon emission computed tomography
TCEP	Tris(2-carboxyethyl)phosphine
TEM	Transmission electron microscopy
TF	Targeting function
TFA	Trifluoroacetic acid
TMAOH	Tetramethylammonium hydroxide
TOP	Trioctylphosphine
TOPO	Trioctylphosphine oxide
TSTU	*N,N,N',N'*-tetramethyl-*O*-(*N*-succinimidyl)uronium tetrafluoroborate
UCNP(s)	Upconverting nanoparticle(s)
ζ-Pot.	Zeta potential